Analysis of the molecular mechanisms of mitotic spindle assembly and checkpoint signalling using the HaloTag system

Daniel Bernard Harry Gold

Reuben College

University of Oxford

A thesis presented for the degree of

Doctor of Philosophy in Biochemistry

Trinity Term 2025

This thesis is dedicated to my family in recognition of all your love and support

Acknowledgements

A thesis would be impossible without the help and support of others. Work that is not solely that of my own is explicitly mentioned in text. This is inclusive of any recent publications where I am a contributing author. I would like to extend my gratitude to the Oxford Medical Research Council Doctoral Training Programme, Reuben College, University of Oxford Department of Biochemistry, and Cancer Research UK for funding my time and research here in Oxford.

Ah where to begin - I've enjoyed my time in Oxford and can't believe it's coming to an end! First, I must thank my supervisor, Prof. Francis Barr, for all his help and guidance during my DPhil, and for agreeing to take on and train a physicist with minimal biochemistry experience, but who was willing to learn. To the Barr lab; Andreas Gerondopoulos, Luke Fulcher, Tomoaki Sobajima, Caleb Batley, Gege Yang, thank you for all your help, your humour, your insightful conversations, and your support. Luke (The Western Blot King), Tomoaki (aka Tomo-Cell-Tracki), and Caleb (The Quote Machine); I'll miss our morning coffee and cinnamon buns. Andreas (Who makes a great Moussaka, apparently), thank you for all your guidance and advice. Gege (The Plant Queen), thank you for all our chats and help over the years. To Ulrike Gruneberg, James Holder, Ian Gibbs-Seymour - thank you for your insightful discussions! To the Micron Imaging Facility, Deirdre Kavanagh, Niloufer Irani, Lothar Schermelleh – thank you for all your imaging expertise and help throughout my DPhil. To all those who have supported me outside of the lab; Fern Pannell, Farnosh Tolou, Milena Nikolajeva, Louisa March, Natasha Black, Megan Ward, Natalie Duffus, Ben Carty, Emma Fitzgibbon, Lauryn Deaville, Katie Hains, Caroline Mawson, Kirren Mahmood, Christian Covill-Cooke, Alexia Cross, Holly Sanderson, Izzy Leitch, Dan Grant – thank you! I couldn't have done this without my support network. And last, but by no means least, to my amazing family; Merle, Brian, Andy, Matt and Rosie. Your unwavering support, belief in me, hours of conversations, advice, and love, have made this all possible. Thanks for also bearing with me while I try to explain a cool experiment I'd done! There is no way I could have done this without you all – thank you, always.

Abstract

Timely alignment and accurate chromosome segregation in mitosis are vital for genomic stability and are required to prevent the emergence of aneuploid cells, a hallmark of many cancers. Central to these processes are kinetochores, large protein complexes which connect mitotic chromosomes to spindle-associated microtubules and act as hubs for spindle assembly checkpoint (SAC) signalling. The SAC ensures that correctly bioriented chromosomes are discriminated from unaligned chromosomes in a process involving the mitotic kinases Aurora B and MPS1. These interact with and phosphorylate the kinetochore microtubule binding protein NDC80 and SAC scaffold protein KNL1, respectively. This thesis uses the synthetic HaloTag sequence integrated into the endogenous genomic loci encoding NDC80, KNL1 and the Aurora B activator and targeting protein INCENP to enable accurate visualisation and rapid PROTAC-mediated degradation in living cells. Using this system, the roles of these proteins in SAC activity, kinetochore function, and genomic stability were investigated. Integration of the mStayGold fluorescent marker into the MPS1 and BUB1 checkpoint proteins in these HaloTag backgrounds enabled the live readout of SAC activity.

In metaphase, microtubule pulling forces separate Aurora B at the inner centromere from its targets at the outer kinetochore. Using super-resolution STED microscopy, I show that NDC80 at kinetochores and Aurora B and CPC$^{Survivin/Borealin}$ at inner centromeres are collapsed together in prometaphase and become spatially segregated in metaphase. In contrast, no discernible separation was detected between the distal and proximal ends of the kinetochore, marked by CENP-A and NDC80 respectively. Structure-guided analysis revealed that Aurora B localisation to inner centromeres is crucial for SAC signalling in prometaphase. Targeted degradation of NDC80 prevents microtubules from attaching to chromosomes, resulting in constitutive SAC signalling and delayed mitotic progression. By contrast, either degradation of the SAC scaffold KNL1 or the Aurora B activator INCENP reduced SAC activity, with KNL1 loss shortening mitosis. Proteomic analysis of INCENP-dependent Aurora B phosphorylation sites in mitosis identified the kinetochore subunit DSN1 and the inner centromere kinesin MCAK. The data presented in this thesis support a spatial separation model for Aurora B in SAC signalling and demonstrate an important role for NDC80 in silencing of the SAC.

TABLE OF CONTENTS

LIST OF FIGURES

LIST OF TABLES

LIST OF ABBREVIATIONS

ANOVA	Analysis Of Variance
AO	Anaphase Onset
APC/C	Anaphase Promoting Complex/ Cyclosome
As	Asynchronous
AURKA	Aurora Kinase A
AURKB	Aurora Kinase B
BIR	Baculoviral Inhibitor of Apoptosis Repeat
BUB1	Budding Uninhibited by Benzimidazoles 1
BUB3	Budding Uninhibited by Benzimidazoles 3
BUBR1	Budding Uninhibited by Benzimidazoles Related 1
CCAN	Constitutive Centromere-Associated Network
CDC20	Cell Division Control Protein 20
CDK	Cyclin Dependent Kinase
CENP	Centromere Protein
CH	Calponin Homology
CPC	Chromosome Passenger Complex
CRISPR	Clustered Regularly Interspaced Short Palindromic Repeats
DAPI	4′,6-Diamidino-2-Phenylindole
DMSO	Dimethyl Sulfoxide
DNA	Deoxyribonucleic Acid
DTAG	Degron Tag ($FKBP^{F36V}$)
DTT	Dithiothreitol
ECL	Enhanced Chemiluminescence
EDTA	Ethylenediaminetetraacetic Acid
EGTA	Egtazic Acid
G1	Gap 1
G2	Gap 2
GFP	Green Fluorescent Protein
H1	Histone 1
H3	Histone 3
H3pT3	Histone H3 Phospho-Threonine 3
HCl	Hydrochloric Acid
HEPES	4-(2-Hydroxyethyl)-1-Piperazineethanesulfonic Acid
HRP	Horseradish Peroxidase
HTEMF	HEPES-Triton-EGTA-$Mgcl_2$-Formaldehyde Fixative
IGEPAL	Octylphenoxypolyethoxyethanol
INCENP	Inner Centromere Protein
IP	Immunoprecipitation
JFX	Janelia Fluor Deuterated Dye
kb	Kilo Base Pairs
kDa	Kilo Daltons
KIF11	Kinesin Family Member 11
KMN	Knl1-Mis12-Ndc80
KNL1	Kinetochore Scaffold 1
KO	Knock Out
KT	Kinetochore
M	Mitosis
MAD1	Mitotic Arrest Deficient 1
MAD2	Mitotic Arrest Deficient 2
MCAK	Mitotic Centromere-Associated Kinesin
MCC	Mitotic Checkpoint Complex

MDM2	Mouse Double Minute 2
MELT	Methionine–Glutamate–Leucine–Threonine
$MgCl_2$	Magnesium Chloride
MIS12	Mis12 Kinetochore Complex Component
MKLP1	Mitotic Kinesin-Like Protein 1
MKLP2	Mitotic Kinesin-Like Protein 2
MPS1	Monopolar Spindle 1
MS	Mitotic Slippage
MT	Microtubule
NaCl	Sodium Chloride
NaF	Sodium Fluoride
NDC80	Nuclear Division Cycle 80
NEBD	Nuclear Envelope Breakdown
NEDD8	Neural Precursor Cell Expressed, Developmentally Down-Regulated 8
NEK2	NIMA (Never in Mitosis Gene A)-Related Kinase 2
NOC	Nocodazole
PAGE	Polyacrylamide Gel Electrophoresis
PBS	Phosphate-Buffered Saline
PCR	Polymerase Chain Reaction
PIPES	Piperazine-N,N′ -Bis(2-Ethanesulfonic Acid)
PP1	Protein Phosphatase 1
PP2A B56	Protein Phosphatase 2a B56
PP6	Protein Phosphatase 6
PRC1	Protein Regulator of Cytokinesis 1
pro-TAME	Pro-Tosyl-L-Arginine Methyl Ester
PROTAC	Proteolysis Targeting Chimera
PSF	Point Spread Function
PTEMF	PIPES-Triton-EGTA-$Mgcl_2$-Formaldehyde Fixative
Rb	Retinoblastoma Protein
RNA	Ribonucleic Acid
ROI	Region Of Interest
RZZ	Rod-Zw10-Zwilch Complex
S	Synthesis
SAC	Spindle Assembly Checkpoint
SD	Standard Deviation
SDS	Sodium Dodecyl Sulfate
SEM	Standard Error of the Mean
SGO1	Shugoshin 1
SIR	Silicon-Rhodamine Dye
STED	Stimulated Emission Depletion Microscopy
STLC	S-Trityl-L-Cysteine
TEMED	Tetramethylethylenediamine
TRIP13	Thyroid Hormone Receptor Interacting Protein 13
VHL	Von Hippel-Lindau
WT	Wild Type

1. Introduction

1.1. An overview of the cell cycle

1.1.1. The mammalian cell cycle & DNA damage checkpoints

Cells are created from existing cells through a cycle where replication and segregation of the chromosomes and division of the cytoplasm are precisely coordinated. In human cells, this cell cycle process consists of two key stages: S-phase when DNA is replicated and Mitosis or M-phase, when the copied chromosomes are segregated to the new daughter cells. These two phases are separated by gap phases G1 and G2 where cells grow and integrate signals modulating cell growth and cell cycle progression. By convention the cycle starts in the G1 phase following chromosome segregation and cell division. Stressed or damaged cells may exit the regular cell cycle during G1 and enter a gap-phase known as G0 and undergo senescence or quiescence, depending on whether this is a permanent or transient outcome (Campisi, 1996; Marescal & Cheeseman, 2020). The movement between these cell cycle phases is regulated by protein phosphorylation mediated by Cyclin Dependent Kinases (CDKs) which bind to and are activated by specific cyclins A, B, D and E in human cells (Sherr et al., 1996). The timely synthesis and degradation of cyclins controls CDK activity and drives progression from one cell cycle phase to the next. Growth factors trigger the synthesis of cyclin D in G1. To trigger S phase entry and DNA synthesis, cyclin E is required; cyclin A is then needed to sustain S phase and progression into G2. Finally, cyclin B promotes entry into mitosis and the process of cell division. Figure 1.1 further outlines these phases, and the specific CDK:cyclin complexes associated with them (Arellano & Moreno, 1997; Evans et al., 1983).

Embedded within the cell cycle are checkpoints which ensure genomic integrity by halting cell cycle progression in the face of any damage sustained to the DNA, sub-optimal growth conditions, or stresses that might impair accurate DNA replication or chromosome segregation

(Funabiki et al., 1996; Hartwell & Weinert, 1989). Checkpoints allow for such issues to be dealt with before progression into the next cell cycle phase. There are three major cell cycle checkpoints crucial for maintaining genome stability: DNA damage checkpoints in G1 and G2, and a mitotic checkpoint monitoring correct alignment of chromosomes on the mitotic spindle. The G1 DNA damage checkpoint acts by inhibiting CDK4/6-cyclin D complexes required for entry into S phase (Sherr & Roberts, 1999). Mitogens found in serum triggers the synthesis of cyclin D and activate CDK4/6 resulting in phosphorylation of the retinoblastoma protein (Rb) which, in its unphosphorylated state, binds to and inhibits E2F family transcription factors. CDK4/6-cyclin D therefore triggers the release of E2F transcription factors from Rb and thus enables gene transcription events driving progression into S-phase (Weinberg, 1995). When DNA damage is present in G1 cells, Rb phosphorylation is prevented due to the activity of a DNA damage responsive transcription factor p53 which triggers synthesis of a CDK-inhibitory protein p21 (El-Deiry et al., 1993; Engeland, 2022). This blocks Rb phosphorylation by CDK4/6-cyclin D and maintains E2F in an inhibited state, thereby preventing S-phase entry (Sherr, 1994).

The G2 DNA damage checkpoint operates by directly modulating the activity of the CDK1-cyclin B complex to prevent entry into mitosis if DNA damage is present. This pathway requires conserved protein kinases and phosphatases, Wee1/Myt1 and CDC25, respectively (O'Connell et al., 1997; Russell & Nurse, 1986). Wee1/Myt1 phosphorylate CDK1 at threonine 14 and tyrosine 15 during G2 and prevent its untimely activation by cyclin B. This phosphorylation is counteracted by the phosphatase CDC25. Both Wee1/Myt1 and CDC25 are under feedback control by CDK1-cyclin B, creating a robust switchlike mechanism controlling CDK activity during mitosis (Gautier et al., 1991; Gould & Nurse, 1989; Novak & Tyson, 1993; Pomerening et al., 2003). Crucially, CDC25 is inhibited by DNA damage preventing CDK1 activation until the damage has been repaired (O'Connell et al., 1997).

Defects in the G1 and G2 DNA damage checkpoints are found in many cancers; most notably the DNA damage responsive transcription factor p53 is one of the most highly mutated genes in cancers (Olivier et al., 2010). These checkpoints are therefore critical for preserving genomic integrity and preventing the propagation of DNA damage by the cell cycle.

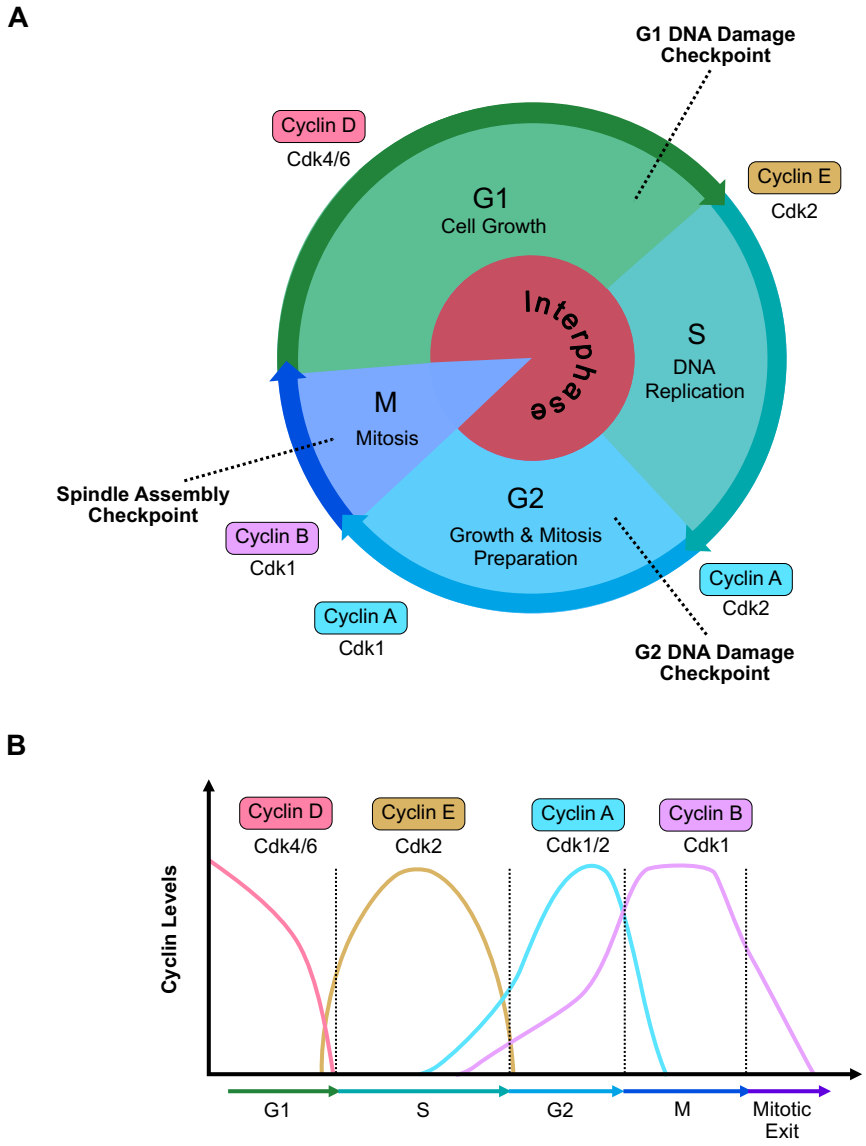

Figure 1.1 - The mammalian cell cycle at a glance

(A) The cell cycle moves in a chronological order, from a growth phase G1, to a DNA replication S phase, to a growth and preparation G2 phase, to active cell division in Mitosis (M phase); arrows show directionality to each stage. Checkpoints help to safeguard the genome against damage/mis segregation defects. (B) Cdk:Cyclin complexes are responsible for transition into each phase (as indicated on the figure).

These interphase checkpoints serve to safeguard the cell from accumulating damage prior to mitosis. During mitosis, the spindle assembly checkpoint (SAC) becomes the next failsafe to protect against incorrect chromosomal alignment and subsequent mis-segregation which would generate cells with altered or damaged chromosomes (discussed further in Introduction 1.1.3).

1.1.2. Mitotic spindle formation & chromosome segregation

Mitosis is a short-lived yet highly active period within the cell cycle, whereby chromosomal DNA must be correctly packaged and segregated to ensure the correct genomic information is passed on to daughter cells. Failure of faithful chromosome segregation in mitosis can have catastrophic cellular consequences leading to apoptosis or the emergence of cells with altered properties that result in diseases, including cancers (Levine & Holland, 2018).

To explain chromosome segregation in mitosis it is necessary to understand how mitotic chromosomes are structured. When chromosomes are replicated in G2, the two copies of sister chromatids are tied together by a ring-like protein complex, cohesin (Michaelis et al., 1997). During mitotic entry cohesin is released from the chromosome arms and retained only at the centromere region (Losada et al., 2002). The chromosome arms are condensed or compacted by two cohesin-related protein complexes called condensin I and II. This creates the characteristic X-shaped mitotic chromosome architecture where the two sister chromatids, which are copies of the same DNA sequence, remain linked at the centromere (Ono et al., 2003). The centromere is also the site of a multi-subunit microtubule-binding complex referred to as the kinetochore. Each sister chromatid has a kinetochore, creating a chromosome with two outward facing microtubule attachment sites. These are crucial for movement of the chromosomes during mitosis (Cheeseman & Desai, 2008).

Paramount for successful segregation of duplicated chromosomes is the formation of a bi-polar mitotic spindle and attachment of chromosomes to this structure. During interphase, centrosomes, the main microtubule organising centres, are duplicated in a manner coordinated with DNA replication. When cells enter mitosis, they become separated and move apart in a process regulated by multiple protein kinases NEK2, Aurora A and CDK1 (Faragher & Fry, 2003; Magnaghi-Jaulin et al., 2019; Nigg, 2007). Microtubules emanating from the now separated spindle poles bind to the kinetochores of the chromosomes and exert pulling forces moving the chromosomes into alignment at the metaphase plate (Risteski et al., 2021).

Completion of chromosome alignment and biorientation is regulated by the spindle assembly checkpoint which prevents exit from mitosis until these conditions are met. Two conserved kinases, Aurora B and MPS1, regulate the correction of improper kinetochore-microtubule attachments by promoting chromosome biorientation and activating a checkpoint signal preventing cyclin B degradation (Lampson & Cheeseman, 2010; Musacchio, 2015) (Discussed further in Introduction 1.3.2). Once spindle assembly is complete, the checkpoint signal is turned off, and the Anaphase Promoting Complex/Cyclosome (APC/C^{CDC20}) becomes active (Sivakumar & Gorbsky, 2015). The APC/C ubiquitylates key inhibitors of mitotic exit, securin and cyclin B, promoting their rapid degradation by the proteasome. Because securin and cyclin B inhibit the cohesin protease separase, their degradation leads to the activation of separase, the cleavage of cohesion, and the triggering of sister chromatid separation in anaphase (Waizenegger et al., 2002). Each chromatid can then be pulled to opposing ends of the spindle by forces generated from bioriented kinetochore-microtubule attachments. Once complete, the nuclear envelope reforms around both sets of newly separated chromosomes before cell furrowing ensues and an actin and myosin contractile ring pinches and separates the two new daughter cells (Barr & Gruneberg, 2007; Cheffings et al., 2016) (Figure 1.2).

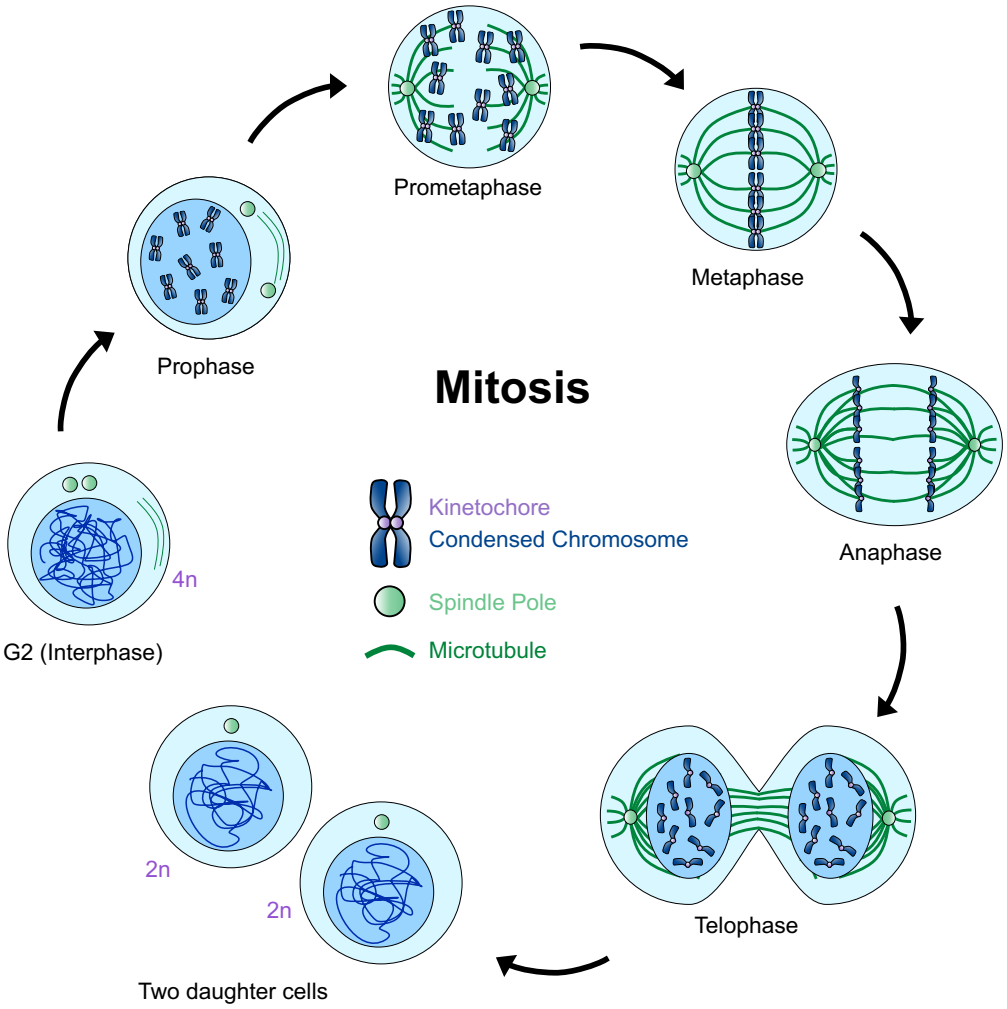

Figure 1.2 - An overview of mitosis

Mitosis is the shortest part of the cell cycle where active cell division occurs, comprising of prophase, prometaphase, metaphase, anaphase, telophase, and resulting in two new, genetically identical, daughter cells.

Hallmarks of failed mitosis include aneuploidy, a non-diploid incorrect number of chromosomes, and the formation of micronuclei, whereby a small pocket of DNA content exists outside of the main nucleus (Mazzagatti et al., 2024). These errors often arise from defects in chromosome segregation, such as improper kinetochore-microtubule attachments. One such attachment defect is a merotelic orientation attachment, whereby a single sister chromatid's kinetochore is attached by microtubules to opposite poles instead of just being

attached to one pole. This can lead to lagging chromosomes left near the spindle equator, and result in aneuploidy (Cimini et al., 2001). Premature loss of sister chromatid cohesion (cohesion fatigue) can also occur, often after a prolonged mitosis (Daum et al., 2011), and leads to merotelic attachments. Mitotic defects such as these can result in genome instability, and drive tumorigenesis and developmental disorders (Thompson & Compton, 2010).

1.1.3. Mechanism of the spindle assembly checkpoint

The overall concept of the Spindle Assembly Checkpoint is simply to sense an incorrectly aligned chromosome and halt any further progression through mitosis until this issue is resolved. In practice, however, it consists of a complex set of protein interactions that work harmoniously to ensure that there are no alignment errors, even down to a single kinetochore level (Musacchio, 2015). Once all kinetochores are attached to microtubules, the APC/C-Cdc20 E3 ligase becomes active towards securin and cyclin B, simultaneously triggering mitotic exit and chromosome segregation (Sivakumar & Gorbsky, 2015) (Figure 1.3 - B). The presence of a chromosome with a single kinetochore which is not attached to the mitotic spindle can trigger the checkpoint. In the absence of a bound microtubule, Aurora B aids recruitment of MPS1 to that kinetochore but not kinetochores on other chromosomes which are attached to the mitotic spindle (Lara-Gonzalez et al., 2021; McVey et al., 2021). MPS1 has been reported to interact with NDC80, promoting MPS1-kinetochore localisation and multisite phosphorylation of MELT (Methionine, Glutamine, Leucine and Threonine) motifs within the N-terminus of KNL1 (Figure 1.3 - A) (Kemmler et al., 2009; London et al., 2012; Nijenhuis et al., 2013; Shepperd et al., 2012; Yamagishi et al., 2012). In human cells, there are approximately 19 MELT motifs reported, however redundancy is noted as not all motifs need to be phosphorylated for SAC activation (Vleugel, Omerzu, et al., 2015). Nonetheless, these phosphorylated motifs act as a platform for BUB3:BUB1, a stoichiometric stable complex (Primorac et al., 2013). BUB1 can then be phosphorylated by CDK1 and MPS1, promoting recruitment of MAD1:C-MAD2 (Closed-MAD2) complexes (Ji et al., 2017; Qian et al., 2017;

Zhang et al., 2017). Once recruited, MAD1:C-MAD2 helps to convert free-floating Open-MAD2 (O-MAD2) in the cytosol to its closed form which is then able to bind to CDC20 (De Antoni et al., 2005). Additionally, phosphorylation of MAD1 by MPS1 has been reported necessary for CDC20 recruitment (Faesen et al., 2017; Ji et al., 2017; Piano et al., 2021). Finally, BUB3:BUBR1 is then able to dock to BUB1 and provides the final piece of the Mitotic Checkpoint Complex (MCC) formed of BUB3:BUBR1:C-MAD2:CDC20 (Sudakin et al., 2001). This complex can then travel through the cytosol, inhibiting active APC/C^{Cdc20} and preventing anaphase onset (Izawa & Pines, 2014). Whilst the unattached status of the kinetochore remains unchanged, BUB3:BUB1 remains bound to KNL1, allowing the cascade of events resulting in MCC generation to continue.

In addition to these KMN-centred signalling events, unattached kinetochores also assemble a fibrous corona, a transient crescent-like layer that expands beyond the KMN network. It is prominently comprised of the RZZ complex (ROD-Zw10-Zwilch) and its adaptor Spindly, as well as checkpoint and motor proteins MAD1, MAD2, CENP-F and CENP-E (McHugh & Welburn, 2017; Mosalaganti et al., 2017). A key role of the corona is to expand the potential binding surface for microtubules, supporting lateral attachments that drive chromosome congression, mediated by CENP-E, and amplify SAC signalling by RZZ recruitment of MAD1-MAD2 (McHugh & Welburn, 2017; Mosalaganti et al., 2017). Once correct end-on attachments are established, Spindly recruits dynein to shed corona components from kinetochores, thereby dismantling the corona and silencing MAD1-MAD2 mediated checkpoint activity (Mosalaganti et al., 2017). CENP-F modulates the rate of dynein-mediated corona disassembly, ensuring corona integrity until proper attachments are made (Auckland et al., 2020). Hence, the corona helps to supplement the KMN network to ensure robust checkpoint signalling at unattached kinetochores.

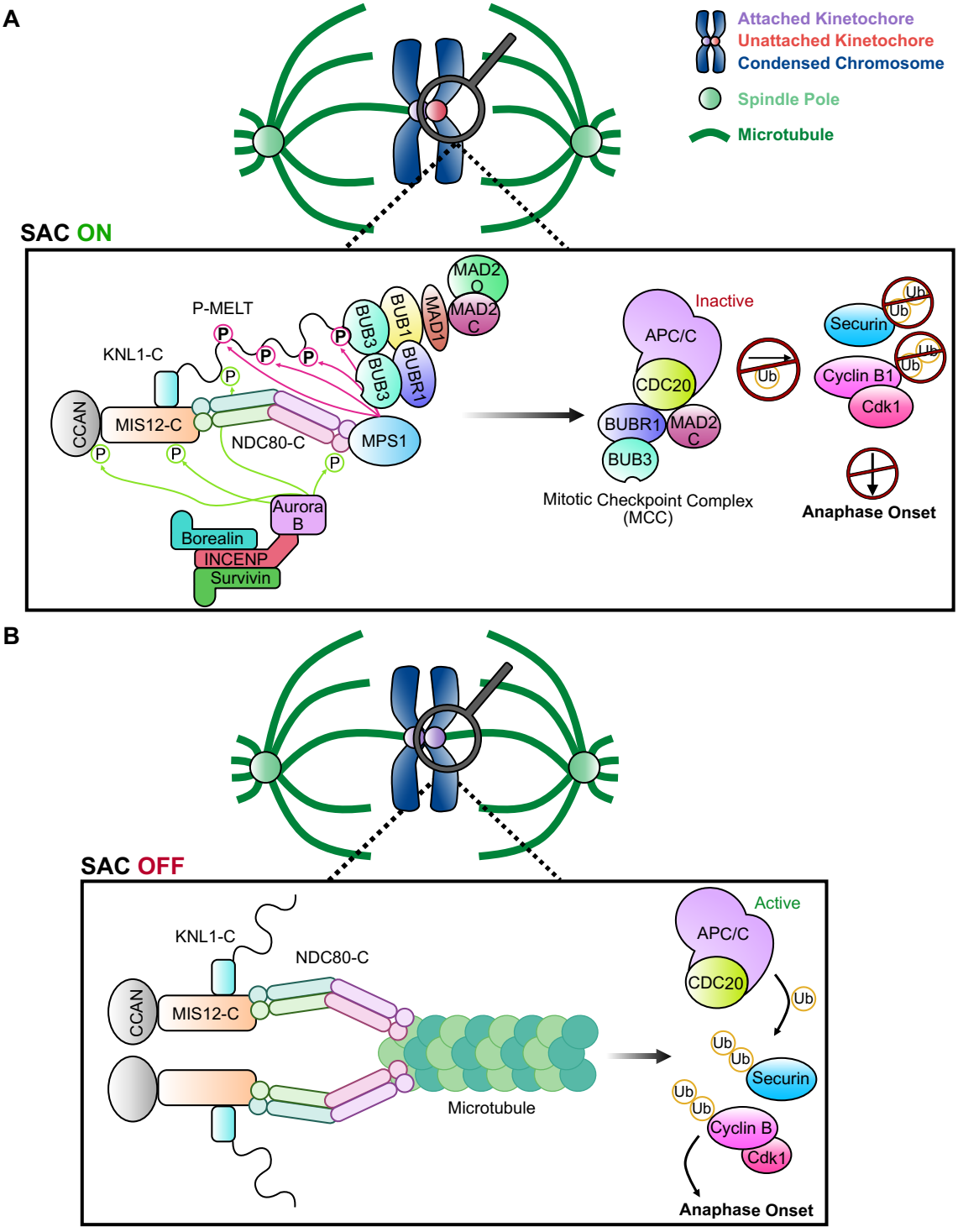

Figure 1.3 - A schematic of the Spindle Assembly Checkpoint.

The mitotic checkpoint exists in two states: (A) SAC Active; No attachment, allowing MCC complexes to form and APC/C-CDC20 to become inhibited. Securin and Cyclin B1 remain active, and the cell stays in mitosis. (B) SAC Inactive state; NDC80 is attached to a microtubule and no MCC assembled. APC/C-CDC20 is able to ubiquitylate securin and cyclin B1, allowing for anaphase onset. Figure inspired from (Musacchio, 2015).

Once correct attachment takes place, the system needs to shut down and allow for progression to anaphase; as such, the SAC must be dismantled. Phosphorylated MELT motifs are dephosphorylated by either PP2A-B56 (Espert et al., 2014) or PP1 (Nijenhuis et al., 2014). Additionally, at microtubule-attached kinetochores, MPS1 levels fall (Kuijt et al., 2020), resulting in reduced KNL1-MELT phosphorylation and BUB3:BUB1 recruitment. Without any BUB1, MAD1:C-MAD2 is no longer recruited, meaning that O-MAD2 is no longer converted to C-MAD2, and will therefore no longer bind CDC20 and create MCC complexes. Whilst this stops any new MCC from being made, the previously generated (and now cytosolic) MCC still needs to be rapidly dismantled; $p31^{Comet}$, a regulatory adaptor protein, binds to C-MAD2 and disrupts the MCC. Once bound, its co-factor TRIP13 (an ATPase) helps to unwind C-MAD2 back to its open, inactive form of O-MAD2, thereby releasing CDC20 which is then free to activate APC/C (Alfieri et al., 2018; Eytan et al., 2014).

Deficiencies in any one of these SAC proteins could result in premature anaphase onset and increase the risk of aneuploid cell divisions (Thompson & Compton, 2010). In a laboratory setting, deletion of just one allele of MAD2 resulted in a defective mitotic checkpoint in both human cancer cells and embryonic fibroblasts (Michel et al., 2001). In a more clinical setting, certain diseases can result from ineffective checkpoint signalling; one such disease arising from this is a rare, recessive condition known as ‘Mosaic Variegated Aneuploidy’, caused by a mutation in BUBR1. This condition can lead to intrauterine growth defects (reduced growth rate in the womb), congenital abnormalities, and carries an increased risk of malignancies in children (Hanks et al., 2004). Hence, correct SAC signalling is vital for ensuring proper kinetochore-microtubule attachments, and genomic integrity in the daughter cells generated.

1.2. Structure & function of the kinetochore

1.2.1. The centromere & inner kinetochore

Kinetochores are the key structures required for chromosome segregation and checkpoint signalling. In human cells these assemble at a unique site, the centromere, on each sister chromatid (Navarro & Cheeseman, 2021). The centromere is a region of DNA on the chromosome specifically marked by CENP-A, a unique variant of Histone H3, deeming the chromatin as centromeric (Figure 1.4). In human cells, centromeres are monocentric, with each chromosome containing a single centromere. This is comprised of repeats of α-satellite DNA, where CENP-A is deposited, marking centromere identity (McKinley & Cheeseman, 2015).

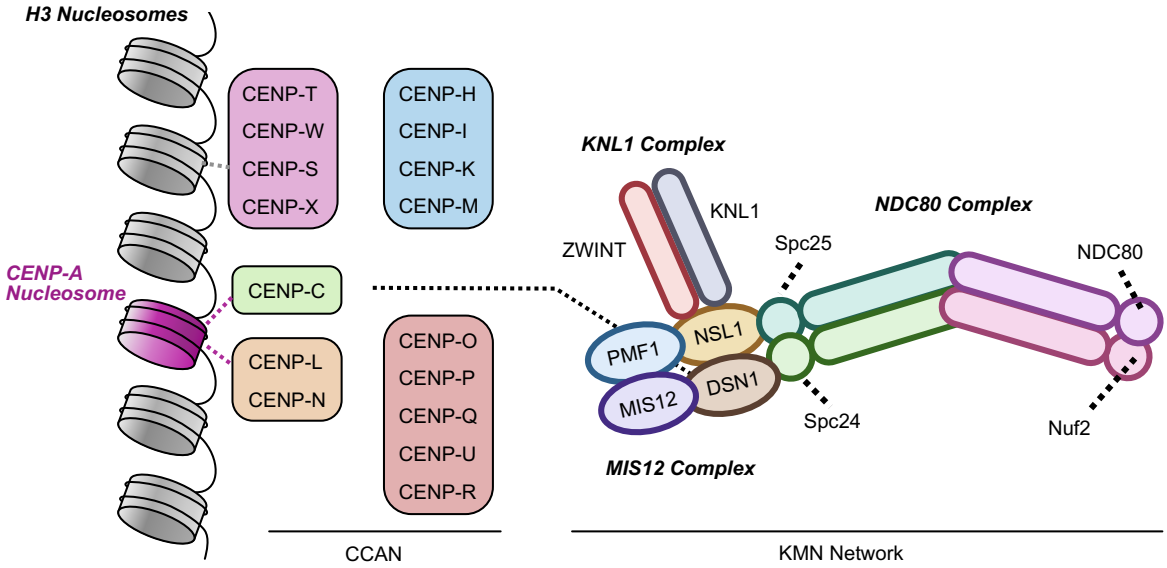

Figure 1.4 - CCAN and KMN Network

A simplified schematic of the CCAN interacting with H3 and CENP-A nucleosomes, as well as interactions with the outer-kinetochore KMN network (Pesenti et al., 2022; Yatskevich et al., 2022).

The CENP-A centromere is recognised by a 16-protein complex known as the CCAN (Constitutive Centromere Associated Network) (Pesenti et al., 2022; Yatskevich et al., 2022). This consists of five sub-complexes each with their own roles in providing a stable platform for the kinetochore: CENP-C, CENP-L-N, CENP-H-I-K-M, CENP-T-W-S-X and CENP-O-P-Q-U-

R (Pesenti et al., 2022; Yatskevich et al., 2022) (Figure 1.4 - CCAN). CENP-C and CENP-L-N have been shown to bind directly to the CENP-A nucleosome (Mckinley et al., 2015), with CENP-C shown to also bind to DSN1 of the MIS12 complex (Gascoigne et al., 2011; Petrovic et al., 2010). CENP-C:DSN1 interaction shows an example of how the centromeric chromatin and microtubule-binding interface can be bridged via the CCAN and the KMN network (KNL1-MIS12-NDC80).

The CENP-H-I-K-M subcomplex is proposed to bind to CENP-C and CENP-L-N, providing structural rigidity and stability to CENP-A nucleosome binding, as well as interacting with and contributing to outer-kinetochore function (Foltz et al., 2006; Okada et al., 2006). The CENP-T-W-S-X subcomplex has been shown to bind canonical H3 and provides a parallel, but distinct, pathway for KMN attachment (via NDC80-C or MIS12-C) to the CCAN, independent of CENP-C (Hori et al., 2008; Nishino et al., 2013). This creates redundancy, ensuring that there is robust kinetochore assembly if one pathway is compromised. The CENP-O-P-Q-U-R subcomplex has been implicated in PLK1 (Polo-like kinase 1) regulation, notably in its recruitment to kinetochores (Bancroft et al., 2015; Kang et al., 2011) and in chromosomal alignment (Pesenti et al., 2018). At the kinetochore, PLK1 phosphorylates KMN network components to help mediate SAC activity and correct microtubule attachment (Kim, 2022).

Together, these CCAN subcomplexes establish a stable inner-kinetochore platform that can support outer-kinetochore assembly.

1.2.2. The outer kinetochore KMN network

The KMN network comprised of the KNL1-complex (KNL1, ZWINT), MIS12-complex (MIS12, DSN1, NSL1, PMF1), and NDC80-complex (NDC80, NUF2, Spc24/25) form the outer-kinetochore (Polley et al., 2024; Yatskevich et al., 2024) (Figure 1.4 - KMN Network). Each part of the complex has distinct roles.

The MIS12 complex is the inner-most part of this network, and has been shown to bind directly to CENP-C, thus mediating attachment to the inner-kinetochore (Screpanti et al., 2011). Depletion of any part of the MIS12 complex has been shown to result in defects in chromosomal alignment and subsequent delays in mitosis (Kline et al., 2006), highlighting the necessity of this complex for kinetochore assembly.

KNL1 is attached to the outer kinetochore by its C-terminus, which binds to the MIS12 complex (Petrovic et al., 2014, 2016). Its N-terminus is a large disordered region, implicated in providing a scaffold for checkpoint signalling proteins to bind and form mitotic checkpoint complexes, and release these for inhibition of the APC/C (Figure 1.3 - A) (Vleugel et al., 2013). As discussed in Introudction 1.1.3, 19 MELT motifs have been reported on KNL1 in human cells, serving as key phosphorylation sites for the MPS1 kinase (Vleugel et al., 2013). It has been reported that MPS1 preferentially phosphorylates threonine residues within these motifs, and that the amino acid sequences surrounding these motifs were shown to affect the efficiency of MPS1 phosphorylation and hence stability of BUB1 recruitment (Vleugel et al., 2013). Removal of KNL1 by RNA interference has been shown to prevent BUB checkpoint protein recruitment to kinetochores, and resulted in chromosome alignment and segregation issues (Kiyomitsu et al., 2007). Hence, KNL1 is necessary for SAC signalling.

The NDC80 complex (NDC80-C) is the outer-most part of the KMN network shown to bind to MIS12, and hence the rest of the kinetochore, by SPC24 and 25 (Polley et al., 2024). At the opposite end, NDC80 and Nuf2 subunits form a long rod-like coiled coil, terminating in calponin

homology (CH) domains which mediate microtubule binding and bridge the attachment between the kinetochore and mitotic spindle (Alushin et al., 2010; Ciferri et al., 2008; Pesenti et al., 2018; Volkov et al., 2018; Wei et al., 2006). This interaction is crucial for mediating chromosomal alignment, and ensuring correct attachments prior to anaphase onset. Previous data have shown that distruption of this complex by RNA interference can lead to aberrant issues in cell growth (Ju et al., 2017), and mutations in the CH domain of NDC80 by RNA interference and subsequent rescue led to defective kinetochore-microtubule attachments (Sundin et al., 2011). Hence, NDC80-C is an essential gene, crucial for ensuring accurate chromosomal alignment and faithful segregation.

In summary, the KMN network facilitates both stable microtubule attachments and acts a platform for SAC signalling. In the following sections, I will discuss how Aurora kinases promote chromosome alignment and mitotic spindle formation, and regulate processes at the kinetochores and centromeres necessary for SAC signalling.

1.3. Post translational control of spindle assembly by Aurora kinases

Activation and inhibition of protein function occurs by post-translational modifications (PTMs). One of the most notable PTMs is phosphorylation, whereby kinases add phosphate groups to the protein which can either activate or inhibit it depending on the context. Similarly, phosphatases counterbalance kinase activity by removing these phosphate groups, thereby regulating protein activity (Cohen, 2000; Hunter, 2007). Specific kinases and phosphatases target certain proteins; this section will focus on Aurora kinases, and their roles in mitotic spindle regulation and error correction. Aurora serine/threonine kinases were identified as conserved regulators of mitosis and meiosis. They come in three variations; Aurora A & B, which are mitotic, and Aurora C which is meiotic (Goldenson & Crispino, 2014). This thesis is focussed on the roles of Aurora A & B, and Aurora C will not be discussed further.

1.3.1. Aurora Kinase A is necessary for spindle formation and pole-based error correction

The Aurora A kinase is predominantly localised to centrosomes and spindle-associated microtubules via its binding partners CEP192 (Holder et al., 2024; Joukov et al., 2014) and TPX2 (Bayliss et al., 2003; Bird & Hyman, 2008) respectively; this binding allows for full auto-catalytic activation of the kinase at threonine 288 (pT288) (Eyers et al., 2003). Aurora A function has been implicated in centrosome maturation, bipolar spindle assembly and chromosome separation (Barr & Gergely, 2007). Within a bipolar spindle context, Aurora A contributes to pole-based error correction by an activity gradient; kinetochores closer to the pole will be subject to higher Aurora A kinase activity resulting in elevated phosphorylation of NDC80 and movement toward the central spindle (Figure 1.5)(Ye et al., 2015).

More recently, Aurora A kinase has also been shown to phosphorylate the N-terminus of NDC80 at microtubule-attached kinetochores, contributing to spindle size regulation (Sobajima et al., 2023). Aurora A kinase activity is counterbalanced by Protein Phosphatase 6 (PP6), whose catalytic subunit PPP6C is responsible for dephosphorylating T288 on Aurora A (Zeng et al., 2010). Removal of PPP6C by CRISPR/Cas9-mediated protein knockout leads to hyper-phosphorylation of Aurora A, resulting in excessive phosphorylation of NDC80, enlarged mitotic spindles, and the formation of micronuclei in subsequent G1 cells (Sobajima et al., 2023). Hence, precise modulation of Aurora A kinase activity is essential for spindle formation and genomic stability.

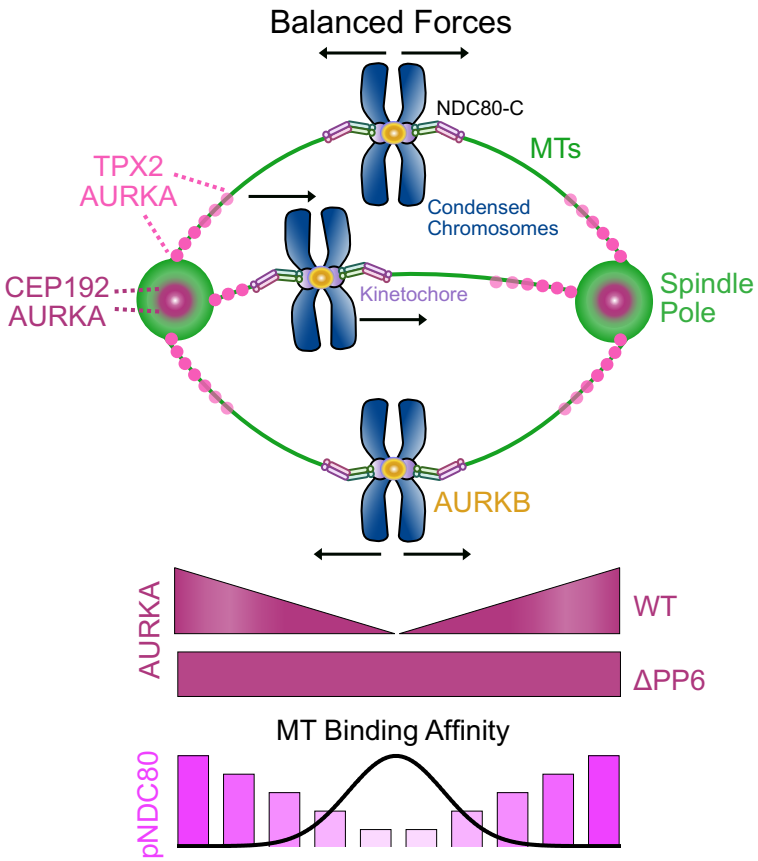

Figure 1.5 - The mitotic spindle and Aurora kinases

A figure outlining a basic schematic for Aurora kinase localisation with respect to the mitotic spindle and chromatin. Also highlighted are Aurora A kinase and NDC80 activity gradients along the spindle (Ye et al., 2015).

1.3.2. Aurora B kinase is required for chromosome condensation, biorientation, and SAC signalling

Aurora B is the catalytic subunit of the Chromosome Passenger Complex (CPC), consisting of Borealin, Survivin and its scaffold, the inner centromere protein (INCENP) (Carmena et al., 2012; Ruchaud et al., 2007). INCENP recruits and activates Aurora B via its IN-box domain, and spatially targets the kinase to pericentromeres in prometaphase, and to the central spindle in anaphase, thereby orchestrating Aurora B activity throughout mitosis (Sessa et al., 2005; Wheatley et al., 2001). During early prophase, Aurora B is responsible for phosphorylating

histone H3, specifically at serine 10 and 28, promoting chromosome condensation and facilitating the displacement of heterochromatin protein 1 (HP1) (Hirota et al., 2005) (Figure 1.7 - Late G2-Prophase). Inhibition of Aurora B during this phase has been shown to cause defects in chromosome structure, such as lack of constriction at centromeres (Hirota et al., 2005), thus highlighting its importance in mitotic progression.

As cells transition into prometaphase, Aurora B is predominantly localised at the inner centromere between two sister chromosomes through the coordinated action of the CPC. Within the complex, Survivin binds to phosphorylated Histone H3 at threonine 3 (H3pT3), while Borealin interacts directly with nucleosomes, acting cooperatively to stabilise pericentric localisation (Abad et al., 2019). INCENP helps to maintain complex integrity by forming a three-helical bundle with Survivin and Borealin (Jeyaprakash et al., 2007; Niedzialkowska et al., 2012), as well as playing a role in activating Aurora B (Sessa et al., 2005). Here, the CPC acts as a 'tension sensor' for monitoring and correcting incorrect microtubule-kinetochore attachments, such as syntelic, single pole, attachments (Lampson & Cheeseman, 2010) (Figure 1.7 - Late Prometaphase-Metaphase). Under low tension, one model suggests that Aurora B can phosphorylate its kinetochore substrates (e.g. NDC80, KNL1, DSN1, MCAK) to destabilise incorrect microtubule attachments and allow for correct re-attachment (Andrews et al., 2004; DeLuca et al., 2006; Welburn et al., 2010). Once correct attachment has occurred, Protein Phosphatase 1 (PP1) acts counteractively to dephosphorylate these sites and maintain stable attachment status (Liu et al., 2010; Nijenhuis et al., 2014). In parallel, to ensure no premature chromosome de-condensation and to maintain sister chromatid cohesion, the Protein Phosphatase 2A B56 (PP2A-B56) is recruited by Shugoshin 1 (SGO1) at centromeres to counteract Aurora B phosphorylation of cohesin subunits (Liu et al., 2013; Meppelink et al., 2015). Simultaneously, in this low-tensioned state, Aurora B can phosphorylate the kinetochore, allowing MPS1 binding and promoting spindle assembly checkpoint signalling to continuously inhibit APC/C until correct chromosomal alignment (Nijenhuis et al., 2013) (Figure 1.3).

Once errors have been corrected and tensioned biorientation has occurred (i.e. each kinetochore pair is correctly attached to microtubules emanating from opposite poles), Aurora B-mediated phosphorylation of kinetochore substrates is reduced (Liu et al., 2009). There is some debate about the mechanism(s) of how this system is regulated. One concept is termed the ‘spatial separation’ model. In this model, it is proposed that attached kinetochores are pulled away from Aurora B, physically displacing it from its substrates, preventing further phosphorylation and stabilising the system (Liu et al., 2009). Evidence for the spatial separation model shows that if Aurora B is artificially relocated closer to the kinetochore (i.e. able to reach its substrates irrespective of tension), the spindle assembly checkpoint remains active and stable bioriented attachments are prevented (Hayward et al., 2022; Liu et al., 2009). This would imply that Aurora B must be physically displaced from its substrates to prevent phosphorylation (Figure 1.6 - A). An alternative mechanistic framework for reduced Aurora B kinase activity under tension proposes that regulation occurs within the kinetochore itself via an ‘intra’-kinetochore stretch (Cheeseman & Maiato, 2021; de Regt et al., 2022; Maresca & Salmon, 2009; Uchida et al., 2009, 2021). This model suggests that Aurora B kinase activity emanates from the pericentromeric region, and under a tensioned state, is unable to phosphorylate kinetochore substrates. This is said to be due to small displacements within the kinetochore architecture e.g. the most distal component, NDC80, undergoes a conformational change preventing Aurora B accessibility (de Regt et al., 2022; Uchida et al., 2021) (Figure 1.6 – B). These two models may operate in a complementary manner to ensure accurate chromosome segregation.

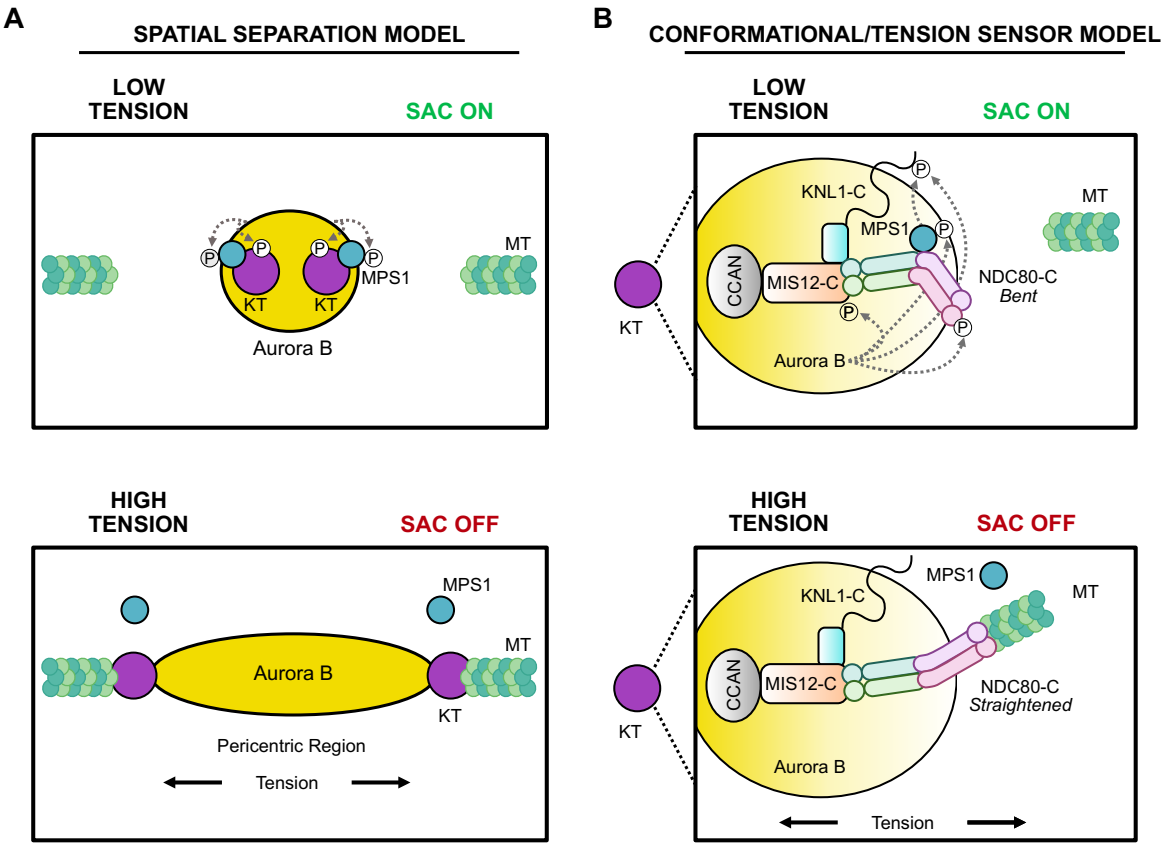

Figure 1.6 - Aurora B regulation models

(A) The spatial separation model, implying Aurora B displacement from kinetochores regulates its ability to phosphorylate its substrates. (B) The 'intra'-kinetochore stretch model, suggesting a gradient of Aurora B activity affects tensioned kinetochores from being phosphorylated distally from the pericentromere, and NDC80 undergoes a conformational change under tension. Figure inspired from (Welburn et al., 2010).

Once its function as a chromosome error corrector is complete and the SAC is satisfied, anaphase onset begins. As chromosomes segregate, Aurora B is re-localised to the central spindle by a kinesin motor protein MKLP2 (Gruneberg et al., 2004) (Figure 1.7 - Anaphase). Aurora B then phosphorylates a second kinesin motor MKLP1 to help stabilise antiparallel non-kinetochore microtubules as they mature to form the central spindle (Neef et al., 2006). Aurora B then cooperates with other central spindle proteins to regulate contractile ring assembly and cell furrowing (Minoshima et al., 2003) (Figure 1.7 - Telophase). Additionally,

after its SAC-related roles, it has been suggested that Aurora B may act as a sensor towards incomplete chromosome separation, preventing premature de-condensation by retention of Condensin I, should a lagging chromosome be detected (Afonso et al., 2014). This differs from the SAC, as at this point the cell has already committed to dividing; hence this pseudo-checkpoint is said to act in prevention of further chromatin damage and tetraploidisation, for example by delaying chromosome de-condensation (Afonso et al., 2014) and abscission (Steigemann et al., 2009). Once chromatin has been cleared from the midbody, PP1 or PP2A act to dephosphorylate Aurora B substrates and allow continuation of anaphase B/ telophase (Afonso et al., 2014).

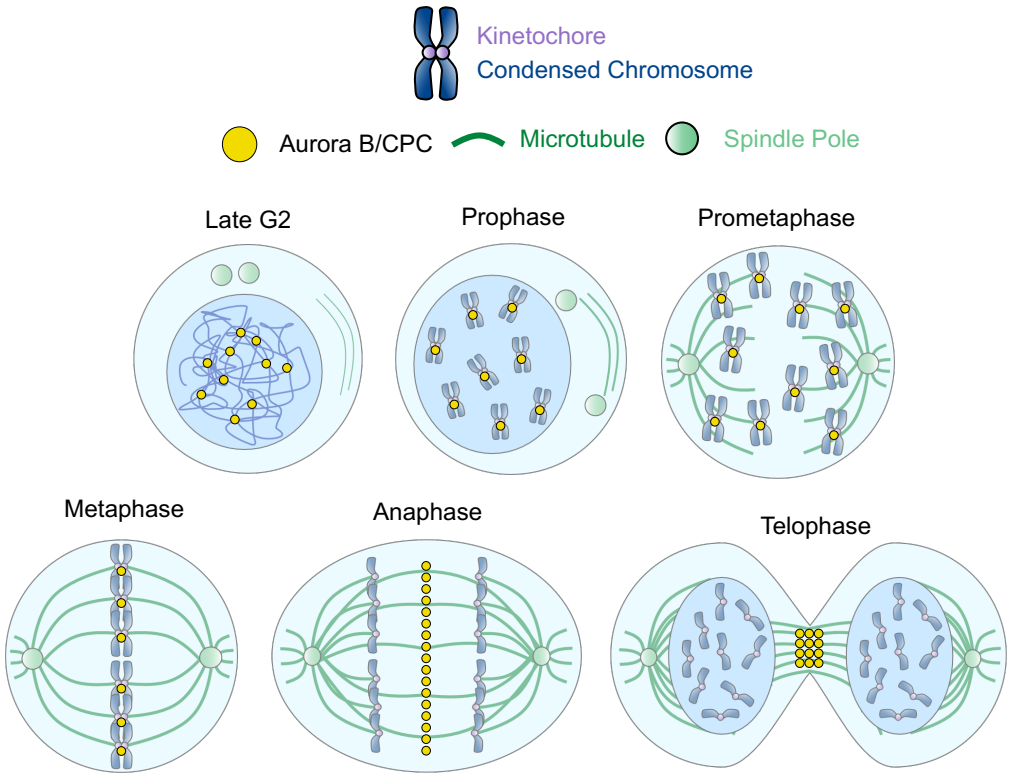

Figure 1.7 - Aurora B kinase throughout mitosis

The Aurora B kinase is first localised on chromatin in late G2/early prophase, helping to phosphorylate Histone H3. It then moves to a centromeric localisation from prometaphase-metaphase sensing incorrect attachment. It then moves to the anaphase central spindle, before condensing around the telophase midbody to aid abscission.

1.4. Thesis Aims

Faithful and accurate chromosome alignment and segregation rely on integration of error correction and spindle assembly checkpoint signalling, processes coordinated by Aurora B-mediated phosphorylation of multiple substrates within the centromere and kinetochore structures. Three key elements are necessary for this regulation to function: (i) the NDC80 complex, which forms the core kinetochore-microtubule binding interface, (ii) the KNL1 scaffold, acting as the main hub for checkpoint protein recruitment, and (iii) the CPC component INCENP, which spatially positions the Aurora B kinase throughout mitosis including at the pericentromere region adjacent to the kinetochore. The aim of this thesis is to understand how microtubule-mediated tension generated during chromosome biorientation regulates the spindle assembly checkpoint.

While many studies have revealed significant insights into the function and interactions of these components, most employ the use of RNA-interference as a means of perturbing protein function. These methods often act over a 48–72-hour period, primarily revealing long-term end-point responses. Such approaches cannot fully resolve the immediate consequences of protein loss, as cells are often able to adapt during this time, or succumb to apoptosis if the target protein is an essential gene. To overcome these limitations, I have integrated synthetic HaloTag sequences into the endogenous loci of key kinetochore and CPC proteins. This system allows for both high-resolution imaging and rapid protein degradation to probe protein localisation and function within a single cell cycle stage. Through applying this system to NDC80, KNL1 and INCENP, I aim to define the mechanistic contributions of these proteins to Aurora B-mediated activation and silencing of spindle assembly checkpoint signalling during the process of chromosome alignment, by investigating the leading models for checkpoint silencing.

2. Results

2.1. Analysis of the outer-kinetochore protein NDC80 during mitosis

2.1.1. Integration of a synthetic HaloTag into endogenous NDC80

The NDC80 complex (NDC80, Nuf2, Spc24 and Spc25) is the major microtubule binding site on chromosomes, essential for mitotic spindle formation and chromosome alignment, and is thought to play a crucial role in the spindle assembly checkpoint (SAC) signalling pathway (Cheeseman et al., 2006; Ciferri et al., 2008; DeLuca et al., 2006; Musacchio, 2015). NDC80 has been reported to be a substrate for both Aurora family kinases, with recent findings suggesting that it is phosphorylated by Aurora kinase A at microtubule-attached kinetochores (Sobajima et al., 2023), extending previous work showing Aurora B mediated phosphorylation of NDC80 was important for correct chromosome alignment and the SAC (DeLuca et al., 2006; Umbreit et al., 2012; Welburn et al., 2010). However, despite these advances' questions remain about how the NDC80 complex promotes both chromosome alignment and the SAC. To explore both the function and dynamic localisation of NDC80 during the different stages of mitosis with high spatial and temporal resolution, a synthetic HaloTag was integrated into the endogenous NDC80 gene locus via CRISPR/Cas9 technology (Methods 4.3). The HaloTag allows for highly efficient detection of targeted proteins using super-resolution and live cell imaging, as well as modulation of protein stability to perturb function (Buckley et al., 2015; Erdmann et al., 2019; Simpson et al., 2020; Thevathasan et al., 2019). The human cell model chosen for this study was the colorectal carcinoma-derived HCT116 cell line. This line was chosen as it has a near-diploid karyotype, is p53 wild-type, is compatible with genetic manipulation, and exhibits altered MDM2-p53 regulation, suggesting an attenuated mitotic timer response (Kaeser et al., 2004). Together, these characteristics allow perturbations that lead to altered mitotic progression to be investigated.

PCR of the genomic locus of NDC80 indicated successful tag integration, shown by an increase in size of approximately 1 kb for all three isolated clones in comparison to wild-type

and confirmed by genomic DNA sequencing (Figure 2.1 - A). Successful HaloTag integration was also confirmed by immunoblotting with NDC80 and HaloTag antibodies which revealed that NDC80 exhibited a change in electrophoretic mobility to a higher molecular weight, and a positive HaloTag signal was seen at the same molecular weight as the NDC80 band, respectively (Figure 2.1 - B). A chromosome spread assay was performed to determine NDC80-HaloTag localisation at individual mitotic chromosomes using the HaloTag-binding JFX549 dye (Methods 4.6.2). Each individual chromosome showed two closely positioned signals adjacent to the compression marking the centromere region (Figure 2.1 - C), indicative of the expected kinetochore localisation (Suzuki et al., 2015). Further supporting this conclusion, immunofluorescence staining of cells revealed overlap of the NDC80-HaloTag detected using JFX549 with the centromere protein CENP-C and NDC80 detected using a specific antibody (Suzuki et al., 2015). In addition, some NDC80-HaloTag JFX549 signal was observed coincident with bipolar mitotic spindle structures positive for the microtubule binding protein TPX2 (Figure 2.1 - D) (DeLuca et al., 2018; Sobajima et al., 2023). Taken together, these results are consistent with successful tag integration without compromising NDC80 localisation to the kinetochore, or its function in mitotic spindle formation.

After clone selection, initial screening suggested that both putative diploid and tetraploid clones had been isolated. Immunofluorescence microscopy was performed using JFX549 to detect NDC80-HaloTag combined with antibody staining for pericentrin to test how many centrosomes were present in these cell lines (Figure 2.2 - A). In addition, the number of kinetochores, NDC80 foci, were determined using a custom Fiji macro (Methods 4.7.1.1). This approach revealed that clones G3 C25 and G4 C3 had a diploid number of NDC80-positive kinetochores, whereas G4 C15 was tetraploid (Figure 2.2 - B). During mitosis, both cell lines had two centrosomes, one at each spindle pole, as expected for a diploid cell (Figure 2.2 - A, pericentrin). However, although metaphase spindle morphology was normal in both cases, spindle size was increased from ~ 8 μm in the C3 diploid cells to ~10 μm in the C15 tetraploid cells (Figure 2.2 - C).

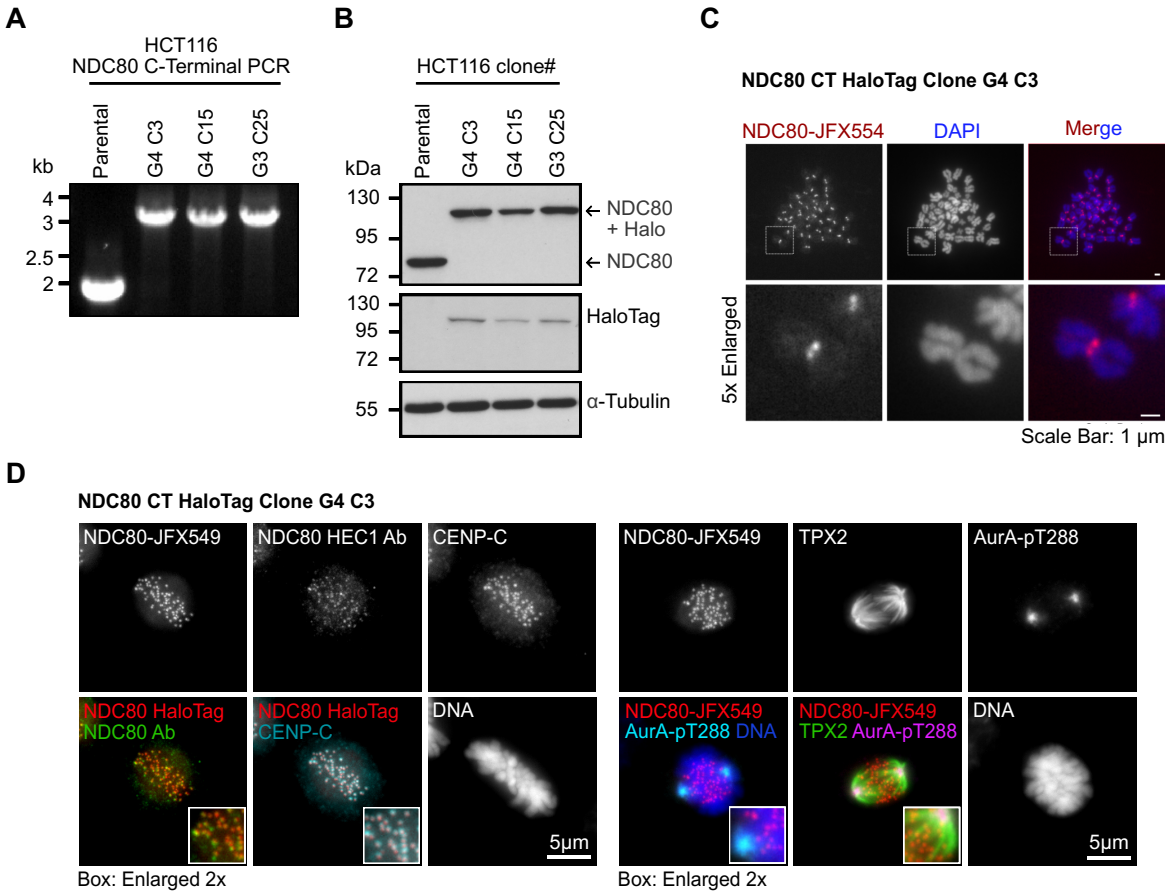

Figure 2. 1 - Generation of NDC80-HaloTag HCT116 cell lines and validation by direct detection with HaloTag-binding JFX dyes

A) PCR of the C-Terminus of NDC80 to determine tag integration. Genomic DNA was extracted from HCT116 wild type and NDC80-HaloTag clone pellets; products were resolved on agarose gel. (B) Western blot of whole-cell lysates for the same cell lines as in (A), immunoblotting with antibodies for NDC80, HaloTag and a-Tubulin. (C) A representative chromosome spread (Methods 4.6.2) highlighting NDC80-JFX554 localisation relative to chromatin (DAPI). (D) Representative images highlighting NDC80-HaloTag localisation relative to key centromeric and spindle markers. Asynchronous cells were incubated with 100 nM JFX549 for 15 minutes and PTEMF fixed for 12 minutes, followed by immunofluorescence staining with antibodies against CENP-C, NDC80, TPX2, AurA-pT288, and DAPI.

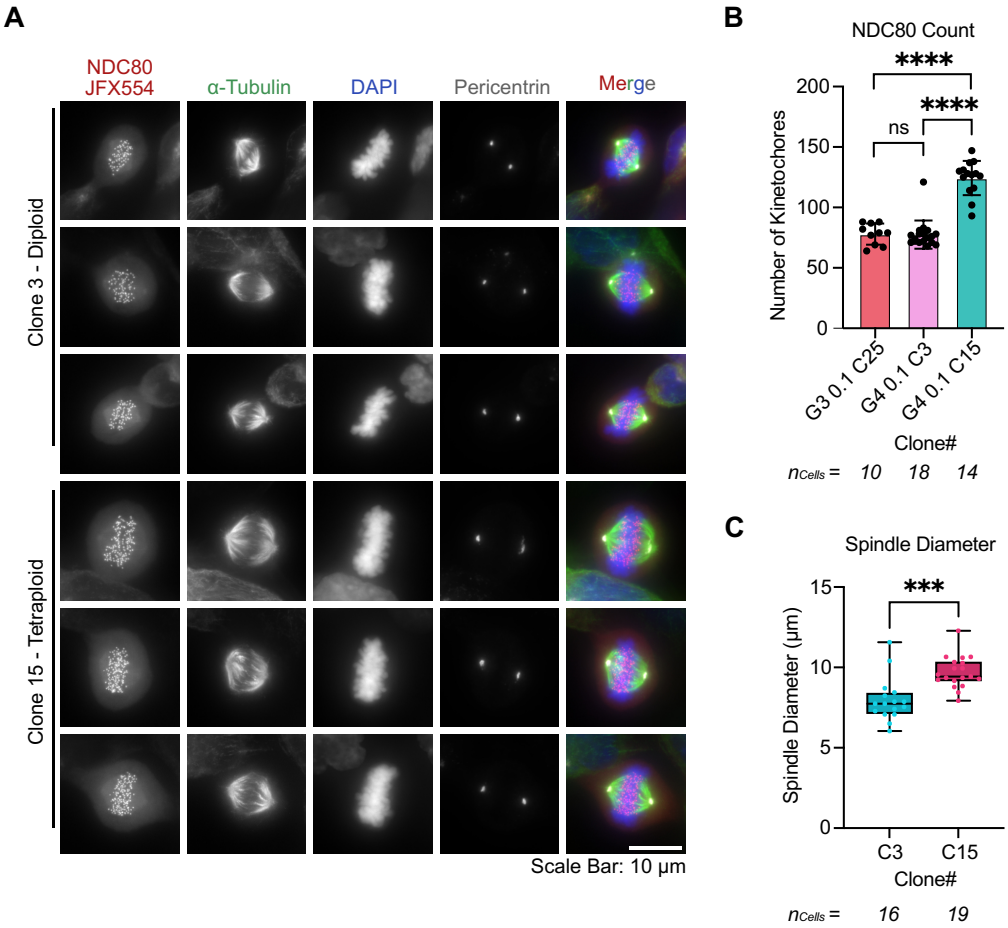

Figure 2. 2 - Diploid and tetraploid NDC80-HaloTag cell lines with normal centrosome numbers

(A) Imaging of both diploid (G4C3) and tetraploid (G4C15) HCT116 NDC80-HaloTag clones to determine ploidy and spindle diameter. Asynchronous cells were incubated in 100 nM JFX554 for 15 minutes prior to 12 minutes PTEMF fixation. Immunofluorescence staining was then performed with antibodies against a-tubulin and pericentrin, with chromatin visualised by DAPI staining. Representative images are shown. (B) A custom Fiji macro was used to count the number of NDC80-JFX554 positive kinetochores present in each clone; total number of cells measured indicated in the figure, bar graph with mean ± SD shown. An ordinary one-way ANOVA was used to test for significance with P<0.0001 (****) and P>0.9999 (ns). (C) Circular spindle diameter measured inclusive of chromatin content between diploid (G4C3) and tetraploid (G4C15) clones; total number of cells measured indicated in the figure, box and whiskers plot with min-max shown. Welch's t-test performed with P = 0.0003 (***).

2.1.2. NDC80-HaloTag interacts with the KMN network

To examine whether the NDC80-HaloTag protein was able to still interact with other members of the KMN network, immunoprecipitation was performed from either G2 or cells at different stages of mitosis (Methods 4.4.3). Immunoblotting revealed that only NDC80-HaloTag and not wild-type samples were immunoprecipitated, and that in all cell cycle phases tested (G2 by CDK1 inhibition, and prometaphase by the spindle poison nocodazole or Eg5 inhibitor STLC), NDC80 can interact with Nuf2, Spc24 and Spc25 which form the outer kinetochore assembly (Figure 2.3 - A). Additionally, increased NDC80 phosphorylation at serine 55 was observed in mitotic cells compared to G2 cells (Figure 2.3 - A). The highest NDC80 pS55 levels were seen in mitotic cells arrested with STLC, with slightly lower levels in nocodazole-arrested cells, consistent with previous findings (Kettenbach et al., 2011; Sobajima et al., 2023). Further immunoblots revealed that NDC80-HaloTag was also able to interact with other members of the KMN network; MIS12-C (MIS12, NSL1, DSN1) and KNL1-C (KNL1, ZWINT) (Cheeseman et al., 2006), with more robust interactions noted in mitotically arrested cells (Figure 2.3 - A).

To determine whether spindle checkpoint surveillance was still functional in NDC80-HaloTag cells, perturbations of spindle formation and chromosome alignment by treatment with two different doses of nocodazole or CENP-E inhibitor respectively were performed to promote SAC signalling. The SAC protein BUBR1 was used as a readout for checkpoint active kinetochores (Banerjee et al., 2022; Chan et al., 1999; Chen, 2002), and NDC80 pS55 used as a readout of microtubule attached kinetochores (Sobajima et al., 2023).

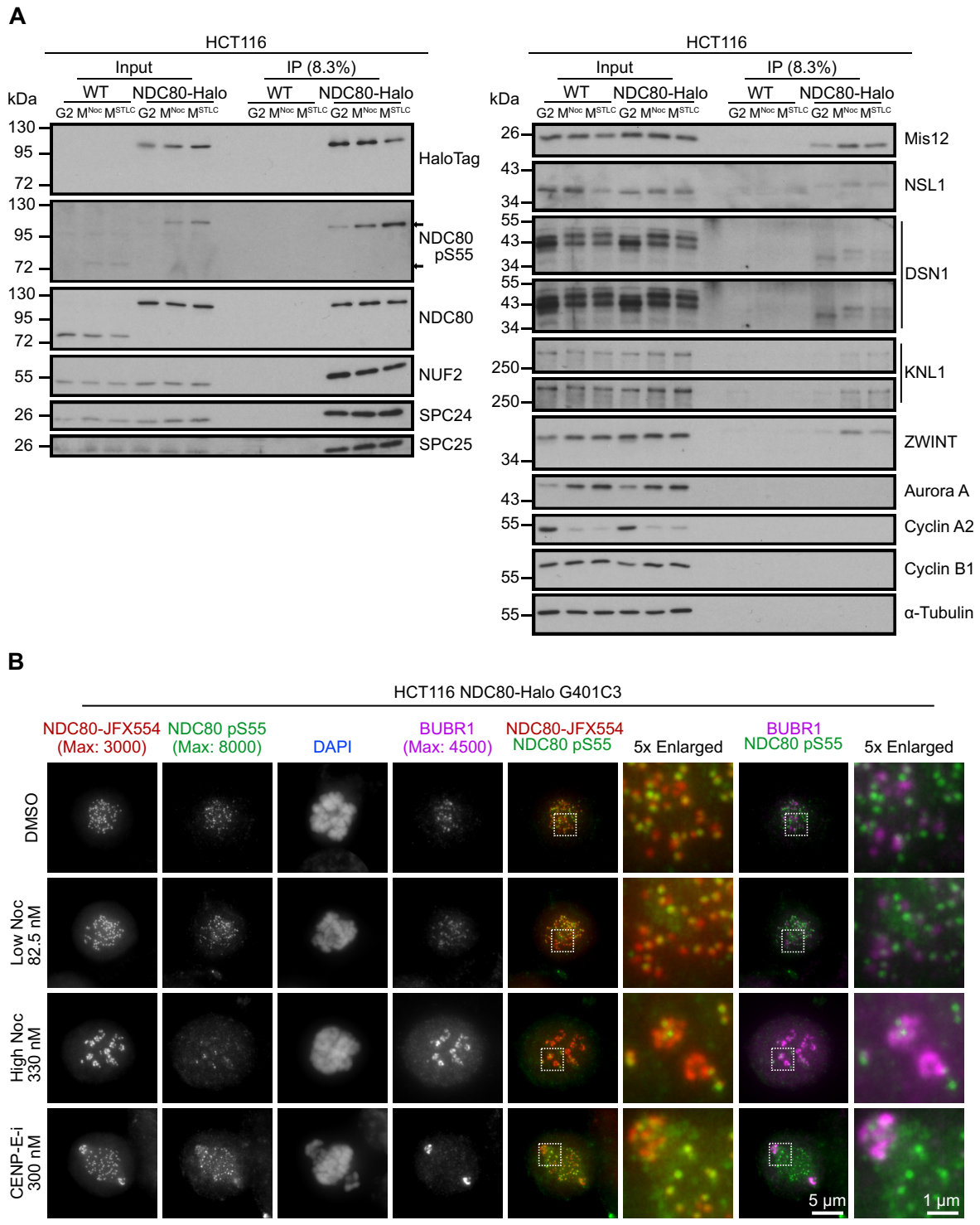

Figure 2. 3 - NDC80-HaloTag interacts with outer kinetochore proteins and localises to the outer kinetochore in mitosis

(A) HCT116 wild-type or NDC80-HaloTag cells were arrested for 18 hours in G2 using 6 µM CDK1 inhibitor RO-3306, or in two-different stages of mitosis using either 330 nM of the spindle poison nocodazole or 10 µM KIF11 inhibitor STLC. NDC80 was immunoprecipitated (IP) (Methods 4.4.3) using

HaloTag-nanobody agarose beads and run on a western blot to check interactions with known KMN network proteins (KNL1-C, MIS12-C, NDC80-C). Wild-type cells used as an IP control. (B) Determining NDC80-HaloTag response to spindle perturbations. Cells were arrested in mitosis using either low-dose nocodazole (82.5 nM) for minor spindle perturbations, high dose nocodazole (330 nM) for spindle collapse, or CENP-E-inhibitor (300 nM) to affect chromosome congression. Cells were treated with 100 nM JFX554 for 15 minutes before being fixed using ice-cold methanol for 5 minutes, and immunofluorescence stained with antibodies against NDC80-pS55 and BUBR1. Chromatin visualised by DAPI staining.

Under low doses of nocodazole which only partially block spindle formation, NDC80 pS55 was still present due to continued microtubule-kinetochore interactions (Figure 2.3 - B, Low Noc). Under those conditions, NDC80 pS55 and BUBR1 signals were largely mutually exclusive, supporting the conclusion that BUBR1 is recruited to kinetochores where microtubule interactions have been lost (Figure 2.3 - B, Low Noc). At a high dose of nocodazole almost all NDC80 pS55 was abolished whereas higher levels of BUBR1 were seen, consistent with the loss of kinetochore-microtubule attachments and full SAC activation (Figure 2.3 - B, High Noc). With inhibition of CENP-E, chromosome congression was impeded and some chromosomes remained unaligned at spindle poles (Guo et al., 2012; Yang et al., 2024). These chromosomes were BUBR1 positive and showed lower levels of NDC80 pS55 (Figure 2.3 - B, CENP-E-i), potentially suggesting that the chromosome is attached to the spindle via CENP-E rather than microtubule-binding to NDC80-C at the kinetochore. Taken together, these data indicate that NDC80-HaloTag can function as previously reported (Sobajima et al., 2023), both in the presence and absence of anti-mitotic drugs that perturb mitotic spindle assembly.

2.1.3. NDC80 re-localises from centrosomes to kinetochores in early mitosis

NDC80-HaloTag was used to study live-cell dynamics by labelling with the cell permeable dyes JFX549 and SiR-DNA to visualise both NDC80-HaloTag and chromosomes respectively. Using a spinning disk with a temperature-controlled chamber (Methods 4.6.4), living cells were imaged from G2 to metaphase (Figure 2.4). Interestingly, NDC80-HaloTag was found to localise to centrosomes in late G2 as they become separated, and then rapidly relocate to kinetochores at G2-M as the DNA condenses into individualised chromosomes, which then align into the metaphase plate (Figure 2.4).

To investigate this NDC80 complex re-localisation step further, higher-resolution imaging was performed using a high-resolution spinning disk microscope system to track NDC80-HaloTag JFX554 from G2 to prometaphase with higher spatial and temporal resolution (Figure 2.5 - A). NDC80-HaloTag initially associated with the centrosomes and forming spindle poles, before weak punctate signals in the nuclear region were observed. Approximately 10 minutes after the initial centrosome signal was observed, there was a rapid relocation of NDC80-HaloTag to the kinetochores with loss of the centrosomal signal. These dynamics are shown schematically in Figure 2.5 - B. Due to photodamage affecting cell viability it was not possible to follow cells for longer periods on this system. Therefore, the lower resolution spinning disk was used to follow NDC80-HaloTag during mitotic exit from anaphase to telophase. This revealed that ‘reverse translocation’ is seen from kinetochores back to the centrosomes which will be inherited by the new daughter cells (Figure 2.6).

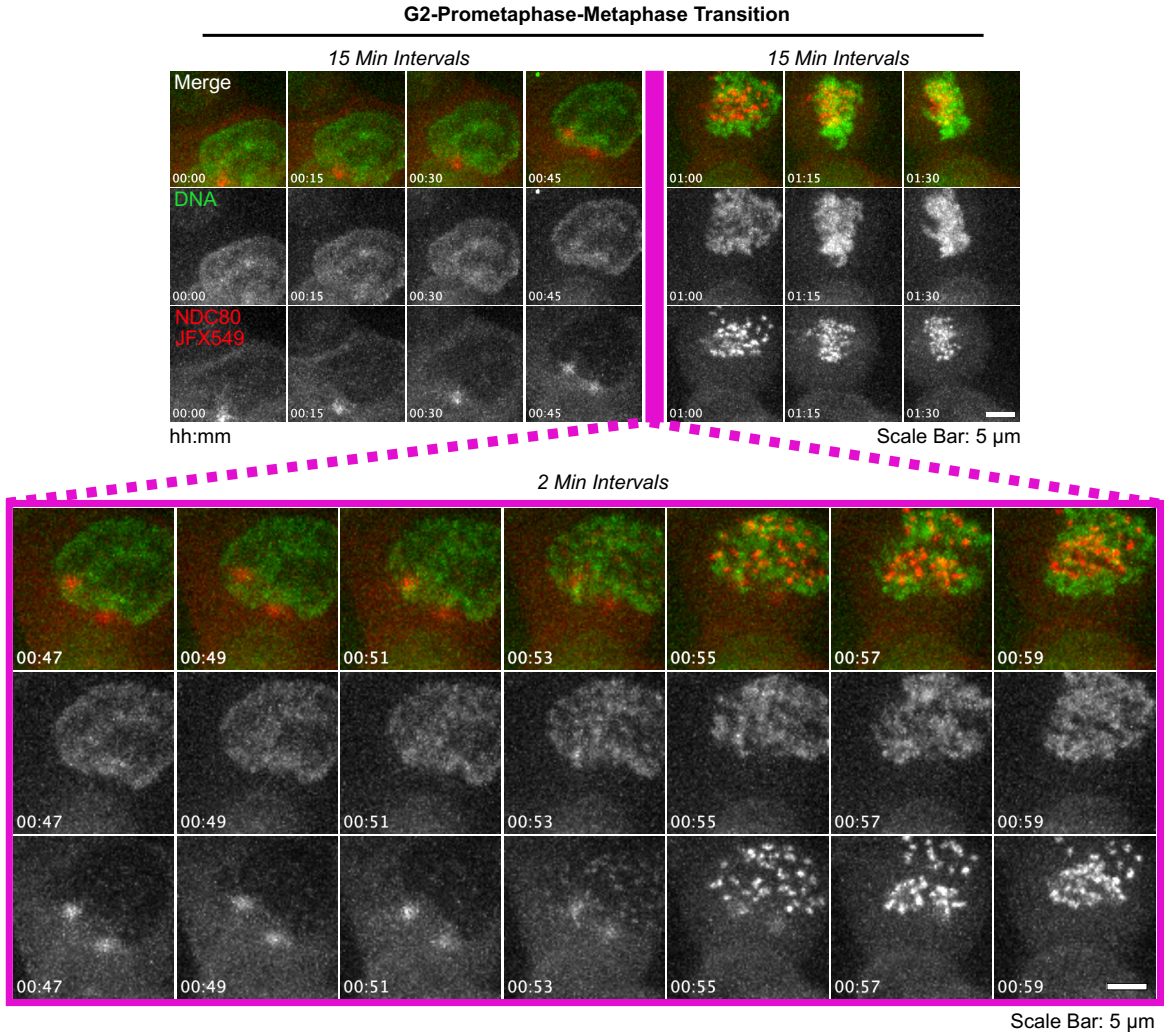

Figure 2. 4 - NDC80-HaloTag undergoes dynamic re-localisation from centrosomes in G2 to kinetochores in prometaphase and metaphase

Live-cell spinning disk imaging of HCT116 NDC80-HaloTag cells. JFX549 (NDC80) and SiR-DNA (DNA), showing NDC80 localisation relative to DNA from G2-Metaphase with 15-minute intervals shown between frames. 50 nM SiR-DNA was added for 3 hours and 100 nM JFX549 was added for 15 minutes and excess dye washed out in SiR-DNA containing media before imaging. The pink box shows shorter 2-minute intervals between adjacent frames, highlighting relocalisation from spindle pole to kinetochore.

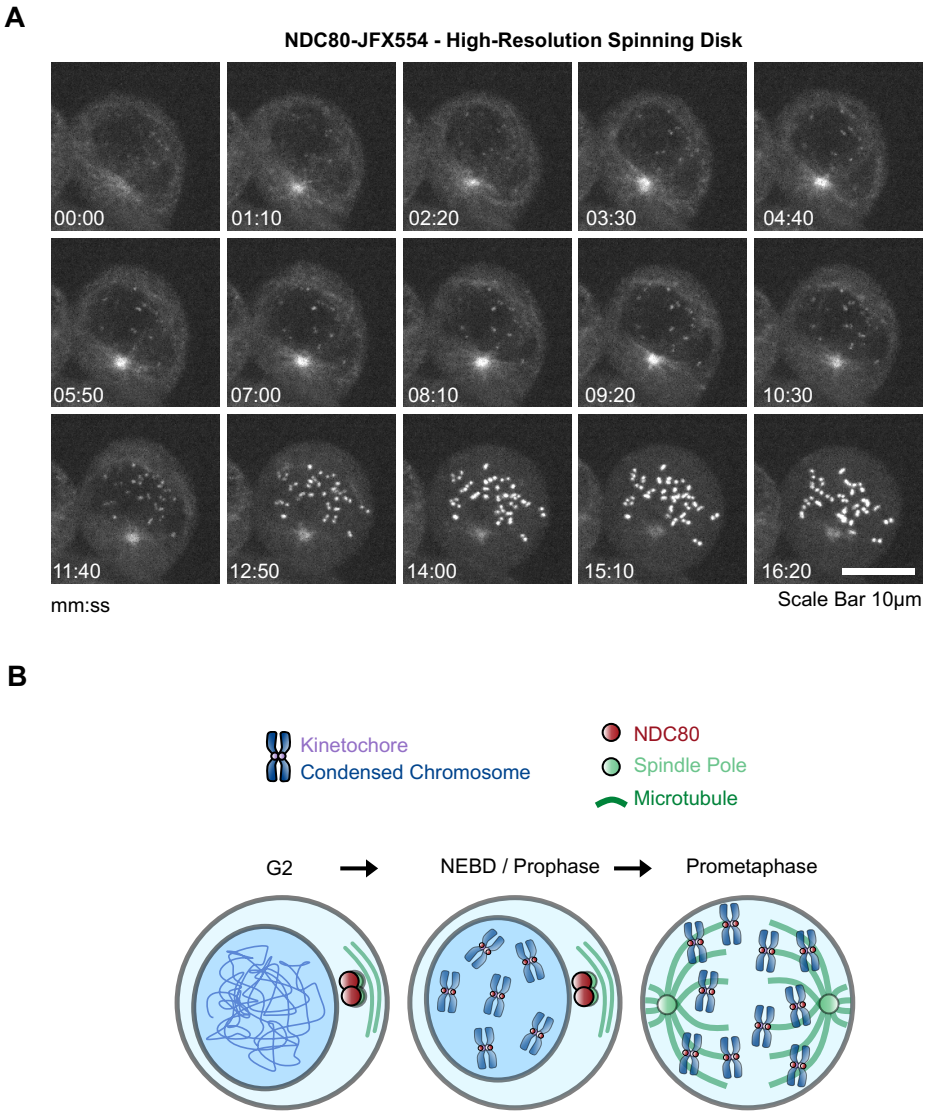

Figure 2. 5 - High temporal resolution imaging of NDC80-HaloTag localisation during the early stages of mitotic entry

(A) Live cell imaging of HCT116 NDC80-HaloTag cells using a high-resolution spinning disk with 1 minute 10 second intervals between frames, showing rapid re-localisation of NDC80-JFX554 from centrosomes in G2 to kinetochores as the cells enter mitosis. The experimental setup was the same as in Figure 2.4, except JFX554 was used to detect the HaloTag. (B) A basic schematic recapitulating the localisation dynamics of NDC80-JFX554 from G2 to prometaphase.

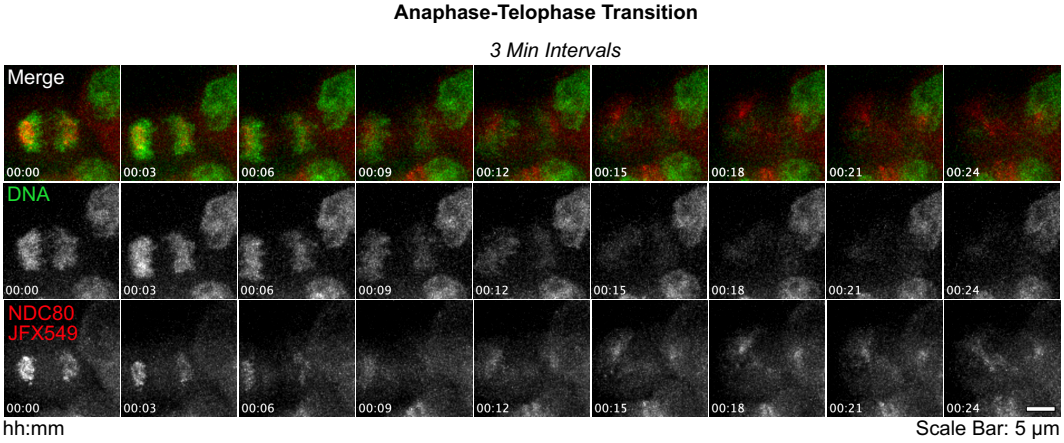

Figure 2.6 - Dynamic re-localisation of NDC80-HaloTag from kinetochores to spindle poles during mitotic exit

Live-cell spinning disk imaging of HCT116 NDC80-HaloTag cells. JFX549 (NDC80) and SiR-DNA (DNA), showing NDC80 localisation relative to DNA from anaphase-telophase, with 3-minute intervals shown between frames. Experimental set up is the same as in Figure 2.4.

In addition to its role in microtubule binding, the NDC80 complex has been proposed to play a crucial function in SAC activation at the outer kinetochore during mitosis by aiding MPS1 recruitment to the kinetochore (Lara-Gonzalez et al., 2021). The initial recruitment of NDC80-C to centrosomes prior to the outer kinetochore raised questions about the timing of SAC activation relative to outer kinetochore assembly. To address this question, immunofluorescence microscopy for the SAC protein BUBR1 and NDC80-HaloTag-JFX549 was performed, capturing cells progressing from G2 to Metaphase (Figure 2.7). As expected from live-cell observations, NDC80-C was localised to centrosomes in G2, and no BUBR1 recruitment was seen (Figure 2.7 - G2). As NDC80-C began to relocate prior to NEBD, BUBR1 recruitment was not initially observed (Figure 2.7 - G2 pre-NEBD). However, once full re-localisation of NDC80-C had occurred, BUBR1 became strongly recruited to kinetochores (Figure 2.7 - Prophase). The BUBR1 signal remained high at kinetochores during prometaphase, and reduced once chromosomes were aligned in metaphase, consistent with previous reports (Taylor et al., 2001).

Similar staining was performed for other core SAC proteins BUB3 and BUB1 including comparison to BUBR1 (Figure 2.8), and for CDC20, MAD1 and MAD2 (Figure 2.9). With the exception of CDC20, the timing of recruitment was similar to that of BUBR1, whereby checkpoint protein recruitment was prominently seen in prophase post-NEBD at unattached kinetochores, and minimally during metaphase when chromosomes were aligned, consistent with previous findings (Howell et al., 2000; Logarinho et al., 2008; Vleugel, Hoek, et al., 2015). For CDC20, kinetochore-like staining was already observed prior to NDC80-C localisation to the kinetochore, (Kallio et al., 2002). For none of the SAC proteins was centrosomal signal seen during G2, suggesting that this is a unique property of NDC80-C. Thus, NDC80-C localisation to the kinetochore appears concomitant with SAC activation and is timed to align with entry into mitosis and chromosome condensation.

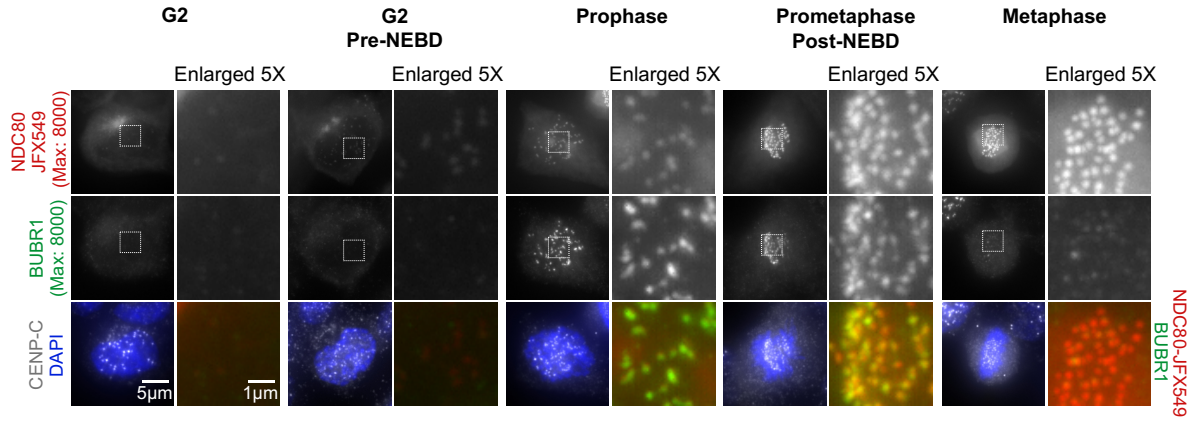

Figure 2. 7 - Spindle assembly checkpoint activation occurs after NDC80-HaloTag localisation to kinetochores during mitotic entry

Asynchronous HCT116 NDC80-HaloTag cells were incubated with 100 nM JFX549 before being PTEMF fixed for 12 minutes. Cells were then immunofluorescence stained with antibodies for the checkpoint protein BUBR1, and centromere protein CENP-C. Chromatin was visualised with DAPI. Representative cells for early G2, late G2 (pre-NEBD), prophase, prometaphase and metaphase are shown.

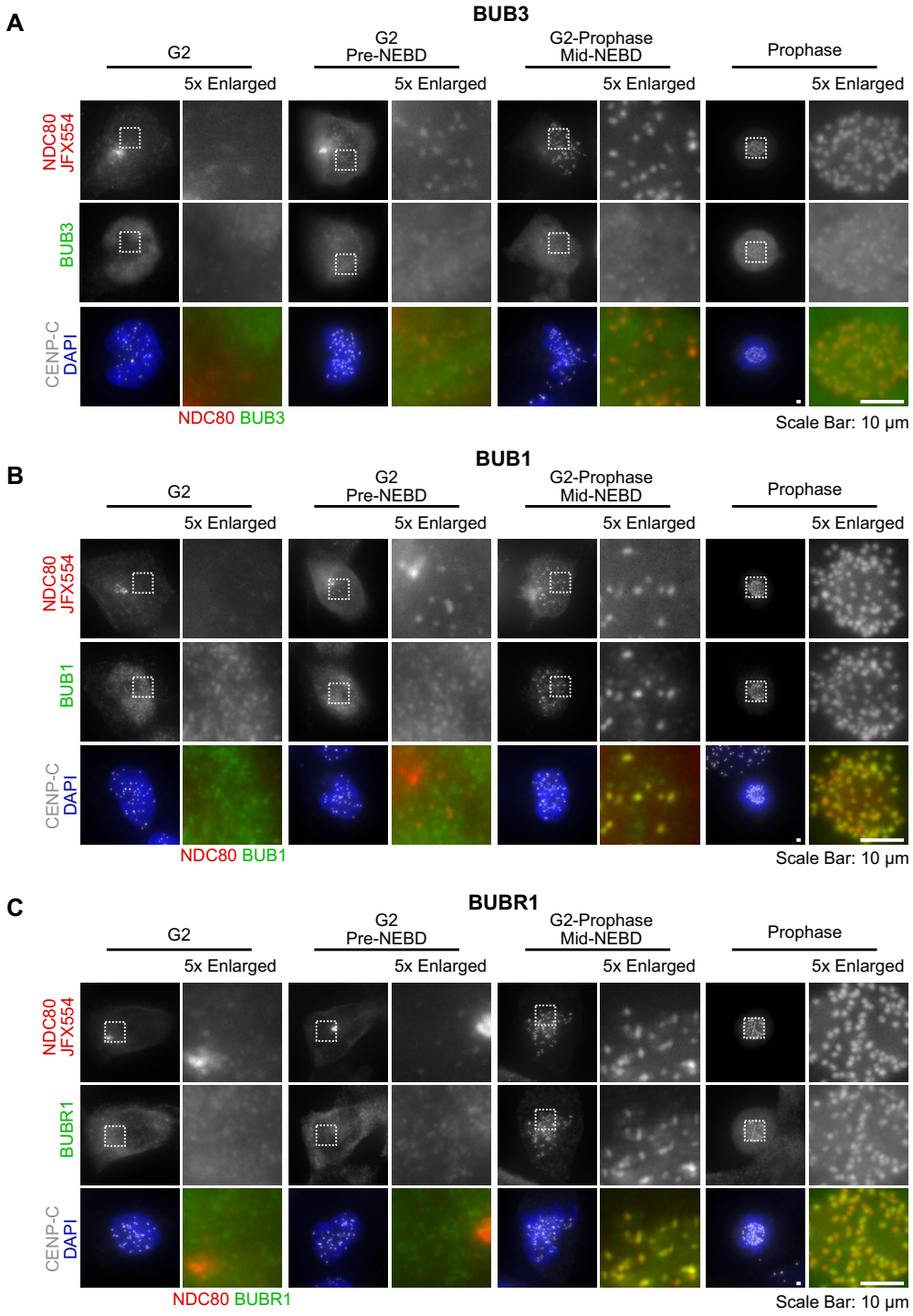

Figure 2. 8 - Localisation of the SAC proteins BUB3, BUB1 and BUBR1 during mitotic entry

HCT116 NDC80-HaloTag cells were arrested in G2 using 6 µM CDK1 inhibitor RO-3306 for 18 hours. Cells were then released from G2 by washout of the CDK1 inhibitor and incubated with 100 nM JFX554 for 15 minutes to detect NDC80-HaloTag. Cells were then HTEMF fixed after 0, 15 or 30 minutes. Cells were then stained with antibodies for CENP-C and either (A) BUB3, (B) BUB1, or (C)BUBR1. Chromatin was visualised using DAPI. Representative cells are shown from G2-Prophase to illustrate early kinetochore localisation of these checkpoint markers.

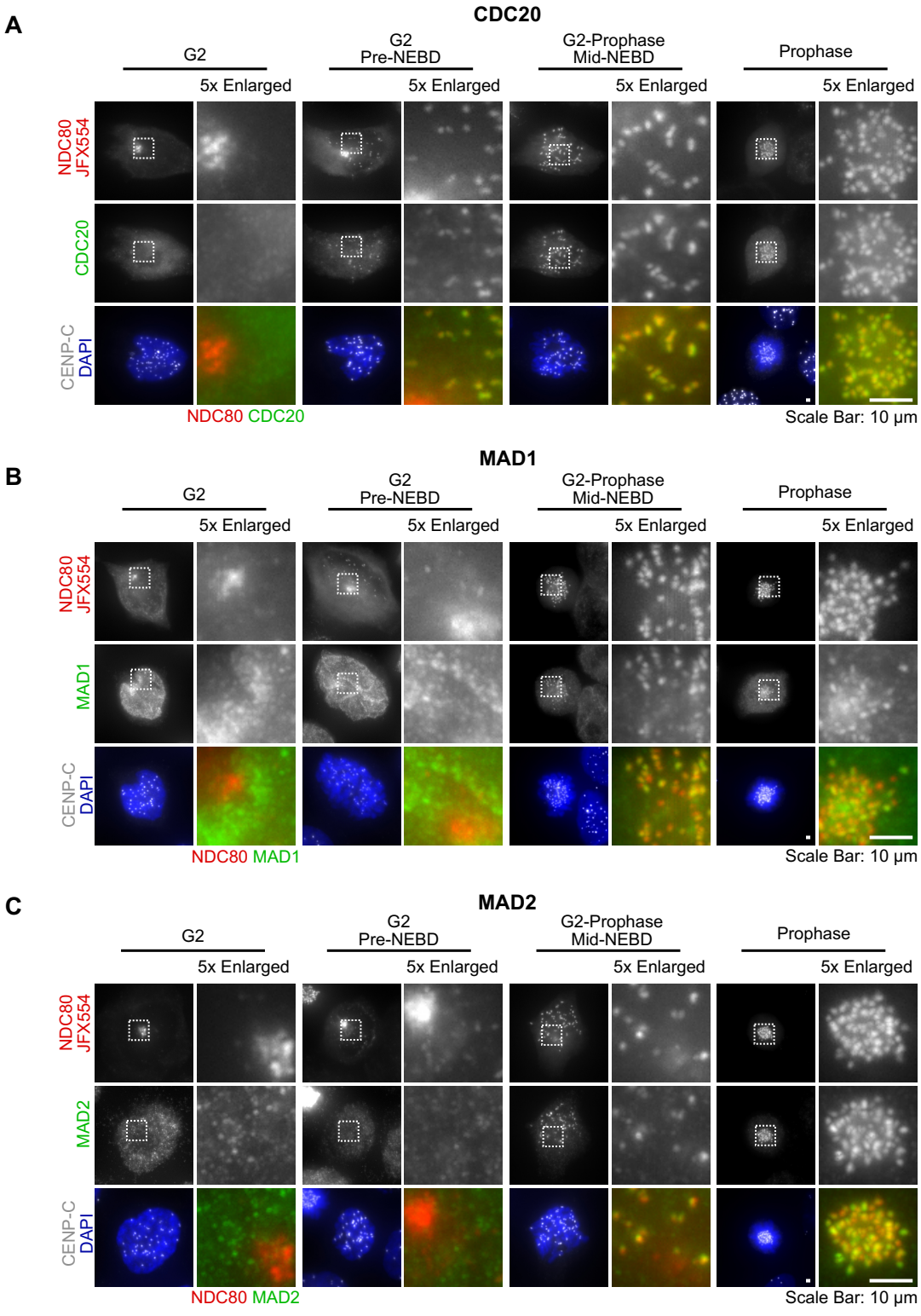

Figure 2. 9 - Localisation of the SAC proteins CDC20, MAD1 and MAD2 during mitotic entry

As in Figure 2.8, except cells were immunofluorescence stained with antibodies for (A) CDC20, (B) MAD1, or (C) MAD2.

2.1.4. Using Halo-PROTAC to investigate the rapid degradation of NDC80 in different ploidy backgrounds

After establishing that NDC80-HaloTag localises correctly and supports chromosome alignment and SAC signalling, the HaloTag was exploited to trigger targeted proteolysis of NDC80 and study its function in these processes. The HaloTag can be bound with a PROTAC, a bifunctional molecule which can bind to both the HaloTag and an E3 ubiquitin ligase. This brings the HaloTag and protein of interest (POI) into proximity to a VHL E3 ligase, causing them to become ubiquitinated and targeted for proteolytic degradation (Methods 4.5.2; Figure 2.10 - A). Adding Halo-PROTAC to the HCT116 NDC80-HaloTag cells over a time course of 0-4 hours resulted in a gradual decay in signal as seen via immunoblots, with near-complete degradation of NDC80 and of Nuf2, with which NDC80 heterodimerises, after 4 hours (Figure 2.10 - B-C, Figure 2.11 - A).

To test whether Halo-PROTAC-mediated degradation of NDC80 occurs via the expected proteolytic pathways, two confirmatory experiments were performed. Once Halo-PROTAC is bound to VHL, Nedd8 is required to cause a conformational change in Cullin 2, part of the Cullin-Ring E3 ligase, enhancing the POI's affinity for ubiquitination (Wong et al., 2016). Inhibition of Nedd8 with pevonedistat prevented neddylation of Cullin 2 and resulted in stabilisation of NDC80 and HaloTag despite the addition of Halo-PROTAC, as seen by immunoblot (Figure 2.11 - B). Similarly, direct inhibition of the proteasome with MG132 blocked any protein degradation (Figure 2.11 - C); even with Halo-PROTAC addition, no degradation of NDC80 or HaloTag was seen across all time points.

In both NDC80-HaloTag diploid (Figure 2.1 - Clone 3) or tetraploid cells (Figure 2.1 - Clone 15), the degradation kinetics of NDC80 and Nuf2 were similar (Figure 2.12 - A-B). The effect of NDC80 degradation on cell proliferation in both ploidy backgrounds was then tested over a period of 1-3 days ± the addition of Halo-PROTAC (Methods 4.4.5). In both instances, cell growth was found to be attenuated to a similar extent in the presence of the Halo-PROTAC

(Figure 2.12 - C). Thus, NDC80 is important for cell proliferation irrespective of ploidy, despite the difference in chromosome numbers and doubling in kinetochores in tetraploid cells.

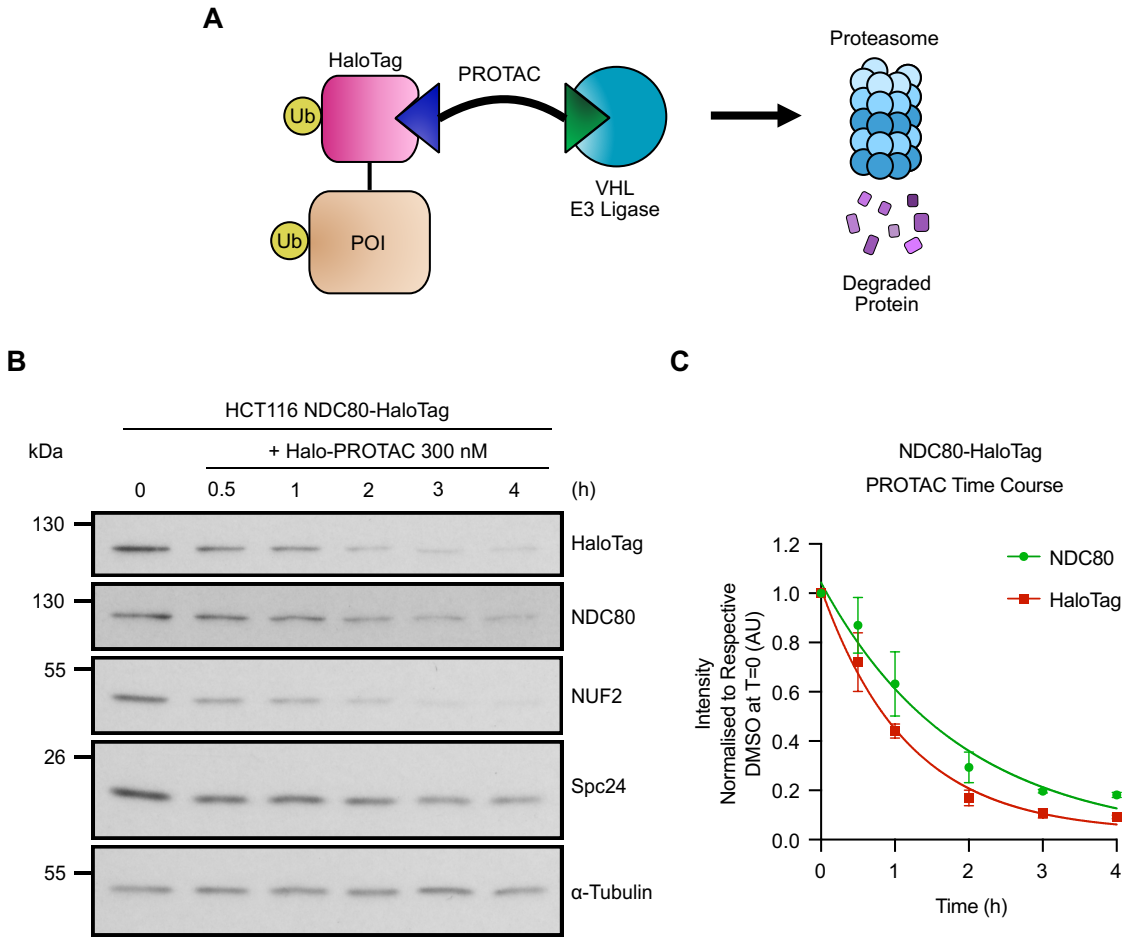

Figure 2. 10 - A Halo-PROTAC triggers NDC80 degradation in NDC80-HaloTag HCT116 cells

(A) A basic schematic explaining how Halo-PROTAC-mediated degradation works via proteasomal degradation. (B) 300 nM Halo-PROTAC was added to asynchronous HCT116 NDC80-HaloTag cells for 0, 0.5, 1, 2, 3, or 4 hours. Mitotic lysis buffer was used to lyse cells, and a Bradford assay performed to normalise whole-protein concentrations to each other. Cells lysates were then run on a western blot to determine levels of the NDC80-complex proteins NDC80, NUF2 and Spc24, as well as HaloTag levels, under PROTAC addition. α-Tubulin used as a loading control. (C) Densitometry quantification of background-subtracted immunoblot bands for HaloTag and NDC80 over time (n=3, mean ± SD). Intensity values for each data set were normalised to T=0 (DMSO). One phase decay curves were fitted to each data set.

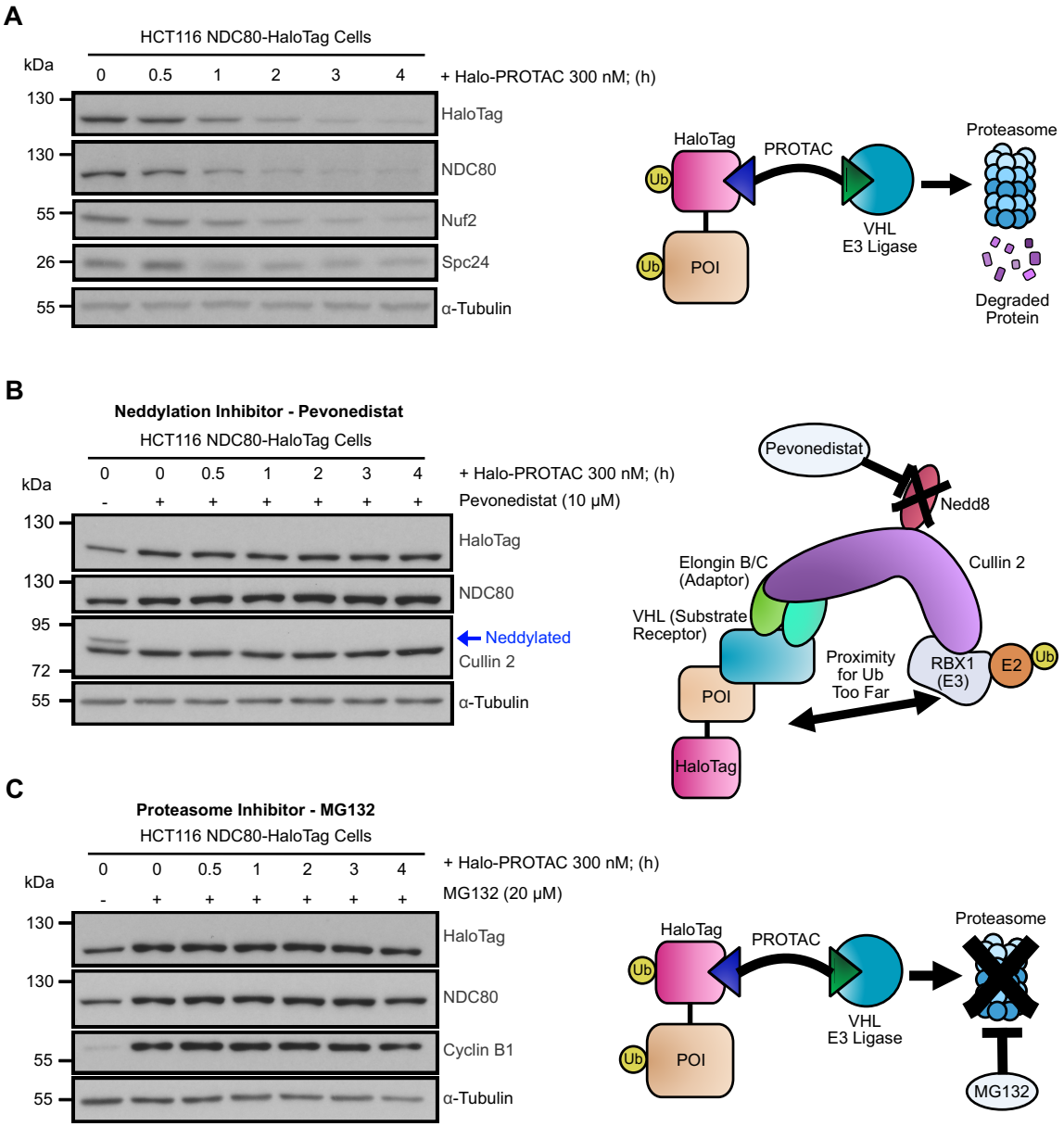

Figure 2. 11 - The Halo-PROTAC acts via a Cullin-Ring ligase and proteasomal degradation pathway

For all blots, 300 nM Halo-PROTAC was added to asynchronous NDC80-HaloTag cells for 0, 0.5, 1, 2, 3, or 4 hours. Cells were also treated as follows: (A) No further treatment. A schematic of Halo-PROTAC-mediated degradation is shown right of the blot. (B-C) In addition to Halo-PROTAC, either (B) 10 μM of the Nedd8 inhibitor Pevondistat or (C) 20 μM the proteasome inhibitor MG132, was added to the six time-course samples for 4 hours, before Halo-PROTAC addition. The left-most sample in each blot had no drugs added, acting as a control. A schematic of (B) Pevondistat's effect on E3-ligase ubiquitination or (C) MG132's effect on the proteasome is shown to the right of their respective blots. Mitotic lysis buffer was used to lyse cells, and a Bradford assay performed to normalise whole-protein

concentrations to each other within each experiment. Lysates were then run on a western blot, with immunoblotting against HaloTag and NDC80 shown on all blots, as well as (A) NUF2, Spc24, (B) Cullin 2 and (C) Cyclin B1 to determine the effects of Halo-PROTAC and relative drug additions. α-Tubulin as a loading control.

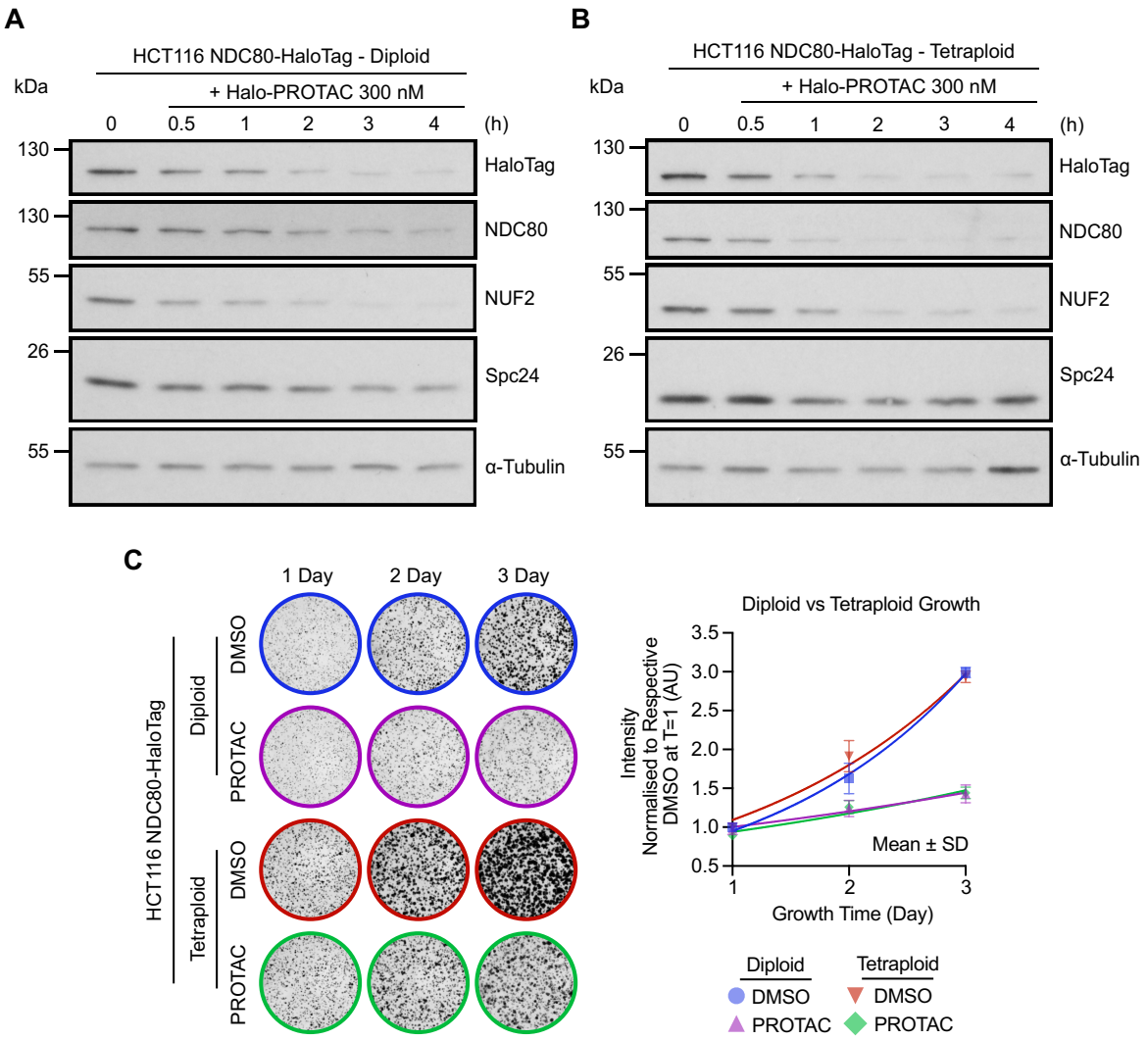

Figure 2. 12 - NDC80 degradation using the Halo-PROTAC affects cell proliferation irrespective of ploidy

(A-B) 300 nM Halo-PROTAC was added to NDC80-HaloTag (A) diploid or (B) tetraploid cells for 0, 0.5, 1, 2, 3, or 4 hours. Mitotic lysis buffer was used to lyse cells, and a Bradford assay performed to normalise whole-protein concentrations to each other within each experiment. Lysates were run on a western blot, immunoblotting for the NDC80 complex proteins NDC80, Nuf2 and Spc24 to determine protein levels under PROTAC addition. The blot in (A) is the same as in Figure 2.10 - A, shown again

for comparison. (C) For both diploid and tetraploid HCT116 NDC80-HaloTag clones, cells were seeded at a low density and grown for 1-3 days ± 300 nM Halo-PROTAC, then fixed and stained for 30 minutes using crystal violet. Cell growth was quantified using densitometry, background subtracted and then normalised to each cell line's respective 1-day DMSO condition (n=3, Mean ± SD). Exponential growth curves were fitted to each data set.

2.1.5. Rapid loss of NDC80 after Halo-PROTAC treatment results in defective chromosome alignment

Having established that NDC80 protein levels were strongly reduced during three hours of Halo-PROTAC treatment (Figure 2.10 - B, Figure 2.11 - A, Figure 2.12 - A), the effect of this treatment on HCT116 NDC80-HaloTag cells actively underdoing mitosis was examined. Cells were first transiently arrested in mitosis using a low-dose of nocodazole and treated with Halo-PROTAC. Nocodazole was then washed out to allow chromosome alignment and spindle formation to complete. Immediately after nocodazole washout, cells were treated with the proteasome inhibitor MG132 for 0-40 minutes to prevent anaphase onset and allow for the accumulation of metaphase cells. This approach enabled scrutiny of the immediate consequences of reduced NDC80 on actively dividing cells, and their ability to form an aligned metaphase plate (Figure 2.13 - A). Over the time measured, both cells from the control and Halo-PROTAC treated groups were able to move from prometaphase to a metaphase-like state (Figure 2.13 - B-C). However, the proportion of cells able to form aligned metaphase plates was lower in Halo-PROTAC treated cells across all time points (Figure 2.13 - B-C), suggesting the process of chromosome alignment was slower or less effective.

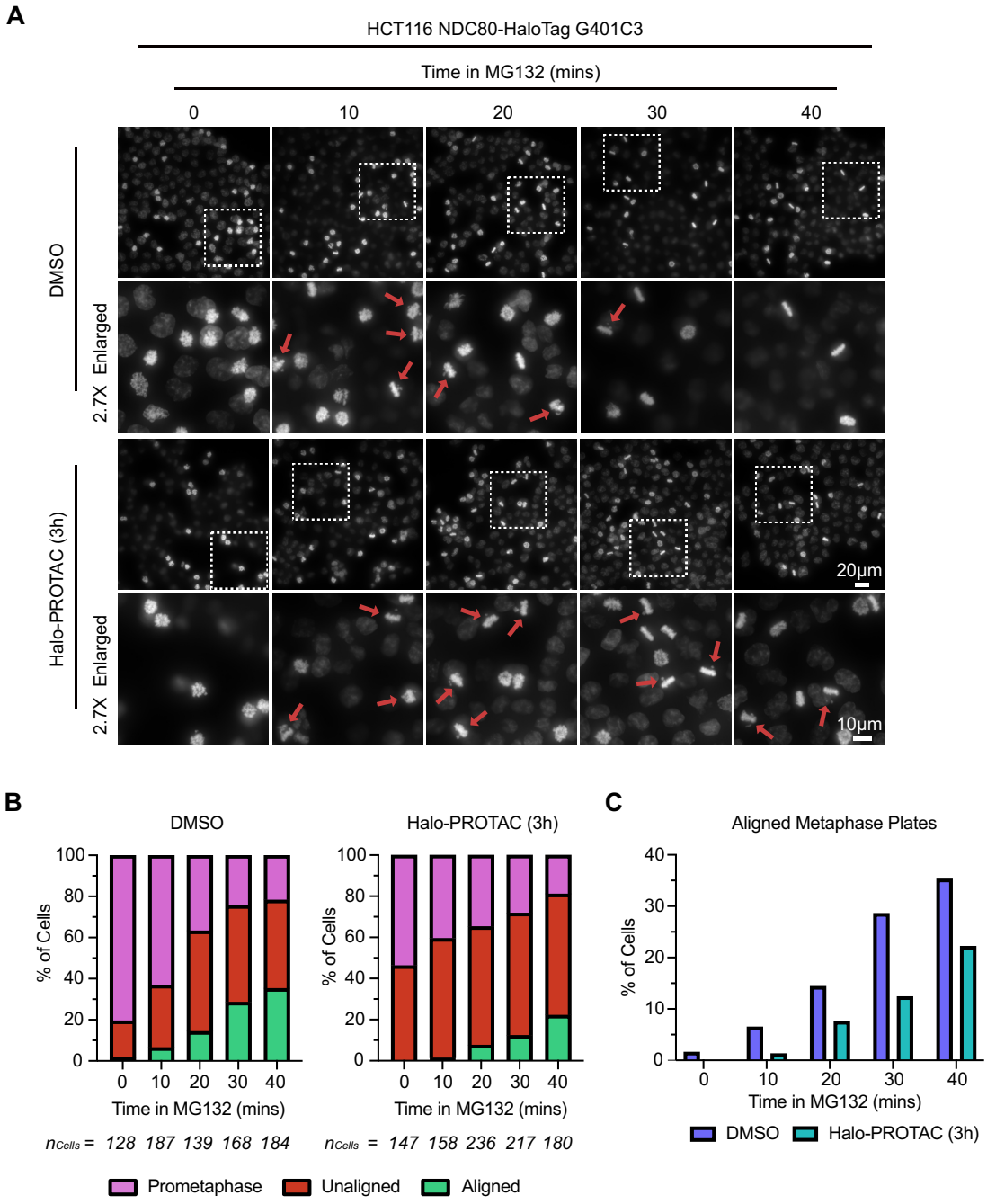

Figure 2. 13 - HCT116 cells show compromised ability to form an aligned metaphase plate after NDC80 degradation.

(A) HCT116 NDC80-HaloTag cells were arrested using low dose nocodazole (82.5 nM) for 2 hours, then treated with either DMSO or 300 nM Halo-PROTAC for a further 3 hours. Cells were then washed out of nocodazole arrest and released into 20 μM MG132. Cells were then PTEMF fixed every 10 minutes for 0-40 minutes; PTEMF fixation at each time point was performed for 12 minutes. Chromatin was then visualised by DAPI staining. Red arrows point to examples of unaligned metaphase plates.

(B) Quantification of prometaphase and aligned/unaligned metaphase cells were performed and plotted as a proportion of the total of number of cells measured per condition. The cell sample number is shown on the figure. (C) A grouped column graph shows the direct comparison of the number of aligned metaphase plates between DMSO/PROTAC treated cells at each timepoint.

2.1.6. Removal of NDC80 results in extended mitotic duration

To assess the biochemical changes in mitosis in NDC80 depleted cells and whether mitotic duration was extended, HCT116 NDC80-HaloTag cells were first arrested in G2 for 18 hours using a CDK1 inhibitor (RO-3306) to prevent mitotic entry whilst simultaneously depleting NDC80 by Halo-PROTAC addition. Cells were then released into mitosis as a synchronous wave by washout of the CDK1 inhibitor, with samples taken for western blot from 0-8 hours. Immunoblots of these samples confirmed NDC80 depletion in the Halo-PROTAC treated cells and extended mitotic duration due to the increased stability of key mitotic proteins such as Cyclin B1 and Geminin, and a marker for CDK1-cyclin B activity PRC1 pT481 (Holder et al., 2020) (Figure 2.14). p21 phosphorylation, as inferred by the upper-p21 band, was also used as an indirect readout of mitosis (Kreis et al., 2016).

Live cell spinning disk microscopy then enabled tracking of individual cells and provided a more dynamic view of chromosomal movement from mitotic entry to exit, and direct measurement of mitotic timings. Dual labelling of both NDC80-HaloTag with JFX554 and DNA with SiR-DNA allowed for simultaneous visualisation of both kinetochores and chromosomes. This revealed two different outcomes in HCT116 cells: either anaphase onset (Figure 2.15 - A), where cells successfully move into anaphase and divide into two daughter cells, or mitotic slippage (Figure 2.15 - B) in which cells exit mitosis without chromosome segregation and cytokinesis into a 4n G1-like state (Lok et al., 2020; Sinha et al., 2019).

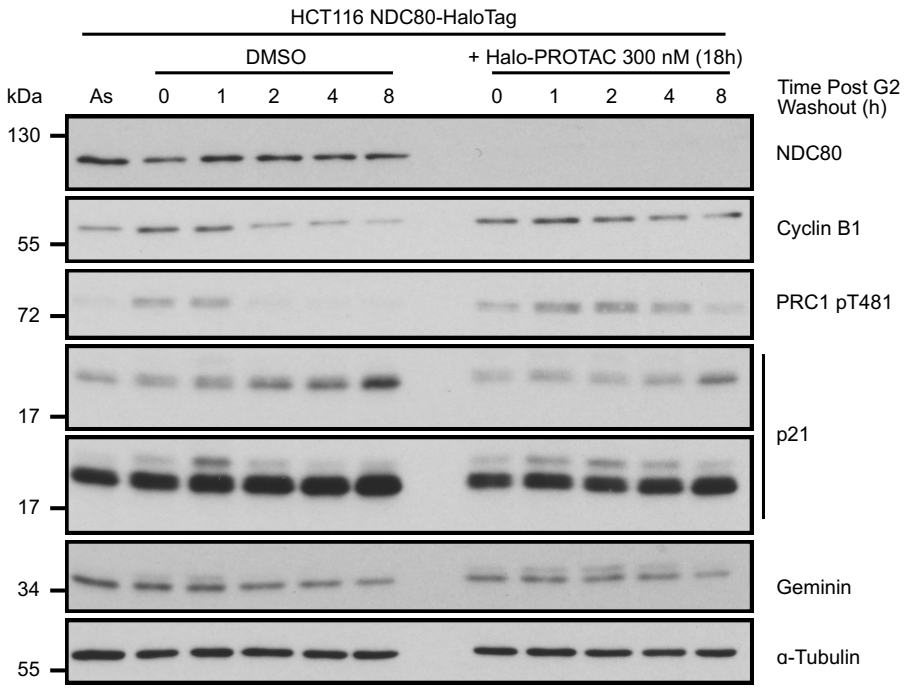

Figure 2. 14 - Biochemical analysis indicates mitosis is extended after NDC80 degradation

HCT116 NDC80-HaloTag cells were arrested in G2 using 6 μM CDK1 inhibitor RO-3306 and treated with either DMSO or 300 nM Halo-PROTAC for 18 hours. Cells were then washed out of CDK1 inhibition for either 0, 1, 2, 4 or 8 hours. Whole-cell lysates were then run on a western blot, immunoblotting for cell cycle markers Cyclin B1, PRC1 pT481 and Geminin to determine which stage they were in. α-Tubulin used as a loading control. An asynchronous (non-arrested/drug treated) sample was loaded on the left-most lane as a control.

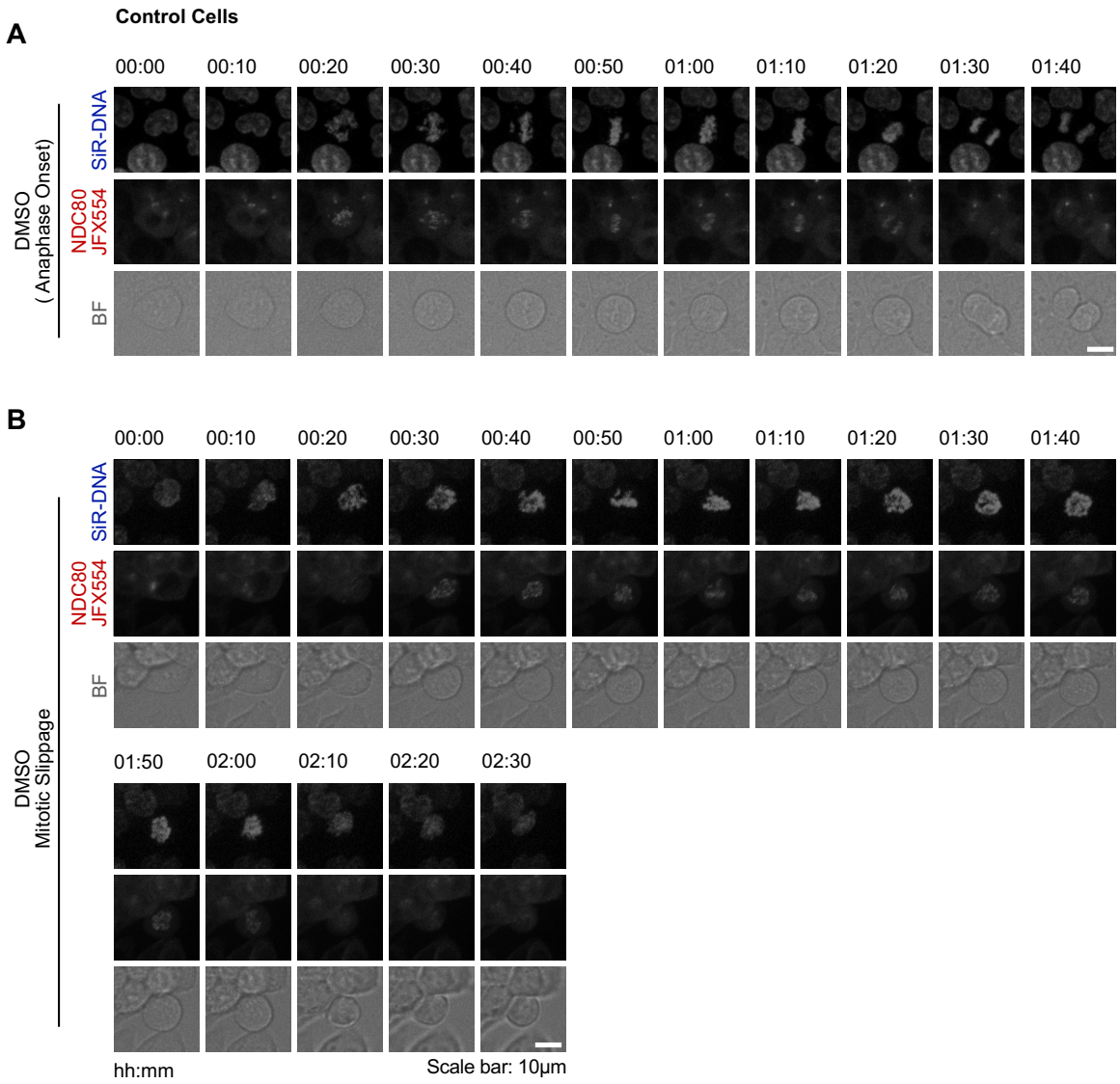

Figure 2. 15 - Live-cell imaging of NDC80-HaloTag cells under control conditions.

HCT116 NDC80-HaloTag cells were labelled with 50 nM SiR-DNA (DNA) for 3 hours, and 100 nM JFX554 (NDC80) for 15 minutes. Excess JFX554 was washed out in SiR-DNA containing media before imaging. Cells were imaged every 10 minutes in far-red, red, and bright-field channels on a spinning disk. Example cells are shown that either (A) undergo anaphase onset and successful division, or (B) undergo mitotic slippage, 'crashing' out of mitosis without division.

Cells treated with Halo-PROTAC for at least three hours to degrade NDC80 were then tracked and imaged as they passed through mitosis (Figure 2.16).

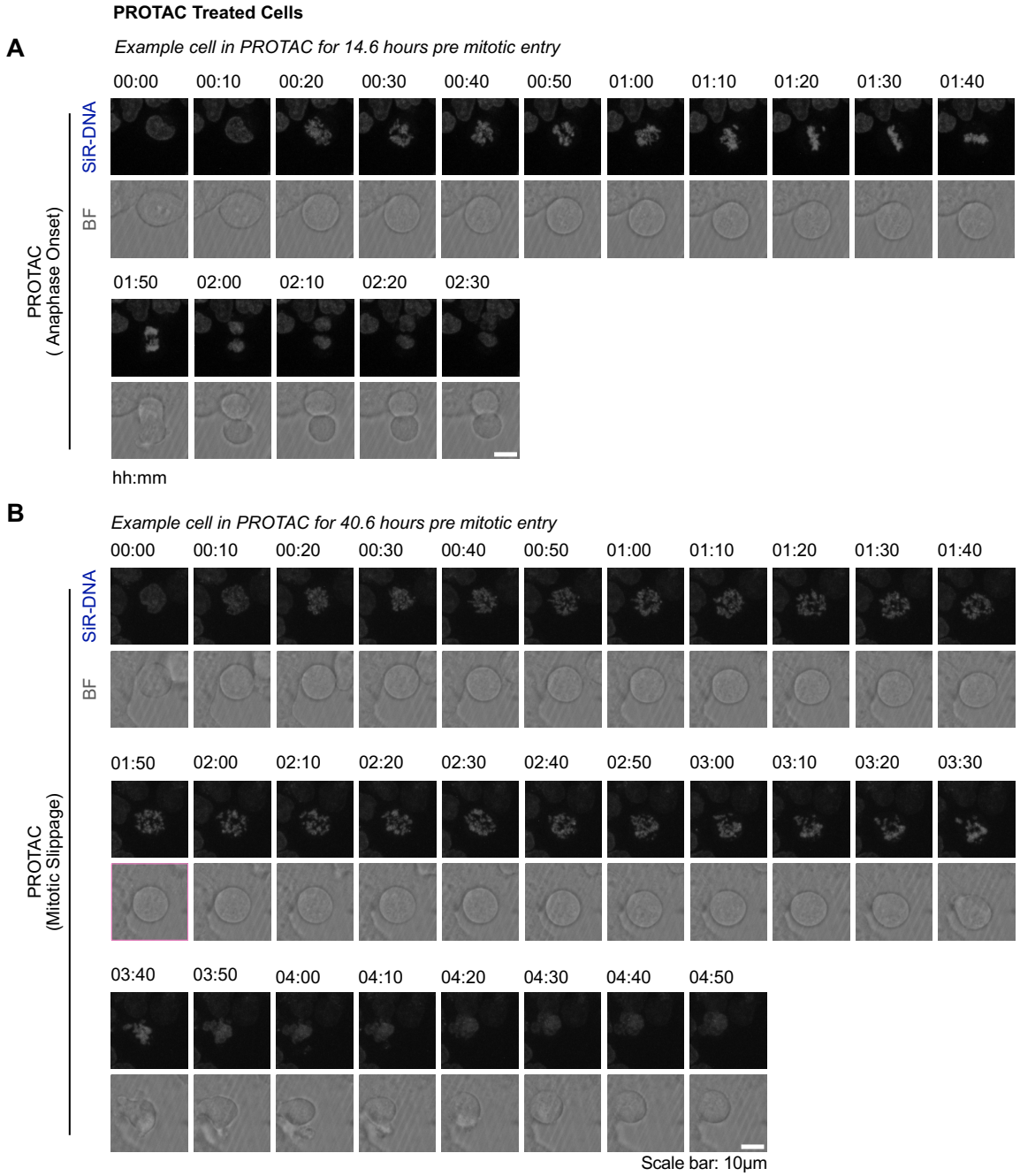

Figure 2. 16 - Live-cell imaging of NDC80-HaloTag cells following Halo-PROTAC addition.

As in Figure 2.15, except cells were labelled with 50 nM SiR-DNA (DNA) only, and treated with 300 nM Halo-PROTAC for 3 hours prior to imaging.

Cells treated with Halo-PROTAC to degrade NDC80 were seen to undergo the mitotic slippage phenotype more often than those treated with DMSO as a control, with approximately 80% of Halo-PROTAC treated cells and 8% of control cells experiencing this cell fate respectively (Figure 2.17 - B). The cells undergoing mitotic slippage after Halo-PROTAC treatment spent ~4 hours in mitosis, compared to ~1 hour for control cells (Figure 2.17 - A). Analysis of mitotic progression showed that there is a positive correlation between the loss of NDC80 caused by PROTAC treatment and extended mitotic timing with mitotic slippage (Figure 2.17 - C). Only cells with short exposure to the PROTAC entered anaphase (Figure 2.17 - C), suggesting that they still retained some NDC80 protein.

To investigate whether these effects on mitosis were exacerbated with increased ploidy, the effect of NDC80 degradation was compared in diploid and tetraploid HCT116 NDC80-HaloTag cells. A similar extended mitotic duration phenotype was observed for both cell lines, with tetraploid cells spending longer in mitosis in the absence of NDC80 than diploid cells (Figure 2.18 - A). For both cell lines, increased time spent in Halo-PROTAC resulted in a higher probability of mitotic slippage (Figure 2.18 - B).

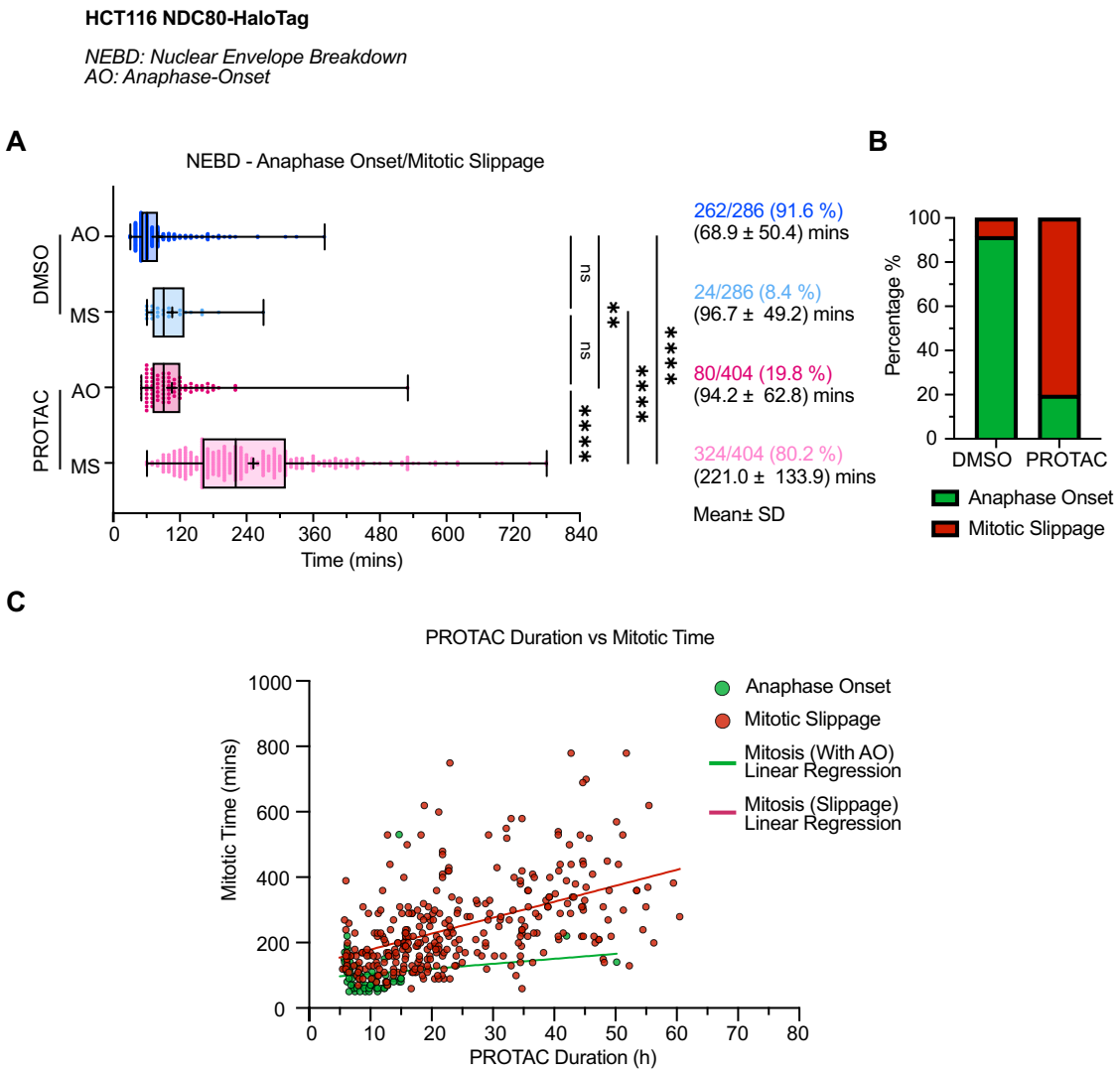

Figure 2. 17 - Mitotic timing and frequency of mitotic slippage both increase in the absence of NDC80

(A) Quantification of the time cells spent in mitosis was measured from Nuclear Envelope Breakdown (NEBD) to either Anaphase Onset (AO) or Mitotic Slippage (MS) for cells treated with either DMSO or Halo-PROTAC in Figure 2.15 and Figure 2.16. Min-max box & whisker plots are shown, with 3 lines representing the 25/50/75 percentile respectively; + symbol indicates the mean. The number of cells tracked and the Mean ± SD of mitotic timing are shown next to each condition. Brown-Forsythe and Welch ANOVA tests were performed for statistical analysis, where P<0.0001 (****) and P=0.0054 (**). For DMSO AO vs DMSO MS (P=0.1051, ns) and DMSO MS vs PROTAC AO (P>0.9999, ns). (B) The proportion of cells undergoing either AO or MS is shown for each condition. (C) For Halo-PROTAC treated cells only; the amount of time each cell spent in mitosis vs the time that cell spent in PROTAC prior to NEBD is shown, with linear regressions fitted.

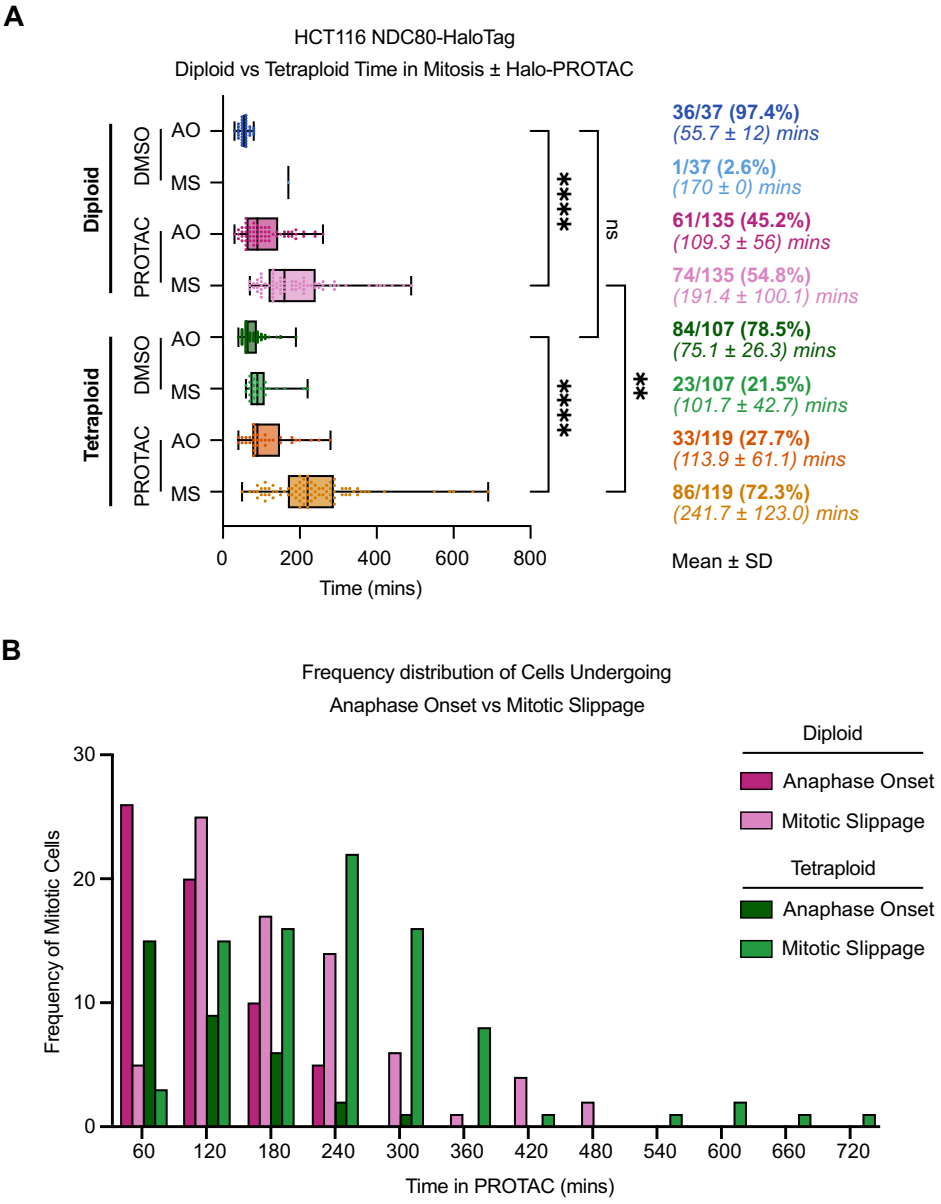

Figure 2. 18 - Mitotic timing increases in the absence of NDC80 regardless of ploidy

(A) Quantifications for the time spent in mitosis for both diploid and tetraploid HCT116 NDC80-HaloTag cells ± Halo-PROTAC addition. Quantifications and data representation are the same as in Figure 2.17. An ordinary one-way ANOVA was used for statistical analysis, with P<0.0001 (****), P=0.0019 (**), and P=0.9190 (ns). (B) For Halo-PROTAC treated cells only, a frequency distribution is shown for cells undergoing AO/MS for increasing times spent in Halo-PROTAC.

2.1.7. The spindle assembly checkpoint is active in the absence of NDC80

The extended mitotic duration observed after Halo-PROTAC mediated degradation of NDC80 suggests that the SAC is still active in these cells. This was surprising given the established role of NDC80 in regulation MPS1-kinetochore localisation and subsequent activation of the SAC (Lara-Gonzalez et al., 2021) , leading to the question as to whether the mitotic delay was in fact SAC-dependent. To understand the relationship between checkpoint signalling and NDC80, a Halo-PROTAC time course was carried out up to 3 hours of treatment, with immunofluorescence staining for two checkpoint proteins BUBR1 (Figure 2.19 - A-B) and MAD1 (Figure 2.20 - A-B). This approach revealed that although NDC80 levels had dropped significantly after 1-hour of Halo-PROTAC treatment, the cells had maintained checkpoint activity at all time points (Figure 2.19 - B and Figure 2.20 - B). An initial increase in checkpoint activity was noted after the immediate loss of NDC80 at the 1-hour Halo-PROTAC addition timepoint for both BUBR1 and MAD1, but in both instances, this returned to the levels observed in control cells after the 2-hour timepoint (Figure 2.19 - C, Figure 2.20 - C).

These results suggest that, although NDC80 is required for chromosome alignment and normal anaphase chromosome segregation, it is not essential for sustained downstream SAC activation or recruitment of spindle checkpoint proteins to the kinetochore. This interpretation is further supported by the live cell imaging data showing that degradation of NDC80 results in mitotic delays up to 4-hours before mitotic slippage occurs, implying the SAC is active in those cells. An alternative possibility is that only low levels of NDC80 are required for regulation of SAC signalling compared to higher levels needed for mechanical coupling to spindle microtubules.

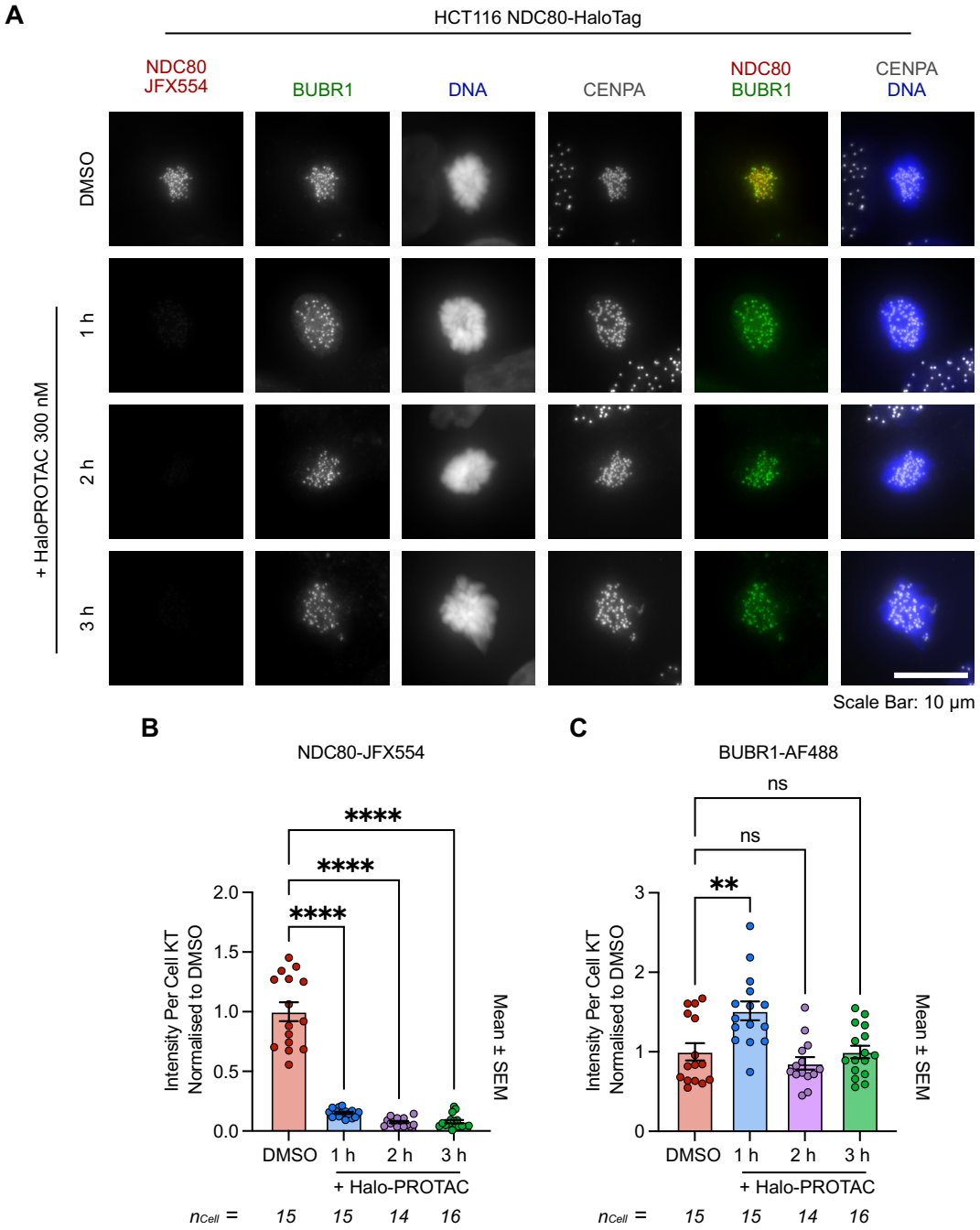

Figure 2. 19 - The SAC protein BUBR1 is present at kinetochores after degradation of NDC80

(A) HCT116 NDC80-HaloTag cells were treated with either DMSO for 3 hours, or 300 nM Halo-PROTAC for 1-3 hours, incubated with 100 nM JFX554 dye for 15 minutes, AND fixed with HTEMF for 12 minutes. Cells were then stained with antibodies for the SAC protein BUBR1 and centromere protein CENP-A. Chromatin was visualised with DAPI. Representative cells from each condition are shown. (B-C) A custom Fiji macro (Methods 4.7.1.1) was used for quantification of the cell-averaged per-kinetochore intensity of either (B) NDC80-JFX554 or (C) BUB1-AF488. All intensities were normalised to their respective DMSO condition, shown on a bar graph with mean ± SEM; the number of cells

*measured are indicated in the figure. An ordinary one-way ANOVA test was used for statistical analysis, with P<0.0001 (****) for both sets of quantifications. For BUB1-AF488 quantifications (C) DMSO vs 1 HR PROTAC (P=0.0015, **), DMSO vs 2 HR PROTAC (P = 0.6678, ns), and DMSO vs 3 HR PROTAC (P>0.9999, ns).*

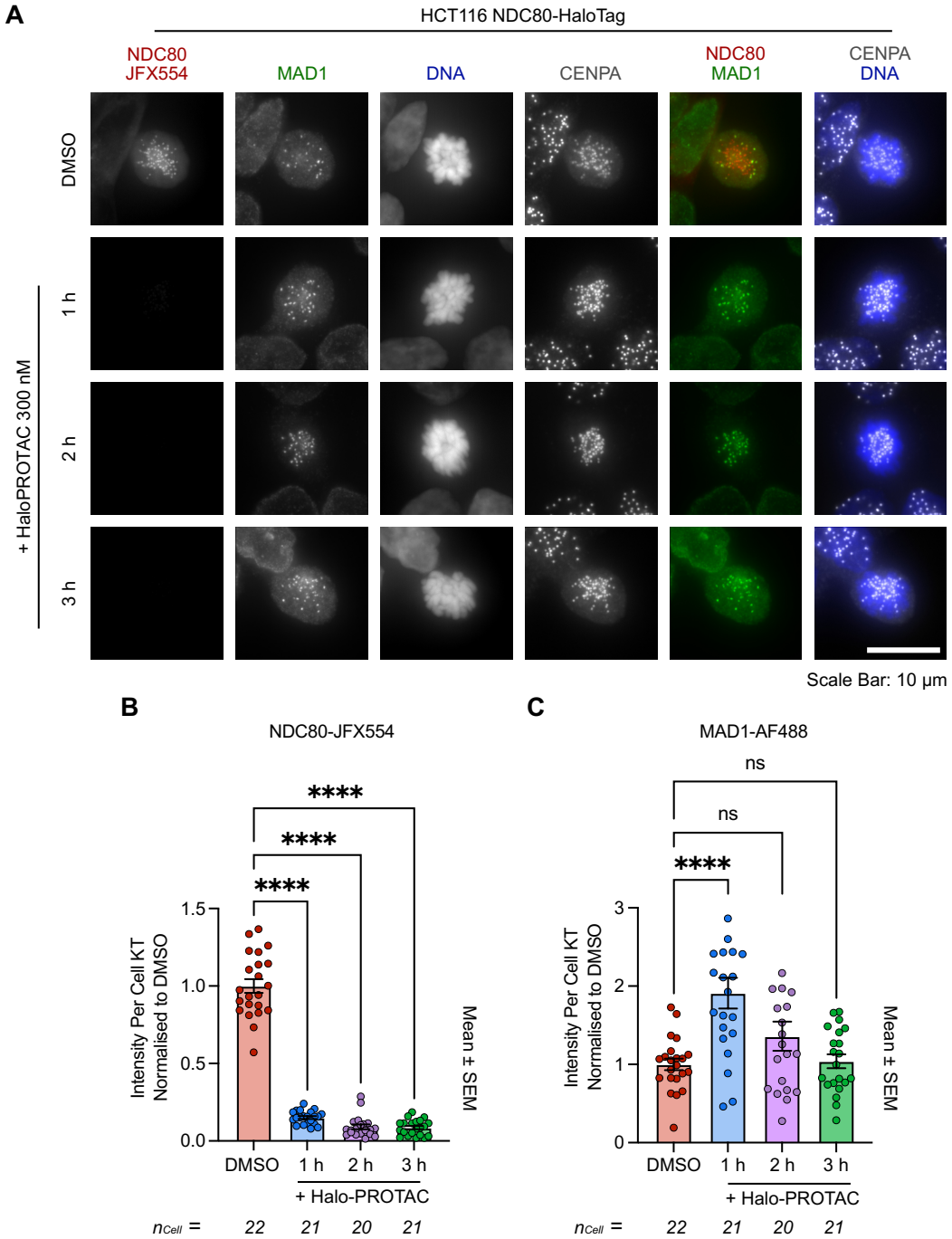

Figure 2. 20 - The SAC protein MAD1 is present at kinetochores after degradation of NDC80

The same experiment and quantifications were performed as in Figure 2.19, except cells were stained with the checkpoint marker MAD1 instead. For MAD1-AF488 statistical analysis (C) DMSO vs 2HR PROTAC (P=0.2283, ns) and DMSO vs 3HR PROTAC (P=0.9960, ns).

2.1.8. NDC80 degradation results in p53-independent proliferative defects

During mitosis the E3 ligase MDM2 targets p53 for degradation by ubiquitylation. Low levels of p53 hence attenuate p21 synthesis, allowing for cell cycle progression beyond the following G1. However, previous studies have shown that extended mitotic duration can trigger a p53-dependent arrest in the subsequent G1 phase. This is due to a reduction in MDM2 levels (by auto-catalysis) below a threshold sufficient enough to degrade p53, resulting in p53 and p21 stabilisation and CDK inhibition (Fulcher et al., 2025; Thompson & Compton, 2010). Given that NDC80 depletion prolongs mitosis, it was important to determine whether the observed proliferative defects were due to loss of viability or loss of proliferation, and what role p53 plays in those outcomes.

To enable this, p53 was knocked out of HCT116 NDC80-HaloTag cells (Methods 4.3). To confirm successful knockout, both parental NDC80-HaloTag and p53 KO cells were treated with the DNA damage reagent hydroxyurea. This treatment triggered p53 stabilisation and an increase in γH2AX in parental cells, and a γH2AX increase alone in the p53 KO cells, as expected (Figure 2.21 - A-B) (Ho et al., 2006). To further confirm p53 KO, both lines were treated with Nutlin 3A, an inhibitor of the p53 ubiquitin ligase MDM2 (Figure 2.21 - C). Cells with wild-type p53 arrested due to an increase in p53 levels, whereas those deficient in p53 continued to proliferate as expected (Figure 2.21 - C-D) (Vassilev et al., 2004).

The effects of NDC80 degradation were then tested in the parental and p53 KO cells. To do this, cells were treated with Halo-PROTAC for 0-8 days and either western blotted (Figure 2.22 - A) or assayed for proliferation (Figure 2.22 - B). In both parental and p53 KO cells after 2 days of treatment, cells were positive for DNA damage marker γH2AX and began to lose mitotic cyclins. Between 2-4 days, apoptotic marker cleaved caspase 3 (Namura et al., 1998) was also present (Figure 2.22 - A). Additionally, cells showed strongly reduced proliferation after NDC80 degradation regardless of p53 status (Figure 2.22 - B). Therefore, although degradation of NDC80 resulted in p53-dependent p21 induction after mitotic slippage, this is

accompanied by DNA damage and unlikely to be solely due to activation of the p53 mitotic timer pathway (Figure 2.22 - A). Supporting this conclusion, p53 KO did not suppress the loss of proliferation seen after NDC80 degradation (Figure 2.22 - B-C). This is in contrast to published work showing that p53 KO can suppress G1 cell cycle arrest after mitotic delays in the absence of DNA damage (Fulcher et al., 2025). These results are consistent with the notion that NDC80 is an essential gene required to generate viable G1 cells lacking DNA damage (Amin et al., 2023; Bharadwaj et al., 2004; Ju et al., 2017).

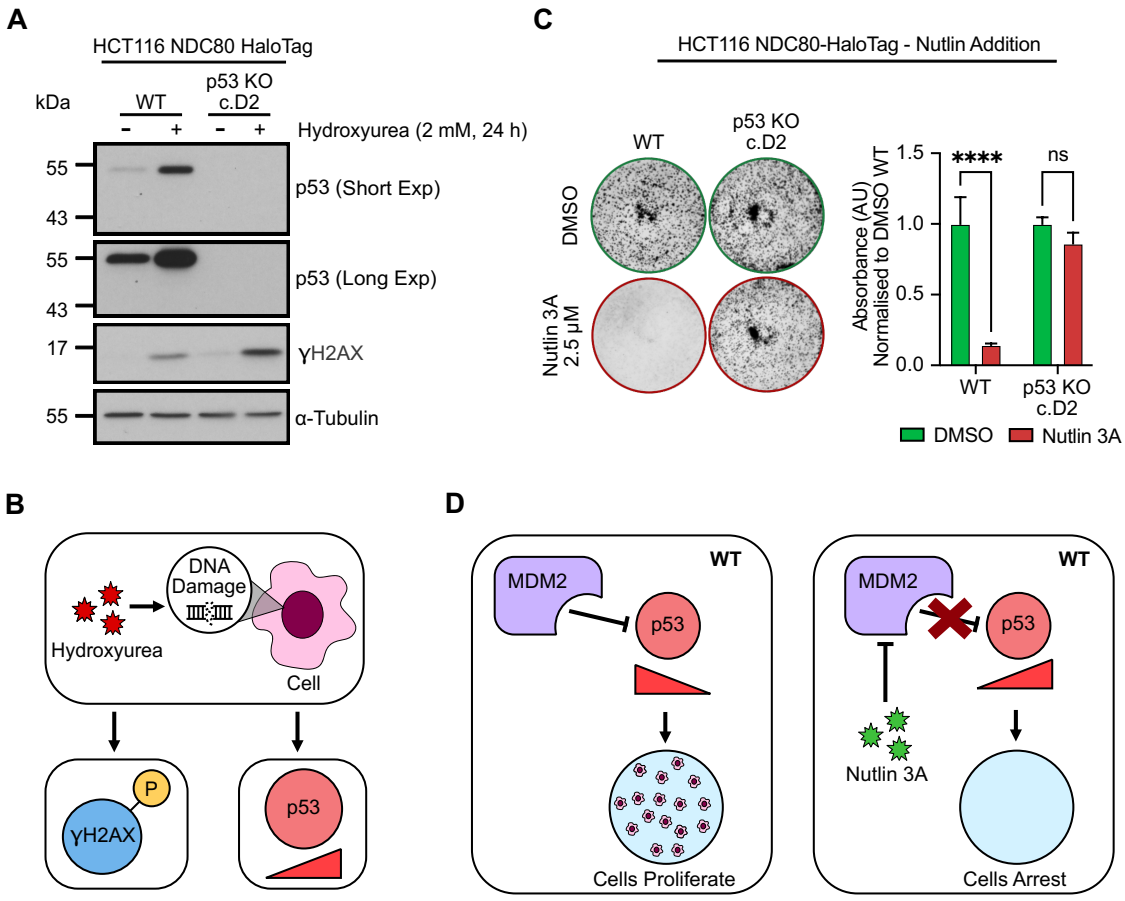

Figure 2. 21 - Generation of a p53-null NDC80-HaloTag HCT116 cell line

(A) In the background of HCT116 NDC80-HaloTag cells, p53 was knocked out using a single guide RNA targeting its N-Terminus (Methods 4.3). 2 mM Hydroxyurea was added to both parental and p53 KO cells, and a western blot run to determine p53 and γH2AX levels by immunoblot. (B) A schematic of hydroxyurea's effects on p53 and γH2AX. (C) Parental and p53 KO cells were seeded at a low density and grown for 5 days ± 2.5 μM Nutlin-3A, before being fixed and stained with crystal violet for 30 minutes. Methanol extraction of crystal violet was performed, and its absorbance at 540nm measured.

Absorbance values were normalised to their respective DMSO controls in each cell line (n=3, Bar graph with Mean ± SD shown). A 2-way ANOVA was used for statistical tests, with P<0.0001 (****) and P=0.3303 (ns). (D) A schematic of Nutlin-3A's effect on cell growth in wild-type cells.

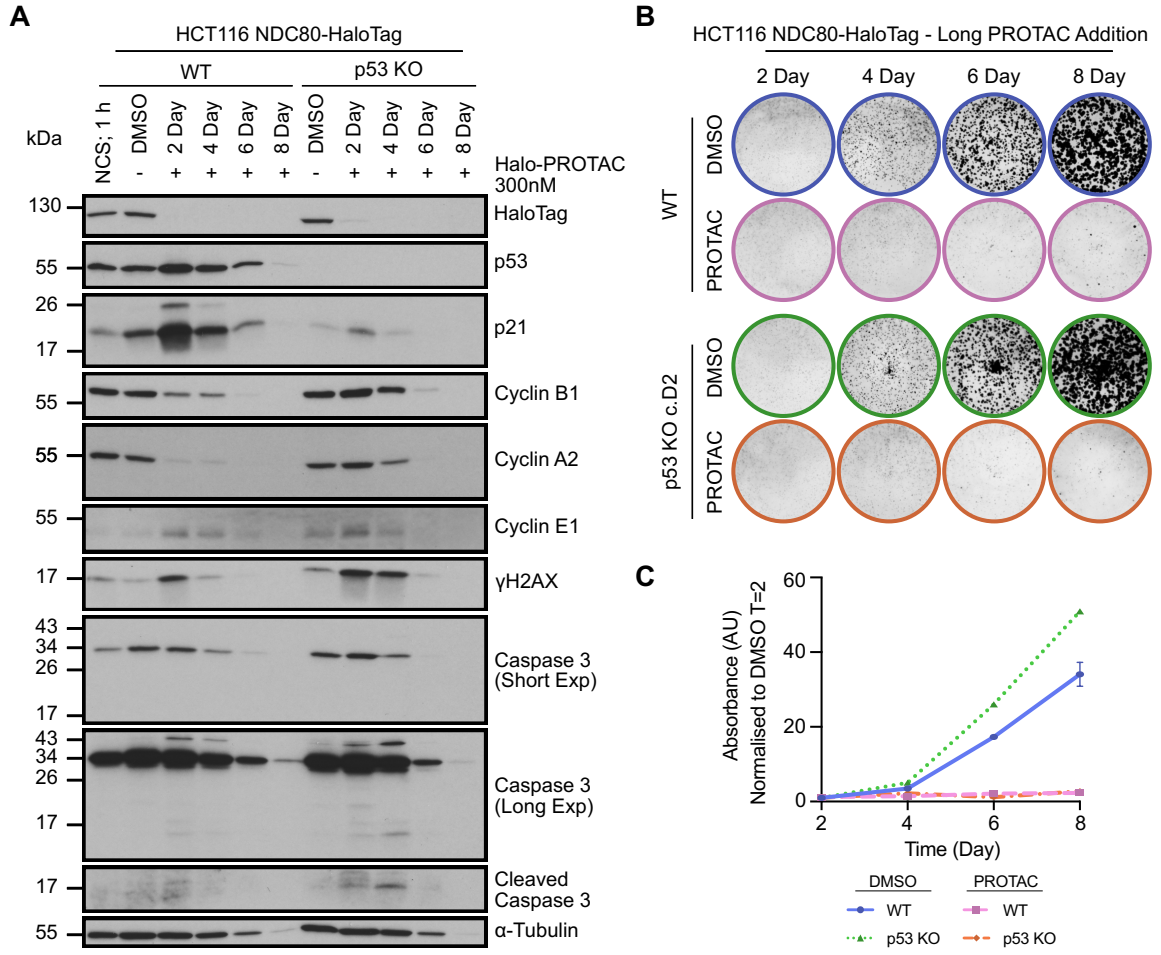

Figure 2. 22 - The requirement for NDC80 in cell proliferation is independent of p53 status in HCT116 cells

For both parental HCT116 NDC80-HaloTag and p53 KO cells - (A) 300 nM Halo-PROTAC was added to cells for 0-8 days. Whole-cell lysates were taken at the same time (8 days) and lysed directly in the same volume of SDS sample buffer. A western blot was performed, immunoblotting with antibodies against cell cycle, DNA damage, and apoptotic markers. A sample with the DNA damage agent NCS was added at 200 ng/ml for 1 hour as a control. (B) Cells were seeded at a low density, and 300 nM Halo-PROTAC added for 0-8 days. At the end of each respective duration of Halo-PROTAC addition, cells were fixed and stained using crystal violet for 30 minutes. (C) For cell growth quantification, methanol was used to extract the dye in each plate. For each sample, absorbance at 540nm was measured. Absorbance was normalised to DMSO T=2 for all values. Mean ± SEM values shown.

2.1.9. Mitotic catastrophe due to synthetic lethality between NDC80 and Protein Phosphatase 6

Recent work has highlighted the role of Aurora A kinase in regulating NDC80 during spindle size control, and shown this is important for accurate chromosome segregation (Hammond et al., 2013; Kettenbach et al., 2011; Sobajima et al., 2023; Zeng et al., 2010). The phosphatase PP6 has been shown to limit Aurora A kinase activity through its catalytic subunit PPP6C, with mutations in PPP6C leading to amplified Aurora A kinase activity and enlarged mitotic spindles with chromosome alignment and segregation defects (Hammond et al., 2013; Kettenbach et al., 2011; Sobajima et al., 2023; Zeng et al., 2010). Genome-wide CRISPR screening in haploid eHAP1 cells identified NDC80 as synthetically lethal with PPP6C; further characterisation in aneuploid HeLa cells showed increased NDC80 phosphorylation by amplified Aurora A kinase activity when PP6 activity was compromised (Sobajima et al., 2023). Thus, when PPP6C was knocked out, cells with constitutively amplified Aurora A kinase activity were sensitised to NDC80 depletion.

To investigate this relationship further, a degron tag ($FKBP12^{F36V}$) was integrated into the endogenous locus of PPP6C in NDC80-HaloTag HCT116 cells. PCR of the genomic locus of PPP6C in parental NDC80-HaloTag and two PPP6C-dTag clones revealed an increase in size by approximately 500 bp (Figure 2.23 - A). Western blots of the same samples showed a change in electrophoretic mobility of PPP6C using a homemade sheep antibody, whereas a rabbit antibody against the native C-terminus of PPP6C was masked by addition of the dTag, leading to loss of signal in the dTag modified samples (Figure 2.23 - B). Integration of the dTag allowed the role of PPP6C and level of Aurora A kinase activity to be explored in cells with normal or reduced amounts of NDC80. The degradation of NDC80 and PPP6C was then tested after the addition of either Halo-PROTAC or dTag-1 (Methods 4.5.3), alone or in combination in HCT116 NDC80-HaloTag PPP6C-dTag clone A9. The Halo-PROTAC

successfully depleted NDC80 without affecting PPP6C levels, and vice versa for dTag-1. Addition of both PROTACs successfully depleted both NDC80 and PPP6C (Figure 2.23 - C).

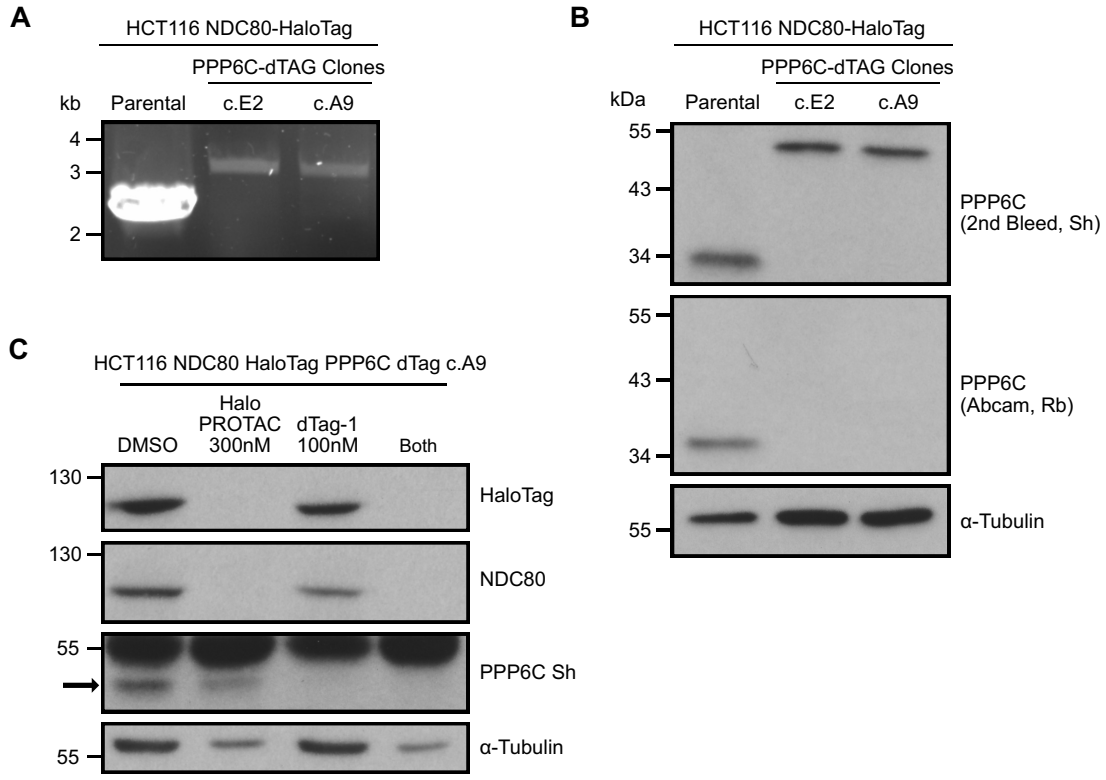

Figure 2. 23 - Generation of a combined PPP6C-dTag NDC80-HaloTag HCT116 cell line

In the background of HCT116 NDC80-HaloTag, a degron-tag ($FKBP12^{F36V}$) was integrated into endogenous PPP6C. (A) PCR of the C-Terminus of PPP6C was performed from the genomic DNA of NDC80-Halo parental and two PPP6C-dTag clones and run on an agarose gel. (B) Similarly, asynchronous whole-cell lysates were taken for the same three cell lines and run on a western blot, immunoblotting with two antibodies against PPP6C to check for tag integration. α-Tubulin was used as a loading control. (C) For one PPP6C-dTag clone (A9), asynchronous cells were treated with either DMSO, 300 nM Halo-PROTAC, 100 nM dTag-1 or both Halo-PROTAC and dTag-1 for 18 hours. Whole-cell lysates were taken and run on a western blot, immunoblotting with antibodies against HaloTag, NDC80 and PPP6C to protein levels. α-Tubulin used as a loading control.

To confirm the effect of PPP6C depletion on Aurora A kinase phosphorylation, dTag-1 was added to both PPP6C-dTag clones E2 and A9. In both instances, western blots confirmed both the depletion of PPP6C and increased Aurora A pT288, a marker for its activation. In contrast, the levels of the Aurora A binding partner TPX2 and Aurora A substrate NDC80 remained unchanged (Figure 2.24 - A). The effect of PPP6C degradation on the mitotic spindle was then followed using immunofluorescence microscopy of HCT116 NDC80-HaloTag PPP6C-dTag cells treated ± dTag-1 (Figure 2.24 - B), showing no discernible change in NDC80 presence/intensity.

Previous reports indicate an increase in spindle size upon removal of PPP6C (Sobajima et al., 2023). To confirm this in the HCT116 NDC80-HaloTag PPP6C-dTag genetic background, cells were depleted of PPP6C and their spindle size measured post-immunofluorescence staining (Figure 2.24 - C). This confirmed an increase in spindle size for PPP6C-depleted cells (Figure 2.24 - C) for both clones tested. In addition, analysis of the frequency of cells at different stages in mitosis indicated a shift towards cells in a prometaphase-like state (Figure 2.24 - D), potentially indicating issues in chromosome alignment.

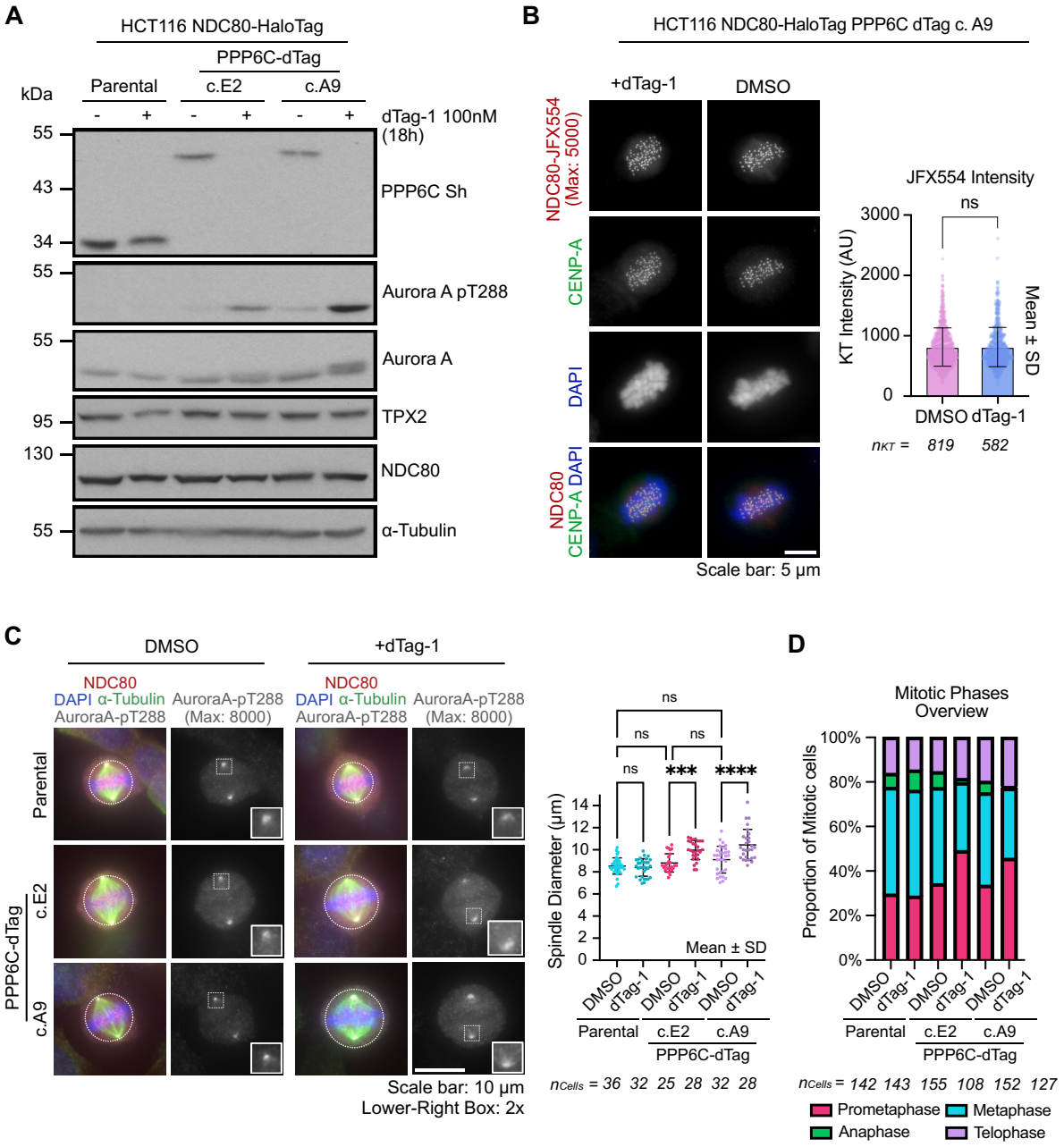

Figure 2. 24 - Degradation of PPP6C results in larger mitotic spindles

(A) Parental HCT116 NDC80-HaloTag and two PPP6C-dTag derived clones were treated with 100 nM dTag-1 for 18 hours, and 20 µM of the APC/C inhibitor proTAME for 2.5 hours. Whole-cell lysates were taken and run on a western blot, immunoblotting for PPP6C and key targets. (B) PPP6C-dTag clone A9 cells were treated with ± 100 nM dTag-1 for 18 hours, and 20 µM proTAME for 4 hours. Cells were then labelled with 100 nM JFX554 for 15 minutes to visualise NDC80, and PTEMF fixed for 12 minutes. Cells were then stained with an antibody against centromere protein CENP-A; chromatin was visualised with DAPI. NDC80-JFX554 intensity was measured on a per-kinetochore basis for both conditions using a custom Fiji macro (Methods 4.7.1.1). An unpaired two-tailed t-test was used for statistical analysis,

with P=0.9414 (ns). Bar graph with mean ± SD shown. (C) Both Parental HCT116 NDC80-HaloTag and two PPP6C-dTag derived clones were treated ± 100 nM dTag-1 for 18 hours, and 20 μM proTAME for 2.5 hours. Cells were then labelled with 100 nM JFX554 for 15 minutes to visualise NDC80, and PTEMF fixed for 12 minutes. Cells were then stained with antibodies against α-Tubulin and Aurora A pT288; chromatin was visualised with DAPI. Spindle size was determined by measuring a circular diameter inclusive of DNA content. Mean ± SD shown. A one-way ANOVA was used for statistical analysis, with P<0.0001 (****) and P=0.0002 (***). For Parental DMSO vs dTag-1 (P=0.9947, ns), Parental DMSO vs C.E2 DMSO (P=0.8588, ns), Parental DMSO vs C.A9 DMSO (P=0.1070, ns), and C.E2 DMSO vs C.A9 DMSO (P=0.8520, ns). (D) Mitotic phase distribution was determined from chromatin morphology (by DAPI staining) for all conditions and shown as a proportion of all mitotic cells. The number of cells measured for each condition are indicated in each figure.

With the double-tag cell line successfully validated, the proliferative capability of NDC80, PPP6C or dual-depleted cells was tested. As previously seen, removal of NDC80 impeded cell proliferation (Figure 2.12 - C, Figure 2.22 - B). Depletion of PPP6C partially affected cell proliferation, and depletion of both proteins caused a complete failure in proliferation (Figure 2.25 - A).

The nuclear morphology of these depleted cells was then determined by immunofluorescence microscopy, with DAPI used to visualise chromatin, Lamin B1 to identify the inner nuclear envelope, and α-Tubulin as a marker for cell size. Degradation of NDC80 resulted in obvious nuclear morphology defects, whereas degradation of PPP6C instead resulted in increased micronucleation, as previously seen with PPP6C KO cells (Sobajima et al., 2023)(Figure 2.25 - B). In contrast, removal of both proteins resulted in highly fragment nuclei consistent with a catastrophic failure of mitosis (Figure 2.25 - B). These findings, using selective and rapid dTag/PROTAC-mediated degradation of PPP6C and NDC80, respectively, support the previous conclusions obtained using other methods in HeLa and eHAP1 cells, that there is synthetic lethality between NDC80 and PP6 (Sobajima et al., 2023).

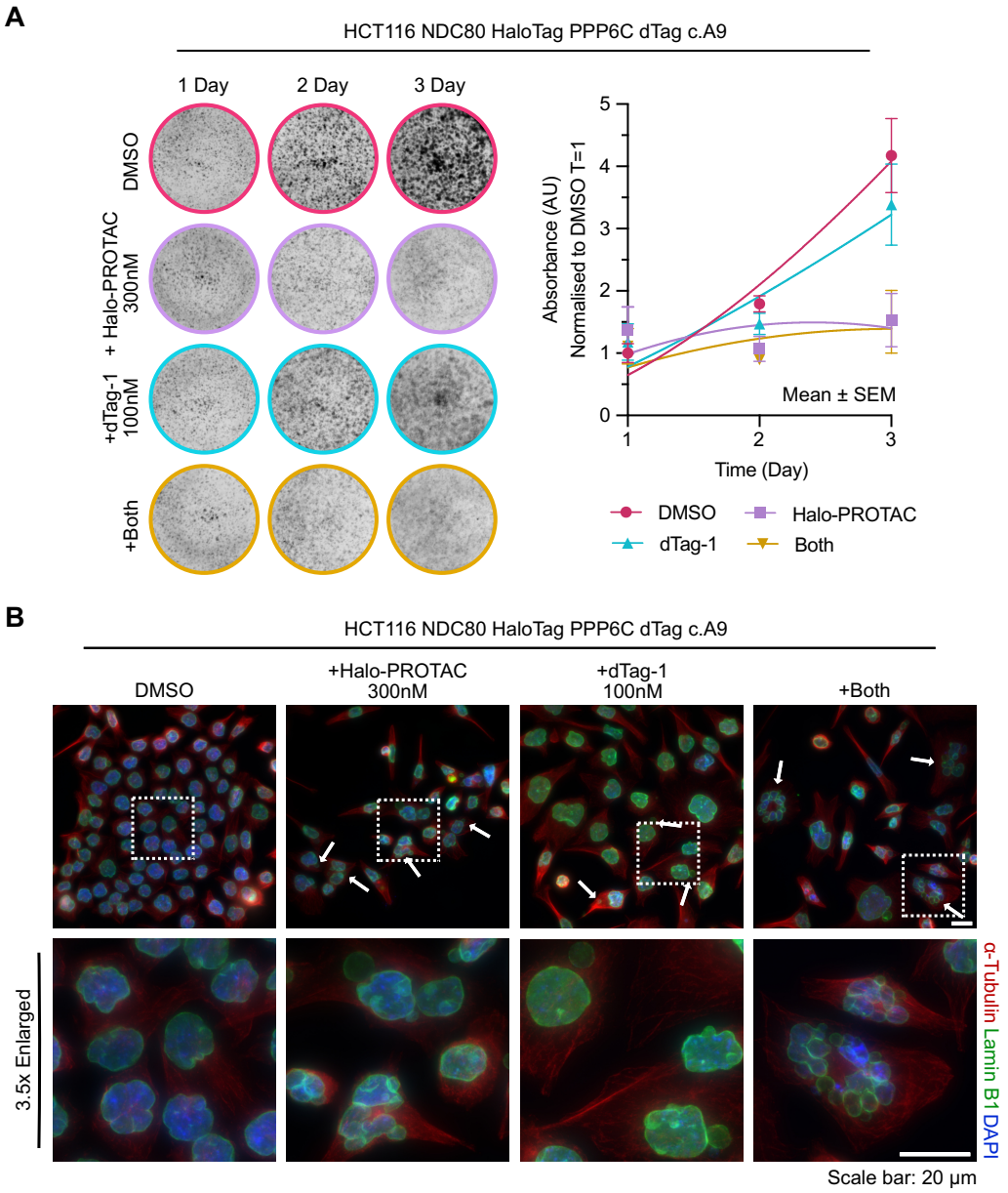

Figure 2. 25 - Synthetic lethality between NDC80 and PPP6C in HCT116 cells

With HCT116 NDC80-HaloTag PPP6C dTag cells (A) Asynchronous cells were seeded at a low density, grown for 2 days, and then treated with either DMSO, 300 nM Halo-PROTAC, 100 nM dTag-1, or both drugs for a further 1-3 days. Cells were then fixed and stained at the end of their respective growth periods using crystal violet for 30 minutes. For quantification of cell growth, methanol extraction of crystal violet was performed, and absorbance at 540 nm measured (n=3). All values are normalised to DMSO at Day 1; mean ± SEM shown. Non-linear beta growth then decay curves fitted. (B) Asynchronous cells were grown for 3 days with either DMSO, 300 nM Halo-PROTAC, 100 nM dTag-1, or both drugs. Cells were then PTEMF fixed for 12 minutes and stained with antibodies for α-Tubulin or Lamin B1. Chromatin was visualised using DAPI.

2.2. Investigation of the spindle assembly checkpoint scaffold protein KNL1

2.2.1. Integration of a synthetic HaloTag into endogenous KNL1 for visualisation and rapid PROTAC-mediated degradation

The results presented thus far indicate that sustained checkpoint signalling could be a driver of prolonged mitosis in an NDC80-depleted background. This was unexpected due to the proposed role of NDC80 in activating the SAC (Lara-Gonzalez et al., 2021). To test whether extended mitosis is a specific effect or would be seen with degradation of other kinetochore proteins, the core checkpoint scaffold protein KNL1 was targeted (Kiyomitsu et al., 2007). Using CRISPR/Cas9 the HaloTag was integrated into the 5'-end of the endogenous KNL1 locus in wild type HCT116 cells to tag the N-terminus of the protein. PCR of the genomic locus of KNL1 revealed an increase in size of approximately 1kb for clone B7 in comparison to the parental cells (Figure 2.26 - A). Western blotting of these samples and additional clones revealed a change in electrophoretic mobility for KNL1, and a corresponding HaloTag-positive band for all clones tested (Figure 2.26 - B).

To ensure correct KNL1 protein localisation after tagging, immunofluorescence microscopy was performed for both parental HCT116 and HaloTag-KNL1 cell lines. Addition of the HaloTag dye JFX554 to both samples and staining with antibodies for both KNL1 and the centromere protein CENP-A revealed only a positive JFX554 signal in the tagged cell line, with good overlap to the KNL1 antibody staining (Figure 2.26 - C). Correct localisation also confirmed by performing a chromosome spread, showing that KNL1 is found to localise to two sites adjacent to the cohesed centromere region of mitotic chromosomes (Figure 2.26 - D). These findings were similar to the NDC80-HaloTag cell lines already analysed (Figure 2.1), demonstrating the general applicability of the HaloTag system for different proteins.

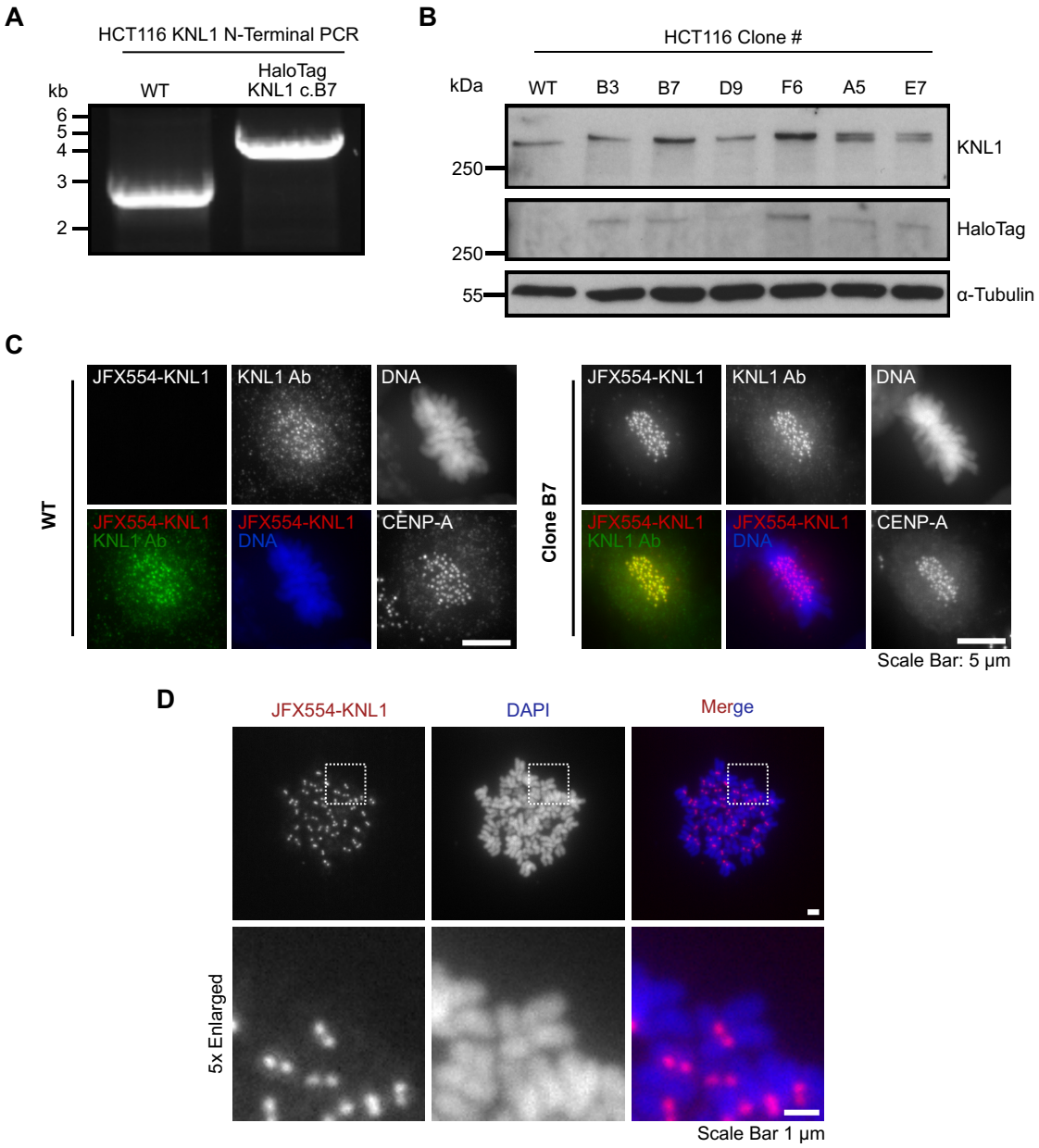

Figure 2. 26 - Generation and characterisation of HaloTag-KNL1 HCT116 cell lines

A) PCR of the KNL1 N-terminus to determine tag integration. Genomic DNA was extracted from HCT116 wild type and HaloTag-KNL1 clone pellets; products were resolved on agarose gel. (B) Western blot of whole-cell lysates for the same cell lines as in (A), with five additional clones, immunoblotting with antibodies for KNL1, HaloTag and a-Tubulin. (C) For both wild-type HCT116 and HaloTag-KNL1 c.B7, asynchronous cells were treated with 100 nM JFX554 for 15 minutes to visualise KNL1. Cells were PTEMF fixed for 12 minutes and stained with antibodies for CENP-A and KNL1. Representative cells are shown. (D) A representative chromosome spread (Methods 4.6.2) shows KNL1-JFX554 localisation relative to chromatin (visualised by DAPI).

With NDC80-HaloTag and HaloTag-KNL1 cell lines available in the same genetic background, this allowed for direct comparison of NDC80 and KNL1 stoichiometry in mitosis while avoiding potential technical limitations such as antibody binding affinity and epitope accessibility. Both cell lines were treated in parallel; cells were arrested in metaphase by addition of MG132, labelled with JFX554 dye, and immunofluorescence-stained with DAPI and CENP-A (Figure 2.27 - A). By determining kinetochore intensities across all channels for both cell lines (Methods 4.7.1.1), there appeared to be a greater distribution of NDC80 and CENP-A signal in comparison to KNL1, with an approximate 3:2 stoichiometric ratio of NDC80:KNL1 observed (Figure 2.27 - B) (Jema et al., 2023). Moreover, the intensity of both outer-kinetochore components correlated with CENP-A signal (Figure 2.27 - C). One possible interpretation of this stoichiometry is that the elevated proportion of NDC80 may reflect a higher reliance on mechanical robustness required for kinetochore-microtubule attachment, whereas fewer KNL1 molecules may suffice for amplification of spindle assembly checkpoint signalling through the mitotic checkpoint complex (MCC).

To determine whether the Halo-PROTAC was able to act in the same way as in the NDC80-HaloTag line, HaloTag-KNL1 cells were treated with Halo-PROTAC over a time course of 0-4 hours. Rapid degradation was observed for HaloTag-KNL1 by Western blot using either KNL1 or HaloTag antibodies, with near-complete degradation observed after two hours of treatment (Figure 2.28 A-B).

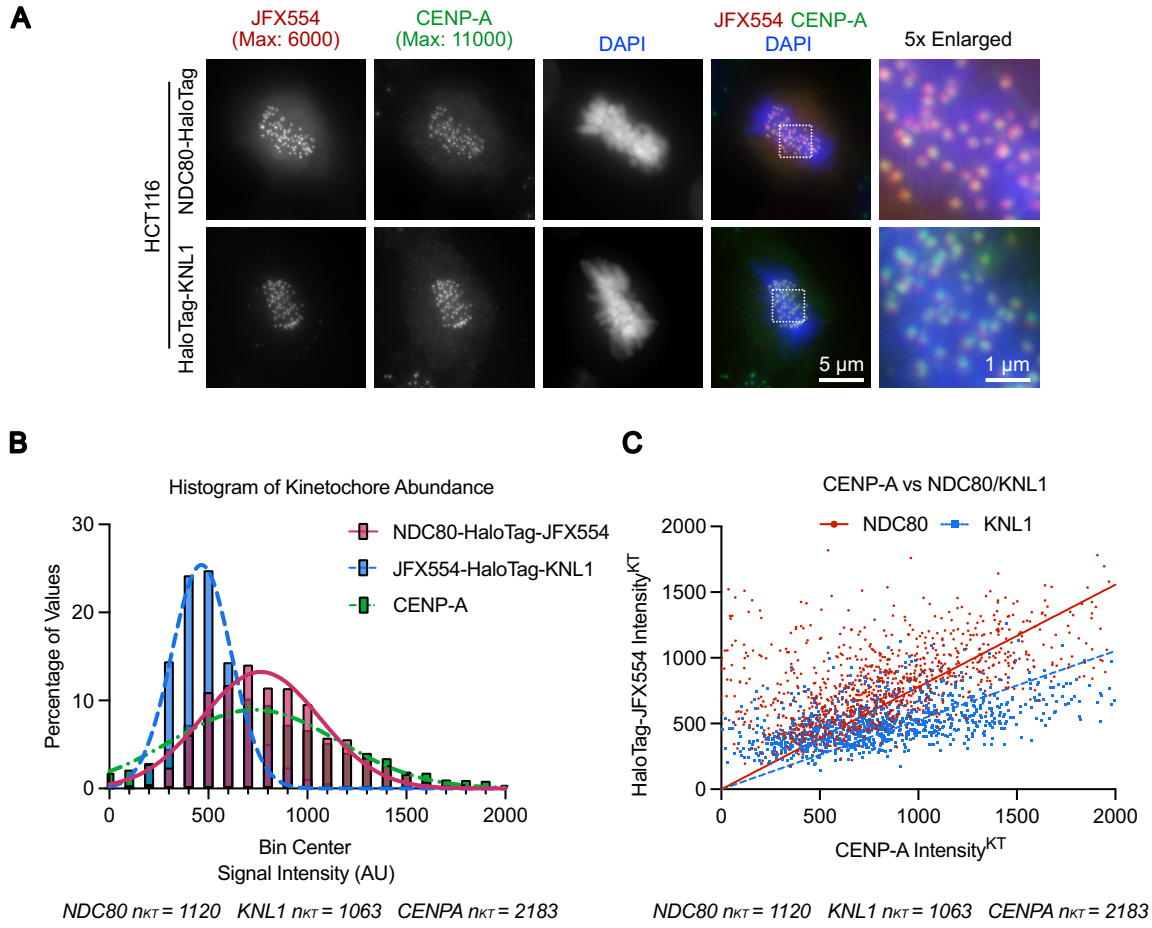

Figure 2. 27 - Comparison of NDC80 vs KNL1 stoichiometry in mitotic HCT116 cells using the JFX-HaloTag-binding dyes

(A) HCT116 NDC80-HaloTag or HaloTag-KNL1 cells were arrested in mitosis using 20 µM MG132 for 4 hours. Cells were treated with 100 nM JFX554 dye, PTEMF fixed for 12 minutes, and immunofluorescence stained with an antibody for CENP-A. Chromatin was visualised by DAPI staining. (B) Intensities of NDC80-JFX554, JFX554-KNL1 or CENP-A per kinetochore were determined using a custom Fiji macro (Methods 4.7.1.1), plotted as a histogram, and fitted with Gaussian curves. The number of kinetochores measured is indicated in the figure. (C) HaloTag-JFX554 intensity for either NDC80 or KNL1 were plotted against CENP-A intensity on a scatter plot, and a linear regression fitted.

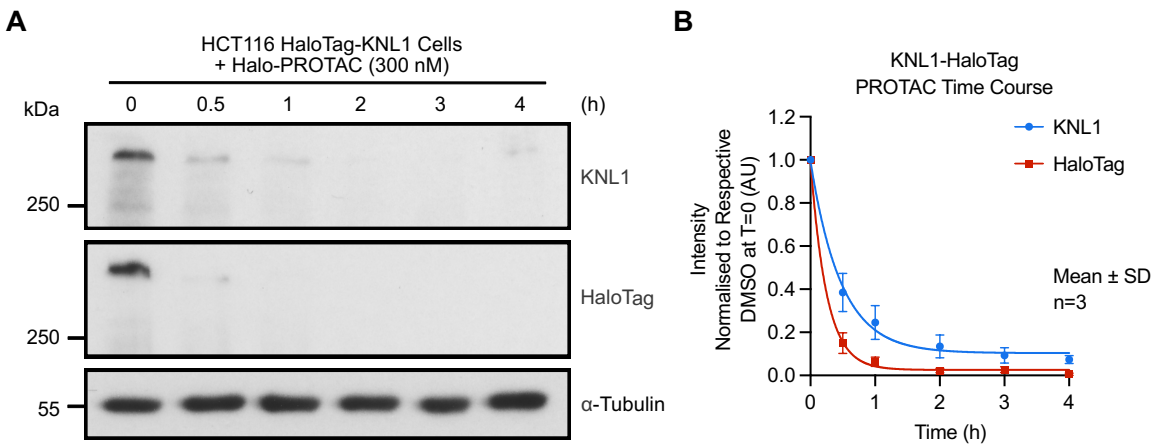

Figure 2. 28 - Time course of HaloTag-KNL1 degradation in HCT116 cells following Halo-PROTAC addition.

(A) 300 nM Halo-PROTAC was added to asynchronous HCT116 HaloTag-KNL1 cells for 0, 0.5, 1, 2, 3, or 4 hours. Whole-cell lysates were run on a western blot to determine KNL1 and HaloTag protein levels under PROTAC addition. α-Tubulin used as a loading control. (B) Densitometry quantification of background-subtracted immunoblot bands for HaloTag and KNL1 over time (n=3, mean ± SD). Intensity values for each data set were normalised to T=0 (DMSO). One phase decay curves were fitted to each data set.

To determine if similar degradation kinetics were observed in single cells, immunofluorescence microscopy was performed. HaloTag-KNL1 cells were treated with Halo-PROTAC for 0-4 hours and arrested in metaphase of mitosis by APC/C inhibition, which prevents mitotic exit independent of SAC activity. HaloTag-JFX554 dye was added to visualise the remaining HaloTag-KNL1 and immunofluorescence staining with antibodies for KNL1 and CENP-A were performed; chromatin was visualised by DAPI staining (Figure 2.29 - A). HaloTag-KNL1 degradation kinetics observed by microscopy were similar to those seen with Western blot, with almost all KNL1 signal being depleted after approximately 2 hours (Figure 2.29 - B). Interestingly, a 30-minute lag was seen between the beginning of the depletion curves for JFX554-KNL1 and KNL1 antibody staining, potentially due to bound-PROTAC molecules inhibiting dye accessibility to the HaloTag.

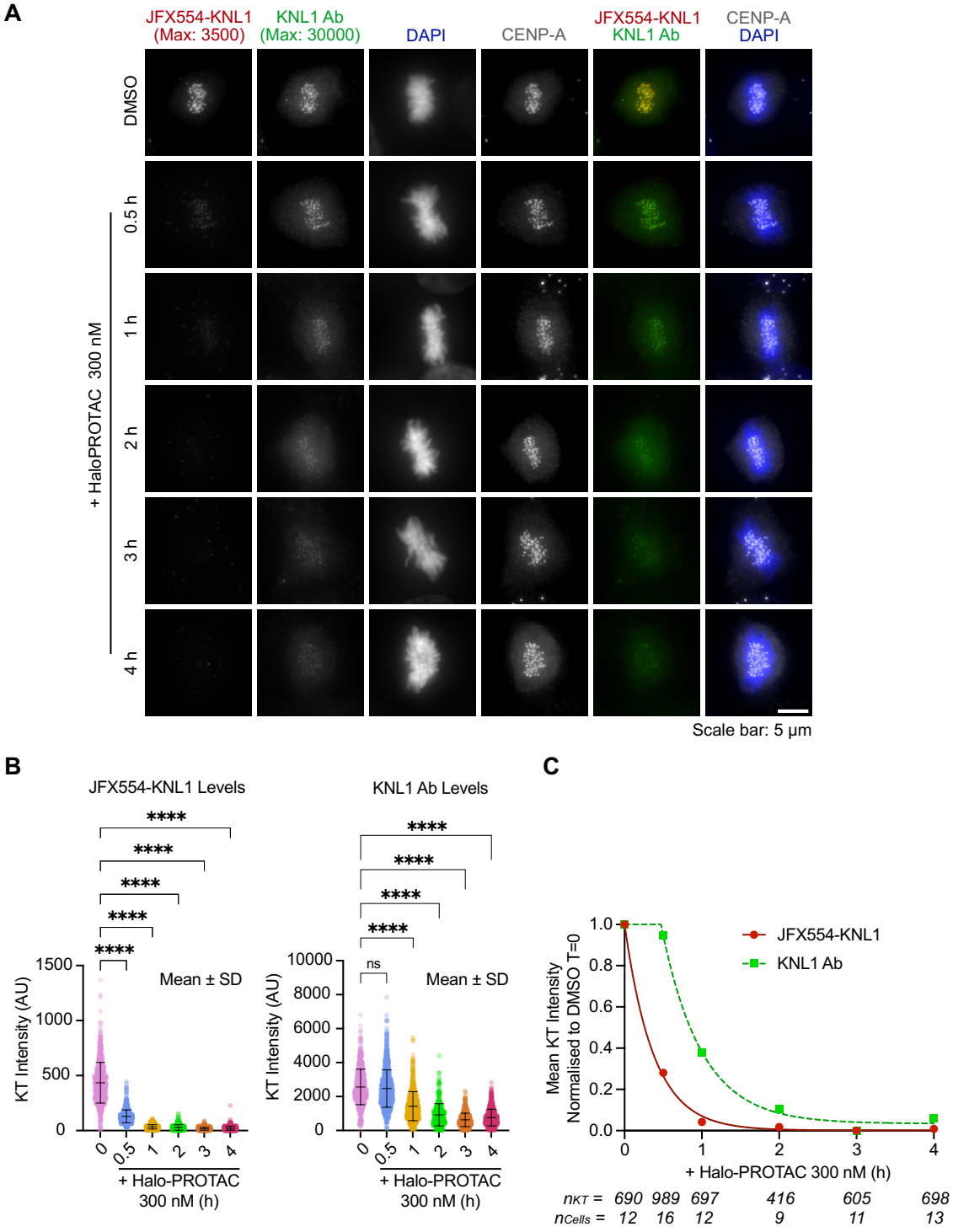

Figure 2. 29 - Immunofluorescence Halo-PROTAC time course using JFX-dyes to directly detect HaloTag-KNL1 in HCT116 cells

(A) HCT116 HaloTag-KNL1 cells were arrested in mitosis using 20 µM proTAME (APC/C inhibitor) for 4 hours, as well as 300 nM Halo-PROTAC for 0, 0.5, 1, 2, 3, or 4 hours. Cells were then incubated with 100 nM JFX554 for 15 minutes to visualise KNL1, followed by PTEMF fixation for 12 minutes. Cells were immunofluorescence stained with antibodies for KNL1 and CENP-A. Chromatin was visualised

using DAPI. (B) Intensities per kinetochore for JFX554-KNL1 and KNL1 antibody were performed using a custom Fiji macro (Methods 4.7.1.1) and plotted as a scatter graph for each time point (Mean ± SD). An ordinary one-way ANOVA was used for statistical tests, with P<0.0001 (****) and P=0.0778 (ns). (C) Mean KT intensities per cell are plotted over time, normalised to each respective DMSO at T=0. One-phase decay curves were fitted, with KNL1 antibody curve having a plateau fitted before the decay. The number of kinetochores and cells measured for both (C) and (D) are shown.

2.2.2. HaloTag-KNL1 and NDC80-HaloTag are integrated into the outer kinetochore

To confirm HaloTag-KNL1 was still correctly incorporated into kinetochores, mass spectrometry was used. Using the same approach as Figure 2.3, immunoprecipitation was performed from NDC80-HaloTag and HaloTag-KNL1 cell lines. In this instance however, immunoprecipitated proteins were sent for analysis by mass spectrometry (Methods 4.4.4). NDC80-HaloTag revealed expected protein interactions with members of the KMN network (e.g. NDC80-C, KNL1-C, MIS12-C) (Figure 2.30 - A). HaloTag-KNL1 revealed similar KMN protein interactions, with the addition of the checkpoint proteins BUB1, BUB3, and BUBR1 (Figure 2.30 - B) - all expected to interact with the KNL1 scaffold to promote MCC formation (Caldas & DeLuca, 2013; Primorac et al., 2013). Key protein interactions were also confirmed via immunoblotting, with NDC80 showing greater binding to other members of the NDC80 complex (NUF2, Spc24/25), and KNL1(CASC5) showing greater binding to ZWINT and BUBR1. Mis12 was observed with similar abundance for both NDC80 and KNL1 samples (Figure 2.30 - C).

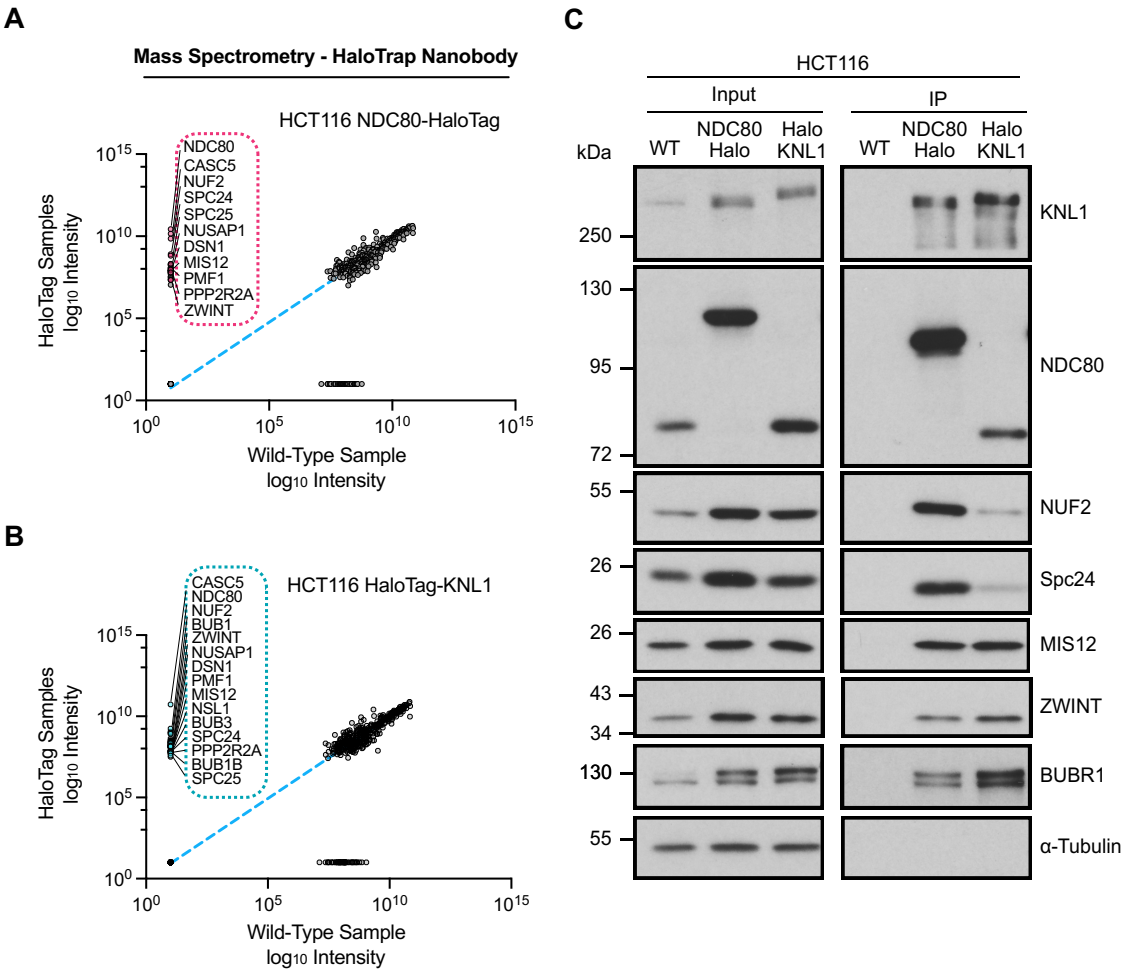

Figure 2. 30 - Immunoprecipitation and Mass Spectrometry analysis of endogenous NDC80-HaloTag and HaloTag-KNL1 complexes in HCT116 cell lines

Immunoprecipitation (IP) was performed (Methods 4.4.3) using HaloTag nanobody beads to identify protein interactions. Either (A) HCT116 NDC80-HaloTag or (B) HCT116 HaloTag-KNL1 cells were immunoprecipitated, with HCT116 wild-type cells used as an IP control and analysed by mass spectrometry (Methods 4.4.4) revealing key protein interactions. Mass spectrometry was performed by the Proteomics Facility at the Department of Biochemistry, University of Oxford. (C) HCT116 wild-type and both NDC80-HaloTag and HaloTag-KNL1 cell lines were arrested in mitosis with 330 nM nocodazole for 18 hours, immunoprecipitated, and run on a western blot to check protein interactions with KMN network proteins.

2.2.3. PROTAC-mediated degradation of HaloTag-KNL1 shortens mitosis

Having established successful protein interaction of HaloTag-KNL1, and the successful degradation of KNL1 with addition of Halo-PROTAC, spinning disk live-cell microscopy was performed to determine if the time spent in mitosis was altered by KNL1 depletion. Control cells were treated with DMSO (solvent control for Halo-PROTAC), and SiR-DNA and JFX554 to visualise chromatin and KNL1, respectively (Figure 2.31 - A). KNL1 was degraded by treating cells with Halo-PROTAC for at least 3 hours before imaging in the presence of SiR-DNA (Figure 2.31 - B).

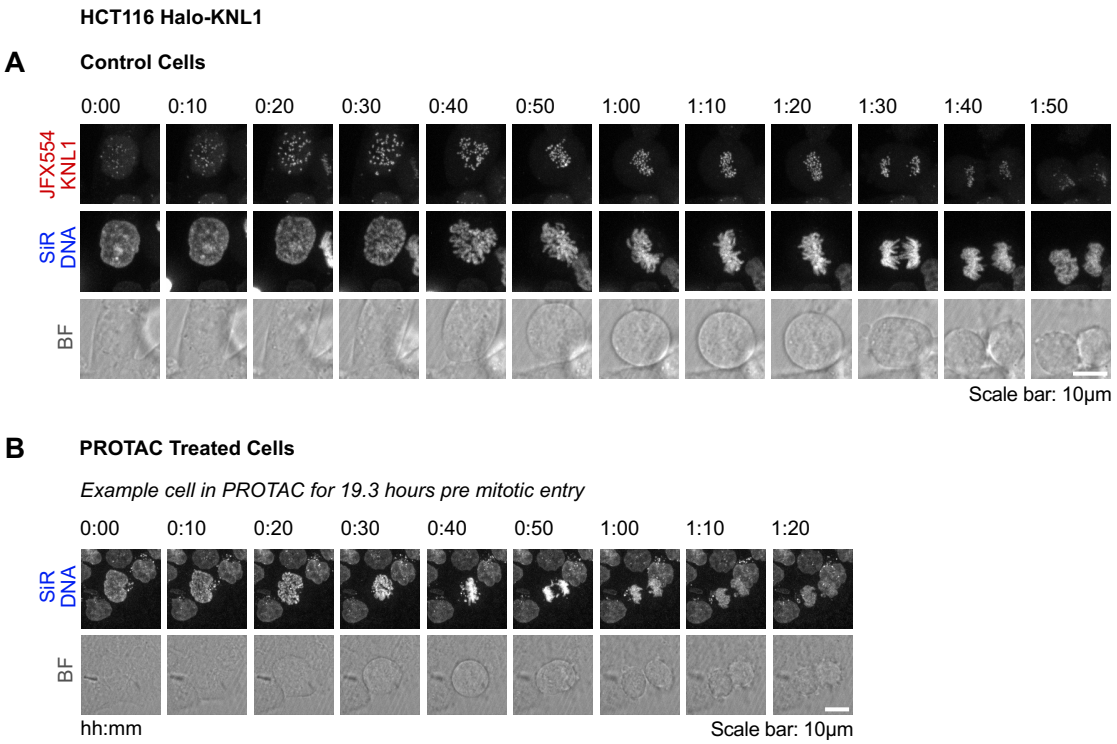

Figure 2. 31 - HaloTag-KNL1 live cell imaging after control or Halo-PROTAC treatments

(A) HCT116 HaloTag-KNL1 cells were labelled with 50 nM SiR-DNA (DNA) for 3 hours, and 100 nM JFX554 (KNL1) for 15 minutes. Excess JFX554 was washed out in SiR-DNA containing media before imaging. Cells were imaged every 10 minutes in far-red, red, and bright-field channels on a spinning disk. An example cell is shown, undergoing anaphase onset. (B) Cells were treated the same as in (A), except cells were labelled with 50 nM SiR-DNA (DNA) only and treated with 300 nM Halo-PROTAC for 3 hours prior to imaging. Only far-red and bright-field channels were imaged.

Compared to the DMSO-treated control cells, KNL1 degradation using the Halo-PROTAC resulted in a shorter time spent in mitosis, with cells spending ~38 minutes in mitosis as opposed to ~46 minutes in the control (Figure 2.32 - A). Additionally, >90% of cells were observed to undergo anaphase onset without mitotic slippage in either the control condition or when KNL1 was degraded (Figure 2.32 - B). There did not appear to be any correlation between time spent in Halo-PROTAC and mitotic duration (Figure 2.32 - C), implying that KNL1 had fallen below the threshold required to support checkpoint activation and thus delay mitotic progression.

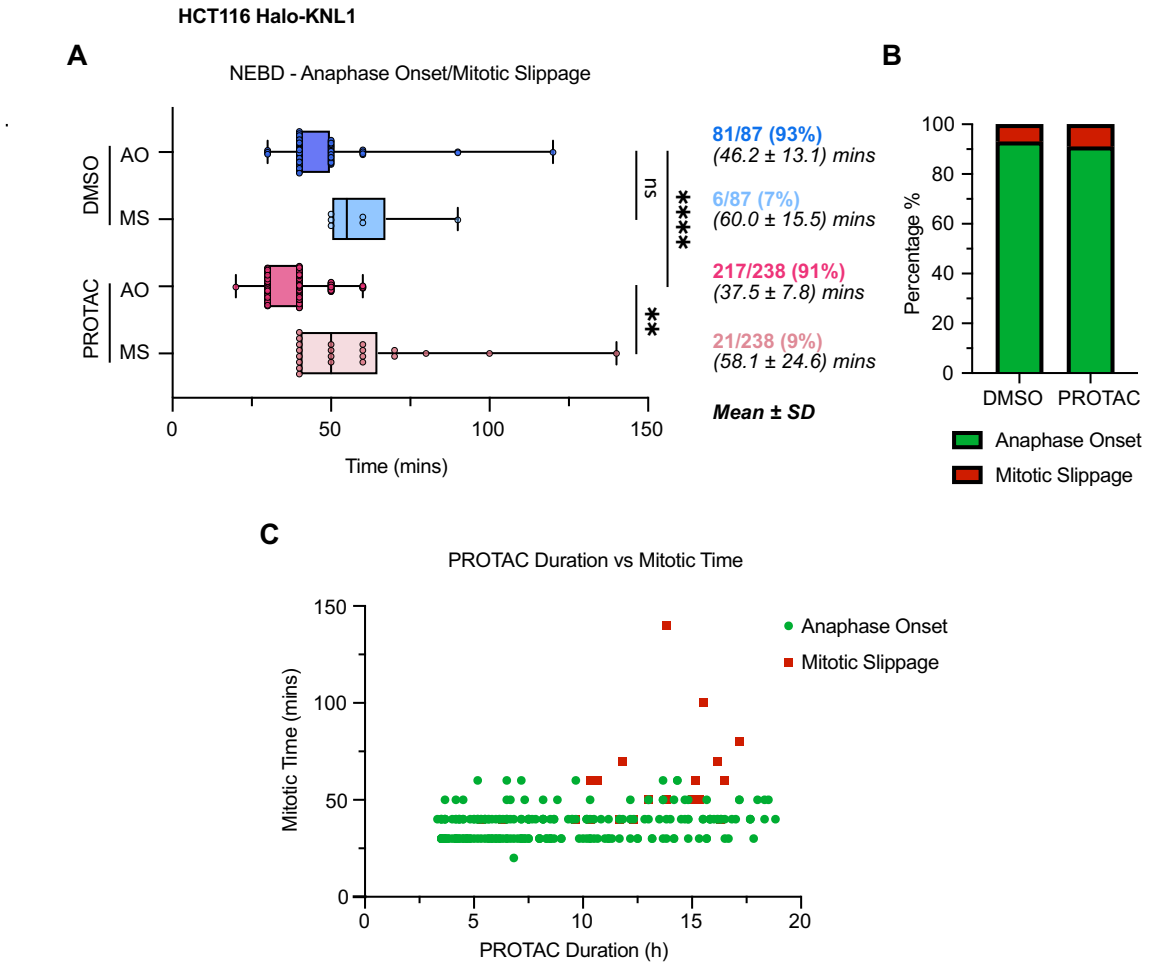

Figure 2. 32 - Time in mitosis decreases when KNL1 is degraded

(A) Quantification of the time cells spent in mitosis was measured from Nuclear Envelope Breakdown (NEBD) to either Anaphase Onset (AO) or Mitotic Slippage (MS) for cells treated with either DMSO or Halo-PROTAC in Figure 2.31. Min-max box & whisker plots are shown, with 3 lines representing the

25/50/75 percentile respectively. The number of cells tracked and the mean ± SD of mitotic timing is shown next to each condition. Brown-Forsythe and Welch ANOVA tests were used for statistical analysis, with P<0.0001 (****), P=0.0032 (**), P=0.1930 (ns). (B) The proportion of cells undergoing either AO or MS is shown for each condition. (C) For Halo-PROTAC treated cells only; the amount of time each cell spent in mitosis vs the time that cell spent in PROTAC prior to NEBD is shown.

As KNL1 provides the platform for MCC formation by MPS1 phosphorylation, the question arose of as to whether this reduced mitotic timing phenotype could be recapitulated by blocking MPS1 activity, and thus MELT-motif phosphorylation in wild-type HCT116 cells (Ji et al., 2017; Stucke et al., 2002). Control cells were treated with SiR-DNA to visualise chromatin (Figure 2.33 - A). MPS1-inhibitor was added to another set of cells (also pre-treated with SiR-DNA) for 15 minutes prior to imaging (Figure 2.33 - B). This revealed a significant reduction in mitotic timing for MPS1-inhibited cells from ~78 minutes to ~35 minutes (Figure 2.33 - C), and an equal propensity for anaphase onset and mitotic slippage was observed for these MPS1 inhibited cells (Figure 2.33 - D). Hence, inhibiting MPS1 kinase activity or removing the KNL1 platform completely can be shown to reduce mitotic timing.

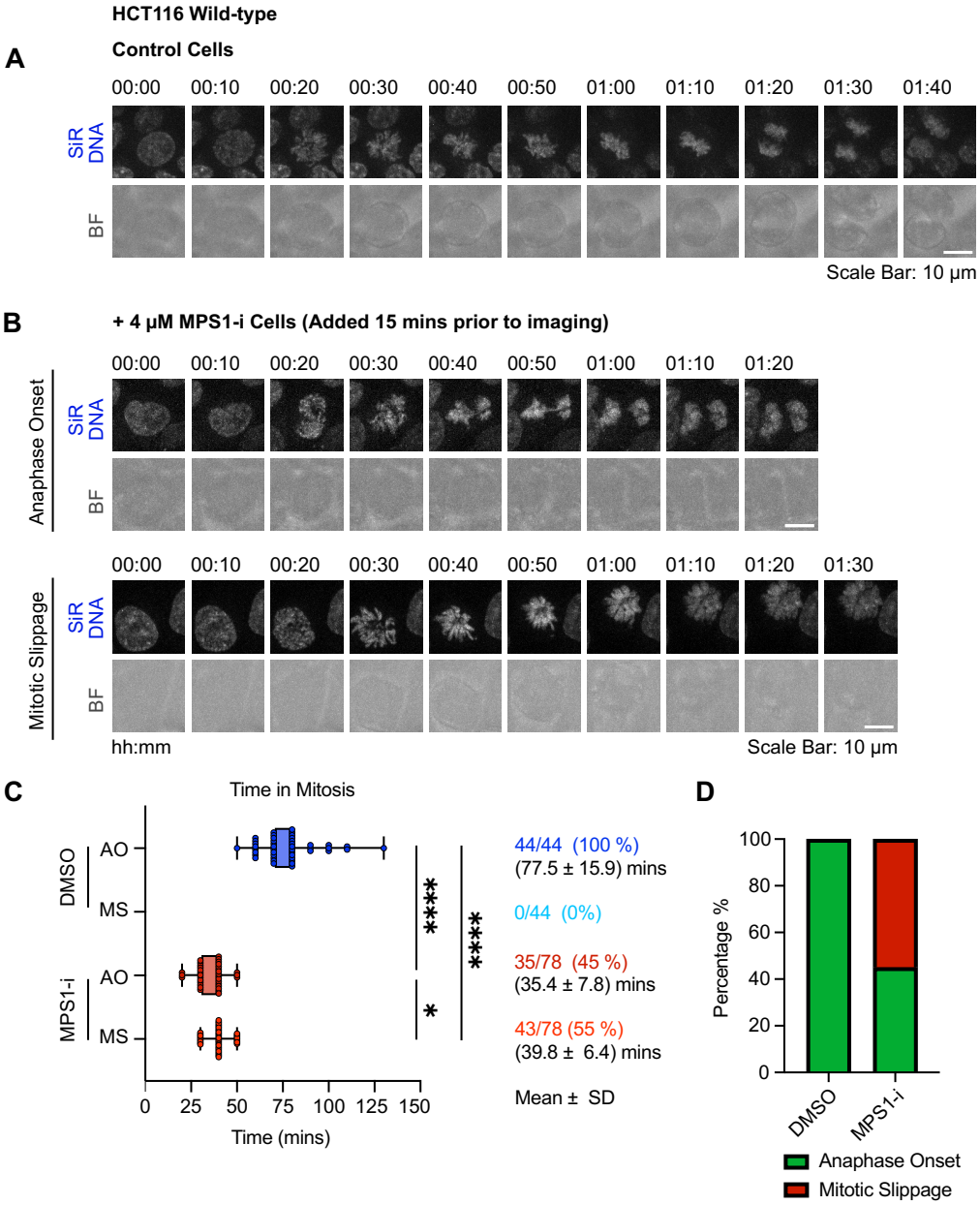

Figure 2. 33 - Time in mitosis decreases when the MPS1 SAC kinase is inhibited

(A) HCT116 wild-type cells were labelled with 50 nM SiR-DNA (DNA) for 3 hours prior to imaging. Cells were imaged every 10 minutes in far-red and bright-field channels on a spinning disk. An example cell is shown undergoing anaphase onset. (B) Cells were treated the same as in (A), except 4 µM MPS1-inhibitor was added for 15 minutes before imaging and remained in the sample for the duration of the imaging session. Example cells are shown either undergoing anaphase onset or mitotic slippage. (C) Quantification for time in mitosis and (D) proportion of cells undergoing AO or MS were performed the same as in Figure 2.32 A and B respectively. For (C), Brown-Forsythe and Welch ANOVA tests were used for statistical analysis with P<0.0001 (****) and P=0.0297 (*).

2.2.4. Rapid PROTAC-mediated degradation of HaloTag-KNL1 reduces NDC80 phosphorylation and checkpoint activity

To provide further evidence of checkpoint inactivation upon KNL1 degradation, HaloTag-KNL1 cells were treated with Halo-PROTAC and immunofluorescence stained for the checkpoint protein BUBR1 (Figure 2.34 - A, BUBR1) to determine checkpoint active kinetochores. Cells were also stained for NDC80 activity via NDC80 pS55 (Figure 2.34 - A, NDC80 pS55) as a readout for microtubule-kinetochore attachment status, as in Figure 2.3 - B. Quantification of kinetochore intensity (Methods 4.7.1.1) averaged over each cell revealed effective degradation of KNL1, and a reduction in BUBR1 levels at kinetochores (Figure 2.34 - B). This agrees with the idea that KNL1 is the major scaffold for checkpoint proteins forming precursors of the MCC at kinetochores (London et al., 2012; Musacchio, 2015; Shepperd et al., 2012; Yamagishi et al., 2012). In addition, a reduction in NDC80 pS55 was also observed (Figure 2.34 - C). This was unexpected since KNL1 is generally not thought to be a major contributor in stable microtubule attachment. However, this may be explained due to altered error correction under these conditions, as previously reported (Caldas et al., 2013). Additionally, there are reports of KNL1-microtubule binding interactions, although these are typically weaker than the robust microtubule binding mediated by the NDC80 complex (Bajaj et al., 2018; Cheeseman et al., 2006).

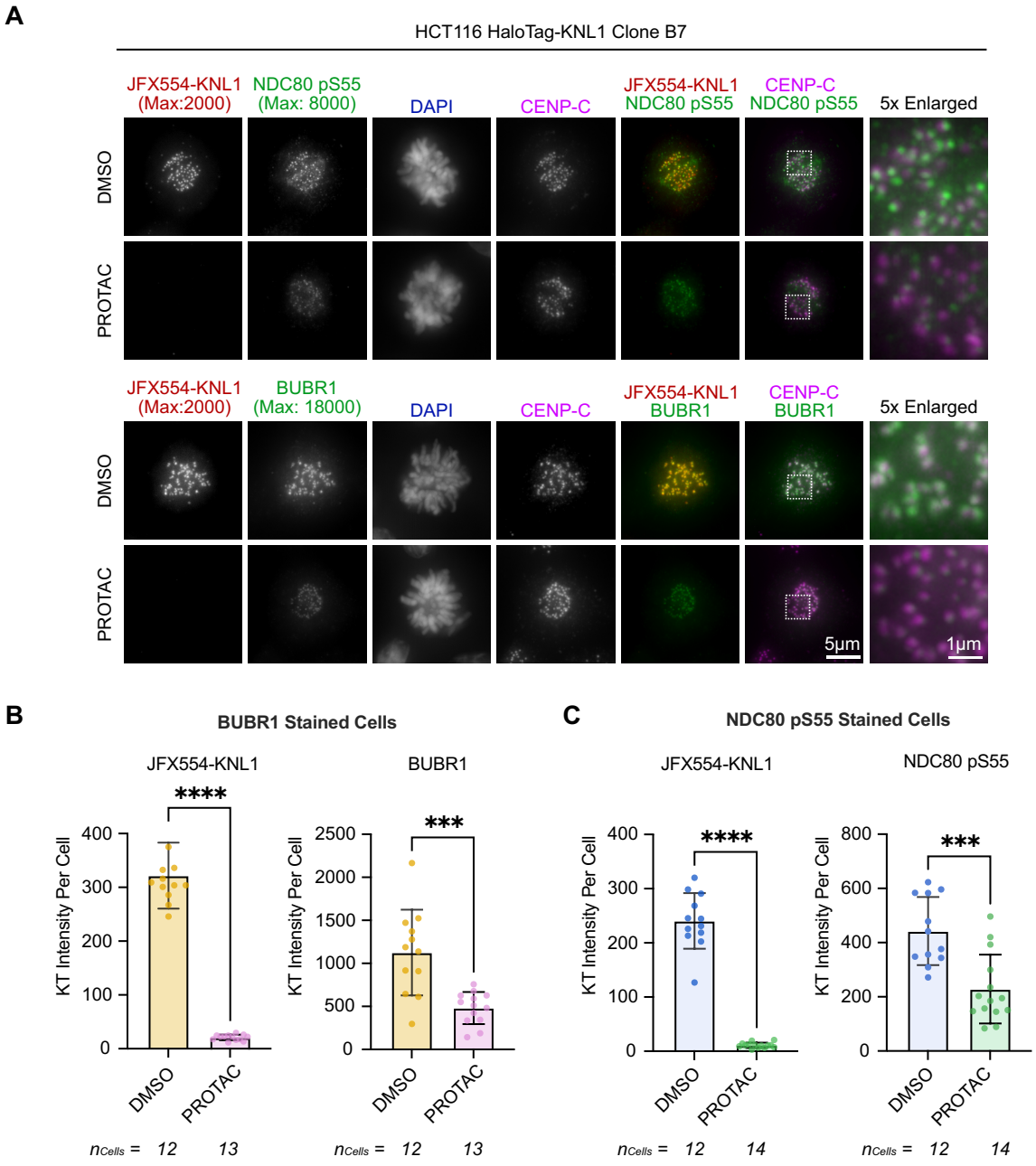

Figure 2. 34 - Degradation of KNL1 reduces NDC80 pS55 and BUBR1 levels at kinetochores

(A) Asynchronous HCT116 HaloTag-KNL1 cells were incubated with either DMSO or 300 nM Halo-PROTAC for 2.5 hours. Cells were then treated with 100 nM JFX554 for 15 minutes and then fixed with ice-cold methanol for 5 minutes. Cells were then immunofluorescence stained with antibodies for NDC80 pS55, BUBR1 and CENPC. Chromatin was visualised using DAPI. (B-C) Intensities per kinetochore of JFX554-KNL1 and either (B) BUBR1, or (C) NDC80 pS55 were determined using a custom Fiji macro (Methods 4.7.1.1) and averaged per cell. Bar graphs with mean ± SD shown; sample number indicated in the figure. Unpaired two-tailed t-tests were used for statistical analysis, with P<0.0001 (****) or P=0.0002 (***).

2.3. Investigation of the Chromosome Passenger Complex protein INCENP

2.3.1. Integration of a synthetic HaloTag into endogenous INCENP

With NDC80 and KNL1 HaloTag lines established, the focus next turned to the chromosome passenger complex scaffold INCENP, responsible for bringing the Aurora B kinase into proximity to kinetochores. Aurora B promotes the retention of MPS1 at unattached kinetochores, thereby supporting subsequent checkpoint activity (Carmena et al., 2012; Saurin et al., 2011). To probe its upstream role in mediating this Aurora B interaction, INCENP was fused with a HaloTag. PCR of the endogenous INCENP locus revealed an increase in approximately 1kb for all clones tested relative to wild-type HCT116 cells (Figure 2.35 - A). Immunoblotting of INCENP-HaloTag clones ± Halo-PROTAC revealed both a change in electrophoretic mobility of INCENP and efficient depletion upon Halo-PROTAC addition (Figure 2.35 - B). HaloTag immunoblots paralleled INCENP results; a positive HaloTag band was seen for all clones tested, degrading with addition of Halo-PROTAC (Figure 2.35 - B). Additionally, phosphorylation of Aurora B at threonine 232 was reduced in the absence of INCENP for all four clones tested, consistent with the reported role of INCENP in activating Aurora B (Xu et al., 2009). Mitotic chromosome spreads were performed for INCENP-HaloTag clone g2F2, revealing pericentric localisation of INCENP, consistent with previous reports (Klein et al., 2006; Samejima et al., 2015) (Figure 2.35 - C).

With pericentric localisation of INCENP-HaloTag confirmed, the next step was to examine co-localisation with the other CPC components. Asynchronous HCT116 wild type and INCENP-HaloTag clone g2F2 cells were treated with JFX554 to visualise INCENP-HaloTag and immunofluorescence stained with antibodies for Survivin and Borealin (Figure 2.36 - A), and separately for INCENP and Aurora B (Figure 2.36 - B). A positive INCENP-JFX554 signal was observed only in HaloTag cells, which colocalised with Survivin and Borealin. Additionally, colocalization was seen against INCENP antibody and Aurora B in both metaphase and anaphase cells.

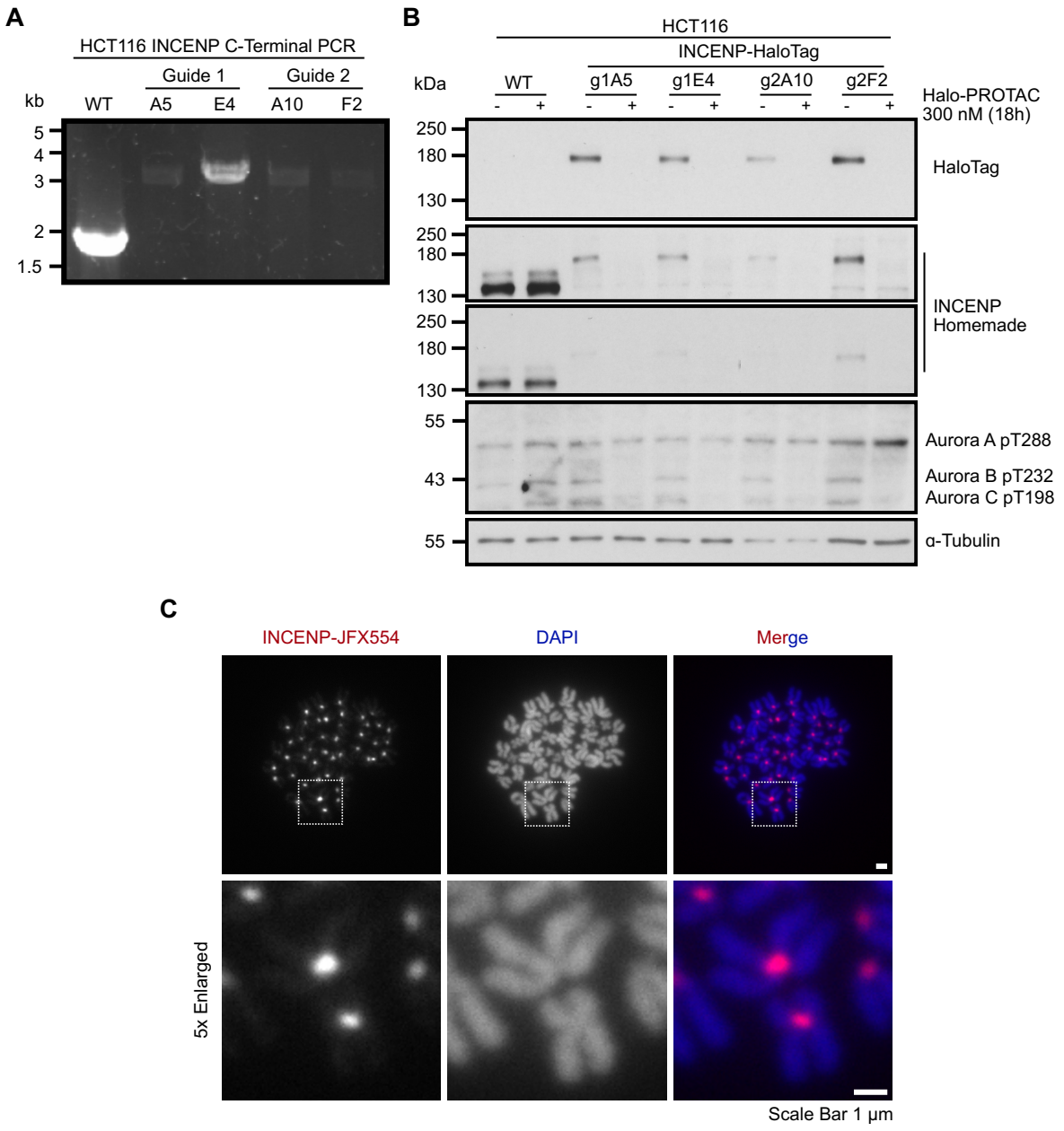

Figure 2. 35 - Generation and characterisation of INCENP-HaloTag HCT116 cell lines

A) PCR of the C-Terminus of INCENP with genomic DNA extracted from HCT116 wild type and INCENP-HaloTag clone pellets; products were resolved on agarose gel. (B) Western blot of whole-cell lysates for the same cell lines as in (A), ± 300 nM Halo-PROTAC treatment for 18 hours, immunoblotting with antibodies for INCENP, HaloTag, phosphorylated Aurora kinases, and a-Tubulin. (C) A representative chromosome spread (Methods 4.6.2) highlighting INCENP-JFX554 localisation relative to chromatin (DAPI).

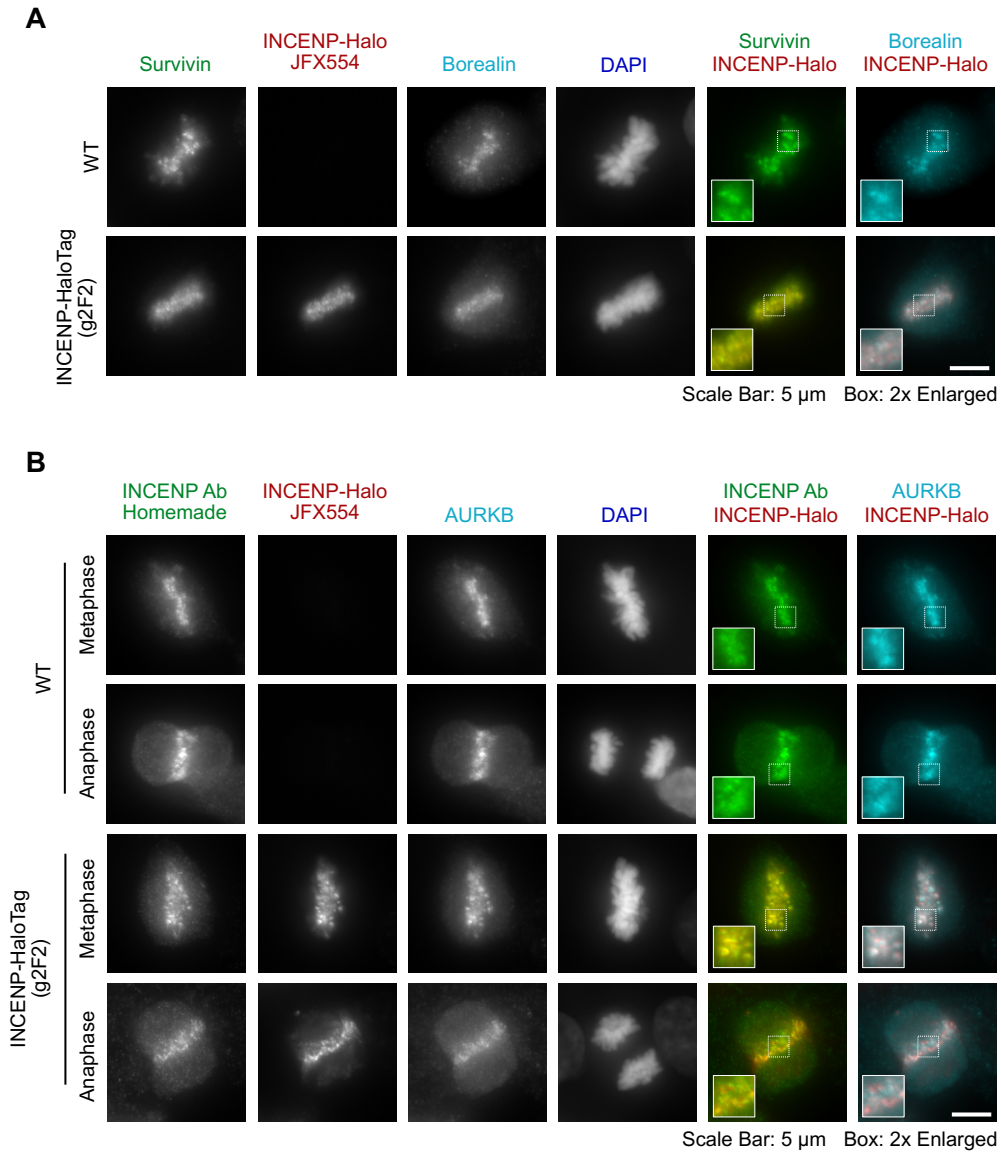

Figure 2. 36 - INCENP-HaloTag localises to the centromeres and central spindle in mitotic and anaphase HCT116 cells, respectively.

Asynchronous HCT116 wild-type or INCENP-HaloTag c.g2F2 cells were incubated with 100 nM JFX554 for 15 minutes to visualise INCENP-HaloTag, Cells were then fixed with PTEMF for 12 minutes and immunofluorescence stained with antibodies for (A) Survivin and Borealin, or (B) INCENP and Aurora B. Chromatin was visualised using DAPI. Representative metaphase and anaphase cells are shown.

To determine INCENP-HaloTag dynamics, live-cell spinning disk imaging was used. INCENP-HaloTag cells were treated with SiR-Tubulin and JFX554, enabling dual-visualisation of both α-Tubulin and INCENP, respectively (Figure 2.37). From prometaphase through to metaphase, INCENP localised to centromeres before it re-localised to the central spindle at anaphase onset, consistent with previous literature (Carmena et al., 2012).

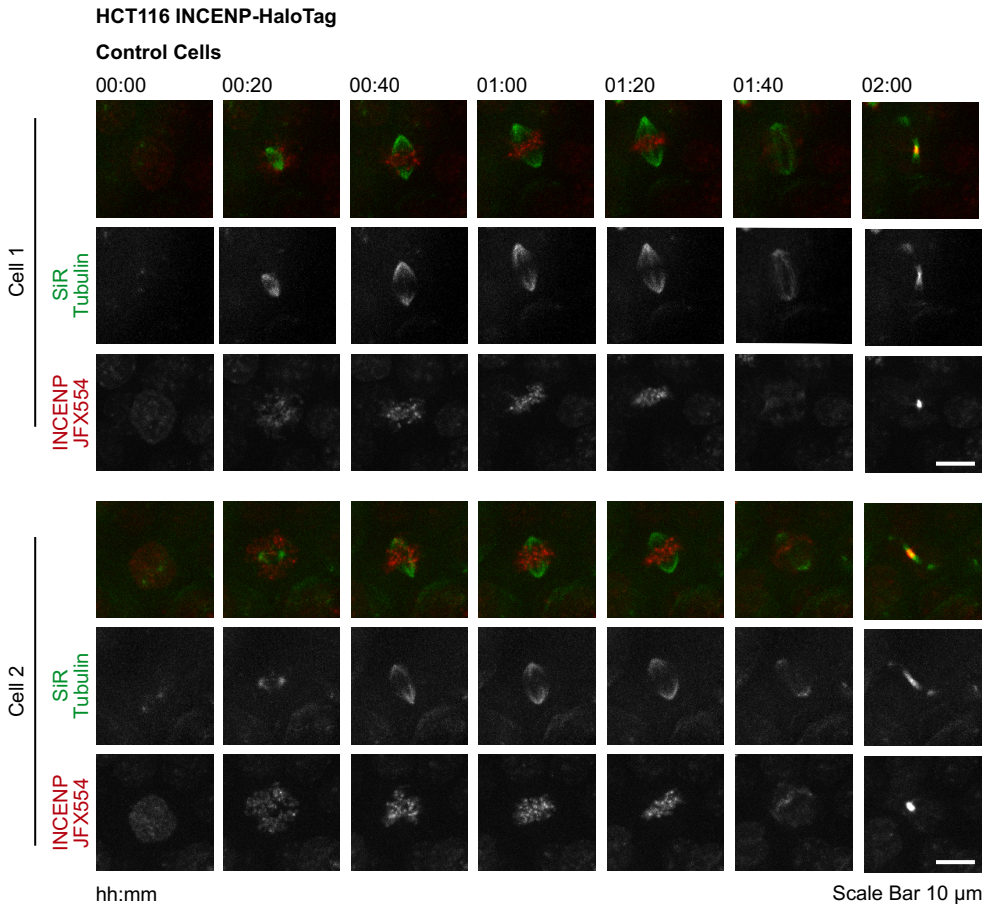

Figure 2. 37 - Live-cell imaging confirms INCENP-HaloTag localises to the centromeres and central spindle in mitotic and anaphase HCT116 cells, respectively.

HCT116 INCENP-HaloTag cells were labelled with 50 nM SiR-Tubulin (α-Tubulin) for 3 hours and 100 nM JFX554 (INCENP) for 15 minutes. Excess JFX554 was washed out in SiR-Tubulin containing media before imaging. Cells were imaged every 10 minutes in far-red, red, and bright-field channels on a spinning disk; two example cells are shown with frame every 20 minutes.

Without INCENP acting as a scaffold for Aurora B and the CPC, localisation of its other components has been reported to be impeded (Honda et al., 2003; Klein et al., 2006). To confirm these findings within the HCT116 INCENP-HaloTag genetic background, INCENP was depleted by Halo-PROTAC and cells stained with antibodies for Aurora B and Survivin. Consistent with previous findings, both Aurora B and Survivin failed to show any specified localisation. In addition, chromatin appeared to exhibit a prometaphase-like morphology in all cases, suggesting defects in chromosomal alignment following INCENP loss (Figure 2.38).

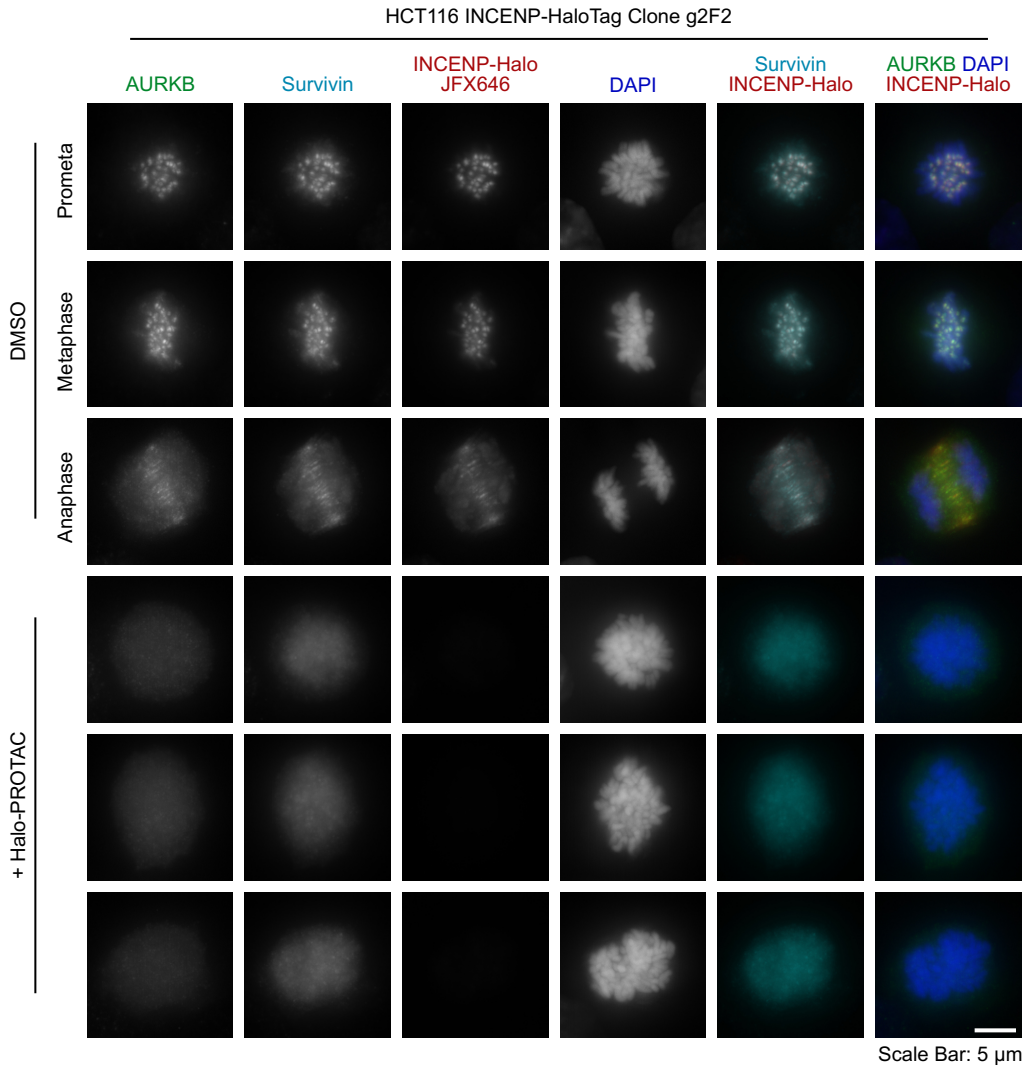

Figure 2. 38 - Degradation of INCENP disrupts inner centromere localisation of Aurora B and the other chromosome passenger complex subunits

(A-B) Asynchronous HCT116 INCENP-HaloTag cells were treated with either (A) DMSO or (B) 300 nM Halo-PROTAC for 18 hours, then arrested in mitosis using low-dose nocodazole (82.5 nM) for the final

4 hours of treatment. Cells were then treated with 100 nM JFX554 for 15 minutes to visualise INCENP, before being washed out of their mitotic arrest by removing nocodazole. 30 minutes post washout, cells were PTEMF fixed for 12 minutes, and immunofluorescence stained with antibodies for Aurora B and Survivin. Chromatin was visualised by DAPI staining. (A) Representative prometaphase, metaphase, and anaphase cells are shown. (B) Three representative Halo-PROTAC treated cells are shown.

2.3.2. INCENP degradation results in mitotic slippage

To investigate the requirement for INCENP at different stages of mitosis, HCT116 INCENP-HaloTag cells were first synchronised in G2 by CDK1 inhibition and then treated with either Halo-PROTAC to trigger INCENP degradation or DMSO as a control where INCENP remains at its normal levels. Cells were then released into mitosis, and samples collected over a 0–4-hour period to monitor key targets of mitotic progression. Depletion of INCENP was confirmed by immunoblotting with INCENP and HaloTag antibodies (Figure 2.39). In agreement with the role of INCENP to activate Aurora B, the Aurora B pT232 activating phosphorylation was strongly reduced (Figure 2.39), In contrast, the pT288 activating phosphorylation on Aurora A remained present (Figure 2.39), showing that INCENP degradation specifically affected Aurora B but not Aurora A kinase activity. The anaphase central spindle component PRC1 undergoes dephosphorylation at T481 and can be used as a marker of mitotic exit (Cundell et al., 2013). Cyclin B degradation and PRC1 pT481 dephosphorylation were not markedly altered in either INCENP depleted or control cells, implying little difference in mitotic timing (Figure 2.39). However, these are ensemble experiments on populations of cells, so small differences in timing <30 minutes would be missed.

To analyse mitotic timing on an individual cell basis, HCT116 INCENP-HaloTag cells were treated with SiR-DNA and either JFX554 (Figure 2.40 - A) or Halo-PROTAC (Figure 2.40 - B) for 3 hours before imaging. Degradation of INCENP resulted in a failure of chromosome condensation, and hence difficulty in alignment to form a clearly defined metaphase plate. This led to a higher propensity for cells to undergo a mitotic slippage phenotype (Figure 2.40

- D). These changes made it difficult to accurately assign the time at which cells entered anaphase due to the lack of chromosome segregation; this was taken at the time chromatin began to de-condense. An increase in time spent in mitosis from ~ 45 minutes to ~60 minutes was observed (Figure 2.40 - C).

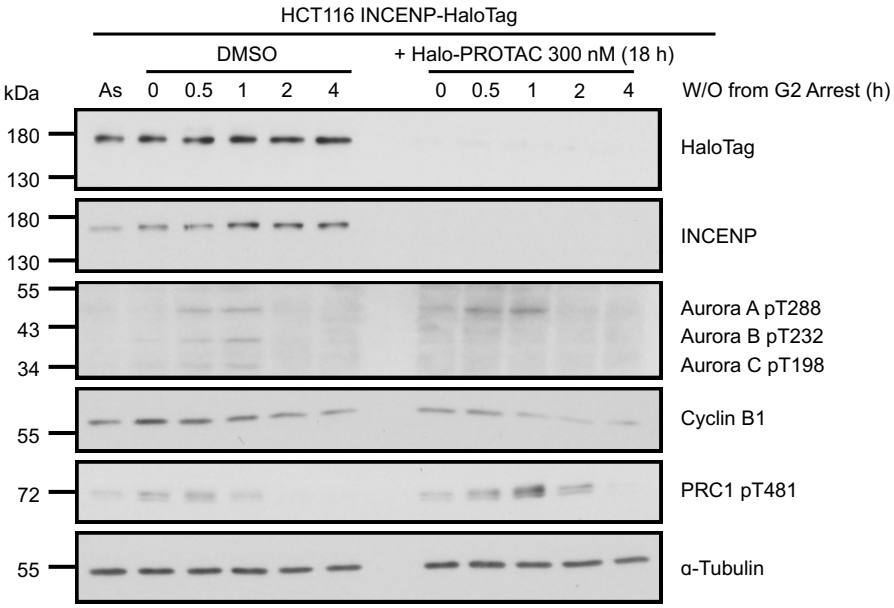

Figure 2. 39 - INCENP degradation does not result in mitotic arrest

HCT116 INCENP-HaloTag cells were arrested in G2 by 6 μM of the CDK1 inhibitor RO-3306 and treated with either DMSO or 300 nM Halo-PROTAC for 18 hours. Cells were then released from G2 by washing out the CDK1 inhibitor, and whole-cell lysates taken from 0-4 hours. A western blot was run, immunoblotting for HaloTag and INCENP to track protein depletion, cell cycle markers to determine cell cycle stage, and α-Tubulin as a loading control. An asynchronous (non-arrested/drug treated) sample was loaded on the left-most lane as a control.

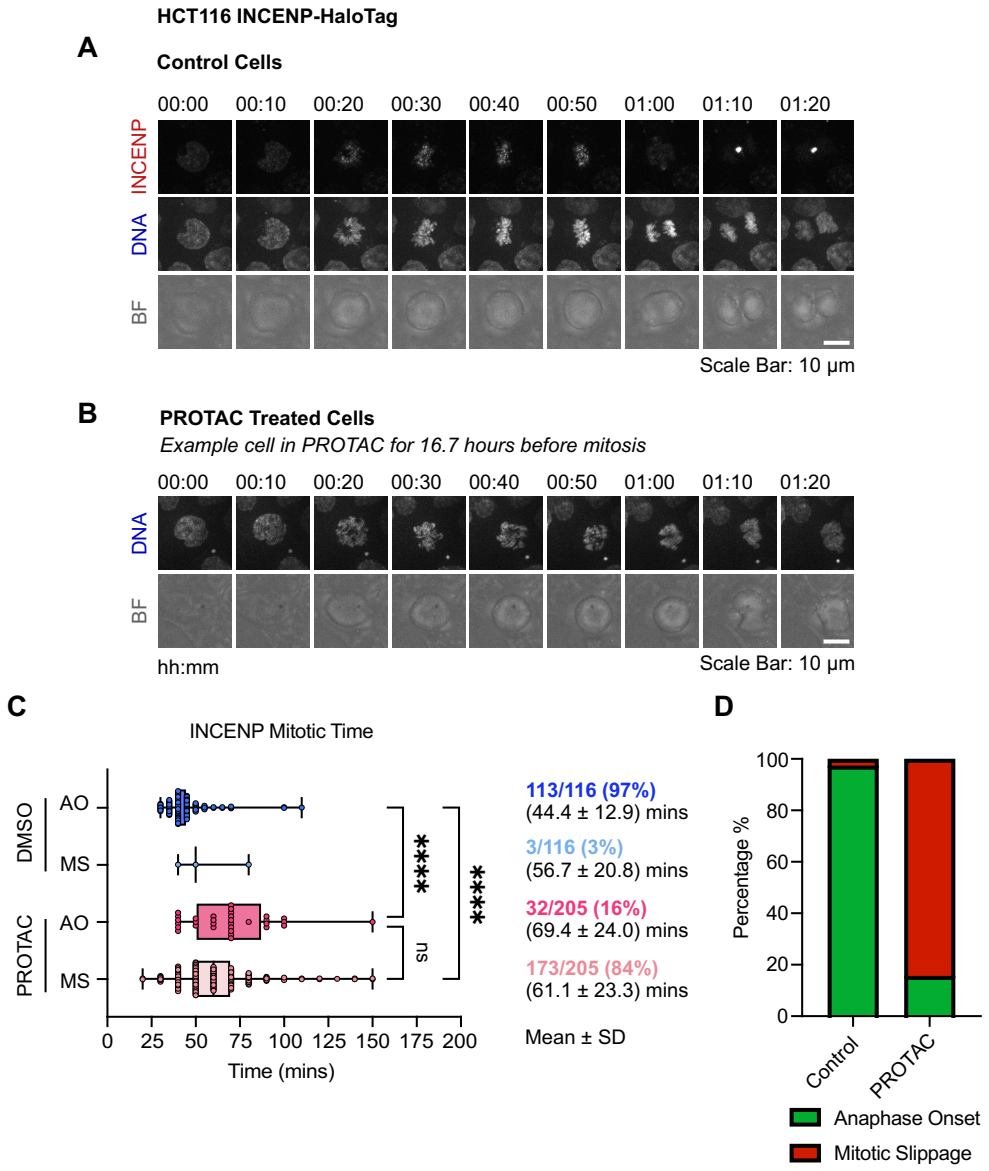

Figure 2. 40 - INCENP-HaloTag live cell imaging ± Halo-PROTAC.

(A) HCT116 INCENP-HaloTag cells were labelled with 50 nM SiR-DNA (DNA) for 3 hours, and 100 nM JFX554 (INCENP) for 15 minutes. Excess JFX554 was washed out in SiR-DNA-containing media before imaging. Cells were imaged every 10 minutes in far-red, red, and bright-field channels on a spinning disk. An example cell is shown undergoing anaphase onset. (B) Cells were treated with both 50 nM SiR-DNA and 300 nM Halo-PROTAC for 3 hours prior to imaging. Only far-red and bright field channels were imaged. A representative cell is shown undergoing mitotic slippage. (C) Quantification for time in mitosis and (D) proportion of cells undergoing AO or MS were performed the same as in Figure 2.32 A and B respectively. For (C), Brown-Forsythe and Welch ANOVA tests were used for statistical analysis with P<0.0001 (****) and P=0.9742 (ns).

2.3.3. INCENP is required for the activity of Aurora B

Given INCENP depletion directly disrupts Aurora B localisation and phosphorylation (Figure 2.38 and Figure 2.39), this provided an opportunity to effectively inhibit Aurora B kinase activity without inhibiting Aurora A, which some Aurora-specific inhibitor drugs have been reported to do over extended exposures (Girdler et al., 2006). HCT116 INCENP-HaloTag cells were synchronised in G2 using CDK1 inhibition and either treated with Halo-PROTAC to degrade INCENP or with DMSO as a control. After washout of the CDK1 inhibitor, cells were then arrested in mitosis with the proteasome inhibitor MG132, and Aurora kinase inhibitory drugs added for 10 or 30 minutes in a staged manner where required within the last 30 minutes of MG132 treatment. This approach lessened the likelihood of off-target inhibition and allowed for any synergistic or additive effects to be observed (Figure 2.41).

Western blotting confirmed successful degradation of both HaloTag and INCENP for Halo-PROTAC treated cells. For both control and Halo-PROTAC treated cells, Aurora A kinase inhibitor was successful with minimal Aurora A pT288 signal seen for these cells (Figure 2.41). For the Halo-PROTAC treated INCENP-HaloTag cells, Aurora B pT232 signal was not detectable, similar to Aurora B inhibited control cells (Figure 2.41). Crucially, total Aurora A and B signals were observed for all samples, showing that the kinases are present but catalytically inactive upon inhibition regardless of approach. In agreement with published findings (Kettenbach et al., 2011; Sobajima et al., 2023), NDC80 phosphorylation at serine 55 was only reduced where Aurora A kinase was inhibited and remained unchanged when Aurora B was inhibited and Aurora B pT232 was absent (Figure 2.41). Altered checkpoint activity could also be indirectly inferred from the loss of the Plk1-dependent BUBR1 doublet in Halo-PROTAC treated cells (Elowe et al., 2007). Finally, a large decrease in H3pS10, another target of Aurora B, was also observed for Halo-PROTAC treated cells, with this signal becoming undetectable upon Aurora B inhibition for both control and Halo-PROTAC treated cells, thus suggesting defects in chromosome condensation or individualisation (Monaco et al., 2005).

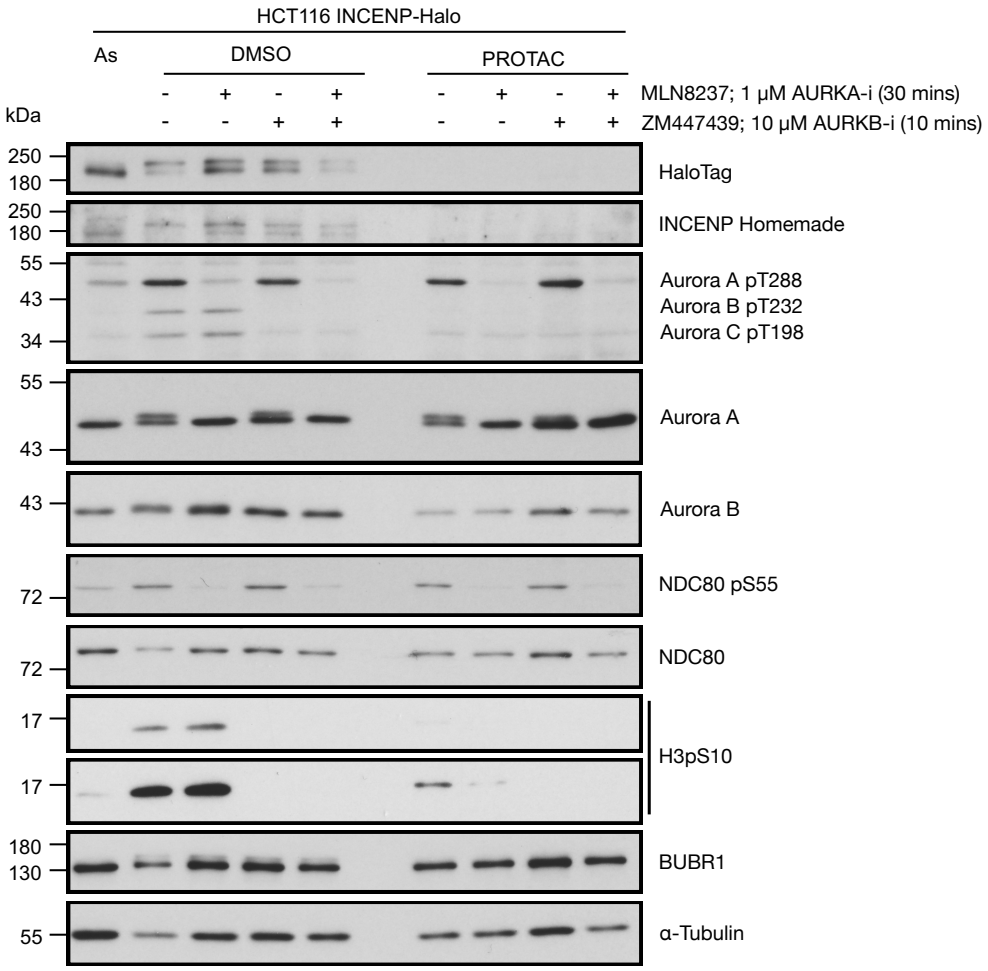

Figure 2. 41 - INCENP is required for the autophosphorylation of Aurora B and not Aurora A.

HCT116 INCENP-HaloTag cells were arrested in G2 using 6 μM CDK1 inhibitor RO-3306 and treated with either DMSO or 300 nM Halo-PROTAC for 18 hours. Cells were then released from G2 by washout of the CDK1 inhibitor into 20 μm MG132 for 3 hours to prevent anaphase onset. They were then either treated with 1 μM Aurora A-inhibitor for 30 minutes, 10 μM Aurora B-inhibitor for 10 minutes, both inhibitors (for their respective times), or no inhibitors. Whole cell lysates were analysed by western blotting, with antibodies for Aurora kinases and key Aurora kinase targets. α-Tubulin and BUBR1 were used as loading controls and to confirm cells were in mitosis, respectively.

This ensemble biochemical data showed a clear reduction in Aurora B pT232 and H3pS10, but unaltered Aurora A pT288 upon INCENP depletion. To test this for single cells, a complementary immunofluorescence microscopy approach was applied to cells treated in a similar fashion. HCT116 INCENP-HaloTag cells were arrested using a KIF11 inhibitor, resulting in a monopolar prometaphase-like state to maximise Aurora A pT288 signal and assess what affects (if any) this had in the absence of Aurora B (Figure 2.42 - A). As expected, in both cases where cells were treated with Halo-PROTAC, INCENP-JFX554 signal was diminished (Figure 2.42 - B). Additionally, Aurora A kinase inhibition reduced Aurora A pT288 signal (Figure 2.42 - C); interestingly, a slightly higher centrosomal level of Aurora A pT288 is noted for INCENP depleted cells despite no biochemical indication of change (Figure 2.41). This may suggest an altered localisation, with reduced cytosolic Aurora A pT288 and more tightly localised enrichment to the spindle pole.

In agreement with loss of H3pS10 seen by Western blotting, there was a broader spread of chromatin for Halo-PROTAC treated cells (Figure 2.42 - D), suggesting that there was less chromosome condensation. Addition of Aurora A kinase inhibitor reduced spindle size in all cases, irrespective of INCENP status, in agreement with previous reports showing that Aurora A mediates spindle size (Sobajima et al., 2023).

These data suggest that INCENP-depleted cells fail to form proper, individualised chromosomes, which may alter kinetochore accessibility. This may reduce chromatin-mediated microtubule attachments and hence reduce TPX2-dependent Aurora A localisation to spindle-associated microtubules, therefore causing Aurora A kinase activity to redistribute to centrosomes where these levels are higher. Additionally, INCENP-depleted cells lose the ability to sense incorrect tension/attachments at the kinetochore, which would affect spindle formation.

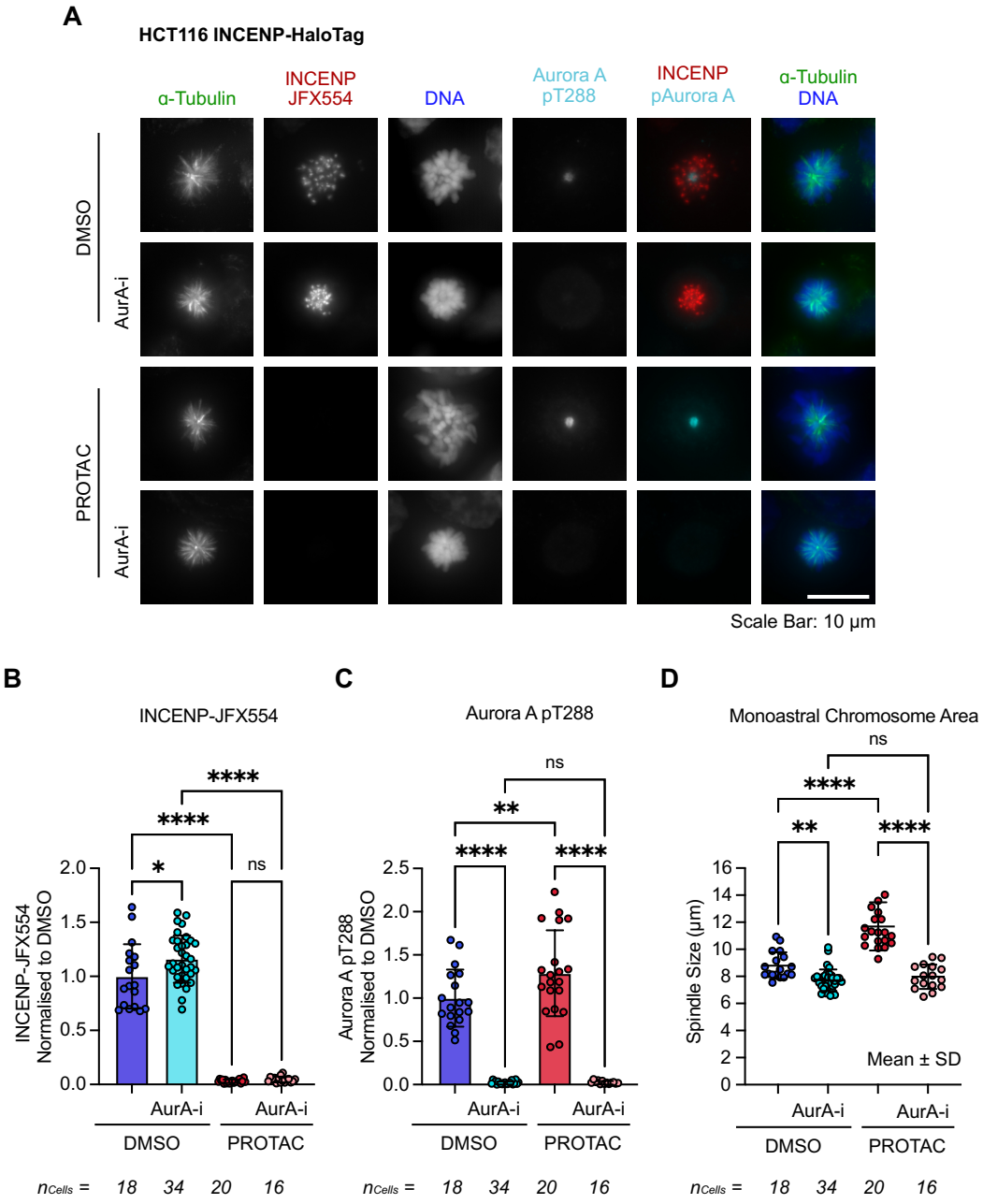

Figure 2. 42 - INCENP degradation alters the localisation of active Aurora A

(A) HCT116 INCENP-HaloTag cells were arrested in G2 using 6 µM of CDK1 inhibitor RO-3306 and treated with either DMSO or 300 nM Halo-PROTAC for 18 hours. Cells were then released from G2 by washout of the CDK1 inhibitor into 10 µM of the KIF11 inhibitor STLC for 3 hours to keep cells in a prometaphase-like state; two conditions were treated with 1 µM Aurora A inhibitor for the last 30 minutes. 100 nM JFX554 was added to all samples to visualise INCENP before HTEMF fixation for 12 minutes. Cells were then immunofluorescence stained with antibodies for α-Tubulin and Aurora A pT288. Chromatin was visualised using DAPI. Representative images are shown for all four conditions. (B) INCENP-JFX554 signal was quantified with chromatin used as a mask. (C) Aurora A pT288 signal

*was quantified using α-Tubulin-determined spindle poles as a mask. (B-C). The signal for each condition was normalised to their respective DMSO-only signal. Bar graphs with mean ± SD shown. The number of cells measured is indicated on the figure. An ordinary one-way ANOVA was used for statistical tests, with P<0.0001 (****). (B) For DMSO vs DMSO + AurA-i (P=0.0213, *) and PROTAC vs PROTAC + AurA-i (P=0.9983, ns). (C) For DMSO vs PROTAC (P=0.0087, **) and DMSO + AurA-i vs PROTAC + AurA-i (P=0.9998, ns). (D) Spindle size was determined by measuring a circular diameter inclusive of chromatin content. . Bar graphs with mean ± SD shown. The number of cells measured is indicated on the figure. An ordinary one-way ANOVA was used for statistical tests, with P<0.0001 (****). For DMSO vs DMSO + AurA-i (P=0.0066, **) and DMSO + AurAi vs PROTAC + AurAi (P=0.9915, ns).*

2.4. A combinatorial approach to investigate spindle assembly checkpoint activity dependence on NDC80, KNL1 and INCENP

2.4.1. Confirming endogenous protein interactions via immunoprecipitation

NDC80, KNL1 and INCENP although all required for normal chromosome segregation, play unique roles in the chromosome structure, alignment, and checkpoint signalling processes. The three stably integrated HaloTag cell lines generated to study endogenous NDC80, KNL1, and INCENP enabled more detailed investigation of these functions. To achieve this, all cell lines were simultaneously tested to further probe loss of function phenotypes after rapid PROTAC-mediated degradation. First, immunoprecipitation was performed using Halo nanobody beads to isolate the respective protein complexes and confirm the expected pattern of interactions (Methods 4.4.3). Immunoprecipitations for NDC80 and KNL1 were performed independently of previous experiments (Figures 2.3 and 2.30) to ensure identical experimental conditions and allow for direct comparison between the three lines.

Cells were arrested in mitosis to ensure all proteins were correctly localised to the kinetochore and centromere region of chromosomes, as already shown. HaloTag Western blots confirmed successful pulldown of each respective HaloTag-modified protein, although some proteolysis was noted. NDC80-HaloTag immunoprecipitated strongly with NUF2, as well as a lesser amounts of KNL1 complex proteins (KNL1, ZWINT - Figure 2.43). HaloTag-KNL1 was isolated together with ZWINT (Figure 2.43), consistent with its established complex (Caldas & DeLuca, 2013). INCENP-HaloTag was isolated together with Aurora B and Survivin; two key components of the CPC (Figure 2.43). Technical issues prevented direct INCENP detection by immunoblot. SGO1 and markers for pericentromeric nucleosomes H3pT3 and H3pS10 which the CPC is known to bind (Abad et al., 2022; Serena et al., 2020) were not observed to co-precipitate with the CPC under these conditions and remained in the unbound fraction (Figure 2.43). This may reflect the use of DNA digestive enzymes or the specific lysis buffer composition, which could interfere with the CPC-chromatin interaction.

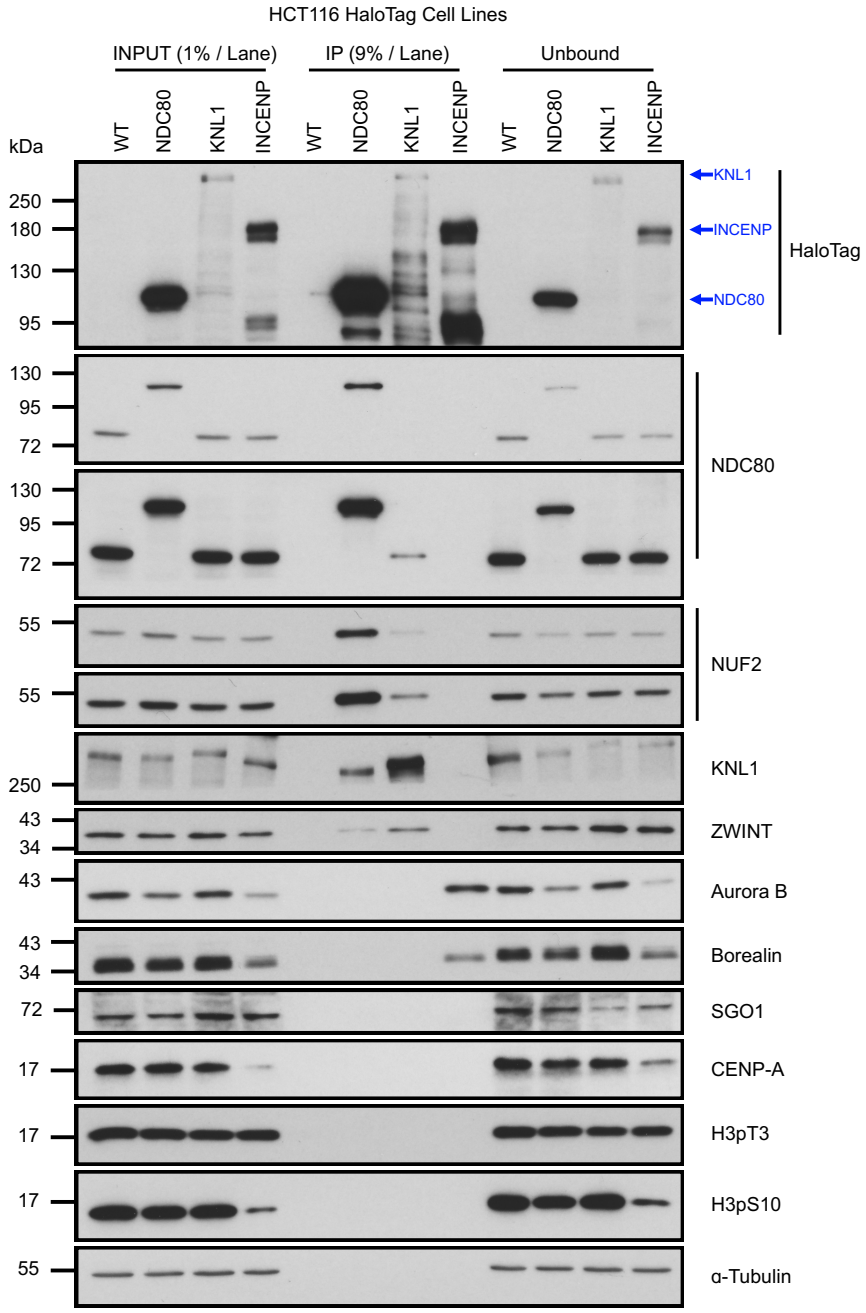

Figure 2. 43 - Analysis of NDC80, KNL1, & INCENP HaloTag complexes using immunoprecipitation and western blotting

HCT116 wild-type, NDC80-HaloTag, HaloTag-KNL1 and INCENP-HaloTag cells were arrested in 10 μM of the KIF11 inhibitor STLC and incubated with HaloTag nanobody beads for immunoprecipitation (IP) (Methods 4.4.3). Input, bead-bound (IP) and unbound lysates were taken and analysed on a western blot. Immunoblotting was performed for antibodies against HaloTag, NDC80, NUF2, KNL1, ZWINT, CPC components and known Aurora B interactors to confirm protein interactions.

2.4.2. Degradation of NDC80, KNL1 or INCENP results in increased genomic instability and cell proliferation defects

Growth assays were then performed to determine the effects on proliferation upon loss of each protein (Figure 2.44 - A). As previously described for NDC80, cells failed to proliferate upon its degradation (Figure 2.12 - C). Similar reductions in cell proliferation were observed after KNL1 and INCENP degradation, suggesting that all three proteins are necessary for sustained cell growth (Figure 2.44 - B).

To compare the morphological consequences of NDC80, KNL1 and INCENP degradation (as performed in Figure 2.25 for NDC80), cells were treated with Halo-PROTAC for 3 days and then stained for chromatin (DAPI), nuclear lamina (Lamin B1) and microtubule architecture (α-Tubulin) to assess cell morphology. Consistent with previous determination, loss of NDC80 resulted in altered nuclear shape and nuclear lamin B1 disorganisation (Figure 2.44 - C, NDC80-Halo). Because the chromosomes cannot attach to microtubules in the absence of NDC80, they remain as a large unsegregated mass. KNL1-deficient cells had small lamin B1-positive micronuclei structures outside the main nucleus (Figure 2.44 - C, Halo-KNL1), suggesting the cells exit mitosis before all chromosomes are captured on the mitotic spindle. INCENP-deficient cells suffered more severe nuclear fragmentation with each fragment wrapped by lamin B1 rather than a single defined nucleus seen in control cells or the micronuclei seen after KNL1 degradation (Figure 2.44 - C, INCENP-Halo). The increased severity of the INCENP phenotypes fits with the notion that Aurora B is required to promote mitotic chromosome condensation as well as spindle checkpoint signalling and chromosome segregation during mitosis. By contrast, NDC80 and KNL1 are necessary for accurate chromosome segregation and checkpoint activity, respectively, but do not contribute to chromosome structure (J. G. DeLuca et al., 2006b; Krenn & Musacchio, 2015; Primorac et al., 2013).

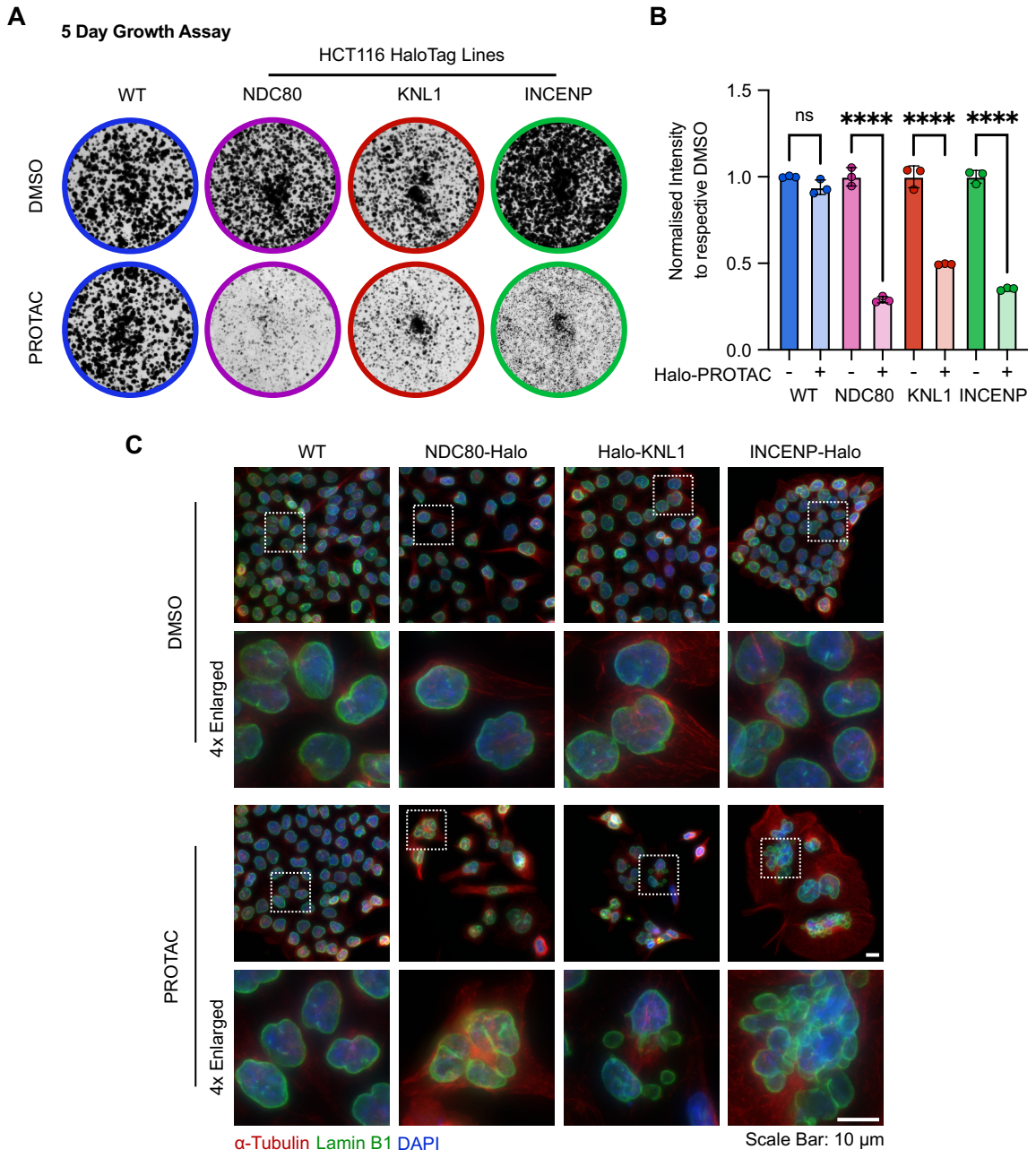

Figure 2. 44 - Degradation of NDC80, KNL1 or INCENP affects cell growth and genome stability

(A) Wild-type HCT116, NDC80-HaloTag, HaloTag-KNL1 or INCENP-HaloTag cells were grown for two days, then treated with either DMSO or 300 nM Halo-PROTAC for a further five days. Cells were then fixed and stained with crystal violet for 30 minutes. (B) Cell growth was determined by densitometry in Fiji. Each cell line intensity was normalised to its respective DMSO control (n=3; bar graph with mean ± SD shown). An ordinary one-way ANOVA was used for statistical tests, with P<0.0001 (****) and P=0.0560 (ns). (C) The same cell lines were grown for two days and then treated with DMSO or 300 nM Halo-PROTAC for a further three days. Cells were then PTEMF for 12 minutes and stained with antibodies for α-Tubulin and Lamin B1. Chromatin was visualised using DAPI.

2.4.3. Generation of BUB1 and MPS1-mStaygold lines to track spindle assembly checkpoint activity after targeted outer kinetochore disruption

To more accurately track SAC function, the spindle checkpoint proteins MPS1 and BUB1 were CRISPR/Cas9 tagged with mStayGold (Ivorra-Molla et al., 2023) in the NDC80, KNL1 and INCENP HaloTag cell lines. This allowed for investigation of their activity in both fixed and living cells. NDC80-HaloTag and INCENP-HaloTag cells lines were generated with MPS1-mStayGold or BUB1-mStayGold, and a HaloTag-KNL1 cell line was created with BUB1-mStayGold. Successful tag integration was determined by Western blotting (Figure 2.45). In all cases, both MPS1 and BUB1 showed a change in electrophoretic mobility when tagged. For BUB1-mStayGold NDC80 and KNL1 lines, heterozygous clones were achieved, as only one allele was altered whilst the other remained at the endogenous molecular weight. For all cell lines, Halo-PROTAC was added to one sample to show successful depletion of the expected HaloTag protein, whilst the mStayGold-tagged protein remained unchanged (Figure 2.45). Interestingly, a PTM band was observed for INCENP under NDC80 depletion for both BUB1 and MPS1 lines, potentially showing sustained INCENP/Aurora B activity due to the prolonged mitosis phenotype.

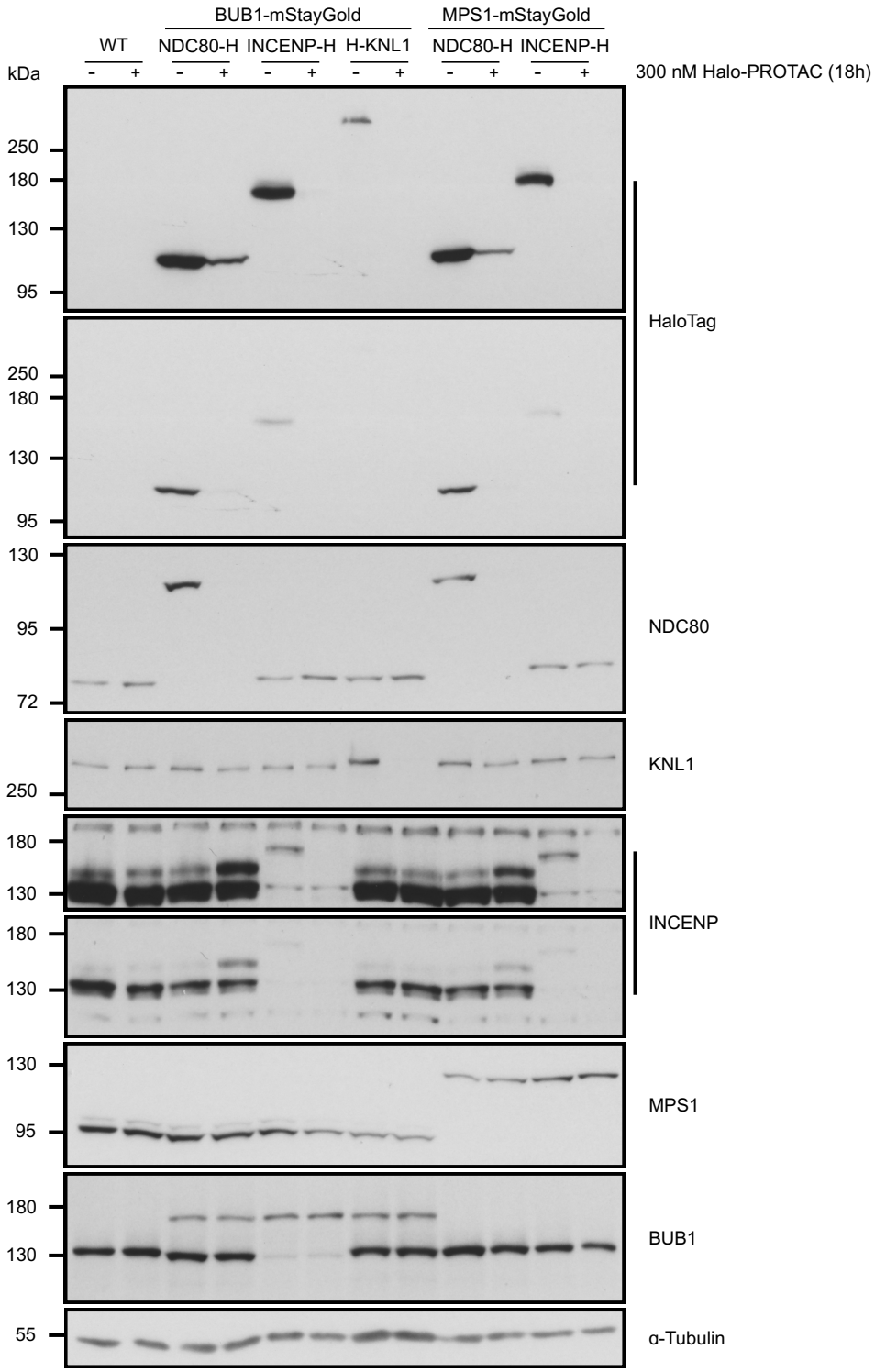

Figure 2. 45 - Generation of BUB1 or MPS1-mStayGold lines in HaloTag HCT116 cells

HCT116 wild-type, NDC80-HaloTag BUB1-mSg, INCENP-HaloTag BUB1-mSg, HaloTag-KNL1 BUB1-mSg, NDC80-HaloTag MPS1-mSg and INCENP-HaloTag MPS1-mSg cells were treated with DMSO or 300 nM Halo-PROTAC for 18 hours. Whole-cell lysates were then run on a western blot. Immunoblotting was performed with antibodies for HaloTag, NDC80, KNL1 and INCENP to check for non-impeded Halo-PROTAC depletion, and BUB1 and MPS1 to check successful tag integration.

With checkpoint marker tag integration confirmed by western blot, live-cell imaging was performed to monitor checkpoint activity for both control conditions and after degradation of NDC80, KNL1 or INCENP. Initially, NDC80-HaloTag MPS1-mStayGold cells were imaged either under control conditions, treating cells with SiR-DNA and JFX554 (Figure 2.46 - A), or Halo-PROTAC and SiR-DNA (Figure 2.46 - B). For control cells (Figure 2.46 - A), MPS1 recruitment was seen as NDC80 re-localised to kinetochores in early prophase, consistent with previous checkpoint marker staining data (Figure 2.8, Figure 2.9). MPS1 recruitment to unattached kinetochores is transient and dynamic and is rapidly reduced once microtubule attachment and chromosome alignment have occurred (Dou et al., 2015; Howell et al., 2004). This transient nature is seen in control cells, with MPS1 signal lost as the mitotic spindle forms (Figure 2.46 - A). For Halo-PROTAC treated cells, there is no obvious MPS1 recruitment seen at prophase (Figure 2.46 - B).

MPS1 phosphorylates MELT motifs on KNL1, promoting MCC formation and inhibiting APC/C^{CDC20}, thus keeping cells in mitosis until all kinetochores are correctly attached and aligned (Musacchio, 2015; Pachis & Kops, 2018). Interestingly, cells in which NDC80 was degraded spent an extended period in mitosis from ~185 minutes for cells undergoing anaphase onset, or ~290 minutes for cells undergoing mitotic slippage (Figure 2.47 - A). The proportion of cells undergoing each fate is shown in Figure 2.47 - B. This was a surprising result since no discernible MPS1 recruitment to kinetochores above the cytosolic signal was observed during prophase for these cells, which would suggest failure of downstream checkpoint activity. However, previous data reported in this thesis have shown that both BUBR1 and MAD1 checkpoint proteins were still recruited to kinetochores after NDC80 degradation (Figure 2.19 and Figure 2.20), indicating that the SAC remained active despite compromised MPS1 recruitment. This may imply a secondary, MPS1-independent pathway for checkpoint activation, or as some previous studies have reported, that cytosolic MPS1 can under some circumstances trigger the SAC (Chen et al., 2018). In addition, the sustained SAC activity may indicate a role for NDC80 in checkpoint silencing.

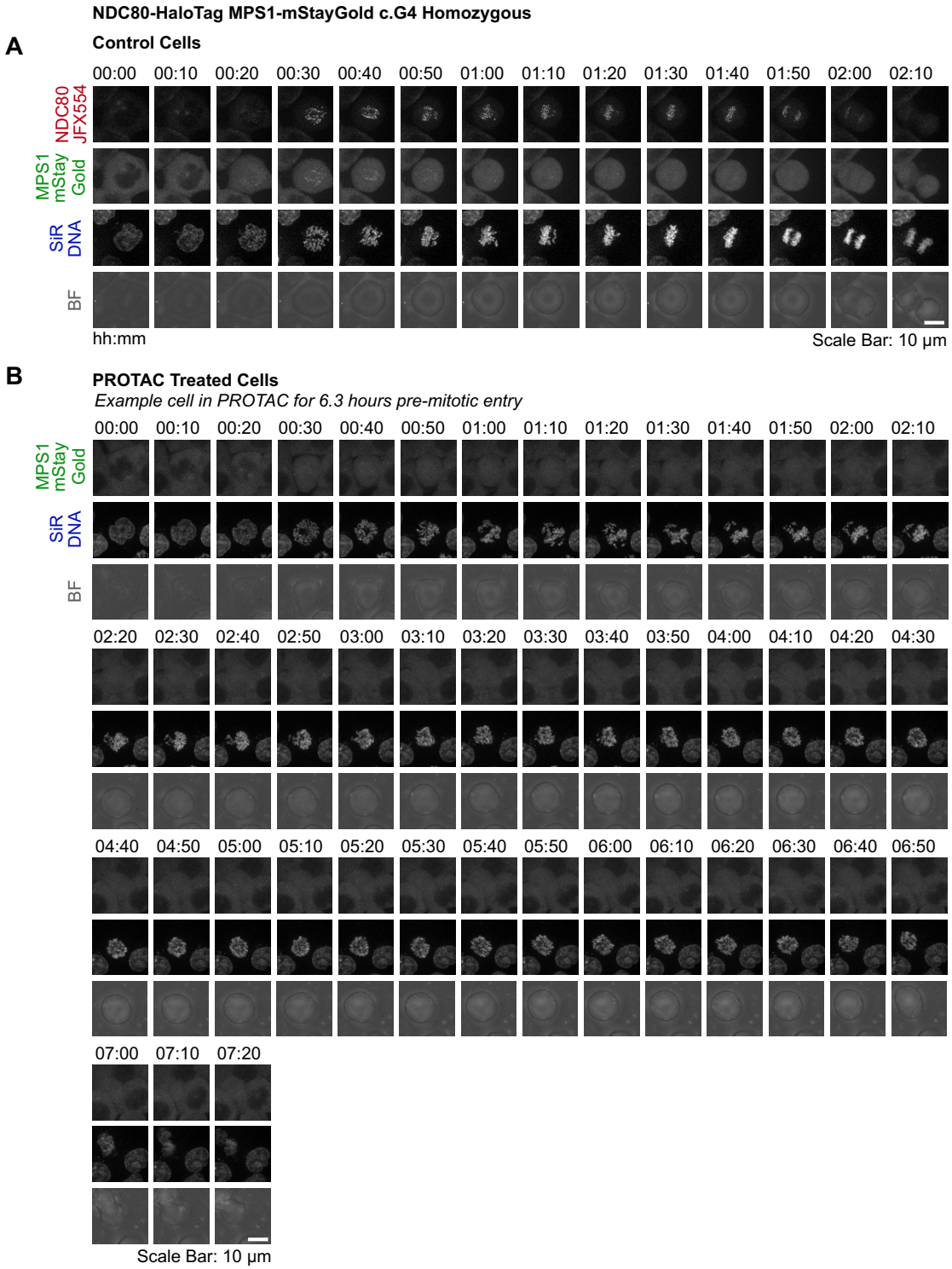

Figure 2. 46 - NDC80-HaloTag MPS1-mStayGold cells tracked over time ± Halo-PROTAC

(A) HCT116 NDC80-HaloTag MPS1-mStayGold cells were prepared the same as in Figure 2.15, and imaged every 10 minutes in far-red, red, green, and bright-field channels on a spinning disk. An example cell is shown, undergoing anaphase onset. (B) Cells were treated the same as in Figure 2.16, with only far-red, green and bright-field channels imaged.

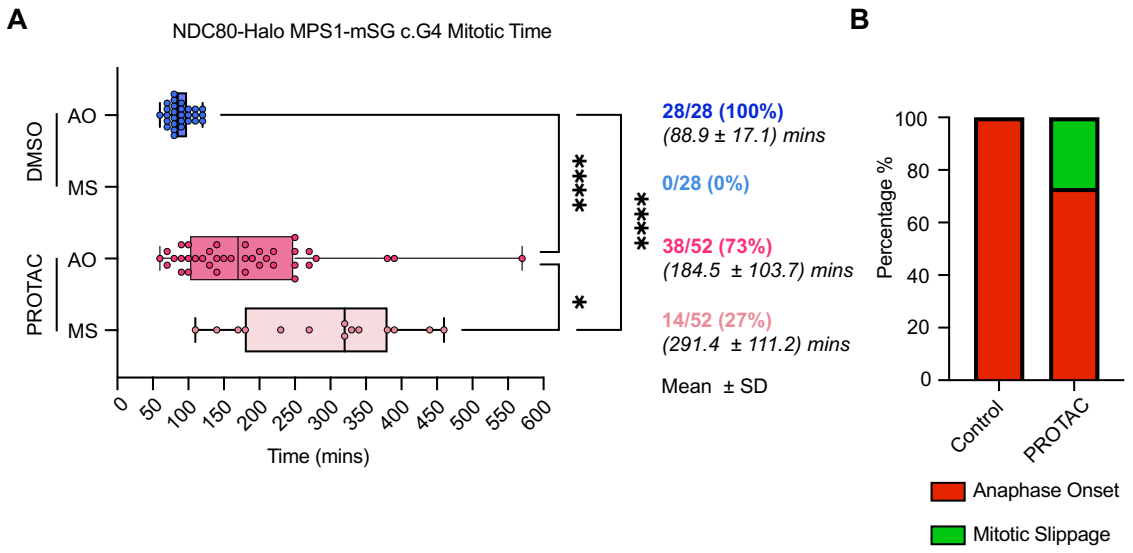

Figure 2. 47 - Tracking MPS1-mStayGold after degradation of NDC80

(A) Quantification for time in mitosis and (B) proportion of cells undergoing AO or MS were performed the same as in Figure 2.32 A and B respectively. For (A), Brown-Forsythe and Welch ANOVA tests were used for statistical analysis with P<0.0001 (****) and P=0.0143 (*).

To further explore SAC activity downstream of MPS1, the behaviour of the checkpoint protein BUB1 was followed in NDC80-HaloTag BUB1-mStayGold cells ± HaloPROTAC treatment. NDC80-HaloTag BUB1-mStayGold cells were treated either with DMSO as a control (Figure 2.48 - A) or Halo-PROTAC (Figure 2.48 - B). Labelling with JFX554 (NDC80) in control cells, and SiR-DNA (chromatin) under both conditions allowed DNA, NDC80 (control only) and BUB1 signals to be measured in real time. Initial observations of mitotic timing are consistent with previous data obtained in this thesis; NDC80 reduction resulted in an increased time in mitosis (Figure 2.49 - A). It should be noted that, for this cell line derivative, control cells appeared to spend longer in mitosis than the NDC80-HaloTag cell line (Figure 2.17 - A), and a smaller proportion of cells underwent mitotic slippage (Figure 2.49 - B).

Tracking BUB1 signal over time by measuring the integrated intensity over the whole cell (Methods 4.7.1.3) revealed a sharp rise in BUB1 signal at NEBD for control cells, which gradually dissipated as cells progressed through mitosis and chromosomes became aligned,

eventually reaching near-zero levels as cells moved into anaphase (Figure 2.49 - C, Control). For Halo-PROTAC treated cells, a similar sharp rise in BUB1 signal was also observed at NEBD, reaching around 75% of initial control cell intensity (Figure 2.49 - C, PROTAC). This signal also dissipated over time, though it took around three times longer to reach near-zero levels, corresponding to the increased mitotic timing observed (Figure 2.49 - A). Example cells at the beginning and end of an imaging acquisition are also shown (Figure 2.49 - D), indicating that the decline in signal observed was not due to photobleaching of the fluorophore.

Sustained BUB1 recruitment to kinetochores after NDC80 degradation was intriguing, since this process is downstream of MPS1 phosphorylation and the cells lack any discernible MPS1 signal at kinetochores above the cytosolic pool under these conditions (Figure 2.46 - B). One explanation is that BUB1 displays a slower turnover rate and more stable kinetochore localisation than MPS1 (Howell et al., 2004). Alternatively, this could indicate that NDC80, due to its role in mediating attachment of chromosomes to the spindle and biorientation, is in fact crucial for SAC silencing.

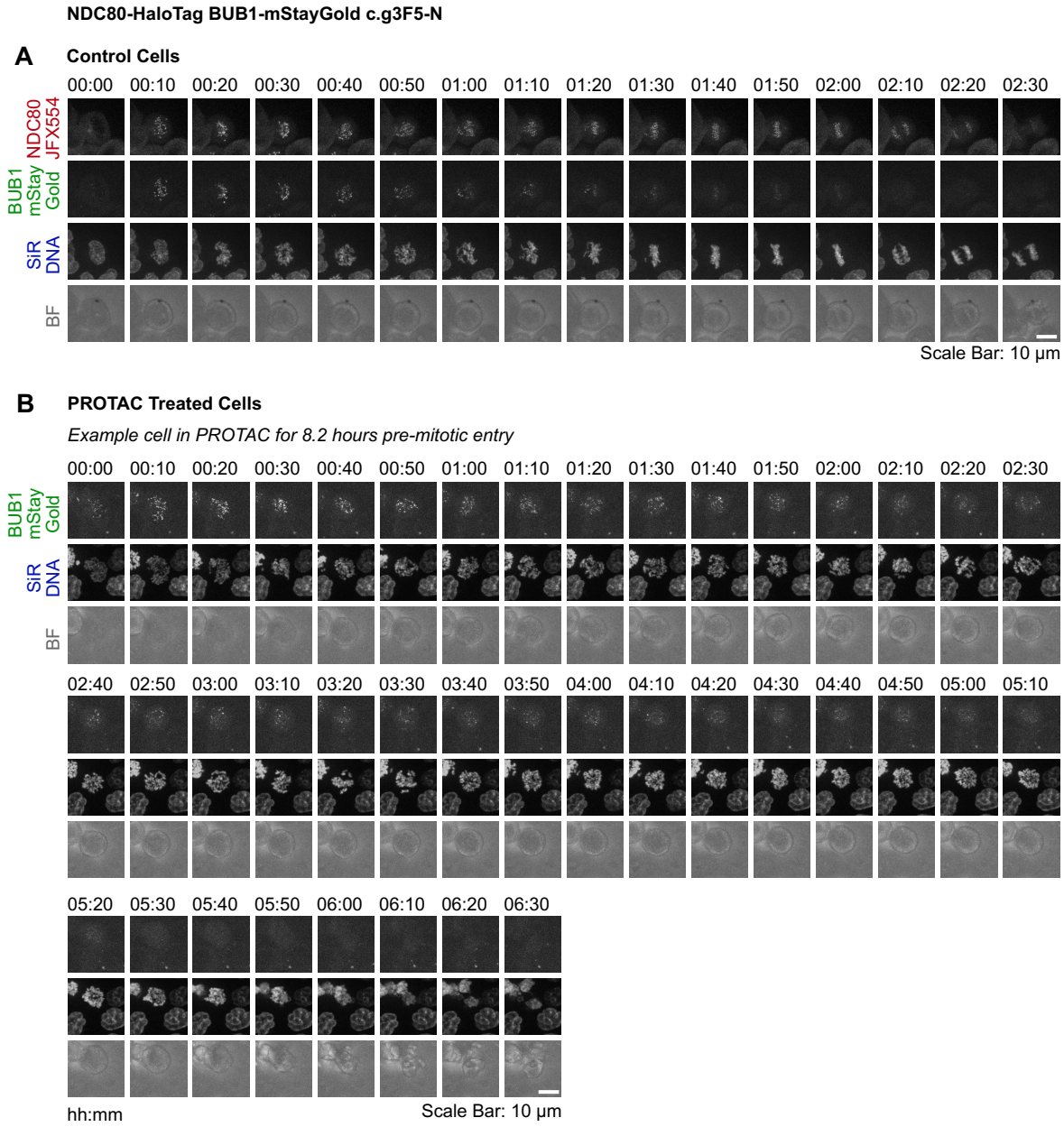

Figure 2. 48 - NDC80-HaloTag BUB1-mStayGold cells tracked over time ± Halo-PROTAC

As in Figure 2.46, except with NDC80-HaloTag BUB1-mStayGold cells.

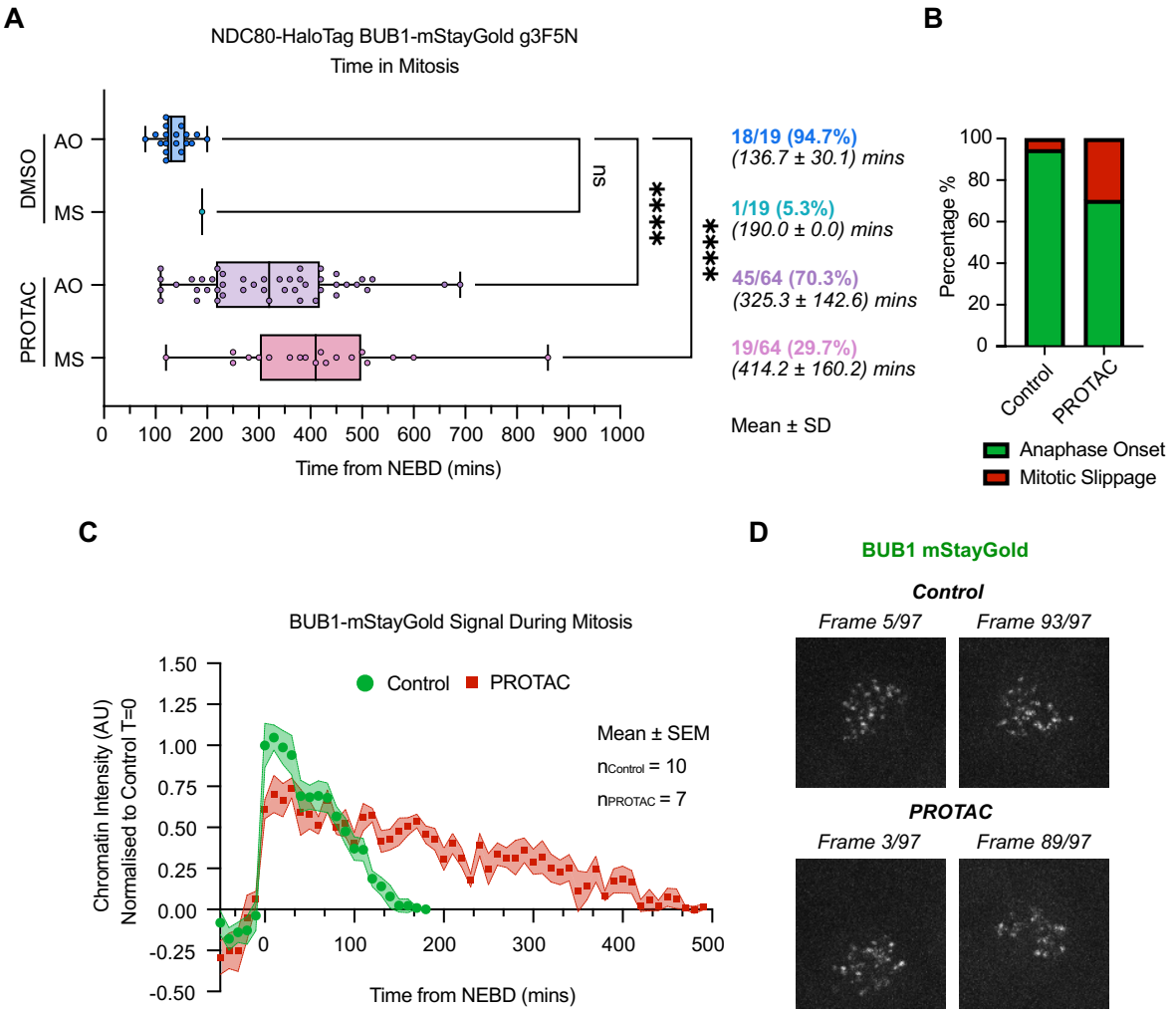

Figure 2. 49 - Tracking BUB1-mStayGold over time following the degradation of NDC80

(A-B) Quantification for time in mitosis and proportion of cells undergoing AO or MS were performed the same as in Figure 2.32 A and B respectively. For (A), An ordinary one-way ANOVA test was used for statistical analysis with P<0.0001 (****) and P=0.9716 (ns). (C) BUB1-mStayGold intensity over time was measured (Methods 4.7.1.3). All measurements were normalised to the intensity at Control T=0. Mean ± SEM values are shown. The number of cells measured are indicated in the figure. (D) Example mitotic cells at both the beginning and end of an imaging acquisition are shown for both control and Halo-PROTAC treated cells. The BUB1-mStayGold channel is shown to not bleach over extended imaging periods.

Live cell imaging was performed under the same conditions for HaloTag-KNL1 BUB1-mStayGold cells (Figure 2.50). As seen with NDC80-HaloTag BUB1-mStayGold cells, time spent in mitosis was increased for control HaloTag-KNL1 BUB1-mStayGold cells (Figure 2.51 - A) in comparison to the HaloTag-KNL1 line (Figure 2.32 - A). Nonetheless, shorter mitotic duration was observed under Halo-PROTAC addition, consistent with previous data observed in this thesis (Figure 2.51 - A). Measuring BUB1 intensity over time revealed an initial peak at NEBD which dissipated over time until anaphase onset, similar to that observed for the NDC80-HaloTag cell line (Figure 2.51 - C, Control). BUB1 recruitment was strongly reduced in Halo-PROTAC treated HaloTag-KNL1 cells (Figure 2.50 - B and 2.51 - C, PROTAC), consistent with the notion the KNL1 helps to recruit BUB1 to kinetochores. Nearly all control and Halo-PROTAC treated cells underwent anaphase onset (Figure 2.51 - B).

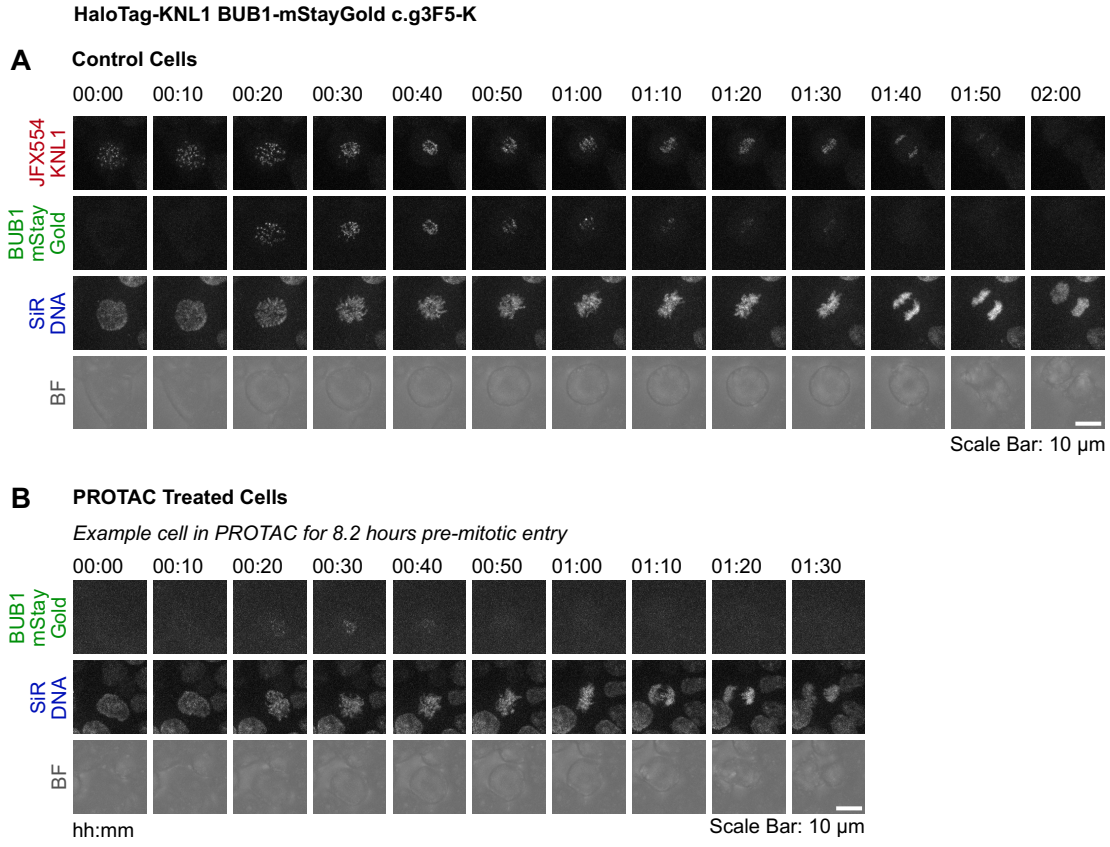

Figure 2. 50 - HaloTag-KNL1 BUB1-mStayGold cells tracked over time ± PROTAC

As in Figure 2.48, except with HaloTag-KNL1 BUB1-mStayGold cells

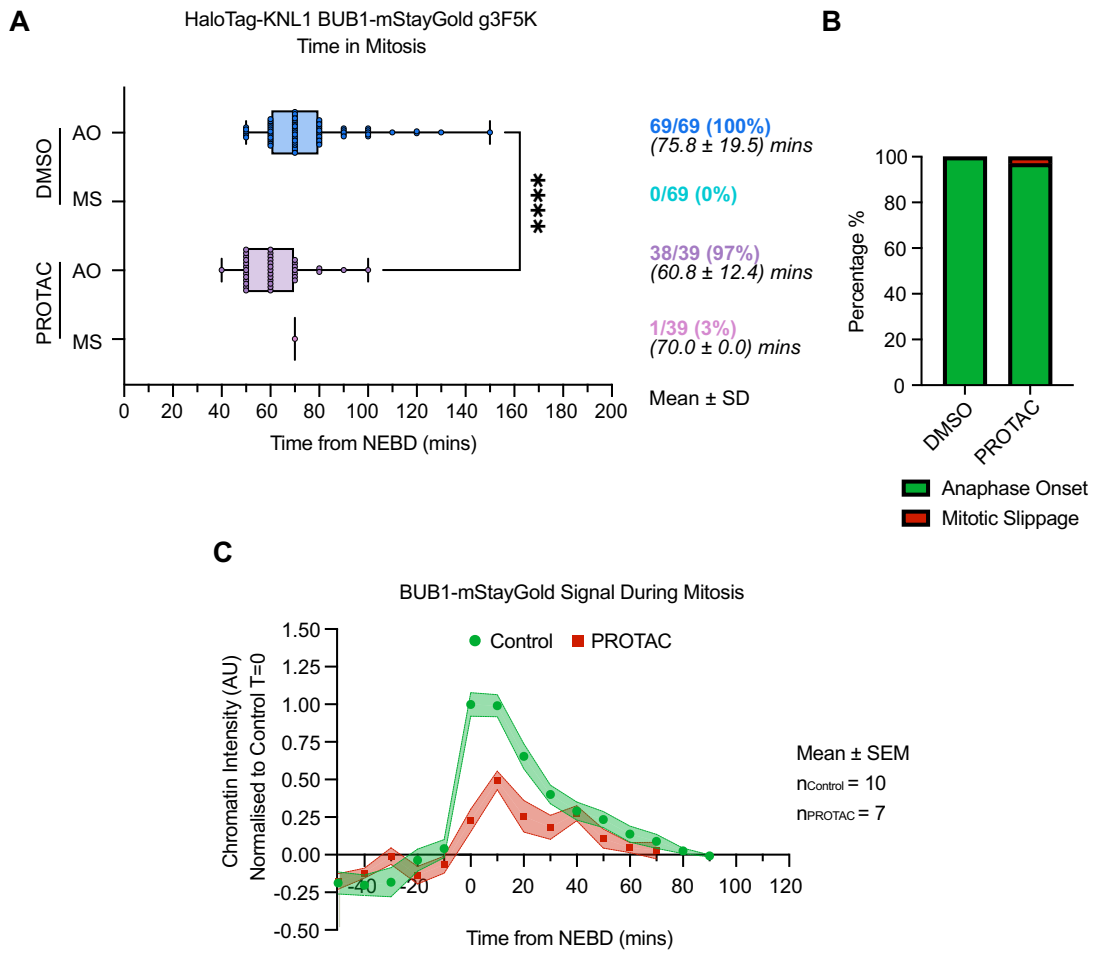

Figure 2. 51 - Tracking BUB1-mStayGold over time after the degradation of KNL1

As in Figure 2.49, except with HaloTag-KNL1 cells. For (A), An ordinary one-way ANOVA was used for statistical tests, with P<0.0001 (****).

INCENP-HaloTag BUB1-mStayGold cells were also treated under the same experimental conditions (Figure 2.52). For control cells, BUB1 intensity over time paralleled that of the other BUB1-mStayGold lines, with an initial peak observed at NEBD and a gradually degrading signal over time until anaphase onset (Figure 2.53 - C, Control). In contrast, the majority of Halo-PROTAC treated INCENP-HaloTag cells showed strongly reduced BUB1 recruitment to kinetochores (Figure 2.52 - B, Figure 2.53 - C, PROTAC) and underwent mitotic slippage (Figure 2.53 - B), indicating a SAC defect. Supporting this view, mitotic timing was shortened from 109.4 minutes in control cells to 89.6 minutes after INCENP depletion where the majority of cells undergo slippage (Figure 2.53 - A).

In summary, analysis of the checkpoint sensor kinase MPS1 and downstream checkpoint effector BUB1 reveal import differences in their behaviour. NDC80 does not appear to be essential for checkpoint activation. Instead, NDC80 degradation results in prolonged checkpoint signalling and increased time in mitosis. By contrast, degradation of KNL1 results in loss of BUB1 and reduced time in mitosis, indicative of a failure in spindle checkpoint activation. Degradation of INCENP also results in loss of BUB1, consistent with its role in spindle checkpoint activation, however due to the large-scale chromosomal defects it is difficult to draw any conclusions about timing of mitosis. Together, these findings suggest that NDC80 may be important for spindle checkpoint silencing, and that MPS1 localisation to kinetochores is not essential for spindle checkpoint under all conditions.

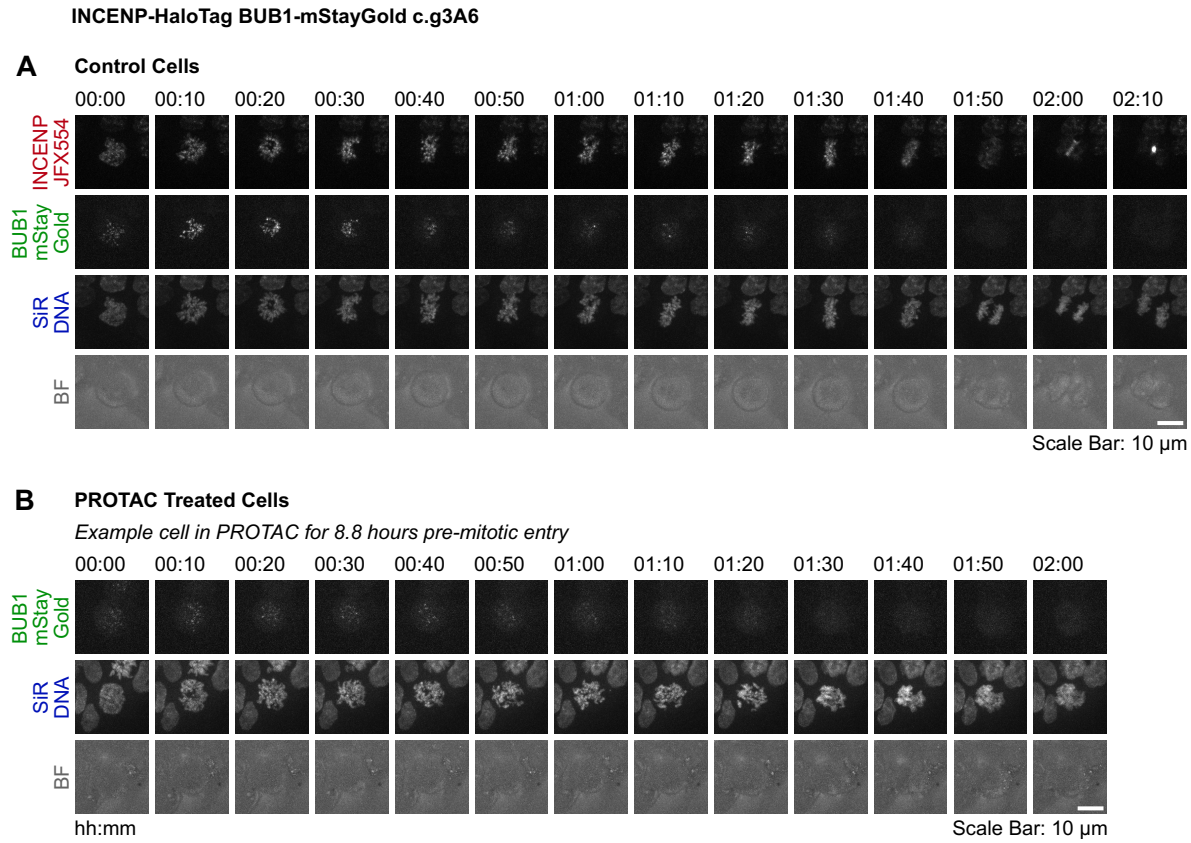

Figure 2. 52 - INCENP-HaloTag BUB1-mStayGold cells tracked over time ± Halo-PROTAC

As in Figure 2.48, except with INCENP-HaloTag BUB1-mStayGold cells.

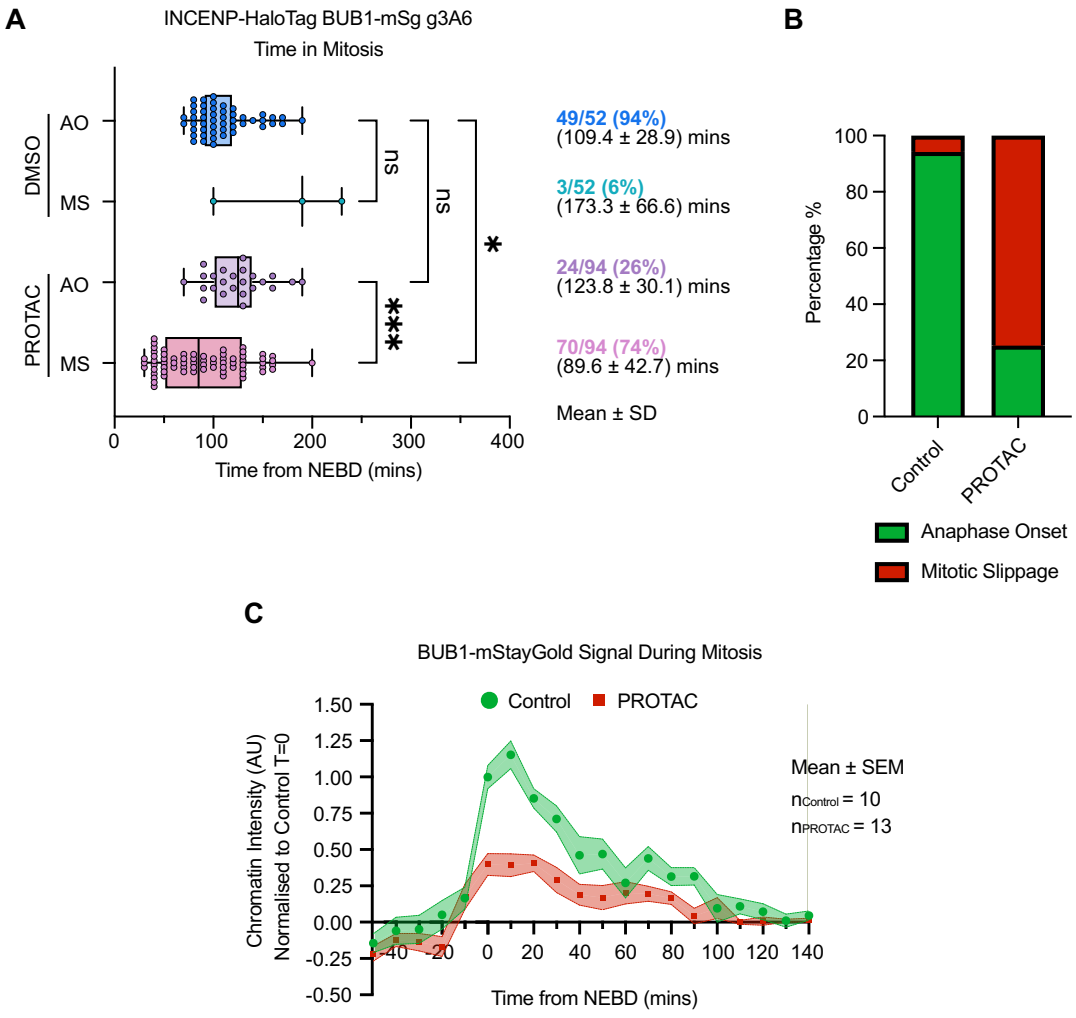

Figure 2. 53 - Tracking BUB1-mStayGold over time after the degradation of INCENP

*As in Figure 2.49, except with INCENP-HaloTag cells. For (A) Brown-Forsythe and Welch ANOVA tests were used for statistical analysis; DMSO AO vs DMSO MS (P=0.5161, ns), DMSO AO vs PROTAC AO (P=0.2102, ns), DMSO AO vs PROTAC MS (P=0.0123, *), and PROTAC AO vs PROTAC MS (P=0.0003, ***).*

2.4.4 Recruitment of BUB1 to kinetochores is reduced in the absence of NDC80, KNL1 or INCENP

Whilst live-cell imaging allows for a dynamic view of BUB1 as a readout for spindle checkpoint activity, fixed cell imaging can be used to determine individual kinetochore intensities at a higher resolution. HCT116 NDC80-HaloTag BUB1-mStayGold cells were synchronised in G2 using CDK1 inhibition and treated with either Halo-PROTAC to degrade NDC80 or DMSO as a control. Cells were released into mitosis by washout of the CDK1 inhibitor and left in fresh media for 25 minutes. Addition of high dose spindle poison nocodazole was then added to disrupt any microtubule-kinetochore binding. This allowed for the ability of NDC80-deficient cells to initiate/maintain a checkpoint response to be monitored (Figure 2.54 - A).

Measuring individual kinetochore intensity (Methods 4.7.1.1) and averaging across each cell showed successful degradation of NDC80, monitored using JFX554, to less than 3% of the level in control cells (Figure 2.54 - B, NDC80-JFX554). By contrast, the average BUB1-mStayGold signal for all kinetochores within a cell was significantly but only slightly attenuated to ~78% of the control cell signal (Figure 2.54 - B, BUB1-mStayGold). On a per-kinetochore basis, the level of BUB1 is noisy in both the control cells and following NDC80 degradation showing no obvious correlation with the efficiency of NDC80 degradation (Figure 2.54 - C). Indeed, some kinetochores were able to mount a high BUB1 checkpoint response in the absence of NDC80 at similar levels to control cells (Figure 2.54 - C).

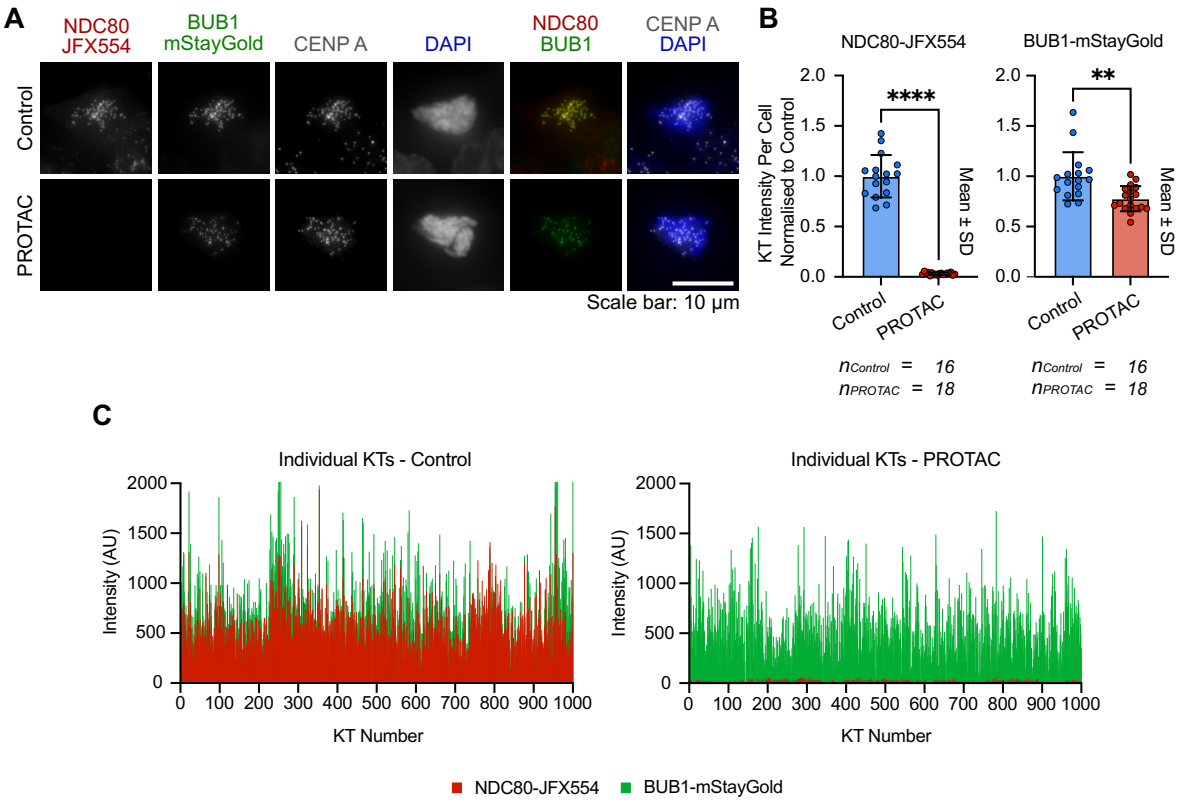

Figure 2. 54 - Determining the response of BUB1 after activation of the spindle assembly checkpoint in the presence or absence of NDC80

(A) HCT116 NDC80-HaloTag BUB1-mStayGold cells were arrested in G2 by 6 µM CDK1 inhibitor RO-3306 and treated with either DMSO or 300 nM Halo-PROTAC for 18 hours. Cells were then released from G2 by washout of the CDK1 inhibitor into fresh growth medium. In the last 15 minutes before fixation, 660 nM nocodazole was added to fully activate the spindle assembly checkpoint, and 100 nM JFX554 to label NDC80. Cells were fixed with HTEMF for 12 minutes, and immunofluorescence stained with an antibody for CENP. Chromatin was visualised using DAPI. Representative images are shown for both conditions. (B) NDC80-JFX554 and BUB1-mStayGold signals were determined on a per-kinetochore basis using a custom Fiji macro (Methods 4.7.1.1) and averaged per cell. Bar graphs with mean ± SD values shown; cell sample number indicated in the figure. Welch's t-test was used for statistical analysis, with P<0.0001 (****) and P=0.0029 (**). (C) Individual kinetochore intensity values measured in (B) plotted.

The same approach was then used to study HaloTag-KNL1 BUB1-mStayGold cells (Figure 2.55 - A). Measuring individual kinetochore intensity and averaging across each cell showed successful degradation of KNL1 monitored using JFX554 to <6 % of the level in control cells (Figure 2.55 - B, KNL1-JFX554). By contrast, the average BUB1-mStayGold signal for all kinetochores within a cell was significantly attenuated to <30% of the control cell signal (Figure 2.55 - B, BUB1-mStayGold). When considering each kinetochore individually in this cell line, measurement of BUB1 indicated KNL1-deficient kinetochores were unable to mount a strong checkpoint response (Figure 2.55 - B and C, BUB1-mStayGold). A small amount of BUB1 signal was still present at some kinetochores, although this did not correlate with the residual levels of KNL1 at single kinetochores (Figure 2.55 - C, Individual KTs - PROTAC BUB1-mStayGold).

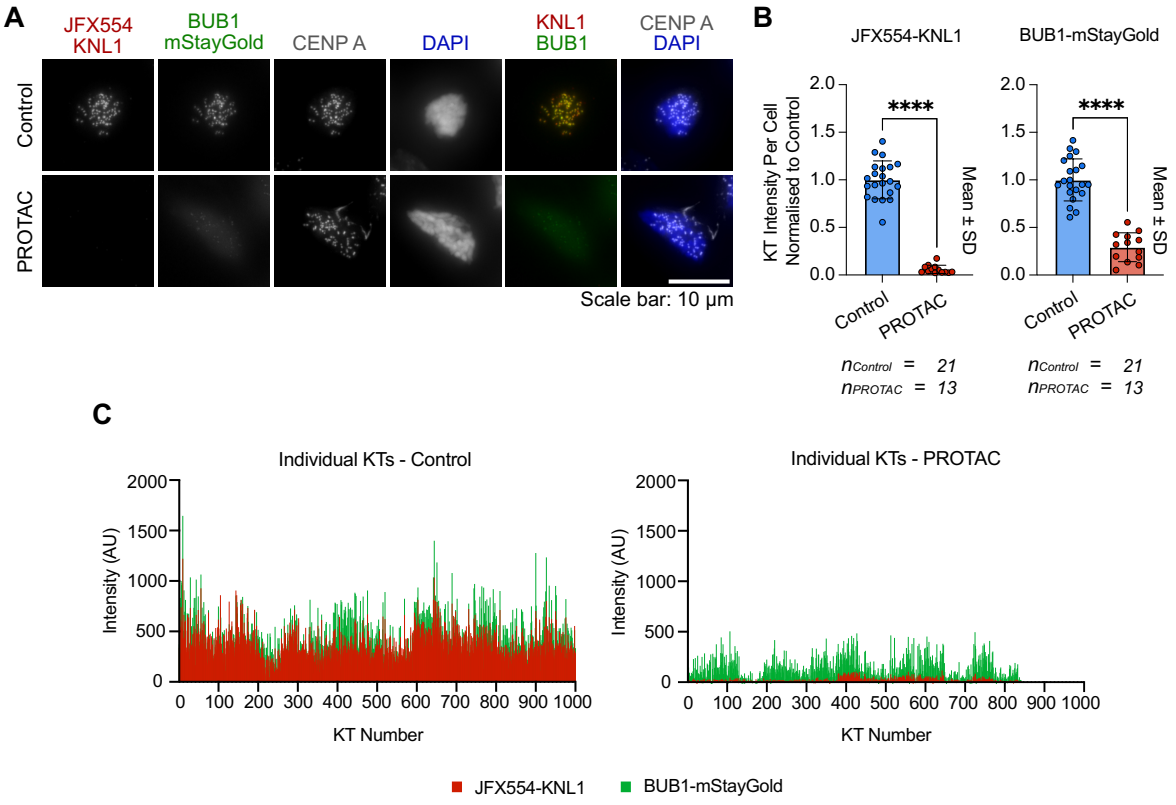

Figure 2. 55 - Determining the response of BUB1 after activation of the spindle assembly checkpoint in the presence or absence of KNL1

As in Figure 2.54, but with HaloTag-KNL1 BUB1-mStayGold cells. For (B) Welch's t-test was used for statistical analysis, with P<0.0001 (****).

For INCENP-HaloTag BUB1-mStayGold cells measuring chromatin-masked intensity across each cell showed successful degradation of INCENP monitored using JFX554 to <3 % of the level in control cells (Figure 2.56 - B, INCENP-JFX554). CENP-A staining confirmed the presence of centromeres in these cells. In contrast, the average BUB1-mStayGold signal for all kinetochores within a cell was significantly attenuated to <45% of the control cell signal after INCENP degradation (Figure 2.56 - B, BUB1-mStayGold). This robust albeit reduced BUB1 checkpoint response was still observed for the majority of individual kinetochores after INCENP degradation (Figure 2.56 - B and C).

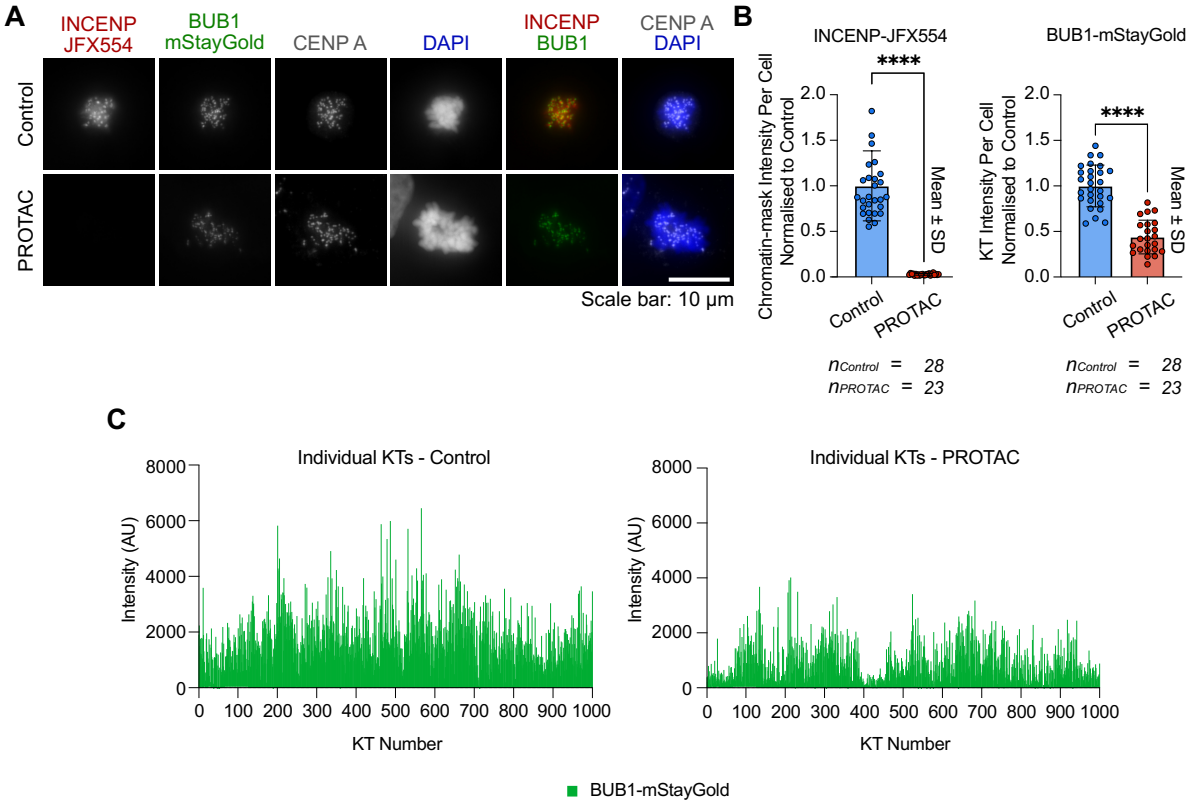

Figure 2. 56 - Determining the response of BUB1 after activation of the spindle assembly checkpoint in the presence or absence of INCENP

As in Figure 2.54, but with INCENP-HaloTag BUB1-mStayGold cells. (B) INCENP-JFX554 signal was instead measured by using chromatin as a mask. BUB1-mStayGold signal was still measured using the custom Fiji Script (Methods 4.7.1.1). Welch's t-test was used for statistical analysis, with P<0.0001 (****).

Taken together the analysis of NDC80, KNL1 and INCENP revealed some surprising findings. NDC80, together with the checkpoint kinases MPS1 and Aurora B, have been proposed to be crucial for the mechanism generating a spindle checkpoint signal. However, as I show here, NDC80 is not required for robust BUB1 recruitment, a marker for checkpoint activation. In contrast, KNL1 the checkpoint scaffold protein is crucial for BUB1 recruitment. Unexpectedly, degradation the Aurora B scaffold and activator INCENP resulted in only a partial loss of BUB1 signal at kinetochores. Given the previously suggested roles of both NDC80 and INCENP in promoting MPS1 recruitment and activation at kinetochores, I then explored whether checkpoint activity was still MPS1-dependent. The effect of MPS1 inhibition was therefore tested in the absence of NDC80, KNL1 or INCENP. Cells were arrested in G2 using CDK1 inhibition and treated with either Halo-PROTAC to trigger NDC80/KNL1/INCENP degradation or DMSO as a control with normal protein levels. Cells were released into mitosis by washout of the CDK1 inhibitor for 25 minutes (NDC80- and INCENP-Halo cell lines) or 15 minutes (KNL1-Halo cell line). A high dosage of the spindle poison nocodazole was then added, in the presence and absence of an MPS1 inhibitor, for 15 minutes prior to fixation. This allowed for the MPS1-dependence of the BUB1 checkpoint response to be monitored when cells enter mitosis after degradation of NDC80, KNL1 or INCENP. The addition of nocodazole allowed for the maximal checkpoint response to be monitored. Representative cells for each condition mentioned for NDC80-HaloTag BUB1-mStayGold cells are shown in Figure 2.57 - A, for HaloTag-KNL1 BUB1-mStayGold in Figure 2.58 - A, and for INCENP-HaloTag BUB1-mStayGold in Figure 2.59 - A.

NDC80, KNL1 and INCENP depletion was successfully observed for the respective Halo-PROTAC treated cells in comparison to the control cells (Figure 2.57 - A and B, NDC80-JFX554, Figure 2.58 - A and B, JFX554-KNL1, Figure 2.59 - A and B, INCENP-JFX554). As expected, addition of an MPS1 inhibitor reduced the levels of BUB1 at kinetochores in all instances compared to respective control cells (Figure 2.57-2.59, DMSO BUB1 Noc + MPS1-i). In NDC80-HaloTag BUB1-mStayGold cells, NDC80 depletion reduced BUB1 signal by

~25% at kinetochores (Figure 2.57 - C, BUB1, Noc DMSO vs PROTAC). MPS1 inhibition alone, reduced the BUB1 signal by >60% (Figure 2.57 - C, BUB1, Noc + MPS1-i DMSO), whereas degradation of NDC80 combined with inhibition of MPS1 lowered BUB1 levels to those like MPS1 inhibition alone (Figure 2.57 - C, BUB1 Noc + MPS1-i PROTAC). These observations suggest that like control cells with normal levels of NDC80, checkpoint activity after NDC80 degradation is MPS1-dependent. By contrast, in HaloTag-KNL1 BUB1-mStayGold cells, degradation of KNL1 appeared to reduce the BUB1 signal at kinetochores >70%, similar to the level seen after inhibition of MPS1 (Figure 2.58, BUB1). This is consistent with KNL1 acting as a direct scaffold for BUB1 recruitment, and MPS1 providing docking sites on KNL1 by phosphorylation. If any residual KNL1 remained after PROTAC addition, MPS1 inhibition would prevent it from recruiting checkpoint proteins.

In INCENP-HaloTag BUB1-mStayGold cells, degradation of INCENP reduced the BUB1 signal to ~45% of the level seen in control cells (Figure 2.59, BUB1, Noc DMSO vs PROTAC). MPS1 inhibition alone reduced the BUB1 signal by >40% (Figure 2.57 - C, BUB1, Noc + MPS1-i DMSO). Degradation of INCENP combined with MPS1 inhibition had an additive effect and further reduced the BUB1 signal at kinetochores to >80% (Figure 2.59, BUB1, Noc + MPS1-i DMSO vs PROTAC). Thus, MPS1 is the major kinase determining the level of BUB1 checkpoint protein recruitment to the kinetochore and Aurora B plays an important but lesser role.

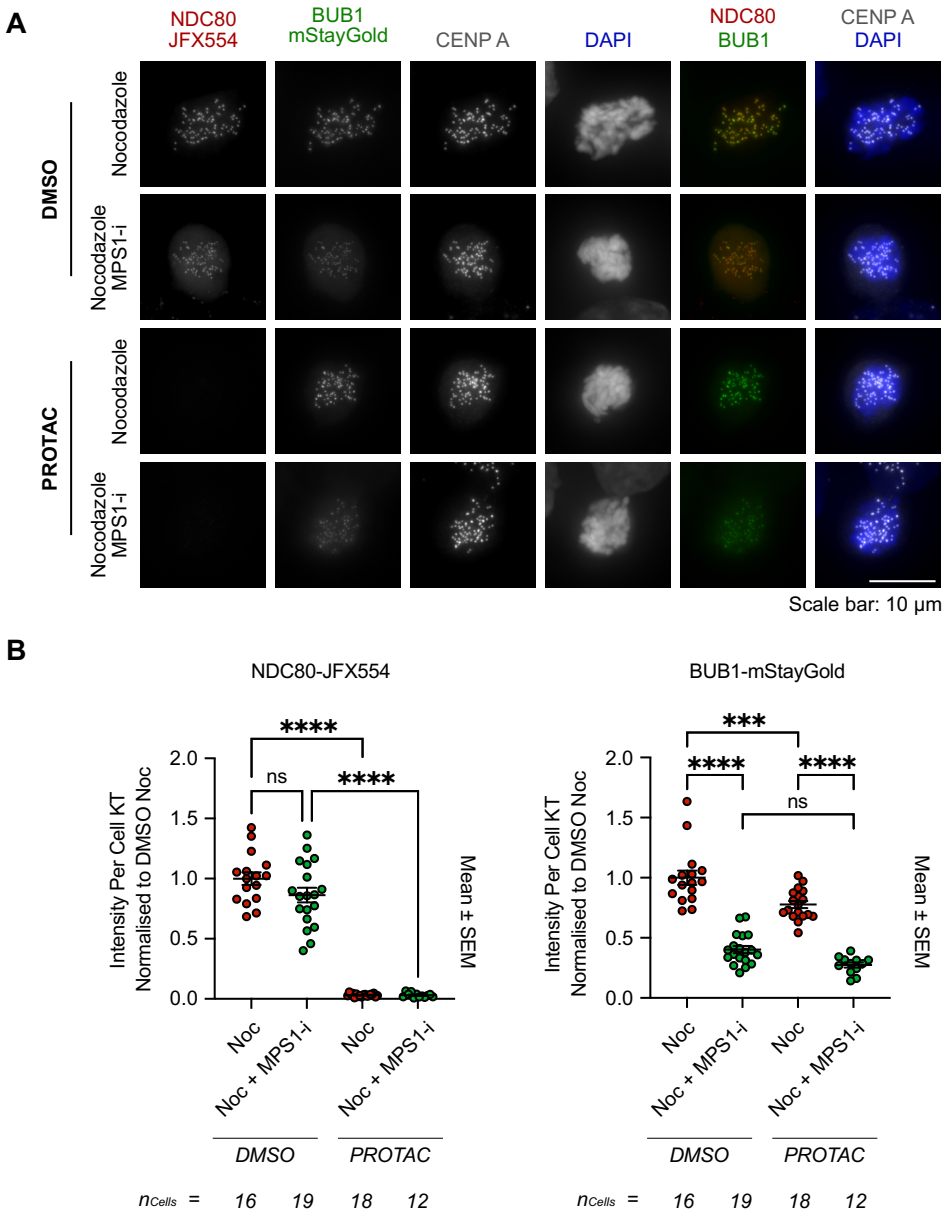

Figure 2. 57 - Comparison of BUB1 levels at checkpoint active and MPS1 inhibited kinetochores in the presence or absence of NDC80

(A) HCT116 NDC80-HaloTag BUB1-mStayGold cells were synchronised in G2 by 6 µM CDK1 inhibitor RO-3306 and treated with either DMSO or 300 nM Halo-PROTAC for 18 hours. Cells were released from CDK1 inhibition by washout of the drug and remained in fresh media for 25 minutes. Cells were then treated with 660 nM Nocodazole ± 4 µM MPS1 inhibitor for 15 minutes. All samples were labelled with 100 nM JFX554 within the same 20-minute period and then fixed with HTEMF for 12 minutes. Cells were then immunofluorescence stained with an antibody for CENP-A. Chromatin was visualised using DAPI. Representative images are shown for all four conditions. (B) NDC80-JFX554 and BUB1-

*mStayGold signals were determined on a per-kinetochore basis (Methods 4.7.1.1) and averaged per cell. Bar graphs with mean ± SEM values shown; cell sample numbers indicated in the figure. Ordinary one-way ANOVA tests were used for statistical analysis, with P<0.0001 (****). For NDC80-JFX554 quantification, DMSO Noc vs DMSO Noc + MPS1-i (P=0.0803, ns). For BUB1-mStayGold quantification, DMSO Noc vs PROTAC Noc (P=0.0004, ***) and DMSO Noc + MPS1-i vs PROTAC Noc + MPS1-i (P=0.1111, ns).*

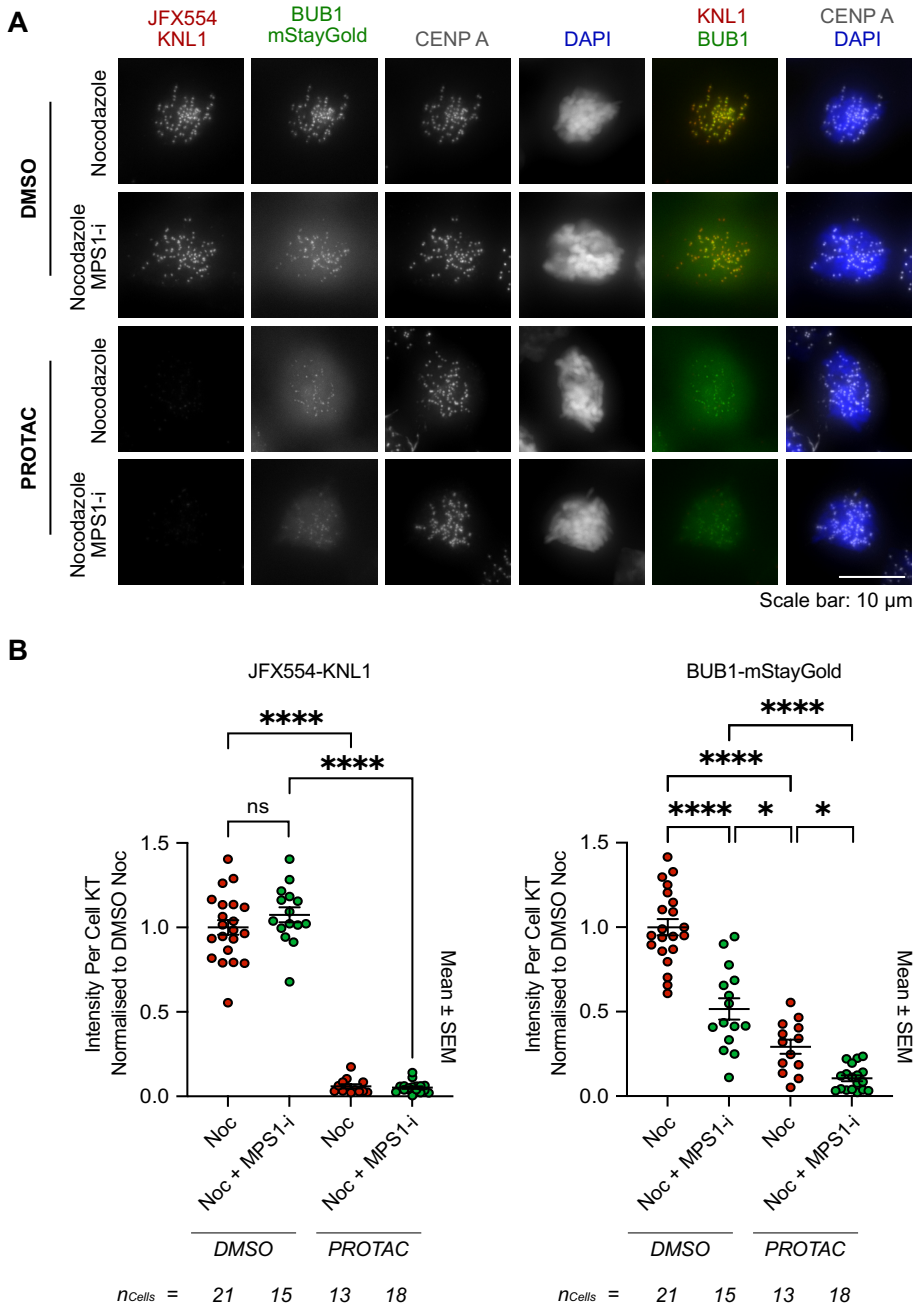

Figure 2. 58 - Comparison of BUB1 levels at checkpoint active and MPS1 inhibited kinetochores in the presence or absence of KNL1

*As in Figure 2.57, but with HaloTag-KNL1 BUB1-mStayGold cells. The only difference in the protocol was the washout time; these cells were left for 15 minutes in fresh media instead of 25 due to KNL1-depleted cells exiting mitosis faster. (B) Ordinary one-way ANOVA tests were used for statistical analysis, with P<0.0001 (****). For JFX554-KNL1 quantification, DMSO Noc vs DMSO Noc + MPS1-I (P=0.3213, ns). For BUB1-mStayGold quantification, DMSO Noc + MPS1-i vs PROTAC Noc (P=0.0113, *) PROTAC Noc vs PROTAC Noc + MPS1-I (P=0.0373, *).*

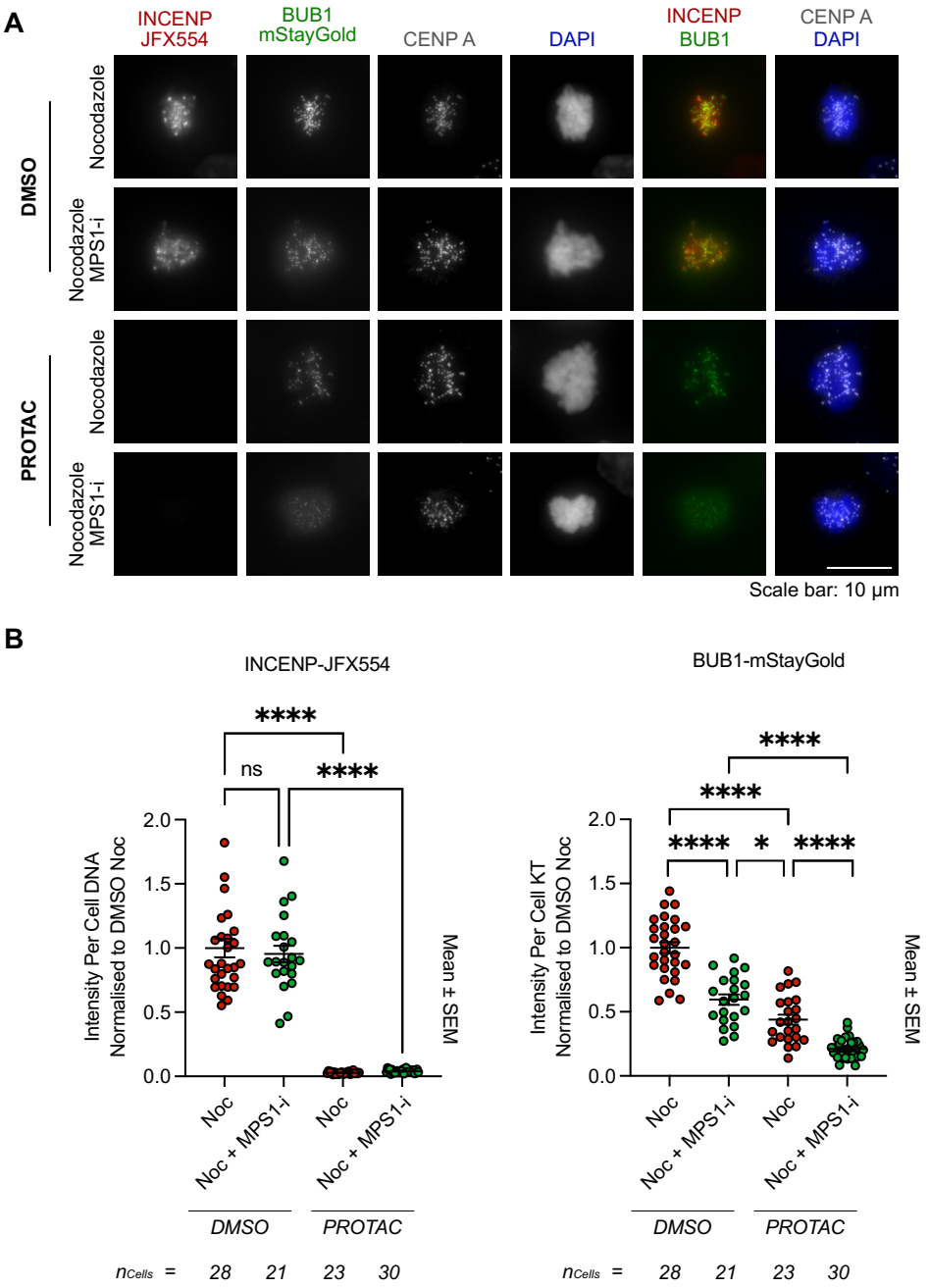

Figure 2. 59 - Comparison of BUB1 levels at checkpoint active and MPS1 inhibited kinetochores in the presence or absence of INCENP

*As in Figure 2.57, but with INCENP-HaloTag BUB1-mStayGold cells. (B) Ordinary one-way ANOVA tests were used for statistical analysis, with P<0.0001 (****). For INCENP-JFX554 quantification, DMSO Noc vs DMSO Noc + MPS1-i (P=0.8799, ns). For BUB1-mStayGold quantifications, DMSO Noc + MPS1-i vs PROTAC Noc (P=0.0214, *).*

2.5. Super-resolution imaging of the outer kinetochore and chromosome passenger complex

2.5.1. The basic principles of STED imaging and improved lateral resolution

Throughout this thesis, standard immunofluorescence widefield microscopy was used to visualise and quantify kinetochore signals. To gain higher spatial precision and resolve finer details, super-resolution STED imaging was next employed for imaging of kinetochore and CPC components.

At its core, STED imaging works by using two lasers; one to excite fluorophores at a dye-specific wavelength, and another red-shifted laser to de-excite them via stimulated emission back down to a ground state (Hein et al., 2008). This depletion laser is shaped into a 'doughnut' form, surrounding the initial excitation spot and effectively supresses fluorophores surrounding the periphery from fluorescing (Hell & Wichmann, 1994). This results in a smaller point spread function and a sharper central illumination, hence acquiring an imaging resolution beyond the diffraction limit (Figure 2.60 - A). Examples of carefully selected fluorophores used (e.g. by considering excitation ranges (Schermelleh et al., 2010)) in this section are shown in Figure 2.60 - B, alongside the STED depletion lasers available for use.

Examples of the STED modes available, as evidenced by imaging of the mitotic spindle by α-Tubulin, are shown in Figure 2.60 - C; cells were prepared and imaged as described in Methods 4.6.3. TauSTED collects and incorporates the spatial fluorescence lifetime gradient and uses this to refine the PSF; a newer technique of TauSTED Xtend furthers this and applies live deconvolution during acquisition, improving resolution without need for additional laser power (Manufacturer's application report; Alvarez et al., n.d.). Measuring line scans of astral tubules emanating from spindle poles in each modality and fitting a Gaussian curve showed a marked improvement in PSF for all STED images (Figure 2.60 - D). Computing full-width at half-maximum (FWHM) quantifiably showed an increase in resolution (Figure 2.60 - E).

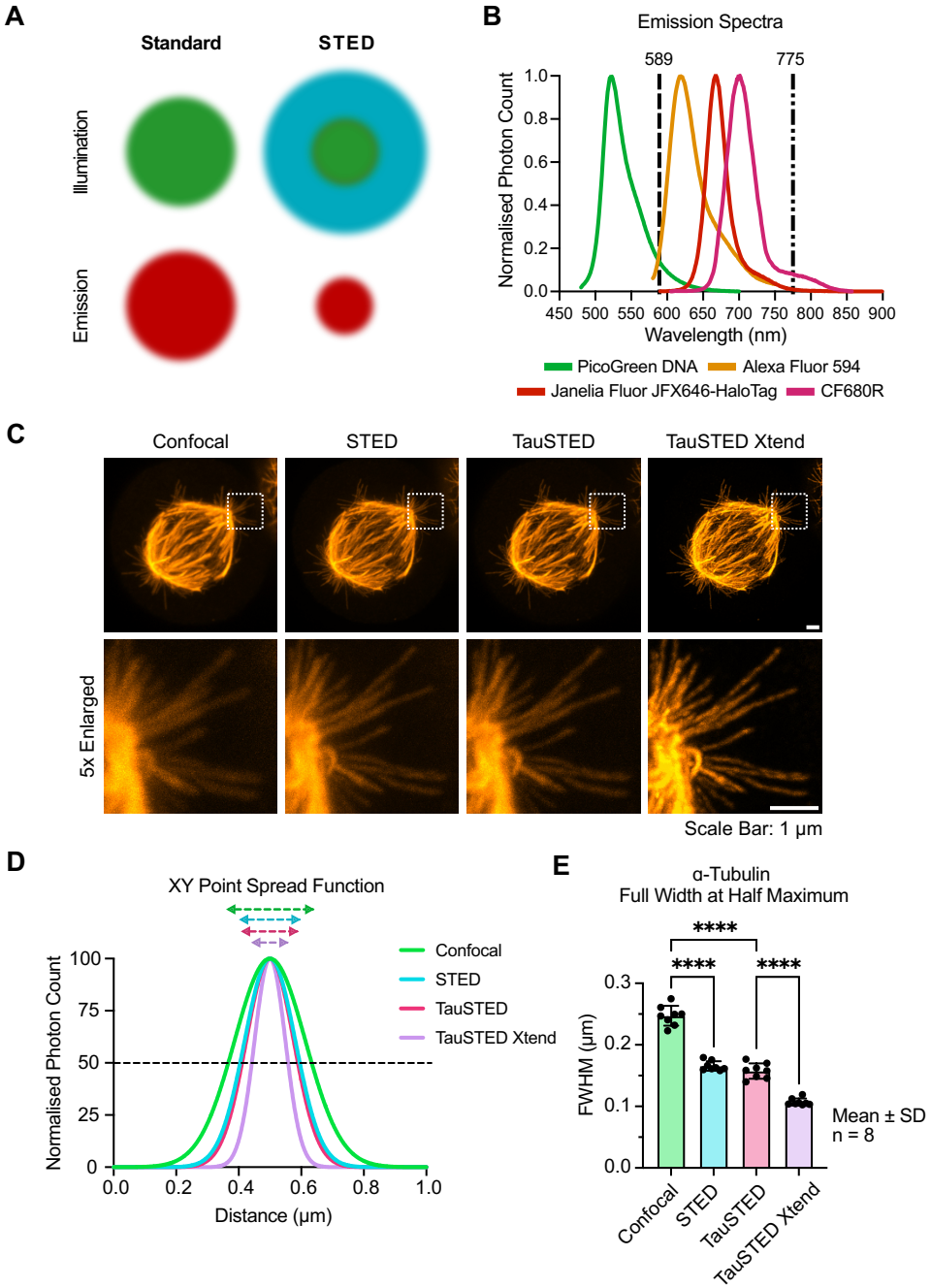

Figure 2. 60 - STED microscopy can be used to improve lateral resolution

(A) A schematic outlining the basic principle of STED imaging. (B) Example of a four-colour dye combination used in STED, with only 589 and 775 nm STED lasers available. (C) Example cell prepared as described in Methods 4.6.3, stained with an antibody for α-Tubulin. Maximum projection of a mitotic spindle imaged over 21 planes with 0.4 µm z-spacing in confocal, STED, TauSTED and TauSTED Xtend imaging modalities. (D) Example line scan over an astral tubule, with fitted Gaussians for each modality. (E) FWHM measurements determined from fitted Gaussians for each modality. A bar graph with mean ± SD shown; cell sample numbers indicated in the figure. An ordinary one-way ANOVA was used for statistical tests, with P<0.0001 (****).

The TauSTED modality was then expanded to incorporate 3-colour imaging. HCT116 NDC80-HaloTag cells were prepared as described in Methods 4.6.3, with NDC80 visualised by far-red Halo dye JFX646, and immunofluorescence antibody staining performed against α-Tubulin and DNA (PicoGreen) (Figure 2.61 - A). A marked improvement in resolution was observed in all channels; NDC80 signal was resolved to a more disc-like appearance, and bunched microtubules were separated.

Pushing this modality further, TauSTED Xtend was applied to a separate set of staining for three kinetochore components: the centromere protein CENP-A, and outer kinetochore components NDC80 and KNL1 (Figure 2.61 - B). Applying TauSTED Xtend also highlighted a disc-like appearance for all kinetochore components and allowed for clear spatial separation of each component not seen by conventional confocal imaging (Figure 2.61 - B). Line scans performed perpendicular to the kinetochore show narrower PSFs for TauSTED Xtend vs confocal images (Methods 4.7.1.2), implying an increase in resolution (Figure 2.61 - C). Further to this, an improvement in the spatial distribution of kinetochore components can be more comfortably measured over a distance of ~ 600 nm in confocal to ~ 250 nm in TauSTED Xtend, providing a more accurate determination of kinetochore architecture by microscopy (Figure 2.61 - C). This is expected from one possible conformation of the kinetochore, given KNL1's large, disordered N-terminus (Polley et al., 2024) (Figure 2.61 - D).

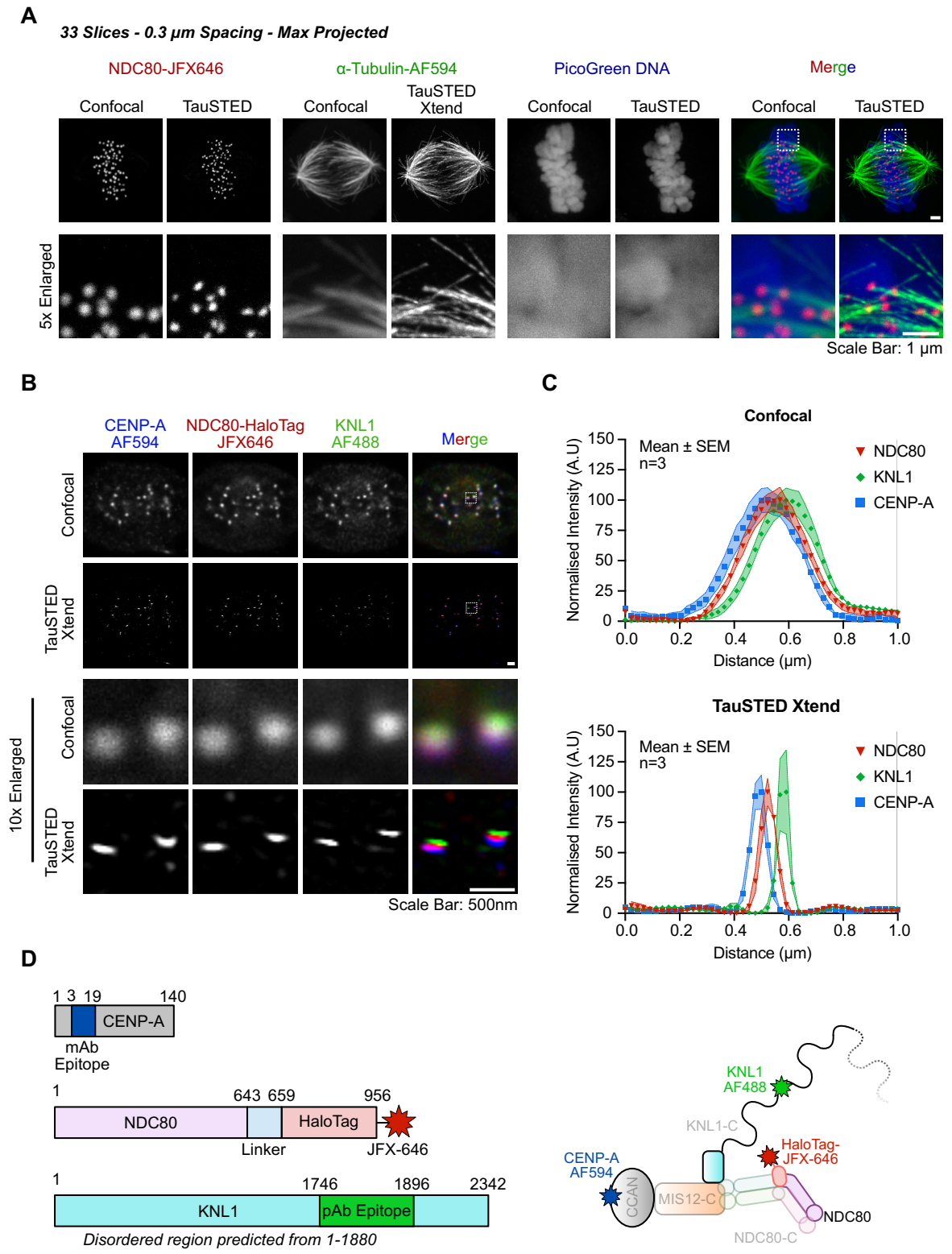

Figure 2. 61 - TauSTED with Xtend capabilities can resolve inner and outer kinetochore components

HCT116 NDC80-HaloTag cells were prepared, fixed, and stained as described in Methods 4.6.3 (A) Three-colour STED imaging of NDC80-JFX554 (TauSTED), immunofluorescence stained α-Tubulin

(TauSTED Xtend), and PicoGreen DNA (TauSTED) to visualise chromatin, with confocal images taken as reference. (B) Three-colour TauSTED Xtend imaging of NDC80-JFX554, and immunofluorescence staining for CENP-A and KNL1; with confocal reference images. (C) Line scans were performed perpendicular to bi-oriented kinetochore surfaces for NDC80, CENP-A and KNL1. n=3, Mean ± SEM shown. (D) Primary antibody binding epitopes for CENP-A and KNL1 indicated, as well as NDC80-HaloTag-JFX-646 estimated C-terminal location. Simplified kinetochore schematic shows one possible conformation of dye locations.

This methodology was then used in HCT116 INCENP-HaloTag cells and pushed even further to four colour TauSTED imaging. INCENP-HaloTag was visualised by JFX646, and immunofluorescence staining was performed for Aurora B, α-Tubulin, and DNA. By carefully selecting three far-red dyes and one green dye, all channels could spectrally separated. For both anaphase (Figure 2.62 - A) and telophase (Figure 2.62 - B) cells, improved resolution is seen in every channel. Side by side comparisons of confocal and TauSTED images are shown in Figure 2.62 - C.

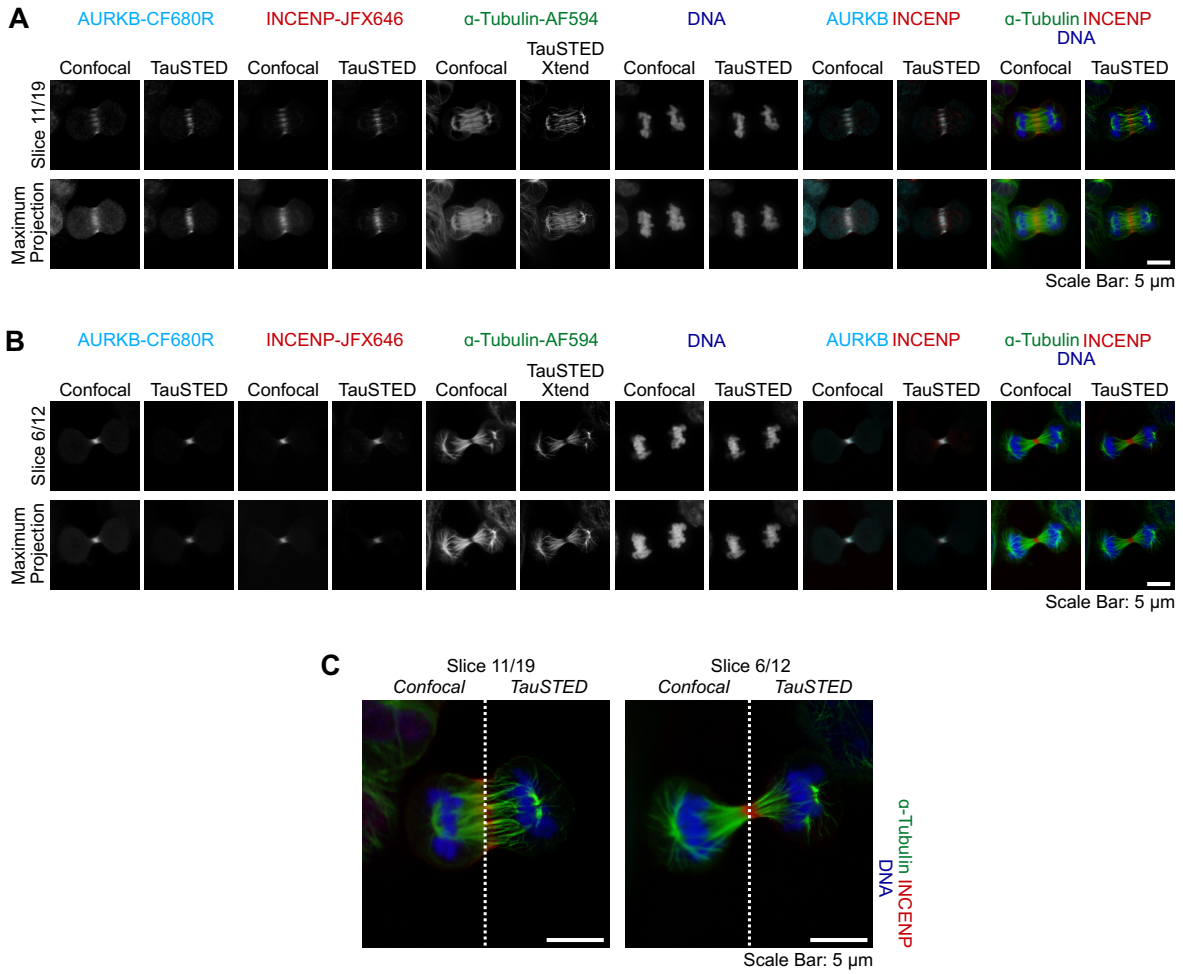

Figure 2. 62 - TauSTED imaging of Aurora B and INCENP in INCENP-HaloTag HCT116 cells

(A-C) HCT116 INCENP-HaloTag cells were prepared as described in Methods 4.6.3, Four-colour TauSTED imaging of INCENP-JFX554 and immunofluorescence-stained Aurora B and α-Tubulin (TauSTED Xtend). PicoGreen was used to visualise DNA. Confocal images taken as reference. Examples are shown of (A) an anaphase cell and (B) a telophase cell. (C) A direct side-by-side comparison of confocal and TauSTED imaging.

2.5.2. Resolving kinetochore, centromeric and pericentromeric localisation of kinetochore and CPC components

With four-colour TauSTED imaging achieved, this technique could then be applied to further investigate kinetochore and CPC localisation with higher resolution. With its role established in initiating checkpoint signalling at unaligned kinetochores through mediating Aurora B localisation (Carmena et al., 2012), super-resolution imaging of the CPC was performed relative to kinetochores to gain a clearer view of its spatial organisation.

Applying four-colour TauSTED imaging to HCT116 NDC80-HaloTag cells allowed for a high-resolution picture of kinetochore localisation from prometaphase (Figure 2.63 - A-B) to metaphase (Figure 2.63 - C-D). Labelling NDC80 with JFX646, and immunofluorescence-staining against the centromere protein CENP-A in this modality allowed for both inter and intra-kinetochore distances to be determined, as well as intensity across pericentric chromatin in each channel (Methods 4.7.1.2). An increase in inter-kinetochore distance was observed when cells move from an un-tensioned prometaphase to a tensioned metaphase state (Figure 2.63 - B, Figure 2.64 - B, Figure 2.65 - B). Due to the narrow PSF obtained from TauSTED imaging, intra-kinetochore distance (between NDC80 and CENP-A) could be estimated by fitting Gaussian curves to line scans across NDC80 and CENP-A signals and finding the difference in the mean of these fits. Using this method, intra-kinetochore distance does not change under tension (Figure 2.63 - D) despite previous suggestions of intra-kinetochore stretch (McVey et al., 2021).

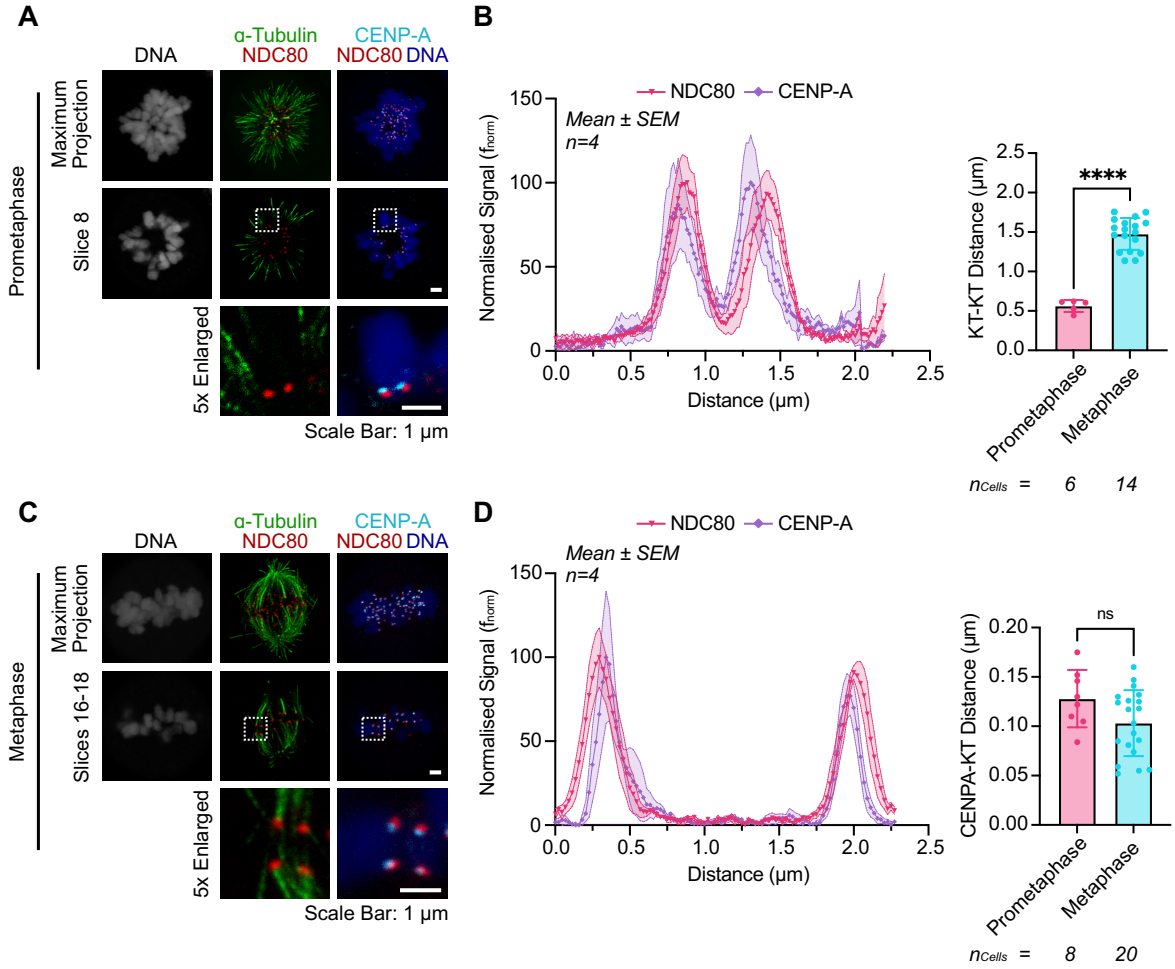

Figure 2. 63 - CENP-A and NDC80 undergo no discernible separation in metaphase

HCT116 NDC80-HaloTag cells were prepared as described in Methods (4.6.3). Four-colour TauSTED imaging was performed for NDC80-JFX554 and immunofluorescence stained CENP-A and α-Tubulin (TauSTED Xtend). PicoGreen was used to visualise DNA. Example cells are shown for (A) prometaphase and (C) metaphase, with both a maximum projection across the whole cell and a single slice/ projection over a few slices. (B, D) Line scans performed across kinetochore pairs to determine signal intensity, KT-KT distance, and intra-kinetochore distance (Methods 4.7.1.2). For both line scan quantifications, mean ± SEM shown. For KT-KT and CENP-A-KT distances, bar graphs with mean ± SD shown. Two-tailed, unpaired t-tests used for statistical analysis, with P<0.0001 (****), P=0.0778 (ns). Cell sample numbers indicated in the figure (Ruza et al., 2025).

Similar line scan quantifications were performed using NDC80-HaloTag cells, visualising NDC80 by JFX646 and co-staining against DNA, Aurora B and either Borealin (Figure 2.64) or Survivin (Figure 2.65). For Borealin-staining, examples are shown of prometaphase (Figure 2.64 - A) and metaphase (Figure 2.64 - C) cells. Spatial distribution of kinetochore and CPC components were described by line scans (Figure 2.64 - B, D). Aurora B and Borealin co-localised on pericentric chromatin, as evidenced by a broad peak sitting between two NDC80 peaks which marked the boundaries of pericentric chromatin. This broad peak became extended during chromosome biorientation but remained localised to pericentric chromatin. A similar distribution of signal is seen between Survivin-stained prometaphase (Figure 2.65 - B) and metaphase (Figure 2.65 - D) cells.

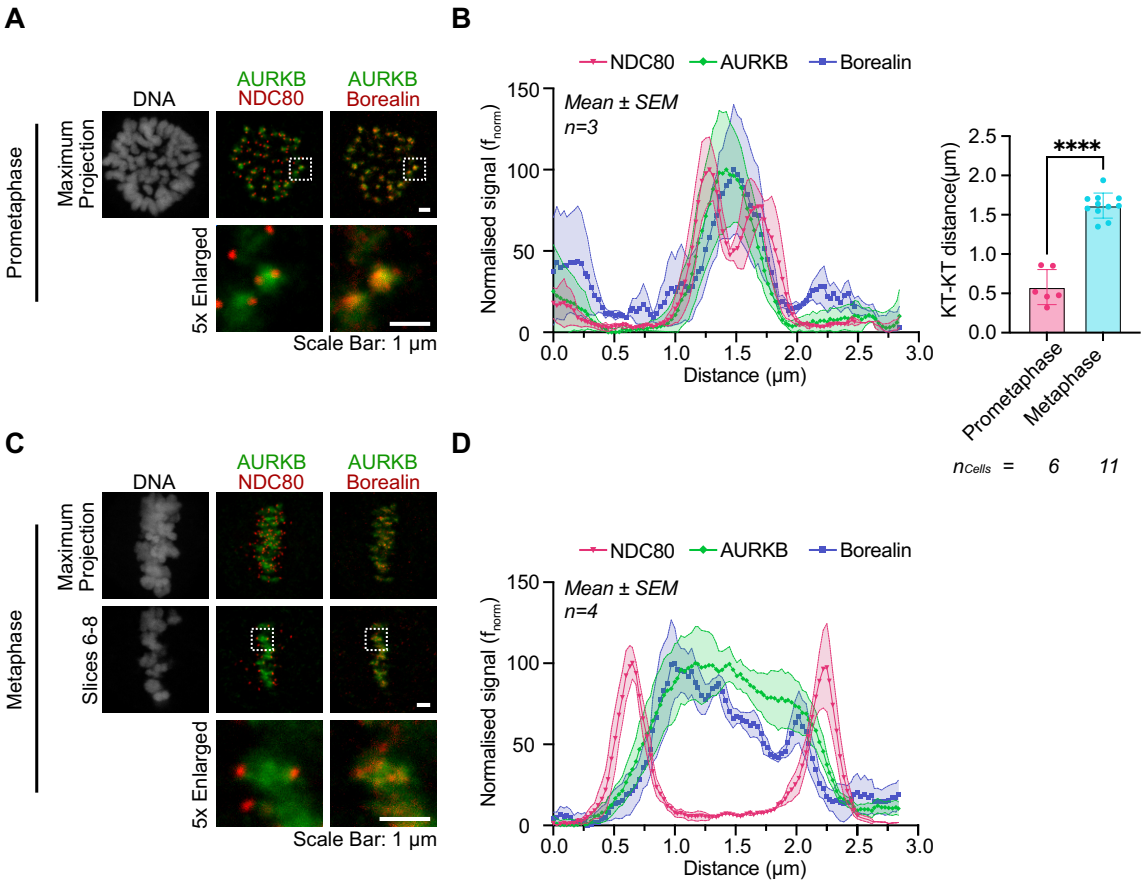

Figure 2. 64 - NDC80 and CPC-Borealin are spatially separated in metaphase

As in Figure 2.63, except cells were immunofluorescence stained for Aurora B and Borealin. No intra-kinetochore distance was measured (Ruza et al., 2025).

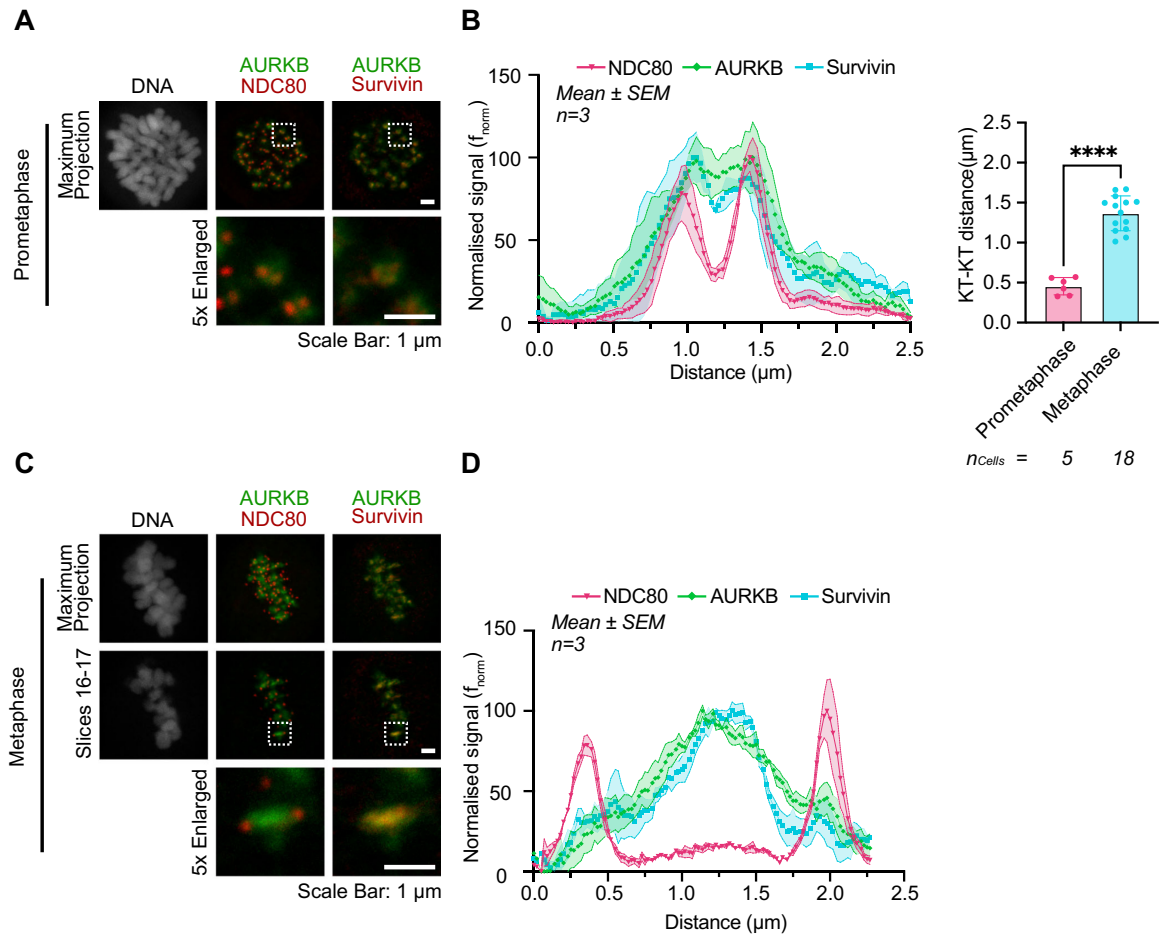

Figure 2. 65 - NDC80 and CPC-Survivin are spatially separated in metaphase

As in Figure 2.63, except cells were immunofluorescence stained for Aurora B and (Ruza et al., 2025).

Taken together, these data suggest that the CPC remains bound to pericentric chromatin which becomes extended upon chromosome biorientation as the kinetochore is physically moved by microtubule pulling forces. This then displaces Aurora B away from the kinetochore, preventing its phosphorylation and reducing checkpoint activity. This, and the absence of evidence for intra-kinetochore stretch from this data, would favour a spatial separation model for Aurora B-mediated kinetochore interaction (Lampson & Cheeseman, 2010; Liu et al., 2009).

2.5.3. Aurora B remains pericentromeric in the absence of SGO1

Additional four-colour TauSTED imaging was performed with NDC80-HaloTag cells staining for DNA, CPC component Aurora B, and Shugoshin 1 (SGO1) which is responsible for protecting centromeric cohesion during chromosome alignment (Kitajima et al., 2006). Unlike CPC components, SGO1 appeared to localise adjacent to kinetochores, potentially acting as a pericentric boundary (Figure 2.66 A, C). This localisation did not change under tension (Figure 2.66 B, D).

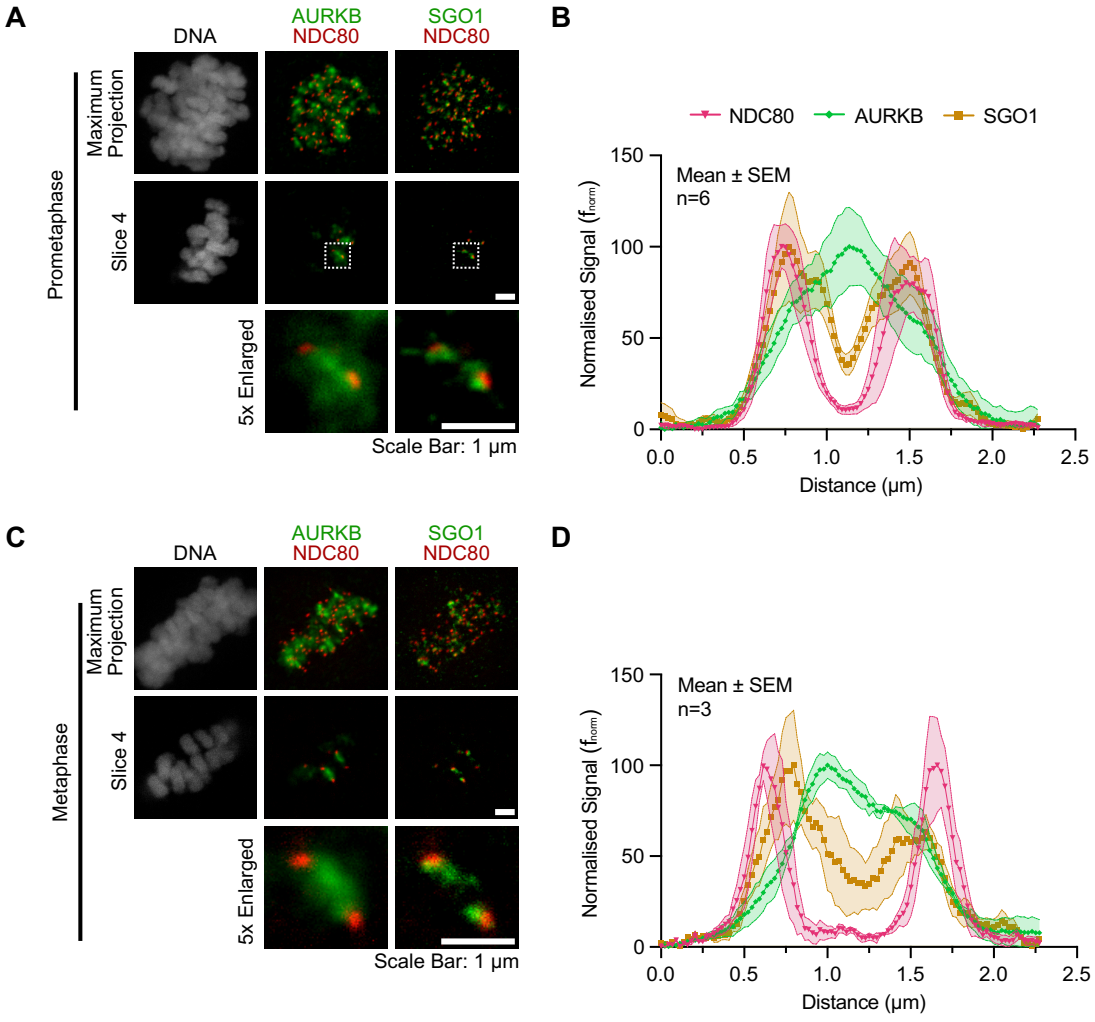

Figure 2. 66 - SGO1, CPC and NDC80 localisation using TauSTED imaging

As in Figure 2.63, except cells were immunofluorescence stained for Aurora B and SGO1. No KT-KT distance measured (Ruza et al., 2025).

To investigate this further, RNA interference against SGO1 was performed, and cells were stained and imaged as in Figure 2.66. Control cells (Figure 2.67 - A) showed SGO1 localisation consistent with previous observations in both prometaphase and metaphase (Figure 2.66 A, C). In contrast, SiSGO1-treated cells (Figure 2.67 - B) exhibited defective chromosome cohesion and showed no discernible attempt at chromosome alignment. Aurora B was able to localise to pericentric chromatin despite the absence of SGO1.

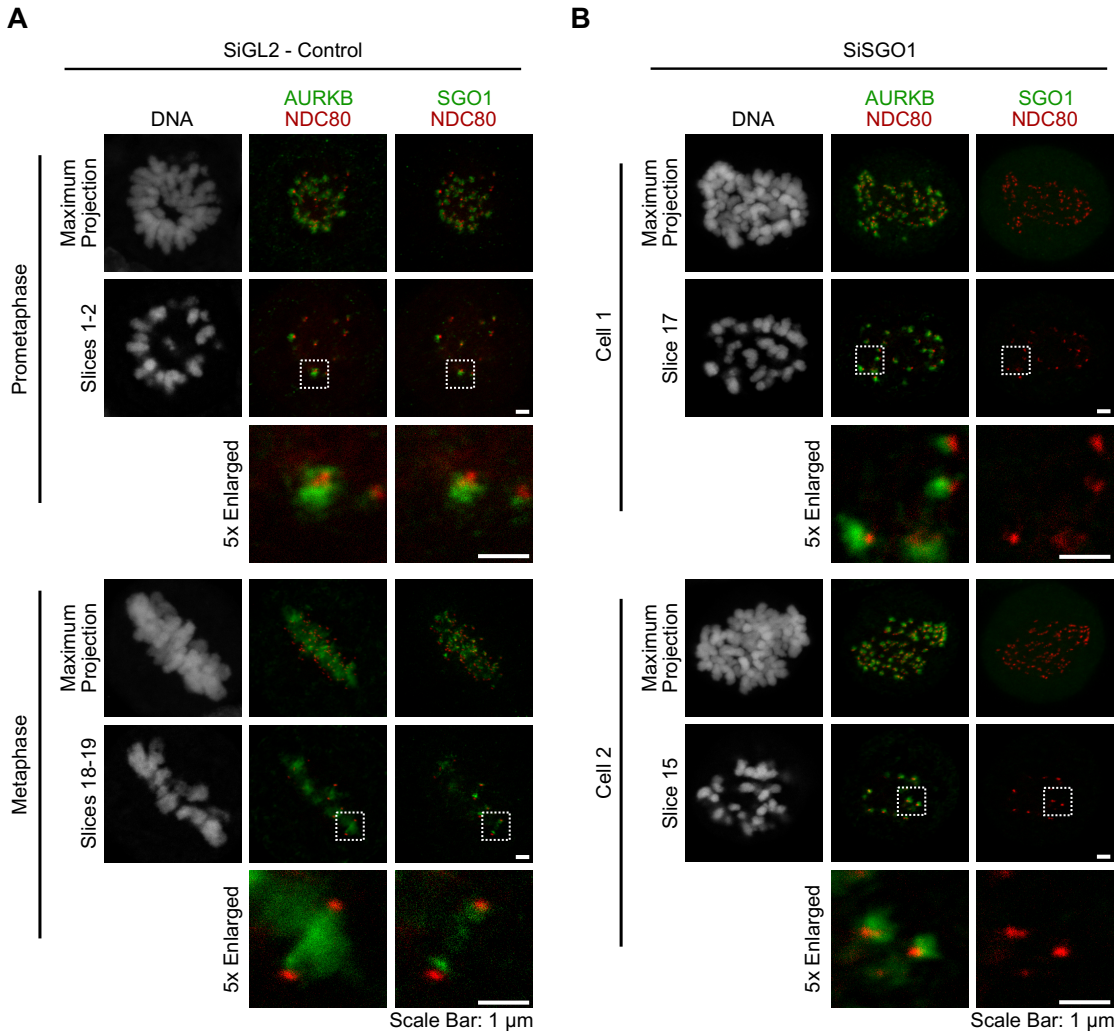

Figure 2. 67 - Aurora B remains localised to pericentric chromatin in the absence of SGO1

As in Figure 2.66, except cells were treated with either (A) SiControl or (B) SiSGO1 for 72 hours prior to fixation (Methods 4.6.3). (A) For control cells, examples of prometaphase and metaphase are shown. (B) For SiSGO1 treated cells, two examples are shown in a prometaphase-like state due to loss of sister-chromatid cohesion (Ruza et al., 2025).

2.6. Chromosome Passenger Complex structure and INCENP-dependent phosphorylation

2.6.1. CPC structure and checkpoint signalling

With super-resolution imaging showing defined localisation of CPC components to pericentromeric chromatin, the mechanistic question arose of as to how Aurora B sequestered within the CPC can phosphorylate kinetochore and checkpoint substrates. To investigate the structural basis of this localisation, cryo-electron microscopy was used to solve structures of the CPC in complex with H3pT3-phosphorylated nucleosomes (Dr Reinis Ruza, Barr Group). This revealed that the Borealin N-terminus acts as a flexible pivot interacting with the nucleosome acidic patch, allowing for movement of the entire CPC whilst remaining anchored to nucleosomes, whereas the BIR domain of Survivin acts as tethering point to the T3-phosphorylated tail of Histone H3 (Ruza et al., 2025). Taken together, these results suggest how CPC affinity for H3pT3 nucleosomes is enhanced without spatial restriction (Figure 2.68).

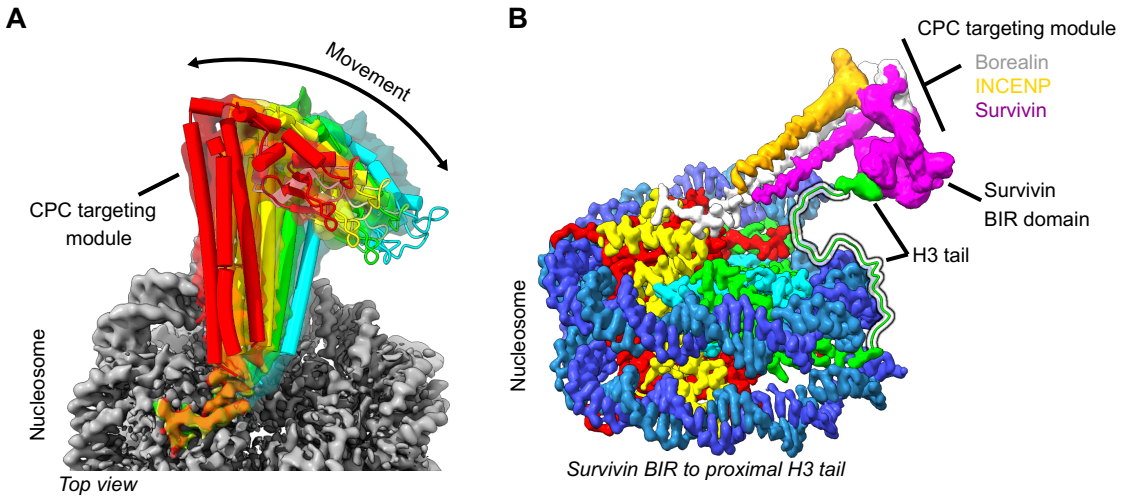

Figure 2. 68 - CPC structure reveals a pivot-tether model for increased affinity to H3pT3 nucleosomes

(A) Cryo-electron microscopy resolved CPC. The Borealin N-Terminus is bound to the H3pT3 nucleosome surface, and acts as a pivot. Selected classes from 3D classification are shown; red (10.4% of particles); yellow (10.0%), green (10.5%); cyan (10.0%). (B) H3pT3 nucleosome with Histone H2A

(red), H2B (yellow), H3 (green), H4 (cyan), DNA (blue), and the CPC subunits borealin (grey/white), survivin (magenta), INCENP (gold/orange). Data collected and analysed by Dr Reinis R Ruza, co-author of (Ruza et al., 2025).

To test the effects on MPS1 checkpoint initiation, mutations in the Borealin pivot and dimerization domains (Figure 2.69 - A-B) and in the Survivin-H3pT3 binding domain (Figure 2.69 - C-D) were introduced by RNA interference and rescue experiments in HeLa MPS1-GFP Flip-In cells by Dr Chyi Wei Chung (Ruza et al., 2025). Complete removal of Borealin abolished MPS1 signal at the kinetochore (Figure 2.69 - A, B - No Rescue). A wild-type Borealin construct restored both CPC localisation and the MPS1 signal at kinetochores under checkpoint active conditions (Figure 2.69 - A, B - WT). Rescue with an N-terminal truncated Borealin lacking the nucleosome acidic patch binding RK motif partially restored CPC localisation and maintained MPS1 signal at kinetochores (Figure 2.69 - A, B - 10-280). In contrast, the H3pS10 signal, was greatly reduced. Rescue with a combined N-terminal truncation and dimerization mutant of Borealin completely abolished its localisation and further attenuated MPS1 signal at kinetochores (Figure 2.69 - A, B - 10-221); H3pS10 signal, which acts as a marker for Aurora B activity (Hirota et al., 2005), was even further reduced implying a global loss in Aurora B activity towards chromatin.

Similarly, complete removal of Survivin abolished MPS1 signal at kinetochores (Figure 2.69 - C, D - No Rescue). Rescue with wild-type Survivin restored both Survivin localisation and MPS1 recruitment to kinetochores (Figure 2.69 - C, D - WT), whereas the H3pT3 binding mutant failed to restore Survivin localisation, and consequently did not restore MPS1 kinetochore localisation (Figure 2.69 - C, D - E65A-H80A). Notably, this mutant of Survivin did not change H3pS10-phosphorylation, suggesting that Aurora B catalytic activity towards chromatin remained intact, but activity specifically towards centromeric chromatin, and hence checkpoint initiation, was compromised.

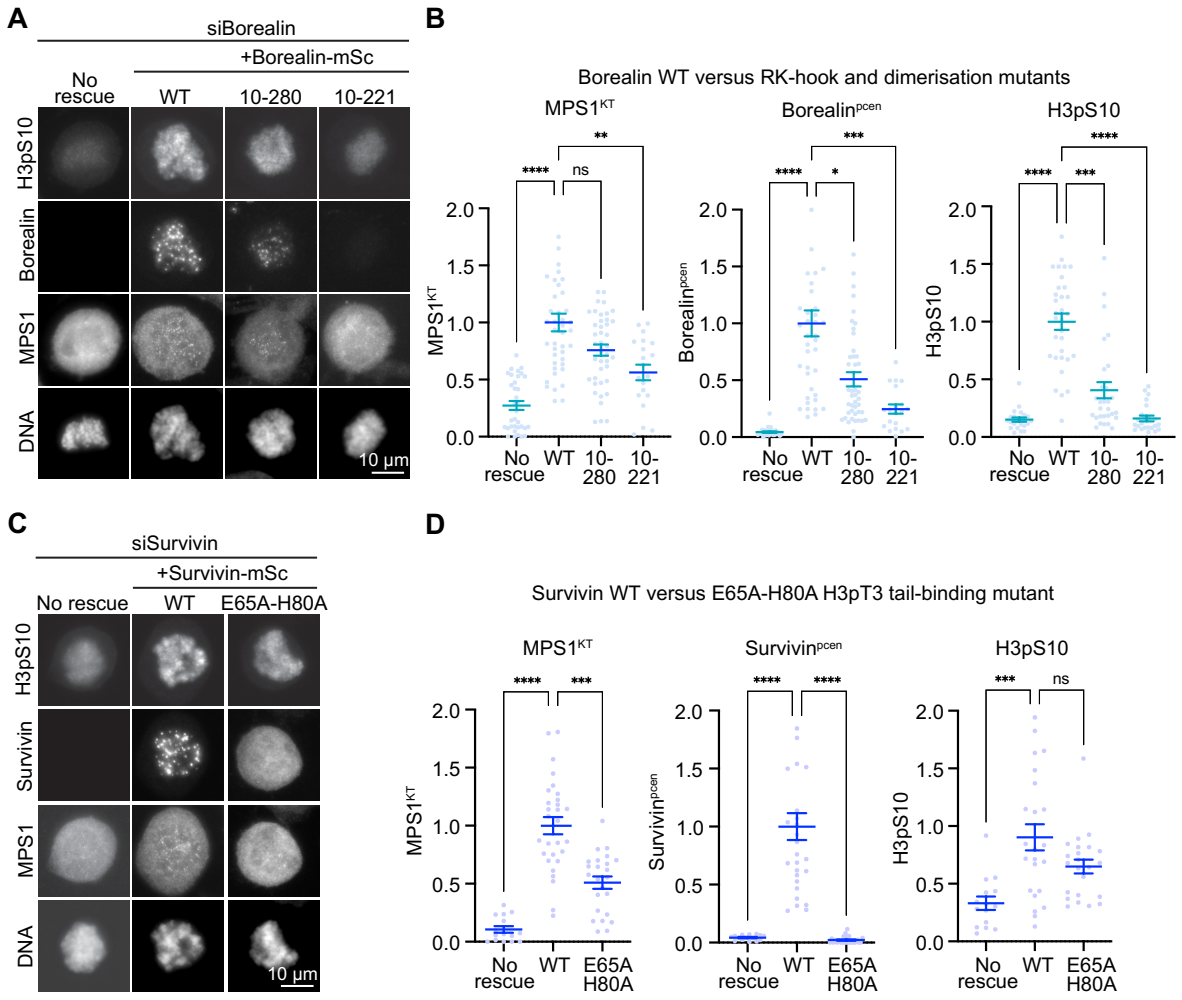

Figure 2. 69 - Borealin and Survivin mutants affect MPS1, CPC, and H3pS10 enrichment

(A, C) HeLa Flp-In T-REx MPS1-GFP cells were used to test MPS1 kinetochore localisation, Borealin/Survivin pericentric enrichment and H3pS10 chromatin enrichment under SiRNA depletion and rescue assays. (A) SiBorealin was either left un-rescued, rescued with wild-type sequence, rescued with a 9 amino-acid N-terminal deletion (10-280), or rescued with a C-terminal dimerization domain deletion and a 9 amino-acid N-terminal deletion (10-221). (C) SiSurvivin was either left un-rescued, rescued with wild-type sequence, or rescued with the H3pT3 binding point mutant E65A-H80A. Quantifications for MPS1 kinetochore intensity, Borealin/Survivin pericentric intensity, or H3pS10 chromatin intensity are shown for (B) SiBorealin or (D) SiSurvivin cells. Data collected and analysed by Dr Chyi Wei Chung, co-author of (Ruza et al., 2025).

2.6.2. Whole-cell phosphoproteomics to identify CPC^{INCENP}-dependent phosphorylation events

With effects on checkpoint protein phosphorylation observed by mutating CPC components, a more holistic approach was taken to determine global changes in mitotic phosphorylation by complete removal of the CPC via INCENP-HaloTag-mediated degradation. Cells were synchronised in G2 by CDK1 inhibition, treated with either Halo-PROTAC or DMSO control, released into mitosis by washout of the CDK1 inhibitor, and accumulated up to metaphase by MG132-based proteasome inhibition. Cells were then lysed, phospho-enriched, and prepared for mass spectrometry as described in Methods 4.4.4.

As expected, INCENP depletion led to a reduction in INCENP phosphorylation due to removal of the protein (Figure 2.70). It also decreased phosphorylation of Histone H3 variants H3.4 and H3.3A at S28, which are known Aurora B substrates (Adams et al., 2001; Goto et al., 2002). Additionally, phosphorylation of Histone variant H1.4 at S36, a putative Aurora B consensus motif, was also downregulated. When phosphorylated, this modification has been associated with weakened chromatin binding (Chu et al., 2011), but not linked directly to Aurora B by previous work. These changes to histone phosphorylation may therefore explain the defective chromosome condensation seen after INCENP degradation (Figure 2.42 - A, PROTAC). By contrast, phosphorylation of NDC80 at S69 remained unchanged under INCENP depletion, consistent with previous reports of N-terminal NDC80 sites being predominantly phosphorylated by Aurora A rather than Aurora B (Sobajima et al., 2023), and my data showing INCENP degradation specifically affects Aurora B activity and not Aurora A (Figure 2.41).

Other INCENP-dependent phosphorylation events may help understand which Aurora B substrates are crucial for error correction and spindle checkpoint signalling in chromosome alignment to the metaphase plate. Amongst the candidate phosphorylation sites downregulated upon INCENP degradation was pS106 on the microtubule depolymerising

protein MCAK/KIF2C (Figure 2.70). MCAK is a previously established target of Aurora B (Andrews et al., 2004), and reduced phosphorylation at this site likely decreases MCAK regulation, potentially impairing error correction and could lead to spindle instability. Also reduced was phosphorylation of the MIS12 complex protein DSN1 at pS109, previously shown to be an Aurora B substrate (Welburn et al., 2010). DSN1 phosphorylation has been linked to outer kinetochore assembly and providing increased sensitivity towards weakening kinetochore-microtubule interactions, leading to subsequent chromosome misalignment (Hadders et al., 2020; Petrovic et al., 2016; Welburn et al., 2010). Another notable candidate was the ssDNA-binding protein RPA1 (RPA70) at pS384, recently implied as an Aurora B target during mitosis. When this phosphorylation site was disrupted by homozygous knock-in of a phospho-dead mutant, it was shown to result in chromosome segregation errors and a higher proportion of apoptosis (Roshan et al., 2023).

Whilst most phosphorylations were unchanged or downregulated, LMNA (Lamin A) at S414 and S632 were notably upregulated. These modifications have not been specifically reported, but lamin A phosphorylation in mitosis is important for in nuclear lamina disassembly (Heald & Yckeon, 1990). Hence, these sites may be upregulated as a compensatory mechanism to disrupted Aurora B activity and the chromosome condensation/segregation errors this presents, resulting in nuclear defects (Figure 2.44 - C, INCENP-Halo). A full list of relevant top hits, their peptide sequence, and gene ontology are shown in Table 2.1.

Taken together, these phosphorylation modifications in the absence of INCENP imply issues with chromosome condensation and segregation, weakened kinetochore-microtubule interaction, and nuclear defects. These effects provide a mechanistic explanation for the increased genomic instability observed in INCENP-depleted cells (Figure 2.44 - C, INCENP-Halo) and highlights the importance of correct Aurora B localisation by the CPC to allow it to phosphorylate its substrates.

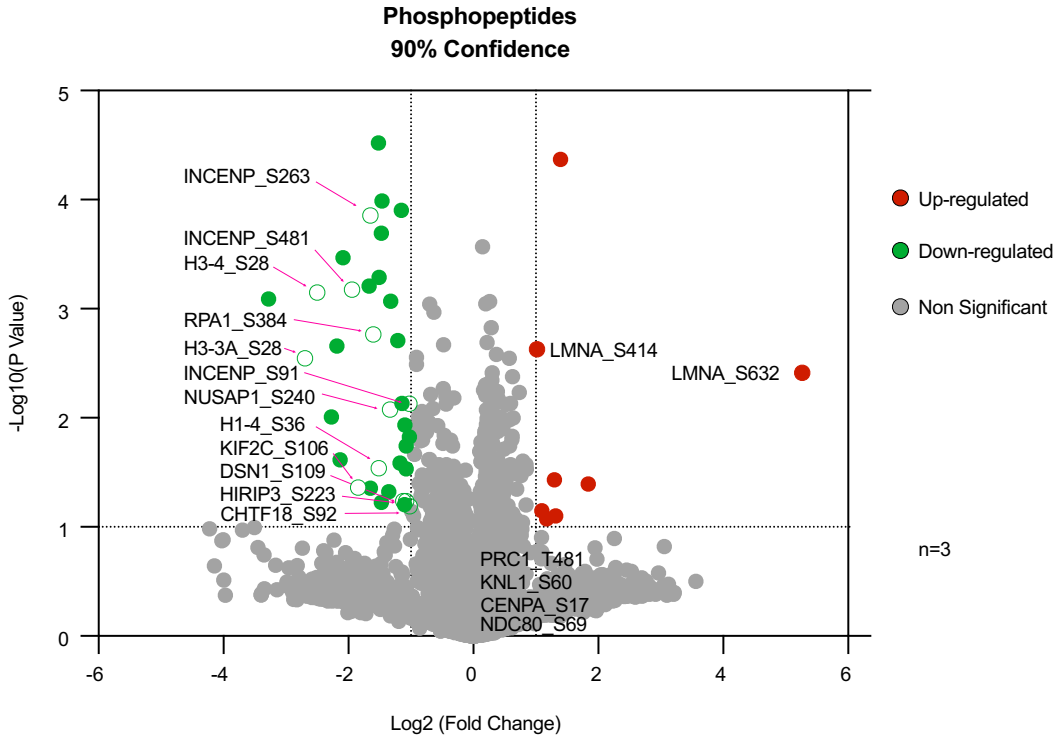

Figure 2. 70 - Whole-cell phosphoproteomics to identify candidate INCENP-dependent phosphorylation sites in mitosis

HCT116 INCENP-HaloTag cells were arrested in G2 with 6 μM CDK1 inhibitor RO-3306 and treated with either DMSO or 300 nM Halo-PROTAC for 18 hours. Cells were then released from G2 arrest by washing out the CDK1 inhibitor and treated with 20 μM MG132 for 3 hours to prevent anaphase onset. Mitotic cells were shaken off, lysed, and snap frozen (Methods 4.4.4). Phospho-enrichment was performed by Dr James Holder. Samples were sent for mass spectrometry, performed by Dr Sean Burnap. DIA-NN software was used to search for phospho-sites with 90% confidence (Methods 4.4.4). Potential key hits have been labelled and further explored in Table 2.1.

Protein	Site	Up/Down Regulated	Peptide Sequence	Gene ontology annotations
INCENP	S481	Down	PRSKTPSSPCPASKV	Aurora B/Chromosome Alignment/Segregation
INCENP	S263	Down	KLRIAQVSPGPRDSP	
INCENP	S91	Down	RRLSRRKSRSSQLSS	
H1.4	S36	Down	GAAKRKASGPPVSEL	Histone/Chromosome condensation
H3.3A	S28	Down	ATKAARKSAPSTGGV	
H3.4	S28	Down	ATKVARKSAPATGGV	
DSN1	S109	Down	KETNRRKSLHPIHQG	MIS12-Complex/Aurora B phosphorylated
KIF2C	S106	Down	KIPAPKESLRSRSTR	Microtubule binding
NUSAP1	S240	Down	VPPRGRLSVASTPIS	Microtubule binding
HIRIP3	S223	Down	GTKSLKESEQESEEE	Chromatin organisation
CHTF18	S92	Down	ADLQPAGSLPHAPRI	DNA binding
RPA1	S384	Down	AIKGARVSDFGGRSL	DNA binding
LMNA	S414	Up	SQTQGGGSVTKKRKL	Nuclear lamina /envelope
LMNA	S632	Up	SYRSVGGSGGGSFGD	

Table 2. 1 - INCENP-dependent phosphorylation site candidates in mitosis

Experiment performed as described in Figure 2.70. This table provides a list of potential key phosphosite hits that are either up or down regulated due to INCENP depletion, alongside their assigned peptide sequence. Putative Aurora kinase consensus sites are underlined.

3. General Discussion

In this thesis I have presented data exploring the spatial separation model for SAC signalling during mitotic spindle formation, and the role of key components NDC80, KNL1, Aurora B and INCENP. Spatial separation of Aurora B from substrates at kinetochores was originally proposed to explain microtubule stabilisation during chromosome biorientation and error correction. Because Aurora B also plays a role in promoting SAC signalling from the kinetochore at non-bioriented chromosomes, spatial separation may also explain how this process is regulated. Here I will discuss how the localisation and dynamics of Aurora B and NDC80 at different stages of mitosis fit into this model. The role of NDC80 is especially intriguing since it is essential for microtubule attachment to the chromosome and hence is required to spatially separate the kinetochores from the inner centromeres in response to spindle forces.

3.1. The Aurora B spatial separation model

3.1.1. Super-resolution STED imaging favours the spatial separation model

Here, I used the improved sensitivity of HaloTag dyes able to provide high-resolution detail in super resolution imaging (Grimm et al., 2021). STED imaging was used to provide a better understanding of the dynamics of kinetochore and CPC components during the transition from an un-tensioned prometaphase state to a tensioned metaphase plate. Using HCT116 NDC80-HaloTag cells allowed for unambiguous identification of kinetochore pairs at the different stages of mitosis. As expected for bi-oriented metaphase chromosomes, the distance between NDC80-defined kinetochore pairs increased under tension (Figure 2.63 - B) (Lampson & Cheeseman, 2010; Ruza et al., 2025). Interestingly, the distance measured between NDC80 and centromeric CENP-A, the most distal and proximal ends of the kinetochore relative to the chromosome, respectively, did not show a clear increase under tension (Figure 2.63 - D) (Ruza et al., 2025). Thus, the kinetochore behaves as a rigid structure under tension and does

not undergo any large-scale rearrangement from prophase to metaphase. By comparison to NDC80, CPC components Aurora B, Borealin (Figure 2.64) and Survivin (Figure 2.65) showed partial overlap with kinetochores during prometaphase, but confinement to the extended pericentromeric chromatin distinct from NDC80 as inter-kinetochore distance increased (Ruza et al., 2025). These observations are consistent with the spatial separation model, in which Aurora B at pericentromeres is spatially separated from substrates at kinetochores, thus preventing their continued phosphorylation (Li et al., 2023; Liu et al., 2009).

3.1.2. Aurora B localisation to the inner centromere is required for the SAC

In the spatial separation model, it is crucial that Aurora B is anchored to the pericentric chromatin during prometaphase and metaphase to ensure robust loss of phosphorylation of kinetochores. With spatial localisation of Aurora B being crucial to its function, structural work to solve the CPC was required to delve deeper into how such specific, yet flexible localisation is attained. Cryo-electron microscopy analysis of the CPC in complex with H3pT3-phosphorylated nucleosomes (Dr Reinis Ruza, Barr Group) (Ruza et al., 2025) revealed a 'pivot-tether' model for the CPC, with the BIR domain of Survivin acting as a tether to H3pT3 and an arginine anchor at the N-terminus of Borealin acting as a flexible tether at the nucleosome acidic patch (Figure 2.68) (Ruza et al., 2025). This supports previous work on CPC localisation (Abad et al., 2019; Du et al., 2012; Jeyaprakash et al., 2011; Kelly et al., 2010; Serena et al., 2020; Wang et al., 2010; Yamagishi et al., 2010). Together, these binding sites stabilise CPC association with chromatin, while allowing flexibility in Aurora B positioning due to the extended helical region of INCENP (Jeyaprakash et al., 2007; Samejima et al., 2015). Mutation of the BIR domain of Survivin to prevent H3pT3 binding disrupted Survivin accumulation at pericentric chromatin and furthermore significantly reduced MPS1 localisation to kinetochores (Dr Chyi Wei Chung, Figure 2.69 - C-D). Removal of the N-terminal arginine anchor of Borealin disrupted its pericentric localisation and Aurora B phosphorylation of H3pS10 but had less effect on MPS1 (Dr Chy Wei Chung, Figure 2.69 - A-B). However,

removal of both the N-terminal arginine anchor and C-terminal dimerization domains of Borealin reduced MPS1 kinetochore localisation (Dr Chy Wei Chung, Figure 2.69 - A-B). Thus, the CPC interacts with chromatin through a multivalent binding mechanism and is required to promote SAC signalling. This leaves open the question of which substrates are phosphorylated by Aurora B to regulate both kinetochore-microtubule attachments and the SAC at non-bioriented chromosomes (Liu et al., 2009). However, these findings support the view that spatial localisation of Aurora B to pericentric chromatin is crucial to phosphorylate its substrates in mitosis.

3.1.3 NDC80 is crucial for SAC silencing

Tension-generated chromosome biorientation is necessary for SAC silencing. The generation of tension and sustained SAC silencing is therefore predicted to require microtubule-binding to NDC80 at the outer kinetochore. In addition, NDC80 has also been proposed to play a direct role in SAC activation by acting as a binding/interaction site for the SAC kinase MPS1 (Hiruma et al., 2015; Ji et al., 2015; Kemmler et al., 2009; Nijenhuis et al., 2013). Using NDC80-HaloTag cell lines I was able to trigger rapid NDC80 degradation as cells entered mitosis by treatment with Halo-PROTAC (Figure 2.10). Western blot indicated that NDC80-depleted cells took longer to degrade key mitotic regulators such as cyclin B1 and longer to dephosphorylate CDK substrates such as PRC1 pT481, implying an extended time spent in mitosis (Figure 2.14). Single cell imaging showed that NDC80-depleted cells entering mitosis struggled with chromosomal alignment and, after a prolonged period spent in mitosis, suffered a higher likelihood of mitotic slippage (Figure 2.15, Figure 2.16, Figure 2.17). This observation was irrespective of ploidy (Figure 2.18), with long-term alignment defects leading to genomically unstable cells (Figure 2.25 - B) regardless of p53 status (Figure 2.22). This implied extended SAC activity could be behind maintaining this mitotic-arrest state, despite the absence of NDC80.

This result was surprising as NDC80 has been reported to be necessary in checkpoint activation, with MPS1 postulated to interact with NDC80, allowing MPS1-KT recruitment, subsequent KNL1 MELT motif phosphorylation and SAC signalling (Hiruma et al., 2015; Ji et al., 2015; Kemmler et al., 2009; Nijenhuis et al., 2013). Once NDC80 is stably bound by a microtubule and biorientation occurs, MPS1 becomes lost from the kinetochore, greatly impeding the SAC and in most cases, silencing it (Hiruma et al., 2015; Ji et al., 2015; Pleuger et al., 2024). This implies that NDC80-mediated MPS1 localisation to the kinetochore is necessary for checkpoint activation. The data presented here, however, suggests continued SAC activity in the absence of NDC80. It was therefore critical to understand what was happening to MPS1 and downstream checkpoint activity under these conditions. MPS1-mStayGold tag integration into NDC80-HaloTag cells revealed a failure of MPS1 to localise to kinetochores in the absence of NDC80 (Figure 2.46 - B), consistent with previous work suggesting MPS1-NDC80 interaction(Kemmler et al., 2009). However, a similar approach taken with BUB1-mStayGold cells, a downstream checkpoint protein, revealed continued BUB1 kinetochore localisation throughout the extended mitotic duration (Figure 2.48 - B, Figure 2.49 - C). It should be noted that not every kinetochore was checkpoint active, but enough activity was present to prevent anaphase onset and extend mitotic duration. The slow dissipation in BUB1 signal observed over this extended mitotic duration was not due to photobleaching, as evidenced by mitotic cells at the beginning and end of an acquisition being of similar intensity (Figure 2.49 - D), as well as the notable photostability improvement of mStayGold in comparison to other green, fluorescent markers (Ando et al., 2024). Testing MPS1 dependence on downstream BUB1 checkpoint activity in both NDC80 positive and null cells revealed equal sensitivity, reducing the checkpoint signal in both cases (Figure 2.57 - B, BUB1-mStayGold, DMSO vs PROTAC, Noc + MPS1-i). It could be postulated that such checkpoint activity is due to cytosolic MPS1 transiently interacting with the kinetochore. Hence, continued checkpoint activity was observed in the near-absence of NDC80 or robust MPS1-kinetochore localisation.

In contrast, removal of the checkpoint scaffold KNL1 was shown to reduce mitotic timing (Figure 2.31 - B, Figure 2.32 - A), consistent with loss of SAC activity, and resulted in rapid anaphase onset and cell division. As a result, instances of both lagging chromosomes and chromosome bridges, both hallmarks of chromosome mis-segregation, were observed (Figure 2.31 - B, Figure 2.50 - B). Live readout of BUB1-mStayGold within this cell line showed weak BUB1 signal in comparison to control cells (Figure 2.51 - C); residual KNL1 not yet degraded by Halo-PROTAC likely accounts for the small levels of BUB1 seen, though these levels were not sufficient to hold cells in mitosis. Hence, under these conditions, changes in force/tension did not lead to SAC activation/silencing, nor was the ability for microtubule binding impeded. This would imply that the initial microtubule attachments made were deemed stable due to insufficient error correction. On a per-kinetochore basis, removal of KNL1 by Halo-PROTAC reduced BUB1 levels beyond MPS1 inhibition alone. Combined inhibition of MPS1 and removal of KNL1 was sufficient to almost completely silence the SAC (Figure 2.58 - B, BUB1-mStayGold), consistent with the idea that any residual KNL1 was denied MELT motif phosphorylation by MPS1.

Overall, these results suggest that NDC80 is essential for checkpoint silencing but not as crucial for checkpoint activation. In the spatial separation model NDC80-mediated microtubule-kinetochore attachments are necessary to couple microtubule pulling forces to spatial separation of kinetochores from the pericentromeres. In a high-tension state, these forces are necessary to spatially separate the kinetochore from Aurora B and allow for subsequent loss of substrate phosphorylation (Figure 3.1 - A). Conversely, in a low-tension state, Aurora B is still able to access its substrates and continue phosphorylating them (Figure 3.1 - B). In the absence of NDC80, no tension, and hence no chromosome bi-orientation, can be achieved due to lack of microtubule binding machinery, permitting continued Aurora B activity towards its substrates (Figure 3.1 - C). Hence, the spatial separation model is consistent with data generated in this thesis, with continued activation of the SAC shown to

be possible in the absence of NDC80. Crucially, in the absence of NDC80 SAC silencing is compromised, most likely due to the failure to generate and maintain a high-tension state.

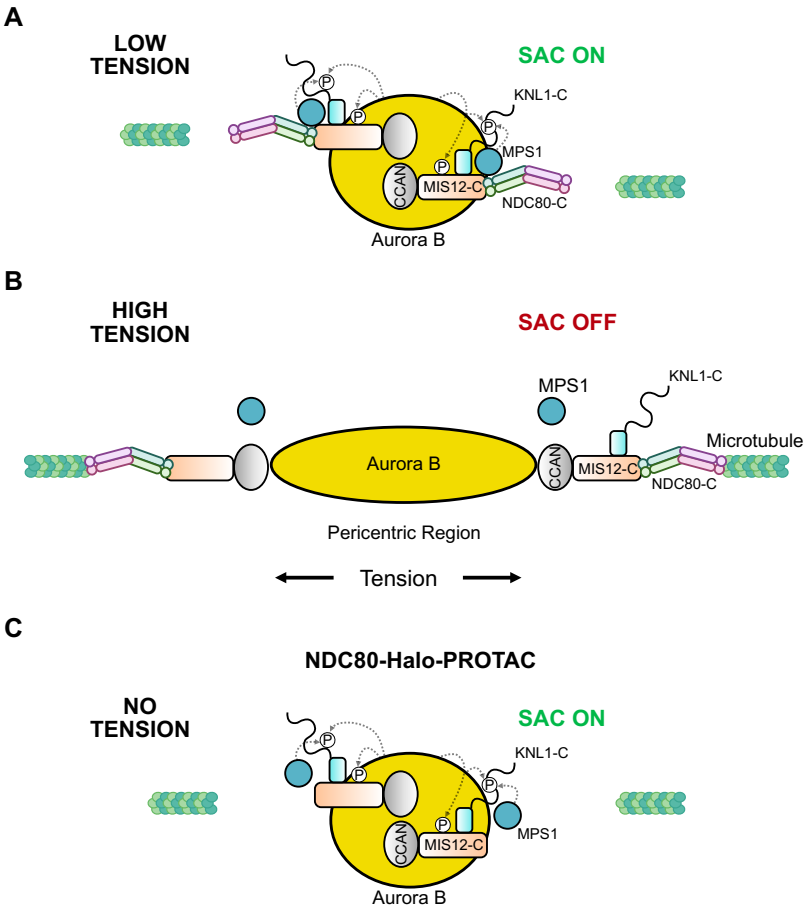

Figure 3.1 - Spatial separation model with loss of NDC80

(A) In a tensioned state, Aurora B is physically separated from its substrates, preventing their phosphorylation. This stabilises microtubule-KT attachments and results in SAC silencing. (B) In a low-tension state, Aurora B can reach and phosphorylate its substrates promoting microtubule release and the SAC. (C) Without NDC80, a low-tension state is maintained allowing for continuous Aurora B phosphorylation of its substrates.

3.2. SAC activation occurs after NDC80 relocalisation from centrosomes to kinetochores during mitotic entry

Further experimentation of NDC80's role in the SAC was performed by determining its dynamics as cells move into mitosis. NDC80 has been robustly shown to localise to kinetochores both via MIS12 (Petrovic et al., 2010) and CENP-C/CENP-T interactions (Suzuki et al., 2015). Dynamic tracking of NDC80-HaloTag signal by live cell imaging revealed a translocation step, where NDC80 is shown to rapidly move from centrosomes to kinetochores (Figure 2.4); a reverse translocation step is also noted from M-G1 (Figure 2.6). Biochemically, immunoprecipitation of NDC80 showed reduced binding to KNL1-C and MIS12-C in G2 compared to two mitotically arrested states (Figure 2.3 - A). Employing high-resolution imaging of the G2-M transition with short time intervals showed a very brief partial relocalisation period, after which full relocalisation occurs (Figure 2.5 - A). The functional consequences of this translocation show that checkpoint activity is only initiated upon full relocalisation of NDC80 to centromeres, as evidenced by BUB3, BUB1, BUBR1, MAD1 and MAD2 staining (Figure 2.7, Figure 2.8, Figure 2.9). These are also shown to be fully kinetochore localised, with no discernible centrosomal signal seen in G2. CDC20, however, appeared to show signal coinciding with partial translocation of NDC80 at mid-NEBD/prophase. CDC20, when part of the mitotic checkpoint complex (CDC20, BUB3, BUBR1, MAD2) binds and inhibits APC/C (Izawa & Pines, 2014; Kallio et al., 2002; Sudakin et al., 2001); its early presence at kinetochores may serve as a platform, priming them for MCC formation at pilot NDC80 molecules. Conversely, live cell tracking of the checkpoint scaffold protein KNL1 revealed robust kinetochore localisation as cells move from G2 to mitosis (Figure 2.31 - A), in contrast to NDC80. This is interesting as it implies that the platform for checkpoint complexes to assemble exist at the kinetochore prior to NDC80 arrival, but that these complexes only start to recruit once NDC80 is fully bound. In the intermediary partial re-localisation stage, it could be argued that kinetochore-bound NDC80 has a free site for MPS1 interaction which has not yet been utilised. Hence, perhaps some form of conformational change may happen to the

kinetochore architecture post-NDC80 relocalisation to allow this interaction and SAC activation. The mechanism of NDC80 recruitment to the centrosome during the G2/M transition remains to be determined. One possibility is that NDC80 appearing at the centrosome could signify early binding to the emerging microtubules as they begin to emanate from the centrosome to form the mitotic spindle. Previous recent work has shown that NDC80 is phosphorylated predominantly by Aurora A kinase (Sobajima et al., 2023), which is localised largely to the centrosomes and spindle poles in G2 and early mitosis. It is tempting to speculate that centrosome-localised NDC80, due to its close proximity to Aurora A, could be regulated by Aurora A to influence its localisation as the cell progresses through M phase. Such a possibility requires further mechanistic dissection.

With both NDC80 and KNL1 localisations accurately determined by HaloTag visualisation, a revised model can be created to describe kinetochore formation from G2 to mitosis. In late G2, NDC80 and KNL1 exist separately (Figure 3.2 - A), with NDC80 at centrosomes and KNL1 at the kinetochore. At NEBD/Prophase, NDC80 begins to re-locate to kinetochores. Given its centrosome localisation and microtubule binding domains, it is postulated that NDC80 movement could occur via microtubule plus end-mediated transfer (Figure 3.2 - B). This may explain why centrosome signal decreases as partial relocalisation occurs, until all signal is transferred over to kinetochores (Figure 2.5 - A). Once full relocalisation has taken place and the KMN network is complete, kinetochores become checkpoint active (Figure 2.7, Figure 2.8, Figure 2.9). This suggests that MPS1-NDC80 mediated interaction may phosphorylate KNL1 only once full kinetochore assembly has been achieved (Figure 3.2 - C).

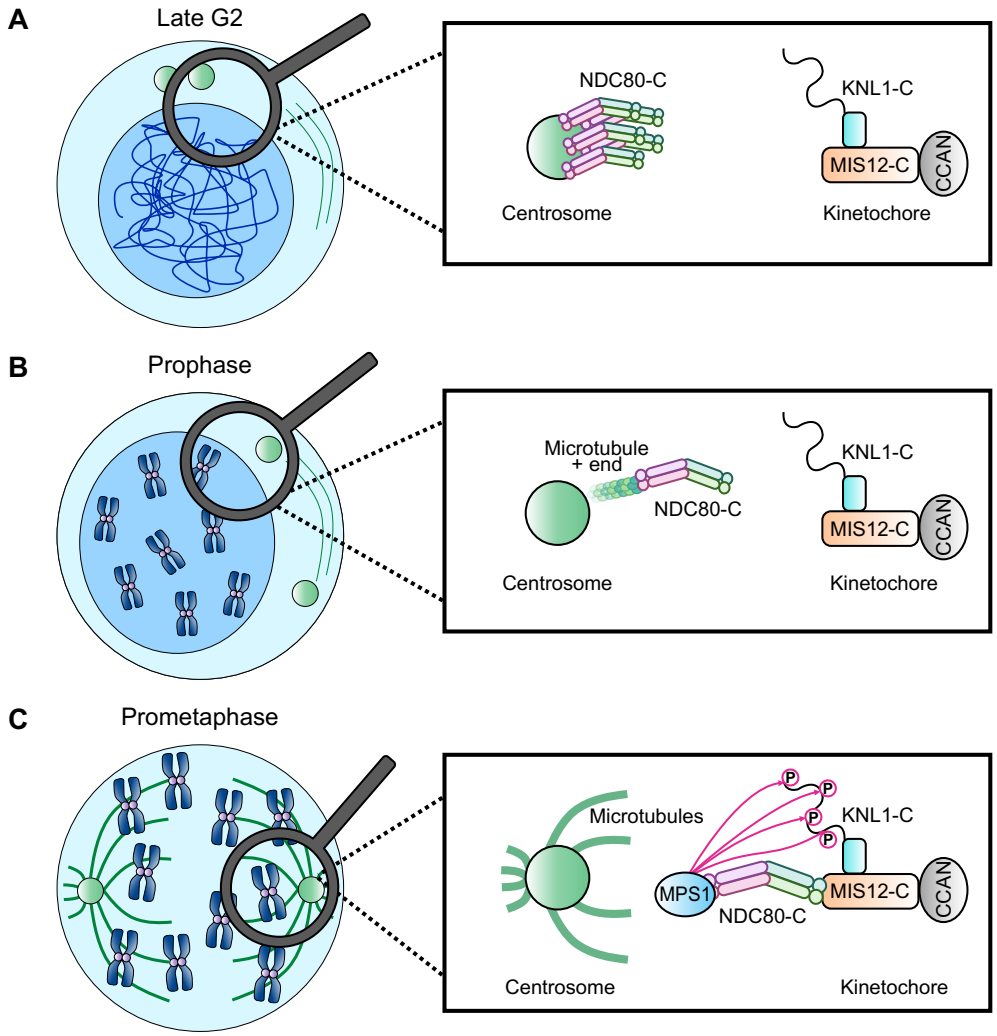

Figure 3.2 - NDC80 recruitment to kinetochores; an updated model

From experimental data obtained in this thesis, NDC80 is shown to be centrosome localised at late G2. NDC80 then rapidly re-locates to kinetochores during NEBD, postulated to be via microtubule plus ends. Once NDC80 is bound to the kinetochore, MPS1 can interact and begin phosphorylation of KNL1 MELT motifs, allowing for rapid activation of the SAC.

Additionally, stoichiometric analysis between NDC80 and KNL1 revealed a 3 NDC80 : 2 KNL1 ratio (Figure 2.27) in mitotic cells. This differs from previous in vitro structural models of the KMN network which show a 1:1:1 ratio between network proteins (Polley et al., 2024). However, the stoichiometric ratio observed does align with previous fluorescence-based studies which reported ~244 NDC80 complexes per kinetochore, of which ~151 were part of

the KMN network (Suzuki et al., 2015); giving an approximate 3:2 ratio of NDC80:KNL1. This may imply that KMN network components are more flexible than a strict 1:1:1 stoichiometric ratio, or alternatively, that excess NDC80 exists outside of the main KMN network which may bind directly to CENP subunits (Suzuki et al., 2015) e.g. by direct NDC80-CENP-T interaction (Takenoshita et al., 2022). Mechanistically, these observations are consistent with a model which places greater reliance on NDC80 for physical movement of chromosomes about the mitotic spindle, with KNL1 serving as a signalling hub or amplifier to ensure that checkpoint activity is maintained.

3.3. CPC^{INCENP} is required for Aurora B localisation and full SAC activation

To investigate Aurora B-dependent checkpoint activation further, the inner centromere protein INCENP was targeted for HaloTag integration because of its role in mediating Aurora B kinase localisation and activation during mitosis (Xu et al., 2009). Confirmatory experiments showed that Halo-PROTAC depletion of INCENP resulted in loss of defined localisation for the other CPC components tested (Figure 2.38, Aurora B and Survivin), consistent with INCENP being a scaffold for other CPC components (Klein et al., 2006). Additionally, removal of INCENP greatly reduced phosphorylation of known key Aurora B substrates, including Aurora B itself at T232, and Histone H3 pS10 (Figure 2.41). These reductions were further exacerbated by chemical inhibition of any non-localised Aurora B. Notably, NDC80 pS55 remained unchanged under both INCENP removal and Aurora B inhibition but was absent in Aurora A inhibited cells (Figure 2.41). This is consistent with recent observations showing Aurora A-mediated phosphorylation of some N-terminal NDC80 sites at microtubule-attached kinetochores (Sobajima et al., 2023).

Interestingly, INCENP removal resulted in cells having a higher propensity for undergoing a mitotic slippage phenotype (Figure 2.40 - D, Figure 2.53 - B), though no hyper-extension of mitotic time was observed (Figure 2.40 - C, Figure 2.53 - A), unlike in NDC80-depleted cells.

When tracking BUB1-mStayGold intensity within this cell line, substantially less signal was seen for Halo-PROTAC treated cells in comparison to control cells (Figure 2.53 - C). This would imply that, despite reduced checkpoint activity, there was still enough to allow timely progression through mitosis. Interestingly, the SAC did seem to turn off at mitotic exit despite no discernible alignment (Figure 2.52 - B). This was interesting as the kinetochore architecture to generate tension was still present, but unable to sense correct attachment nor form bi-orientated chromosomes. This could in part be due to a lack of chromosome condensation, and perhaps limited accessibility of microtubules to the kinetochore due to this morphology. One could also postulate that the SAC activity present in the absence of INCENP (and hence displacement of Aurora B) is solely from MPS1 phosphorylation of KNL1 MELT motifs, and that once MPS1 activity is reduced by NDC80-mediated kinetochore attachment, this phosphorylation reduces. Consistent with this idea, BUB1 checkpoint activity appeared to be synergistically reduced by both removal of INCENP and inhibition of MPS1 (Figure 2.59 - B, BUB1-mStayGold). Without Aurora B phosphorylation of KNL1, NDC80, or MIS12 complexes, no error correction can take place, and the SAC cannot be maintained (Welburn et al., 2010), resulting in APC/C mediated mitotic exit despite the absence of chromosome alignment.

3.3. Aurora B dependent phosphorylation across the proteome

To gain a better idea of Aurora B substrates across the proteome, whole cell phosphoproteomics analysis was performed (with the help of Dr James Holder and Dr Sean Burnap) (Figure 2.70) comparing mitotically arrested control and INCENP-depleted cells. These results revealed a large reduction in Histone H3 and H1 phosphorylation, whose loss is consistent with issues in chromosome condensation (Adams et al., 2001; Chu et al., 2011; Goto et al., 2002). The ssDNA-binding replication protein RPA1 was also found to be downregulated, which is of interest given recent work highlighting that mutation of this site resulted in chromosome segregation errors (Roshan et al., 2023). The only set of sites to show a strong up-regulation belonged to Lamin A, implying issues in nuclear envelope morphology

(Heald & Yckeon, 1990). The specific phospho-sites identified, and their implications are discussed further in Results 2.6.2.

Also of interest was significant reduction in phosphorylation of the microtubule-depolymerising kinesin MCAK. Aurora B has been previously shown to both target MCAK to the centromere/pericentromere region and to regulate its activity in depolymerising microtubules, with loss of function experiments for MCAK shown to result in syntelic errors in microtubule-kinetochore attachments (Andrews et al., 2004). Further work revealed that Aurora B phosphorylation of MCAK at multiple sites produced a graded level of microtubule depolymerisation activity (McHugh et al., 2019). Thus, under higher tension, reduced phosphorylation and weaker centromere targeting of MCAK could be found as proximity to Aurora B decreases, allowing for greater levels of dynamic microtubule turnover. Thus, the Aurora B-MCAK activity gradient may function act as an indirect modulator of tension, facilitating chromosome biorientation by spatially regulated signalling. Within the framework of the spatial separation model, the specific localisation of MCAK relative to Aurora B and the outer kinetochore becomes crucial. If it is enriched at centromeres adjacent to CENP-A and the outer kinetochore, it is likely to be phosphorylated by Aurora B under low-tension conditions, thereby dampening, but not abolishing, its depolymerising activity. However, if MCAK is mainly present at pericentromeres, then it would travel with Aurora B but become separated from microtubules bound to the outer kinetochore. Further work using super-resolution imaging to study MCAK localisation on chromosomes as they become bioriented should help address these questions.

Similar to MCAK, reduction in phosphorylation of DSN1, part of the MIS12 complex, was also observed after PROTAC-mediated INCENP degradation. Previously, Aurora B-dependent phosphorylation of DSN1 has been implicated in providing additional sensitivity to the microtubule binding activity of the KMN network, such that when combined with further KMN phosphorylation overall microtubule attachment is reduced (Welburn et al., 2010). Structural

and biochemical work indicated that DSN1 phosphorylation can enhance the CENP-C-MIS12 interaction, thereby promoting kinetochore assembly (Petrovic et al., 2016). However, individual phosphomimetic and phosphoinhibitory mutations of DSN1, did not appear to reduce cell viability or kinetochore assembly in cells (Welburn et al., 2010). How can these findings on the role of DSN1 phosphorylation be explained? One potential model is that phosphorylation of DSN1 induces a conformational change that modulates kinetochore architecture, making the kinetochore permissive for error correction and SAC signalling by facilitating MPS1 recruitment, rather than acting as a strict requirement for kinetochore assembly. Further work will be needed to answer these important questions.

3.4. Final comments

Integration of the HaloTag system has enabled robust analysis of NDC80, KNL1, and INCENP in relation to SAC activity, dynamics, mitotic timing, proliferative capabilities, cellular architecture, and Aurora B positioning. Immediate loss-of-function phenotypes were determined without prolonged RNA interference treatment, reducing the risk of off-target effects, cellular adaptation, and apoptosis.

Super-resolution analysis of the kinetochore and CPC provided further evidence for the spatial separation model in which Aurora B must be physically separated from its substrates under tension to reduce phosphorylation. Additional evidence comes from NDC80 degradation, which both collapse kinetochore pairs into an un-tensioned state and sustains prolonged SAC activity. This observation implies that whilst NDC80 contributes to robust SAC activation, it is critical for SAC silencing; its removal markedly prolongs mitosis due to sustained SAC activity. In contrast, KNL1 proved essential for SAC activation, with its removal reducing BUB1 recruitment and shortening mitotic timing. INCENP was required for CPC localisation, and therefore Aurora B targeting. In its absence, chromosomes failed to condense properly, and cells exhibited a higher propensity to undergo mitotic slippage. Additionally, widespread reduction in Aurora B-dependent phosphorylation sites were observed across the proteome,

suggesting further issues with chromosome condensation, segregation, error correction, and SAC signalling. Further work could test how Aurora B signalling changes under different mitotic conditions, such as additional inhibition of non-localised Aurora B, or perhaps monopolar- or G2-arrested cells to establish differentials in substrate targeting across cell cycle/mitotic stages.

An additional insight from this work is that NDC80 is initially absent from the kinetochore in G2 and rapidly re-localises at mitotic entry, completing the KMN network and enabling SAC signalling. This updated model is an interesting observation, but proposes some outstanding questions to be addressed; how does NDC80 find the kinetochore surface so rapidly? Why do 'pilot' microtubules not remain attached once NDC80 has become kinetochore localised? Is there a biological reason for a partial kinetochore assembly; does this prevent premature checkpoint activation? These questions leave further work for determining the mechanistic reasoning behind this phenomenon.

Another interesting question is how NDC80-depleted cells exit mitosis. It could be postulated that other pathways (such as $p31^{Comet}$) may help to gradually reduce cytosolic MCC to permit mitotic exit in the absence of tension. Nevertheless, NDC80 does appear to partially contribute to checkpoint activation, and to MPS1 kinetochore localisation, suggesting that more than one pathway is required to robustly underpin checkpoint activity. Such pathways could include direct Aurora B phosphorylation of KNL1, and fibrous corona-mediated MAD1-MAD2 recruitment, though further testing of these dependencies is required.

Together, these findings demonstrate that precise regulation of kinetochore composition and Aurora B activity are crucial for mitotic progression and genomic integrity. Disruption of any of these key components compromises both cell division and long-term proliferative capacity. This may contribute to the chromosomal instability and aneuploidy commonly observed in cancer, highlighting the broader relevance of kinetochore and Aurora B regulation to disease.

4. Materials & Methods

4.1. Reagents and Antibodies

Standard lab reagents and consumables were purchased from ThermoFisher Scientific, Sigma Aldrich/Merck and VWR. Primary and secondary antibodies have been listed in tables 4.1 and 4.2 respectively; where these are commercially available, a catalogue number has been provided.

Table 4. 1 - List of primary antibodies used for Western Blot (WB), Immunofluorescence (IF), or Stimulated Emission Depletion microscopy (STED).

Antibody [Clone]	Company	mAb/ pAb	Catalogue#	Species	Dilution	Use
α-Tubulin [DM1A]	Sigma-Aldrich	mAb	T6199	Mouse	1:1000 1:10000	IF WB
α-Tubulin	ABCD	mAb	ABCD_AA345	Rabbit	1:250	STED
Aurora A [1G4]	CST	mAb	4718S	Rabbit	1:1000	IF, WB
Aurora A pT288 [C39D8]	CST	mAb	3079S	Rabbit	1:1000	IF, WB
Aurora B [6/AIM1]	BD Transduction	mAb	611083	Mouse	1:1000, 1:100	IF/WB STED
Aurora B	Abcam	pAb	Ab2254	Rabbit	1:100	STED
Phospho-Aurora A/B/C [D13A11]	CST	mAb	2914S	Rabbit	1:1000	WB
Borealin [A-5]	Santa Cruz	mAb	Sc-376635	Mouse	1:200	IF/WB STED
BUB1	Bethyl	pAb	A300-373A	Rabbit	1:1000	IF/WB
BUB3 [EPR5319(2)]	Abcam	mAb	Ab133699	Rabbit	1:1000	IF
BUBR1	Millipore Bethyl	pAb pAb	MAB3612 A300-386A	Mouse Rabbit	1:1000 1:1000	IF IF/WB
Caspase 3	CST	pAb	9662S	Rabbit	1:1000	WB
Cleaved Caspase 3 [5A1E]	CST	mAb	9664S	Rabbit	1:1000	WB
CENP-A [3-19]	GeneTex	mAb	GTX13939	Mouse	1:1000	IF
CENPC	MBL	pAb	PD030	Guinea Pig	1:2000	IF
Cyclin B1 [GNS3]	Millipore	mAb	8A5D12	Mouse	1:5000	WB
Cyclin A2 [E399]	Abcam	mAb	Ab32498	Rabbit	1:10,000	WB
Cyclin E1 [EP435E]	Abcam	mAb	Ab33911	Rabbit	1:1000	WB

CDC20	ProteinTech	pAb	10252-1-AP	Rabbit	1:1000	IF
Cullin 2	Invitrogen	pAb	51-1800	Rabbit	1:1000	WB
DSN1	ProteinTech	pAb	17742-1-AP	Rabbit	1:1000	WB
Geminin [A-3]	Santa Cruz	mAb	Sc-74496	Mouse	1:200	WB
HaloTag	Promega	mAb	G9211	Mouse	1:1000	WB
Histone H3pT3	Millipore	pAb	07-424	Rabbit	1:1000	WB
Histone H3pS10 [6G3]	CST	mAb	9706	Mouse	1:1000	WB
INCENP	Homemade	mAb	--	Rabbit	1:1000	IF/WB
KNL1	ProteinTech	pAb	28695-1-AP	Rabbit	1:1000	IF/WB
Lamin B1	Abcam	pAb	Ab16048	Rabbit	1:1000	IF
MAD1	GeneTex	pAb	GTX105079	Rabbit	1:1000	IF
MAD2	Bethyl	pAb	A300-301A	Rabbit	1:1000	IF
MIS12 [2G5F6]	ProteinTech	mAb	67475-1-IG	Mouse	1:1000	WB
MPS1 [NTc.3472-1]	Millipore/ Upstate	mAb	05-682	Mouse	1:1000	WB
NDC80 pS55	Homemade	pAb	--	Sheep	1:1000	IF
NDC80 pS55	GeneTex	pAb	GTX70017	Rabbit	1:1000	WB
NDC80 HEC1 [9G3]	Abcam	mAb	Ab3613	Mouse	1:1000	IF/WB
NUF2 [E-6]	Santa Cruz	mAb	Sc-271251	Mouse	1:200	WB
NSL1	Bethyl	pAb	A300-795A	Rabbit	1:1000	WB
p53 [DO7]	CST	mAb	48818	Mouse	1:1000	WB
p21 [12D1]	CST	mAb	2947	Rabbit	1:1000	WB
Pericentrin	Abcam	pAb	Ab4448	Rabbit	1:2000	IF
PPP6C [EPR8764]	Abcam	mAb	Ab131335	Rabbit	1:1000	WB
PPP6C	Homemade	pAb	--	Sheep	1:1000	WB
PRC1 pT481 [EP1514Y]	Abcam	mAb	Ab62366	Rabbit	1:5000	WB
SGO1 [3C11]	Abcam	mAb	Ab58023	Mouse	1:1000 1:100	WB STED
SPC24	ProteinTech	pAb	26268-1-AP	Rabbit	1:1000	WB
SPC25	ProteinTech	pAb	26474-1-AP	Rabbit	1:1000	WB
Survivin [EPR2675]	Abcam	mAb	Ab134170	Mouse	1:1000 1:250	IF/WB STED
TPX2 [18D5-1]	Abcam	mAb	Ab32795	Mouse	1:1000	IF/WB
ZWINT	ProteinTech	pAb	12282-2-AP	Rabbit	1:1000	WB
γ-H2A.X [2F3]	Biolegend	mAb	613402	Mouse	1:1000	WB

Table 4. 2 - List of secondary antibodies used for WB, IF, and STED, and fluorescent probes

Antibody	Company	Species	Catalogue#	Dilution
Alexa Fluor 488-Donkey-Anti-X	Thermo Fisher	Mouse Rabbit Sheep	A21202 A21206 A11015	1:1000 All
Alexa Fluor 555-Donkey-Anti-X	Thermo Fisher	Mouse Rabbit	A31570 A31572	1:1000 All
Alexa Fluor 594 Plus-Donkey-Anti-X	Thermo Fisher	Mouse Rabbit	A32744 A32754	1:250-1:500 All
Alexa Fluor 647-Donkey-Anti-X	Thermo Fisher	Mouse Rabbit	A31571 A31573	1:1000 All
Alexa Fluor 647-Donkey-Anti-X	Jackson ImmunoResearch	Guinea Pig	706-605-148	1:1000
CF680R-Donkey-Anti-X	Biotium	Rabbit Mouse	20195-1 20194-1	1:250 1:250
DAPI	Thermo Fisher	N/A	D1306	1:2000
JFX554	Janelia	N/A	(Grimm et al., 2017)	1:10,000
JFX646	Janelia	N/A	(Grimm et al., 2017)	1:10,000
HRP-Donkey-Anti-X	Jackson ImmunoResearch	Mouse Rabbit Sheep	715-035-150 711-035-152 713-035-147	1:2000-1:5000 All
PicoGreen	Invitrogen	N/A	P7589	1:500-1:1000

4.2. Cell culture

HCT116 cells were purchased from ATCC (CLL-247) and cultured in McCoy's 5A medium (Gibco #16600082) with 10 mM Sodium Pyruvate (Thermo Fisher #11360088), 100 µg/ml Penicillin-Streptomycin (Thermo Fisher #15140122) and 10% ([vol/vol]) FBS. The mycoplasma status of the parental cell lines was confirmed to be negative by the EZ-PCR Mycoplasma Test Kit with internal control (Geneflow K1-0210), and cell line authenticity determined by STR profiling (Northgene). During routine passaging, cells were washed with 1X PBS, incubated with TrypLE Express Enzyme cell dissociation reagent (Gibco #12605036) for 5 minutes at 37°C, resuspended in media, and diluted to a lower confluency in a fresh dish. Where cells were to be seeded at a particular density, 10 µl of resuspended cells were counted using an automated cell counter (DeNovix Cell Drop), providing a unit of x cells per ml. Cells were maintained in a cell culture incubator (Thermo HERAcell #51013568) set at 37°C with 5% CO_2.

4.3. CRISPR/Cas9 technology

4.3.1. Guide RNA Design

Guide RNAs were designed by downloading the full genebank file for each protein to tag from NCBI (Table 4.3) and opening in Snapgene (V5.0.8). An area surrounding the terminus to tag was selected and a series of guide RNAs determined using various websites (e.g. https://crispor.gi.ucsc.edu) with quality checkers, ensuring minimal off-target effects. A list of guide RNAs used successfully for knock-in/ knockouts are shown in Table 4.3 (custom oligos ordered from ThermoFisher). Forward and reverse primers for each guide were flanked with 5' CACC(G) 3' or 5' AAAC 3' respectively, where 'G' was added if the guide sequence didn't start with a guanine to improve U6 promoter efficiency. Forward and reverse guide primers were fused by mixing in equal parts and heating at 95°C for 5 minutes. Each guide was ligated into the BbsI-HF (NEB #R3539) cut Cas9-containing pX459 vector (Addgene 62988) using T4 ligase (NEB M0202L); guides used for knockouts contained puromycin resistance, whereas those used for knock-ins contained no resistance marker. pX459-guide plasmids were transformed into XL-1 Blue competent cells, around five-ten colonies were selected, grown, mini-prepped (Qiagen #27107), and sanger sequenced (Source Genomics, Cambridge, UK).

Table 4.3 - Gene accession numbers and guide RNAs used for CRISPR editing

Protein	NCBI Accession Number	gRNA	Terminus
NDC80	NP_006092.1	5' tcttcactagaaacatcttg 3'	C-Term
KNL1	NP_733468.3	5' aatggatggggtgtcttcag 3'	N-Term
PPP6C	NP_001116827.1	5' gcgaaggcctcaaaggaaata 3'	C-Term
INCENP	NP_001035784.1	g1: 5' agagctccagaaggttcggt 3' g2: 5' ctggtgcgcttgtgatagcg 3'	C-Term
p53	NP_000537.3	5' gccattgttcaatatcgtccg 3'	N-Term
BUB1	NP_004327.1	5' agattagggccctacgtaat3'	C-Term
MPS1	NP_003309.2	5' agtccaatatattttatagg 3'	C-Term

4.3.2. Molecular cloning & homology cassette design

Homology cassettes were designed to incorporate tags into the endogenous locus of each gene of interest via homologous recombination. Homology regions for each gene of interest were isolated using KOD PCR (Merck #71086) from the genomic DNA of parental HCT116 cells (QuickExtract DNA isolation solution, Lucigen #QE09050). Isolated homology regions were ligated into blunt-end pSCA vector (Agilent #240207) and transformed into XL-1 Blue competent cells. Around five-ten colonies were selected, grown, mini-prepped (Qiagen #27107), and sanger sequenced to check for integration (Source Genomics, Cambridge, UK). KOD PCR of two (minimum 350 bp) homology arms was performed, with primers containing sequences flanking pBlueScript and the specified tag construct. Similarly, KOD PCR of the specified tag construct with primers containing sequences flanking each respective homology arm was also performed. The part of the primer where amplification was to occur had an expected Tm of around 60°C; the part used for Gibson assembly had an expected Tm of around 50°C, optimised for each respective process. pBlueScript vector was cut using the EcoRV-HF enzyme (NEB #R3195) by heating at 37°C for 2 hours, running on a 0.8% agarose gel (Invitrogen #15510-027), visualising bands for extraction with Midori Green DNA stain (Geneflow #S6-0022), and isolating the cut band with the Monarch gel extraction kit (NEB #T1020). Gibson assembly (NEB #E2611) master mix was used to assemble all four parts of the construct (EcoRV-cut pBlueScipt, left/right homology arms, and tag). Once the homology cassette was created, the plasmid was mutagenized using KOD PCR to change 3 base pairs along the gRNA+PAM site, ensuring that once successful integration had occurred, no more Cas9-mediated cutting could occur; these mutations were silent to ensure amino acid composition remained unchanged. Alternatively, some constructs (BUB1-mStaygold, MPS1-mStayGold) were gene synthesized in their entirety (ThermoFisher, GeneArt).

For C-terminal tags, a minimum length of 12AA GGSGGGSGGGG linker replaced the stop codon of the gene, followed by the tag sequence (HaloTag/FKBP-F36V/mStayGold - synthesized using ThermoFisher, GeneArt), GSG-P2A to ensure ribosome skipping, and a

resistance marker (Puromycin/ Blasticidin/Geneticin) to allow for selection of successfully incorporated tags. For N-terminal tags, a similar approach was taken, with the constructs added in the opposite order immediately preceding the first methionine (e.g. HaloTag-GSG-P2A-PURO-Linker-NTerm). Primers used for cassette generation are in Table 4.4.

Table 4.4 - PCR Primers for cassette generation

Target	Purpose	Primers (5'-3')
NDC80	Homology Region 1	Fwd: atgcagtacattgaataaactgcagcc Rev: ctggatttggctcacatgatgtagg
NDC80	Homology Region 2	Fwd: tttgataaatacgaaggtgaaaaccagg Rev: atatgaaaataaatgggtgcggctgg
NDC80	LHA	Fwd: ccgggctgcaggaattcgatataaatacgaaggtgaaaac Rev: ccgccaccaccgctcccaccttcttcagaagacttaatta
HaloTag	Halo + Overhang with NDC80	Fwd: ctaattaagtcttctgaagaaggtgggagcggtggtggcgg Rev: tgatcaacattttatcttcaggcaccgggcttgcgggtca
NDC80	RHA	Fwd: catgacccgcaagcccggtgcctgaagataaaatgttgatcatg Rev: gacggtatcgataagcttgatctacctcagtctcgtgagtag
NDC80-Halo Plasmid	Mutagenesis For Guide+PAM	Fwd: tctcttcactagaaacacctggaagagcagattgctaaag Rev: ctttagcaatctgctcttccaggtgtttctagtgaagaga
PPP6C	Homology Region 1	Fwd: cgatcggcagttttctgagataagc Rev: gtcctaacttttcaacctttccagttgc
PPP6C	LHA	Fwd: gctgcaggaattcgatagttttctgagataagccctggtgg Rev: tttccacctgcactcccataccggtggatcctccgc
FKBP-F36V	dTag + Overhang with PPP6C	Fwd: ggatccaccggtatgggagtgcaggtggaaaccatct Rev: gggcgaaggccttagccctcccacacataaccag
PPP6C	RHA	Fwd: gtgtgggagggctaaggccttcgcccatcc Rev: cggtatcgataagcttgatgtaaactggattgatcacattctactcaactgg
KNL1	Homology Region 1	Fwd: gcgccgctgctctcc Rev: gtgagacagggtcttgaggtagg
KNL1	Homology Region 2	Fwd: ctgcaagctccgcctcag Rev: gggtgccttgtcagtttaccat
KNL1	LHA	Fwd: gctgcaggaattcgatctgcaagctccgcctca Rev:gcttgtactcggtcatttttgaagaaaacttttctgtaacaaatatacaatattagaaaacatga
HaloTag	Halo + Overhang with KNL1	Fwd: ttacagaaaagttttcttcaaaaatgaccgagtacaagcccac Rev: gacaccccatccattccgccgccgcc
KNL1	RHA	Fwd: cggcggcggaatggatggggtgtcttcagagg Rev: cggtatcgataagcttgatgggtgccttgtcagtttaccattg
KNL1-Halo Plasmid	Mutagenesis For Guide+PAM	Fwd: caaaaatggatggggtttcctcagaagctaatgaagaaaag Rev: cttttcttcattagcttctgaggaaaccccatccatttttg

INCENP	Homology Region 1	Fwd: ctgagccggaagtcagggag Rev: gccagctttcattggttctaagca
INCENP	Homology Region 2	Fwd: tcatccgtgaaaggggggtg Rev: gtctttcccaatgaacaaactcccc
INCENP	LHA	Fwd: gctgcaggaattcgattcatccgtgaaaggggggtg Rev: accgctcccaccgtgcttcttcaggctgtaggc
HaloTag	Halo + Overhang with INCENP	Fwd: agcctgaagaagcacggtgggagcggtggtg Rev: gcaggccagcctcaggcaccgggcttg
INCENP	RHA	Fwd: cccggtgcctgaggctggcctgcgg Rev: cggtatcgataagcttgatgtctttcccaatgaacaaactcccc
INCENP -Halo Plasmid	Mutagenesis For Guide+PAM	Fwd: ttcaagaagagcaagcctcgctaccataagcgcaccagctctg Rev: cagagctggtgcgcttatggtagcgaggcttgctcttcttgaa

4.3.3. Cell transfection/nucleofection and antibiotic selection

For cell transfection, mixes were prepared in DNase-free Eppendorf tubes (Eppendorf #0030108035) and consisted of 100 µL Opti-MEM media (Gibco #11058021), 3 µL Mirus-TX2 (Mirus, #MIR6004), and up to 1 µg of plasmid DNA. Ordinarily, 400-500 ng of gRNA and 400-500 ng of homology cassette were added per reaction; for transfection controls, unedited pBlueScript was used instead. Transfection mixes were vortexed briefly and incubated at room temperature for 30 minutes before being added dropwise to cells (one well of a 6-well plate, seeded at a density of 50-80 K around 36-48 hours prior). Two days post-transfection, cells were split evenly amongst a 6-well plate for antibiotic selection with varying concentrations.

Alternatively, where transfection was not successful, nucleofection was used. During routine passaging, 500,000 - 1,000,000 cells were counted, pelleted, and resuspended in 100 µL of nucleofection solution (Nucleofection kit - Lonza #VCA-1003). This solution was gently pipetted into a DNase-free tube containing 4 µg gRNA and 6 µg homology cassette, before being moved into a cuvette provided in the nucleofection kit. The cuvette was placed into an Amaxa Nucleofector and run on the T-0023 programme, after which cells were pipetted into one well of a 6-well plate (containing media). One day later, cells were split evenly amongst a 6-well plate for antibiotic selection with varying concentrations.

The amount of time cells were incubated in antibiotic for selection was dependent on the antibiotic used; in general, puromycin (InvivoGen # ant-pr-1) incubation was 1-2 days, blasticidin (InvivoGen #ant-bl-05) 3-7 days, and geneticin (ThermoFisher Scientific #10131027) 7-14 days (replaced every 3-4 days). Cells were kept under antibiotic selection until control cells were dead, after which the antibiotic was washed out, and transfected cells were allowed to recover. Once recovered, cells were seeded into 96-well plates (at a density of approx. 1 cell / 100 µL), and single-cell derived colonies left to grow for 7-14 days. Once confluent, these clones were expanded into 12-well plates to grow further. Cells were then split into 6-well plates, and a sample taken and lysed for western blot (Methods 4.4.2). KOD PCR validation and sanger sequencing were also performed to check tag integration. Once deemed successful, clones were frozen down in media containing 10% [vol/vol] DMSO (Sigma-Aldrich #276855) and kept in liquid nitrogen for long term storage.

4.4. Biochemical techniques

4.4.1. Drug-specific cell cycle phase arrests/ inhibitors

For certain experiments, synchronisation was required to arrest cells in a particular cell cycle phase, or stage in mitosis. These methods are described below, with details of all drugs shown in Table 4.5.

4.4.1.1. G2 arrest and release

Cells are arrested in G2 by using 6 µM of the CDK-1 inhibitor RO-3306 for 16-18 hours. Cells are then washed out of RO four times, using 2 ml media per wash, allowing for progression into mitosis. Where cells are to be accumulated up to metaphase, 20 µM of the proteasome inhibitor MG132 was added for 3-4 hours. In some experiments (specified in the relevant results figure), additional inhibitors may be added towards the latter end of MG132 incubation (Table 4.5) e.g. Aurora A/B kinase inhibitors.

4.4.1.2. Mitotic arrests

Where cells were to be arrested in mitosis without any preceding G2 arrest, low dose nocodazole (82.5 nM) was added for 3-4 hours before being gently washed out; this dose allowed for spindle re-formation over 15-30 minutes. For mitotic arrests where spindle reformation was not required (e.g. samples for western blots), a higher dose of 330 nM nocodazole or 10 μM proTAME was used for 3-4 hours and not washed out. To arrest cells in a monopole-like state, the Eg5/KIF11 inhibitor STLC was used for 3-4 hours; for perturbed chromosome alignment, a CENP-E-inhibitor was used for 3-4 hours.

4.4.1.3. General drug-based inhibition

To inhibit checkpoint activation, 4 μM of the MPS1-inhibitor AZ3146 was added to cells 15 minutes prior to imaging.

To induce a DNA-damage response, 2 mM of the ribonucleotide reductase inhibitor Hydroxyurea was added for 24 hours. Alternatively, cells could be treated with 200 ng/ml of Neocarzinostatin (NCS). Whilst not directly causing DNA damage, 2.5 μM of the MDM2-inhibitor Nutlin-3A could be used to induce a rise in p53.

To prevent Cullin-mediated E3 ligase ubiquitination, 10 μM of the Nedd8 inhibitor pevonedistat was added to cells for 4 hours. All drugs/inhibitors mentioned are detailed in Table 4.5.

Table 4.5 - Inhibitors/Drugs

Reagent	Source	Catalogue#	Working Concentration	Incubation Time
Aurora A-Inhibitor MLN8237	ApexBio	A4110	1 μM	30 mins
Aurora B-Inhibitor ZM447439	ApexBio	A4113	10 μM	1 hour
CDK1-Inhibitor RO-3306	Tocris	4181	6 μM	16-18 hours
MG132 Proteasome Inhibitor	Merck	474790-5MG	20 μM	3-4 hours
MPS1-Inhibitor AZ3146	Tocris	3994	4 μM	15 mins minimum
S-trityl L-cysteine (STLC) Eg5-Inhibitor	Merck	164739-5G	10 μM	3-4 hours
CENP-E-Inhibitor	Tocris	GSK923295	300 nM	3-4 hours
Nocodazole Spindle Poison	Sigma Aldirch	487928	82.5-330 nM	Depends on use-case.
APC/C-Inhibitor ProTAME	Tocris	7734	10 μM	3-4 hours
DNA Damage Hydroxyurea	Sigma Aldrich	H8627	2 mM	24 hours
MDM2-Inhibitor Nutlin 3A	Selleck Chem	S8059	2.5 μM	Up to 5 days
DNA Damage Neocarzinostatin (NCS)	Sigma-Aldrich	N9162	200 ng/ml	1 hour
NEDD8-inhibitor Pevonedistat	Stratech	S7109-SEL-5mg	10 μM	4 hours

4.4.2. Cell lysis & western blotting

Cell pellets were lysed either directly in 1X SDS sample buffer (Table 4.6) or lysed for 1 hour on ice by the mitotic lysis buffer mixture (Table 4.7) and normalised by Bradford assay before adding 3X SDS sample buffer (final concentration 1X). In either instance, once in 1X SDS sample buffer, samples were boiled at 95°C for 10-15 minutes, vortexing intermittently. Samples were then run on homemade SDS-PAGE gels, with high molecular weight proteins run on lower percentage gels and vice-versa, using a Mini-Protean vertical electrophoresis system (BioRad, #1658000). Gels were then transferred to a nitrocellulose membrane using a Trans-blot Turbo system (BioRad, #1704150); for proteins less than 100 kDa, between 100-180 kDa, and over 180 kDa, 7 Min mixed MW, 10 min High MW or 2x 10 min High MW

protocols were used respectively. Membranes were then blocked in 5% milk [Weight/Vol] in PBS-T for 30-60 minutes before being incubated in primary antibody (Table 4.1) for either 1 hour at room temperature, or up to 16 hours at 4ºC in 5% milk/PBS-T solution. They were then incubated in secondary HRP antibodies (Table 4.2) in 5% milk/PBS-T for 1 hour. Three 10–15 minute washes were performed between each antibody incubation with PBS-T. Bands were visualised by ECL chemiluminescence, exposed to film for different durations, and developed using an OPTIMAX 2010 X-ray Film Processor (PROTEC-Med). All materials used for western blotting have been listed in Table 4.8.

Table 4.6 - SDS sample buffer composition

Reagent	**Company**	**Catalogue#**	**Final Concentration/ Dilution**
Tris-HCL pH 6.8	Sigma-Aldrich	T4661	0.1875 mM
SDS	Sigma-Aldrich	75746	1% [Weight/Vol]
Glycerol	Sigma-Aldrich	G9012	10% [Weight/Vol]
Bromophenol blue	Sigma-Aldrich	B5525	0.05% [Weight/Vol]
β-mercaptoethanol	Sigma-Aldrich	M3148	10% [Weight/Vol]

Table 4.7 - Mitotic lysis buffer composition

Reagent	**Company**	**Catalogue#**	**Final Concentration/ Dilution**
Tris HCL pH 7.4	Sigma-Aldrich	T4661	20 mM
NaCl	Sigma-Aldrich	S3014	150 mM
β-Glycerophosphate	Sigma-Aldrich	G9422	40 mM
NaF	Sigma-Aldrich	201154	10 mM
Na-Vanadate	Sigma-Aldrich	S650	0.3 mM
10% IGEPAL	Sigma-Aldrich	S3014	1% [vol/vol]
1mM EDTA			1 mM
10% Deoxycholate	Sigma-Aldrich	D6750	0.1% [Weight/Vol]
Added Fresh			
1x Protease Inhibitor	Roche	1187358000	1:250
Okadaic Acid	Enzo Life Sciences	ALX-350-011-M001	100 nM
1x Phosphatase Inhibitor Cocktail	Sigma-Aldrich	P0044	1:1000
Microcystin-LR	Enzo Life Sciences	ALX-350-012-M001	200 mM
DTT	Sigma-Aldrich	1158378600	1 mM
Benzonase	Millipore	E1014-25KU	1:3000
Micrococcal nuclease	NEB	M0247S	1:500

Table 4.8 - Western Blotting reagents and materials

Reagent	Source	Catalogue#	Dilution/Concentration/Notes
AMBA Protogel 37:5:1	Geneflow	A2-0072	Depends on gel %
Lower Buffer 4X	Homemade	-	Stock: 0.4% SDS, 1.5 M Tris base, pH 8.8
Upper Buffer 4X	Homemade	-	Stock: 0.4% SDS 0.5M Tris base, pH 6.8
Ammonium Persulfate (APS)	Sigma-Aldrich	A3678	10% Stock - 0.1% working conc (1:100)
TEMED	Sigma-Aldrich	T9281	1:1000 from stock
PBS	PanReac AppliChem	A0965,9100	Made to 10X (1 M) stock
Tween-20	Sigma-Aldrich	P2287	0.1% in PBS-T
PBS-T	Homemade	-	1X PBS + 0.1% Tween-20
Running Buffer	Homemade	-	0.025 M Tris-base 0.192 M Glycine 1% SDS
Dried Skimmed Milk	-	-	5% [Weight/Vol] in PBS-T
Pre-stained protein marker (11-250 kDa)	CST	59329S	5-10 µL per lane
Transfer-Blot Turbo Transfer Packs	BioRad	1704158 1704159	Mini/Midi size (1 or 2 gels)
ECL Detection Reagents	Cytiva	RPN2106	1:1 of each reagent
Amersham Hyperfilm	GE Healthcare	28-9068-37 28-9068-35	Two sizes, dependent on cassette.
Protein Assay Dye	BioRad	50000006	1:5 dilution

4.4.3. Immunoprecipitation

Cells were harvested from at least 2x 10 cm plates seeded at 300,000 cell density at least 2 days prior - dependent on the experiment, cells may have been pre-treated with arrest drugs prior to harvest (Methods 4.4.1) e.g. if treated with nocodazole, a shake off would be performed to collect just the mitotic cells. After 1x wash in PBS, cell pellets were lysed in mitotic lysis buffer (composition - Table 4.7) for 1 hour on at 4°C, before being spun down at 14,000 rpm to separate lysate from insoluble debris. Sample concentrations were normalised to each other based on a Bradford assay, using protein assay dye (BioRad #50000006). From the new, normalised samples, 10% was taken as an input, mixed with 3X SDS sample buffer (Table 4.6), and boiled at 95°C for 10-15 minutes, vortexing intermittently. The remaining 90% of the sample was incubated with 15 µL Halo-Trap agarose beads (ChromoTek #ota) for 4-18

hours at 4ºC to pull down on the HaloTag fused to the protein of interest, and any interacting proteins. Beads were then spun down at 2000 rpm, and an unbound sample taken before washing three times in mitotic lysis buffer. Beads were then resuspended in 2X SDS sample buffer and boiled for analysis by western blot.

4.4.4. Mass spectrometry

For HaloTrap-IP based mass spectrometry, samples were prepared in a similar fashion as described in Methods 4.4.3, except in the final washing step post bead-lysis incubation. Instead, beads were washed twice in mitotic lysis buffer, and twice in a 'reduced' mitotic lysis buffer (20 mM Tri-HCl and 150 mM NaCl) to remove any detergent. Bead-bound samples were then given to the Proteomics facility (Department of Biochemistry, Oxford, UK) for tryptic digest and to be run on the Q-exactive mass spectrometer (ThermoFisher
Scientific) on a 30-minute gradient. Protein identification and abundance were determined by running output m/z data on MaxQuant (V2.5.1.0) software and searching against the human proteome. HaloTag lines vs wild-type intensities were plotted to log base 10 using GraphPad, Prism (V10.5.0); hits that were above a fitted trend line were deemed significant (i.e. low intensity in wild-type, high intensity in HaloTag line).

For whole-cell phosphoproteomics, after any drug-based arrest pertinent to the experiment in question (Methods 4.4.1), cells were lysed in an ice-cold urea-based lysis buffer comprised of 8M Urea (Sigma Aldrich #U5378-5KG), 100 mM Ammonium Bicarbonate (Sigma Aldrich #A6141), 100 nM okadaic acid, protease inhibitor cocktail, phosphatase inhibitor cocktail (details in Table 4.7). Immediately after resuspension, pellets were snap-frozen in liquid nitrogen. Phospho-enrichment was performed by Dr James Holder, as described in (Holder et al., 2020); the only difference being that samples were not dimethyl labelled and were de-salted using Pierce Graphite Spin Columns (Thermo Fisher #88302), as per manufacturer's instructions. Mass spectrometry for these samples was performed by Dr Sean Burnap on a 30-minute gradient using TimsTOF Ultra 2 by Bruker. Phosphoproteomic data was searched

using DIA-NN (V 2.2.0) software against an in-silico generated spectral library from a tryptic digest. This library allowed for phosphorylation with a variable modification of up to 3 modifications per peptide and 2 missed cleavages. Searched data with a 90% confidence phospho-peptide identification was analysed using Jupyter Notebook (V6.4.5) running Python (V3.9). Data was imported as a pandas dataframe (pandas v1.3.4), and filtered to ensure phospho-sites were considered only if detected in at least two out of three replicates for each condition. These data were then log2 transformed (using numpy V.1.22.4), and median normalised (using pandas). Any missing values were imputed with a noise value, determined from the mean minimum intensity over all conditions and repetitions, reduced slightly to avoid biasing further analysis. Log2 fold-change and p values were determined (using scipy V.1.13.1), exported to a csv file, and visualised as a volcano plot using Graphpad, Prism.

4.4.5. Cell proliferation assay

Cells were seeded at a density of 5000/well and grown for 1-2 days. Post-addition of any drugs (as specified in each figure), cells were grown for 5 days unless otherwise stated (e.g. a time course). Cells were then fixed and stained with 5% [Weight/Vol] crystal violet (Sigma-Aldrich #C0775) in 25% [vol/vol] methanol (VWR #20847.307) for 30 minutes at room temperature, washed in water, and left to dry overnight. Plates were then imaged using the Bio-Rad Gel Doc XR+ imaging system (Bio-Rad, 1708195EDU) using Image Lab 6 software (Bio-Rad). Cell proliferation was then assessed in one of two ways; either performing densitometry on the images taken using Fiji/ImageJ software (National Institutes of Health), or by extracting crystal violet dye (using methanol) from each well and determining absorbance at 540 nm.

4.4.6. SiRNA depletion

Where proteins were to be transiently depleted via SiRNA treatment, cells were transfected with the relevant SiRNA (Table 4.9) for 72 hours using Mirus-TX2 (Mirus, #MIR6004). Once depleted, cells were fixed and stained as per the experimental design.

Table 4.9 - SiRNA duplexes

Target	Sequence	Source
Control (GL2)	5'-CGUACGCGGAAUACUUCGAUU-3'	Dharmacon
Shugoshin 1 (SGO1)	5'-CAGUAGAACCUGCUCAGAA-3'	Dharmacon

4.5. HaloTag & Degron-Tag Technologies

4.5.1. Protein Visualisation via HaloTag

The HaloTag is a versatile, synthetic tag that is dual-purpose; it can either be used to visualise a protein of interest or signal it for proteolytic degradation. It can be integrated into the endogenous protein of interest via CRISPR/Cas9 technology (Methods 4.3). For visualisation, cell-permeable dyes can be added whilst cells are in culture, enabling both live and fixed cell imaging. In this thesis, three different JFX dyes are used; JFX549 (red), JFX554 (red) and JFX646 (far red) (Grimm et al., 2021) - Figure 4.1. Dyes were added at a concentration of 100 nM for 15-30 minutes prior to live imaging / cell fixation, with excess dye washed out.

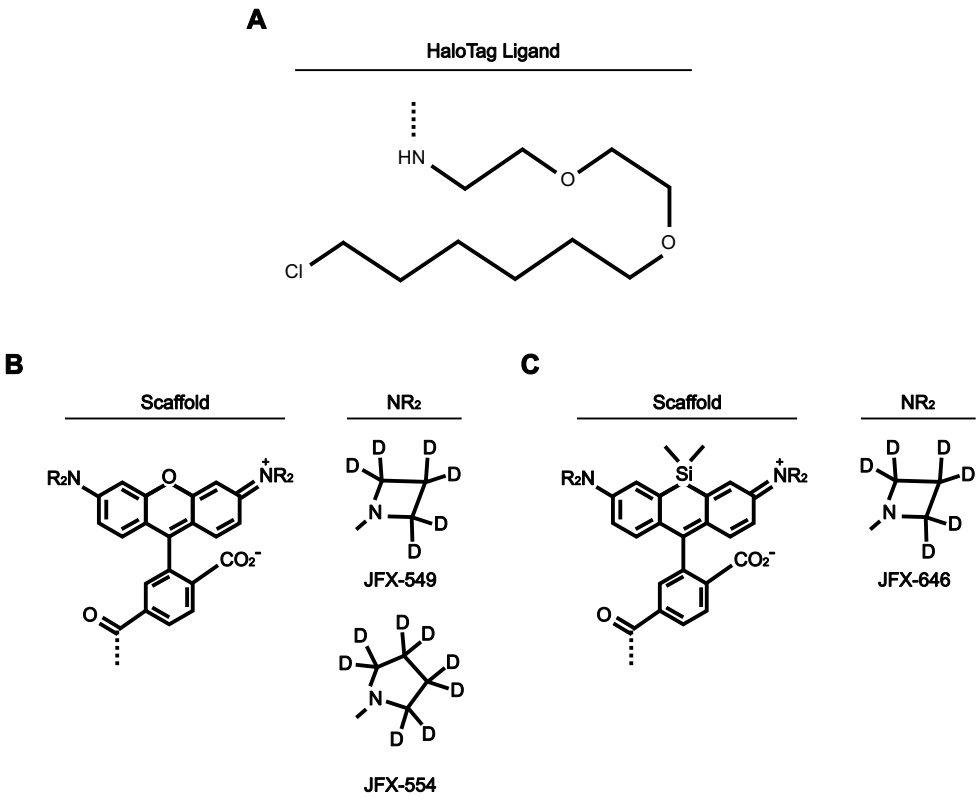

Figure 4.1 - JFX HaloTag dyes

(A) The baseline HaloTag ligand that each dye construct is attached to. (B) Rhodamine-based dye scaffold with two different deuterium-based pyrrolidine rings in place of NR_2, representing JFX549 or JFX554 dyes. (C) Si-rhodamine based dye scaffold with one deuterium-based pyrrolidine ring in place of NR_2, representing JFX646 dye. Figure inspired and adapted from (Grimm et al., 2021).

4.5.2. Proteolysis Targeting Chimera (PROTAC)

A second use of the HaloTag is via a Proteolysis Targeting Chimera (PROTAC), which works to bring the protein of interest fused to the HaloTag into proximity to an E3 ubiquitin ligase, resulting in ubiquitination of the HaloTag and protein of interest, and targeting them for proteolytic degradation - Figure 4.2 (Buckley et al., 2015; Tovell et al., 2019). PROTAC was added once at a 300 nM concentration over all time scales, enabling rapid protein degradation via VHL E3 ligase.

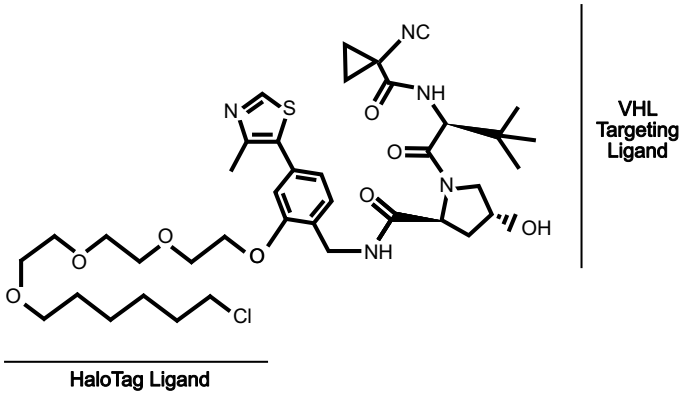

Figure 4.2 - HaloTag PROTAC-E

HaloPROTAC-E is a bifunctional molecule, targeting both the HaloTag ligand and VHL E3 ligase. Figure inspired and adapted from (Tovell et al., 2019).

4.5.3. Degron-Tag

A degron tag (dTag or $FKBP12^{F36V}$) works similarly to the Halo-PROTAC in that it brings together the protein of interest (fused to a dTag) into proximity to an E3 ligase for proteolytic degradation. Due to their different chemical nature, both dTag-PROTAC and Halo-PROTAC can be used independently within a double-tagged cell line, with only one protein of interest being degraded dependent on the PROTAC added. dTag PROTACs also come in a few different forms dependent on the E3 ligase required for degradation; in this thesis, only dTag-1 was used, which targets the protein for VHL-mediated degradation (Nabet et al., 2020)(Figure 4.3). In all instances, 100 nM of dTag-1 was used for protein degradation.

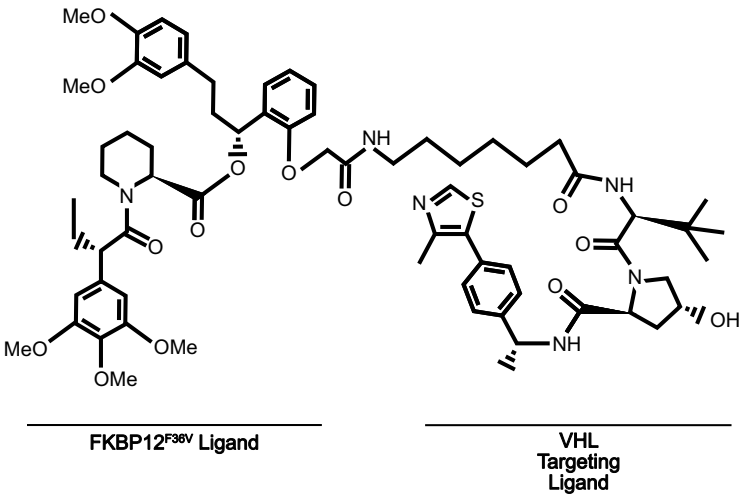

Figure 4.3 - VHL targeting FKBP12^{F36V} dTag-1

dTag-1 is a bifunctional molecule used for targeting FKBP12^{F36V}-fused to a protein of interest, and bringing it into proximity to a VHL E3 ligase. Figure inspired and adapted from (Nabet et al., 2020).

4.6. Microscopy Techniques

4.6.1. Fixed Cell Immunofluorescence

Cells were seeded in 6-well plates containing either 13mm or 16mm circular coverslips for a minimum of two-three days prior to fixation. They were then fixed in one of three ways: ice-cold anhydrous methanol, PTEMF, or HTEMF. For ice-cold anhydrous methanol fixation, methanol was aliquoted and cooled to -20°C. A metal container was placed in contact with ice, and a thin layer of water placed in the container to aid temperature transference. Cells were washed once in PBS, treated with ice-cold methanol, and immediately placed on top of the metal container, in contact with the now ice-cold water, for 5 minutes. The 6-well plate was then removed from the container, and coverslips washed twice in PBS. For PTEMF/HTEMF fixation, cells were washed once in PBS, then treated for 12 minutes with either P/H-TEMF (PIPES-KOH 20 mM pH 6.8 or HEPES 40 mM pH 7.5, Triton X-100 0.2%, EGTA 10 mM, $MgCl_2$ 1 mM, Formaldehyde 4%). Post-fixation, cells were washed twice in PBS.

Once fixed, cells were incubated in primary antibody diluted in PBS (Table 4.1) for 1 hour, washed once in PBS, incubated in secondary antibody diluted in PBS (Table 4.2) for 1 hour, and washed once in PBS. Coverslips were then mounted onto cover glass using mowiol and

left to dry overnight before imaging. All microscopy-based reagent information is shown in Table 4.10.

Samples were imaged on a standard upright microscope system (BX61; Olympus) with filter sets for DAPI, GFP, Cy3, and Cy5 (Chroma Technology Corp.), a 2,048 × 2,048-pixel complementary metal oxide semiconductor camera (PrimΣ, Photometrics), and MetaMorph 7.5 imaging software (Molecular Devices). An LED light source provided illumination (pE300, CoolLED Illumination Systems). Image stacks with a spacing of 0.4 µm through the cell volume were maximum intensity projected and cropped in Fiji/Image J (National Institutes of Health).

Table 4.10 - Immunofluorescence microscopy reagents

Reagent	**Source**	**Catalogue#**	**Working Concentration**
Methanol	VWR	20847.307	-
PIPES	Sigma-Aldrich	P6757	20 mM, pH 6.8
HEPES	Sigma-Aldrich	H7006	40 mM, pH 7.5
Triton X-100	Sigma-Aldrich	T8787	0.2% [vol/vol] in PBS
EGTA	Sigma-Aldrich	E3889	10 mM
$MgCl_2$	Sigma-Aldrich	M8266	1 mM
Formaldehyde	Sigma-Aldrich	F8775-25mL	4% [vol/vol]
PBS	VWR	A09659100	-
Mowiol 488	Sigma-Aldrich	9002895	-
13mm Glass Coverslips	Agar Scientific	AGL46R13-15	-
16mm Glass Coverslips	Agar Scientific	AGL46R16-15	-
Microscope Slides	Thermo Fisher Scientific	10143560	-

4.6.2. Chromosome spreads

Cells were seeded in three 10cm dishes, and when at approx. 50% confluency, treated with 330 nM nocodazole for 5-6 hours; cells were treated with HaloTag-JFX554 dye for the last 30 minutes. Mitotic cells were isolated by shake-off, placed into a 15 mL falcon tube, pelleted at 200 x g at 37°C for 5 minutes, and then re-suspended gently in 5 mL of pre-warmed 75 mM KCl. Cells were incubated in KCl at 37°C, 5% CO_2, for 30 minutes, gently inverting the tube

every 10 minutes to keep cells in suspension. They were then pelleted again at 200 x g at 37°C for 5 minutes before decanting the majority of the KCl; cells were then gently resuspended in the small volume of KCl that remained. Cells were then fixed with 1 mL of a 4ºC cooled fixative solution - 1 part methanol to 2 parts glacial acetic acid (SLS #CHE1014) whilst gently vortexing. This was then topped up to 10 mL total fixative-cell solution and stored in a 4ºC fridge overnight. Cells were then pelleted at 200 x g at room temperature and resuspended in 1 mL of freshly prepared fixative. Glass microscope slides were placed at a 45° angle against a tube rack and washed with double-distilled water. 100 µL of fixed-cell solution was then dropped at a height onto the slide, allowing cell to burst open and chromosomes to spread. 100 µL of fixative solution was used to gently wash the slide, which was then placed on top of a wet paper towel above a heat block set to 60ºC to dry for 2 minutes - any residual condensation was left to dry for 5-10 minutes at room temperature. Three large drops of DAPI-containing mowiol (1:2000 DAPI) was placed on the glass slide, before covering with a coverslip. Slides were then left to dry overnight in a 4ºC fridge for a minimum of 24 hours before imaging (as described in Results 4.6.1).

4.6.3. Stimulated Emission Depletion (STED)

Cells were seeded on high-precision coverslips and grown for 2-3 days. They were then arrested in G2 and released into mitosis, as explained in Methods 4.4.1.1, except for adding MG132 for 1–2 hours instead of 3-4 hours to ensure enough prometaphase cells were still present. 100 nM HaloTag-JFX646 dye was added for 15 minutes prior to fixation to fluorescently label NDC80-HaloTag. Cells were then fixed for 12 minutes with G-PTEMF (0.1% [vol/vol] glutaraldehyde, 20 mM PIPES-KOH pH 6.8, 0.2% [vol/vol] Triton X-100, 10 mM EGTA, 1 mM $MgCl_2$, and 4% [vol/vol] formaldehyde). Fixative was quenched for 15 min with 50 mM NH_4Cl. Coverslips were then incubated in primary antibody (Table 4.1) for 1.5–2 hours, followed by a PBS wash, and a further 1.5-hour incubation with secondary antibodies (Table 4.2). Cells were then post-fixed for 15 min with 0.1% [vol/vol] glutaraldehyde and 3% [vol/vol]

paraformaldehyde to stabilise bound antibodies. Fixative was quenched with 1 mg/ml sodium borohydride for 7 minutes, followed by 100 mM glycine for 15 minutes. Coverslips were then mounted onto cover glass using Everbrite mounting medium and sealed with nail varnish. The next day, samples were imaged using the Leica Stellaris STED system with TauSense and Xtend capabilities. An NKT-Photonics 470 - 790 nm White Light Laser (WLL) was used to excite fluorophores, and either an MPB-589 nm or MPB-775 nm STED laser used for depletion. Images were acquired using a Leica's LAS X software (V4.8), alongside using a HCFL 100x/1.4A Oil objective, a HydX detector, and an average z-spacing of 0.3–0.4 µm. All super-resolution specific reagent information is shown in Table 4.11, and general microscopy reagents in Table 4.10.

Table 4.11 - Super-Resolution specific reagents

Reagent	**Source**	**Catalogue#**	**Working Concentration**
16% Formaldehyde	ThermoFisher Scientific	28908	4% [Weight/Vol] in PBS
25% Glutaraldehyde	Sigma-Aldrich	G5882	0.1% [vol/vol]
Ammonium Chloride	Sigma-Aldrich	A9434	50 mM
Sodium borohydride	Sigma-Aldrich	480886	1 mg/ml
Glycine	Sigma-Aldrich	G7126	100 mM
22m 1.5H High precision Microscope Slides	Marinfeld	0107052	-
Everbrite mounting medium	Biotium	23001	-

4.6.4. Live-Cell imaging

Cells were seeded on 35 mm wide dishes, with a 14 mm 1.5 thickness cover glass bottom (MatTek #P35G-1.5-14-C) and grown for at least 2 days. They were then treated with either 50 nM SiR-DNA (Spirochrome #Sc005) or 50 nM SiR-Tubulin (Spirochrome #Sc002) for at least 3 hours. In the last 15 minutes, cells were treated with 100 nM HaloTag-JFX554 dye; this was then washed out three times in SiR-DNA/Tubulin-containing media, left for 30 minutes

at 37°C and 5% CO_2, and washed out once more prior to imaging to remove any excess, unbound dye.

Dishes were then placed into an environment chamber (Tokai Hit) mounted onto the microscope stage to maintain cells in a 37°C and 5% CO_2 environment throughout the imaging duration. Imaging was performed on an Ultraview Vox spinning disk confocal system running Volocity software (PerkinElmer, V6.3.0) using a 60x/1.42 NA UPlanSApo oil objective on an Olympus IX-81 inverted microscope equipped with an electron multiplying charge coupled device (EM-CCD) camera (Hamamatsu Photonics no. C9100-13). Dependent on the experiment, 488 nm, 561 nm, or 651 nm lasers were used with exposures ranging from 50-200 ms at 1.5-7% laser power; brightfield images at 30-50 ms were also taken for cell morphology refence images. Multi-point acquisition was performed, with images taken over 21-24 planes at 0.9 µm spacing; time intervals are specified in each figure. Maximum intensity projection, image cropping, time in mitosis durations, and intensity quantifications were all performed in Fiji.

For SoRa-capable high-resolution spinning disk imaging, dishes were placed into an environment chamber at 37°C and 5% CO_2 to maintain cell viability during image acquisition. Imaging was performed on an Olympus SoRa spinning disk system running CellSens software (V3.2) using a 60x/1.5 NA UPLAPO OHR oil objective on an Olympus IX-83 microscope stand with a Yokogawa CSU-W1 SoRa super-resolution spinning disk. For kinetochore imaging, a 561 nm laser was used with 350 ms exposure at 4% laser power. Images were taken over 21 planes with 0.9 µm spacing at 70 second intervals. Maximum intensity projection and image cropping was performed in Fiji.

4.7. Computational analysis

4.7.1. Fiji image analysis & macros

Fiji/ImageJ (National Institutes of Health - V2.14) was used for a large proportion of the analysis in this thesis. The following subsections outline the procedures for more in-depth analyses.

4.7.1.1. Kinetochore intensities

To measure individual kinetochore intensities, each kinetochore was identified from a channel of interest, mapped back to a marker channel (a centromere protein) by a binary mask, and selected as a region of interest (ROI). The total mean intensity of each ROI for each channel was then measured over an 8-pixel diameter circle. A background intensity was determined by measuring 52 pixels radially outside of the kinetochore ROI, ensuring that these pixels did not overlap with any other kinetochore ROI. These two values were then subtracted on a per-kinetochore basis to get the signal for each kinetochore over each channel - Figure 4.4. The macro generated for this method was adapted from (Hayward et al). For some quantifications (specified within relevant figures), the mean intensity for all kinetochores in a cell was calculated; a minimum of 20 kinetochores per cell were identified and measured.

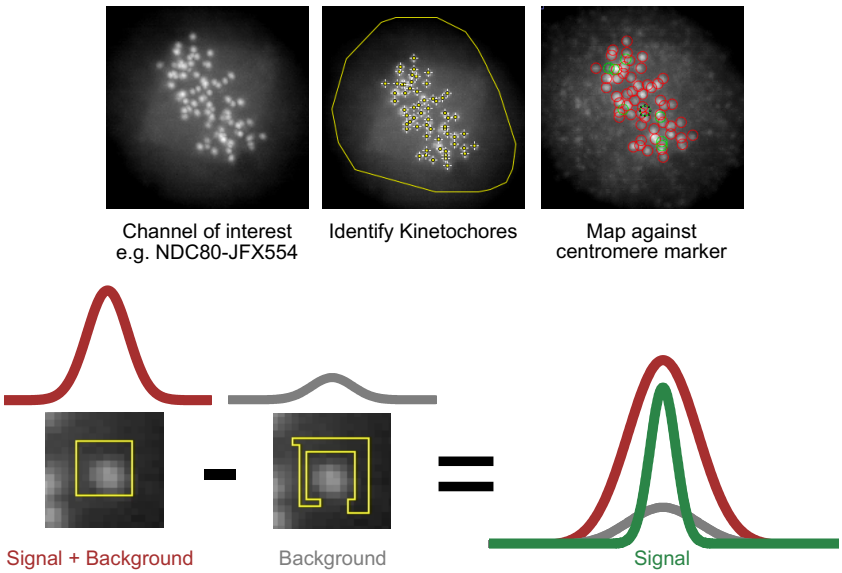

Figure 4.4 - Kinetochore intensity measurements

Kinetochores were identified, mapped back to a marker channel, and measured for both total and background intensities. These two values were then subtracted to give a true signal.

4.7.1.2. Line scan quantifications for STED data

Individual kinetochore pairs were identified, either on a single z-slice or sometimes needing a maximum intensity projection over *x* number of slices. Line scans were then performed by measuring the signal across the pericentric region between two kinetochore pairs over all channels of interest - excess space was left slightly beyond each kinetochore to confidently define the kinetochore and pericentric boundary. Pixel-based distances were then converted to µm, dependent on the scaling of each image when acquired. Data was then normalised in GraphPad, Prism (V.10) with 0 defined as the smallest value in each data set, and 100% defined as the largest mean in each data set. Each line scan was plotted ± SEM, shown as a lightly coloured region about the curve between the SEM boundaries.

Inter-kinetochore distances were measured using a 1-pixel wide line, with each end placed centrally about the kinetochore; a single pair of kinetochores was defined as a replicate *n* within a cell. Intra-kinetochore distances were determined by measuring a line scan across

individual kinetochores and fitting a Gaussian curve to each signal. The difference between means of corresponding CENP-A and NDC80 Gaussians was used as a measure of distance between them, due to the high resolution of the image and sharpness of Gaussian fits. For these quantifications, a single kinetochore was considered a replicate *n* within a cell.

4.7.1.3. Live-cell intensity over time quantifications

Each cell's chromatin was identified using SiR-DNA and used to define the region of measurement; in each time frame, the chromatin mask was re-drawn. Chromatin signal across each channel of interest was then determined. A background signal was determined just outside of the chromatin signal, but still within the cell cytoplasm, allowing for background subtraction over each frame.

4.7.2. Using Prism for statistical analysis

GraphPad Prism (V.10) was used for all statistical analysis. In general (unless otherwise specified); where two values were compared, an unpaired two-tailed t-test was performed and for multiple comparisons, a one-way analysis of variance (ANOVA) was performed. In all cases, p values are defined as follows: $p > 0.05$ (not significant, ns), $p < 0.05$ (*), $p < 0.01$ (**), $p < 0.001$ (***), $p < 0.0001$ (****). The sample number for each test is shown in each figure.

4.7.3. Figure generation

All figures were created using Affinity Designer (V.1.10.8) and exported as high-quality SVG files for use in this thesis.

5. References

Abad, M. A., Gupta, T., Hadders, M. A., Meppelink, A., Wopken, J. P., Blackburn, E., Zou, J., Gireesh, A., Buzuk, L., Kelly, D. A., McHugh, T., Rappsilber, J., Lens, S. M. A., & Jeyaprakash, A. A. (2022). Mechanistic basis for Sgo1-mediated centromere localization and function of the CPC. *The Journal of Cell Biology*, *221*(8). https://doi.org/10.1083/JCB.202108156

Abad, M. A., Ruppert, J. G., Buzuk, L., Wear, M., Zou, J., Webb, K. M., Kelly, D. A., Voigt, P., Rappsilber, J., Earnshaw, W. C., & Arockia Jeyaprakash, A. (2019). Borealin–nucleosome interaction secures chromosome association of the chromosomal passenger complex. *The Journal of Cell Biology*, *218*(12), 3912. https://doi.org/10.1083/JCB.201905040

Adams, R. R., Maiato, H., Earnshaw, W. C., & Carmena, M. (2001). Essential Roles of Drosophila Inner Centromere Protein (Incenp) and Aurora B in Histone H3 Phosphorylation, Metaphase Chromosome Alignment, Kinetochore Disjunction, and Chromosome Segregation. *The Journal of Cell Biology*, *153*(4), 865. https://doi.org/10.1083/JCB.153.4.865

Afonso, O., Matos, I., Pereira, A. J., Aguiar, P., Lampson, M. A., & Maiato, H. (2014). Feedback control of chromosome separation by a midzone Aurora B gradient. *Science (New York, N.Y.)*, *345*(6194), 332. https://doi.org/10.1126/SCIENCE.1251121

Alfieri, C., Chang, L., & Barford, D. (2018). Mechanism for remodelling of the cell cycle checkpoint protein MAD2 by the ATPase TRIP13. *Nature*, *559*(7713), 274–278. https://doi.org/10.1038/S41586-018-0281-1

Alushin, G. M., Ramey, V. H., Pasqualato, S., Ball, D. A., Grigorieff, N., Musacchio, A., & Nogales, E. (2010). The Ndc80 kinetochore complex forms oligomeric arrays along microtubules. *Nature*, *467*(7317), 805–810. https://doi.org/10.1038/NATURE09423

Alvarez, L. A. J., Schwarz, U., Dyba, M., Hecht, F., & Roberti, M. J. (n.d.). *Application Report GENTLE, MULTICOLOR LIVE IMAGING AT THE NANOSCALE WITH TAUSTED XTEND From Eye to Insight*.

Amin, M. A., Chakraborty, M., Wallace, D. A., & Varma, D. (2023). Coordination between the Ndc80 complex and dynein is essential for microtubule plus-end capture by kinetochores during early mitosis. *Journal of Biological Chemistry*, *299*(6), 104711. https://doi.org/10.1016/J.JBC.2023.104711

Ando, R., Shimozono, S., Ago, H., Takagi, M., Sugiyama, M., Kurokawa, H., Hirano, M., Niino, Y., Ueno, G., Ishidate, F., Fujiwara, T., Okada, Y., Yamamoto, M., & Miyawaki, A. (2024). StayGold variants for molecular fusion and membrane-targeting applications. *Nature Methods*, *21*(4), 648–656. https://doi.org/10.1038/S41592-023-02085-6;SUBJMETA

Andrews, P. D., Ovechkina, Y., Morrice, N., Wagenbach, M., Duncan, K., Wordeman, L., & Swedlow, J. R. (2004). Aurora B regulates MCAK at the mitotic centromere. *Developmental Cell*, *6*(2), 253–268. https://doi.org/10.1016/S1534-5807(04)00025-5

Arellano, M., & Moreno, S. (1997). Regulation of CDK/cyclin complexes during the cell cycle. *The International Journal of Biochemistry & Cell Biology*, *29*(4), 559–573. https://doi.org/10.1016/S1357-2725(96)00178-1

Auckland, P., Roscioli, E., Coker, H. L. E., & McAinsh, A. D. (2020). CENP-F stabilizes kinetochore-microtubule attachments and limits dynein stripping of corona cargoes. *The Journal of Cell Biology*, *219*(5). https://doi.org/10.1083/JCB.201905018

Bajaj, R., Bollen, M., Peti, W., & Page, R. (2018). KNL1 Binding to PP1 and Microtubules Is Mutually Exclusive. *Structure*, *26*(10), 1327-1336.e4. https://doi.org/10.1016/j.str.2018.06.013

Bancroft, J., Auckland, P., Samora, C. P., & McAinsh, A. D. (2015). Chromosome congression is promoted by CENP-Q- and CENP-Edependent pathways. *Journal of Cell Science*, *128*(1), 171–184. https://doi.org/10.1242/JCS.163659/VIDEO-6

Banerjee, A., Chen, C., Humphrey, L., Tyson, J. J., & Joglekar, A. P. (2022). BubR1 recruitment to the kinetochore via Bub1 enhances spindle assembly checkpoint signaling. *Molecular Biology of the Cell*, *33*(10). https://doi.org/10.1091/MBC.E22-03-0085

Barr, A. R., & Gergely, F. (2007). Aurora-A: the maker and breaker of spindle poles. *Journal of Cell Science*, *120*(17), 2987–2996. https://doi.org/10.1242/JCS.013136

Barr, F. A., & Gruneberg, U. (2007). Cytokinesis: Placing and Making the Final Cut. *Cell*, *131*(5), 847–860. https://doi.org/10.1016/j.cell.2007.11.011

Bayliss, R., Sardon, T., Vernos, I., & Conti, E. (2003). Structural basis of Aurora-A activation by TPX2 at the mitotic spindle. *Molecular Cell*, *12*(4), 851–862. https://doi.org/10.1016/S1097-2765(03)00392-7

Bharadwaj, R., Qi, W., & Yu, H. (2004). Identification of Two Novel Components of the Human NDC80 Kinetochore Complex. *Journal of Biological Chemistry*, *279*(13), 13076–13085. https://doi.org/10.1074/jbc.M310224200

Bird, A. W., & Hyman, A. A. (2008). Building a spindle of the correct length in human cells requires the interaction between TPX2 and Aurora A. *Journal of Cell Biology*, *182*(2), 289–300. https://doi.org/10.1083/JCB.200802005/VIDEO-6

Buckley, D. L., Raina, K., Darricarrere, N., Hines, J., Gustafson, J. L., Smith, I. E., Miah, A. H., Harling, J. D., & Crews, C. M. (2015). HaloPROTACS: Use of Small Molecule PROTACs to Induce Degradation of HaloTag Fusion Proteins. *ACS Chemical Biology*, *10*(8), 1831. https://doi.org/10.1021/ACSCHEMBIO.5B00442

Caldas, G. V., & DeLuca, J. G. (2013). KNL1: Bringing Order to the Kinetochore. *Chromosoma*, *123*(3), 169. https://doi.org/10.1007/S00412-013-0446-5

Caldas, G. V., DeLuca, K. F., & DeLuca, J. G. (2013). KNL1 facilitates phosphorylation of outer kinetochore proteins by promoting Aurora B kinase activity. *The Journal of Cell Biology*, *203*(6), 957. https://doi.org/10.1083/JCB.201306054

Campisi, J. (1996). Replicative senescence: An old lives' tale? *Cell*, *84*(4), 497–500. https://doi.org/10.1016/S0092-8674(00)81023-5

Carmena, M., Wheelock, M., Funabiki, H., & Earnshaw, W. C. (2012). The chromosomal passenger complex (CPC): from easy rider to the godfather of mitosis. *Nature Reviews Molecular Cell Biology*, *13*(12), 789–803. https://doi.org/10.1038/nrm3474

Chan, G. K. T., Jablonski, S. A., Sudakin, V., Hittle, J. C., & Yen, T. J. (1999). Human Bubr1 Is a Mitotic Checkpoint Kinase That Monitors Cenp-E Functions at Kinetochores and Binds the Cyclosome/APC. *The Journal of Cell Biology*, *146*(5), 941. https://doi.org/10.1083/JCB.146.5.941

Cheeseman, I. M., Chappie, J. S., Wilson-Kubalek, E. M., & Desai, A. (2006). The Conserved KMN Network Constitutes the Core Microtubule-Binding Site of the Kinetochore. *Cell*, *127*(5), 983–997. https://doi.org/10.1016/j.cell.2006.09.039

Cheeseman, I. M., & Desai, A. (2008). Molecular architecture of the kinetochore-microtubule interface. *Nature Reviews. Molecular Cell Biology*, *9*(1), 33–46. https://doi.org/10.1038/NRM2310

Cheeseman, L. P., & Maiato, H. (2021). Chromosomal instability: Stretching the role of checkpoint silencing. *Current Biology*, *31*(8), R386–R389. https://doi.org/10.1016/j.cub.2021.02.014

Cheffings, T. H., Burroughs, N. J., & Balasubramanian, M. K. (2016). Actomyosin Ring Formation and Tension Generation in Eukaryotic Cytokinesis. *Current Biology*, *26*(15), R719–R737. https://doi.org/10.1016/J.CUB.2016.06.071/ASSET/992FB8BB-6365-436D-936D-5E2899D9C4FB/MAIN.ASSETS/GR4.JPG

Chen, C., Whitney, I. P., Banerjee, A., Sacristan, C., Sekhri, P., Kern, D. M., Fontan, A., Kops, G. J. P. L., Tyson, J. J., Cheeseman, I. M., & Joglekar, A. P. (2018). Ectopic activation of the Spindle Assembly Checkpoint signaling cascade reveals its biochemical design. *Current Biology : CB*, *29*(1), 104. https://doi.org/10.1016/J.CUB.2018.11.054

Chen, R. H. (2002). BubR1 is essential for kinetochore localization of other spindle checkpoint proteins and its phosphorylation requires Mad1. *The Journal of Cell Biology*, *158*(3), 487. https://doi.org/10.1083/JCB.200204048

Chu, C. S., Hsu, P. H., Lo, P. W., Scheer, E., Tora, L., Tsai, H. J., Tsai, M. D., & Juan, L. J. (2011). Protein Kinase A-mediated Serine 35 Phosphorylation Dissociates Histone H1.4 from Mitotic Chromosome. *The Journal of Biological Chemistry*, *286*(41), 35843. https://doi.org/10.1074/JBC.M111.228064

Ciferri, C., Pasqualato, S., Screpanti, E., Varetti, G., Santaguida, S., Dos Reis, G., Maiolica, A., Polka, J., De Luca, J. G., De Wulf, P., Salek, M., Rappsilber, J., Moores, C. A., Salmon, E. D., & Musacchio, A. (2008). Implications for Kinetochore-Microtubule Attachment from the Structure of an Engineered Ndc80 Complex. *Cell*, *133*(3), 427–439. https://doi.org/10.1016/J.CELL.2008.03.020/ATTACHMENT/7EB53BE0-3EB5-4D02-B1BB-8F9121EFB2A0/MMC1.PDF

Cimini, D., Howell, B., Maddox, P., Khodjakov, A., Degrassi, F., & Salmon, E. D. (2001). Merotelic kinetochore orientation is a major mechanism of aneuploidy in mitotic mammalian tissue cells. *The Journal of Cell Biology*, *153*(3), 517–527. https://doi.org/10.1083/JCB.153.3.517

Cohen, P. (2000). The regulation of protein function by multisite phosphorylation--a 25 year update. *Trends in Biochemical Sciences*, *25*(12), 596–601. https://doi.org/10.1016/S0968-0004(00)01712-6

Cundell, M. J., Bastos, R. N., Zhang, T., Holder, J., Gruneberg, U., Novak, B., & Barr, F. A. (2013). The BEG (PP2A-B55/ENSA/Greatwall) Pathway Ensures Cytokinesis follows Chromosome Separation. *Molecular Cell*, *52*(3), 393–405. https://doi.org/10.1016/J.MOLCEL.2013.09.005

Daum, J. R., Potapova, T. A., Sivakumar, S., Daniel, J. J., Flynn, J. N., Rankin, S., & Gorbsky, G. J. (2011). Cohesion fatigue induces chromatid separation in cells delayed at metaphase. *Current Biology : CB*, *21*(12), 1018–1024. https://doi.org/10.1016/J.CUB.2011.05.032

De Antoni, A., Pearson, C. G., Cimini, D., Canman, J. C., Sala, V., Nezi, L., Mapelli, M., Sironi, L., Faretta, M., Salmon, E. D., & Musacchio, A. (2005). The Mad1/Mad2 complex as a template for Mad2 activation in the spindle assembly checkpoint. *Current Biology : CB*, *15*(3), 214–225. https://doi.org/10.1016/J.CUB.2005.01.038

de Regt, A. K., Clark, C. J., Asbury, C. L., & Biggins, S. (2022). Tension can directly suppress Aurora B kinase-triggered release of kinetochore-microtubule attachments. *Nature Communications 2022 13:1*, *13*(1), 2152-. https://doi.org/10.1038/s41467-022-29542-8

DeLuca, J. G., Gall, W. E., Ciferri, C., Cimini, D., Musacchio, A., & Salmon, E. D. (2006). Kinetochore Microtubule Dynamics and Attachment Stability Are Regulated by Hec1. *Cell*, *127*(5), 969–982. https://doi.org/10.1016/J.CELL.2006.09.047

DeLuca, K. F., Meppelink, A., Broad, A. J., Mick, J. E., Peersen, O. B., Pektas, S., Lens, S. M. A., & DeLuca, J. G. (2018). Aurora A kinase phosphorylates Hec1 to regulate metaphase kinetochore–microtubule dynamics. *Journal of Cell Biology*, *217*(1), 163–177. https://doi.org/10.1083/JCB.201707160

Dou, Z., Liu, X., Wang, W., Zhu, T., Wang, X., Xu, L., Abrieu, A., Fu, C., Hill, D. L., & Yao, X. (2015). Dynamic localization of Mps1 kinase to kinetochores is essential for accurate spindle microtubule attachment. *Proceedings of the National Academy of Sciences of the United States of America*, *112*(33), E4546–E4555. https://doi.org/10.1073/PNAS.1508791112/SUPPL_FILE/PNAS.201508791SI.PDF

Du, J., Kelly, A. E., Funabiki, H., & Patel, D. J. (2012). Structural Basis for Recognition of H3T3ph and Smac/DIABLO N-terminal Peptides by Human Survivin. *Structure (London, England : 1993)*, *20*(1), 185. https://doi.org/10.1016/J.STR.2011.12.001

El-Deiry, W. S., Tokino, T., Velculescu, V. E., Levy, D. B., Parsons, R., Trent, J. M., Lin, D., Mercer, W. E., Kinzler, K. W., & Vogelstein, B. (1993). WAF1, a potential mediator of p53 tumor suppression. *Cell*, *75*(4), 817–825. https://doi.org/10.1016/0092-8674(93)90500-P

Elowe, S., Hümmer, S., Uldschmid, A., Li, X., & Nigg, E. A. (2007). Tension-sensitive Plk1 phosphorylation on BubR1 regulates the stability of kinetochore–microtubule interactions. *Genes & Development*, *21*(17), 2205–2219. https://doi.org/10.1101/GAD.436007

Engeland, K. (2022). Cell cycle regulation: p53-p21-RB signaling. *Cell Death and Differentiation*, *29*(5), 946–960. https://doi.org/10.1038/S41418-022-00988-Z;SUBJMETA

Erdmann, R. S., Baguley, S. W., Richens, J. H., Wissner, R. F., Xi, Z., Allgeyer, E. S., Zhong, S., Thompson, A. D., Lowe, N., Butler, R., Bewersdorf, J., Rothman, J. E., St Johnston, D., Schepartz, A., & Toomre, D. (2019). Labeling Strategies Matter for Super-Resolution Microscopy: A Comparison between HaloTags and SNAP-tags. *Cell Chemical Biology*, *26*(4), 584-592.e6. https://doi.org/10.1016/J.CHEMBIOL.2019.01.003

Espert, A., Uluocak, P., Bastos, R. N., Mangat, D., Graab, P., & Gruneberg, U. (2014). PP2A-B56 opposes Mps1 phosphorylation of Knl1 and thereby promotes spindle assembly checkpoint silencing. *Journal of Cell Biology*, *206*(7), 833–842. https://doi.org/10.1083/JCB.201406109

Evans, T., Rosenthal, E. T., Youngblom, J., Distel, D., & Hunt, T. (1983). Cyclin: a protein specified by maternal mRNA in sea urchin eggs that is destroyed at each cleavage division. *Cell*, *33*(2), 389–396. https://doi.org/10.1016/0092-8674(83)90420-8

Eyers, P. A., Erikson, E., Chen, L. G., & Maller, J. L. (2003). A novel mechanism for activation of the protein kinase Aurora A. *Current Biology : CB*, *13*(8), 691–697. https://doi.org/10.1016/S0960-9822(03)00166-0

Eytan, E., Wang, K., Miniowitz-Shemtov, S., Sitry-Shevah, D., Kaisari, S., Yen, T. J., Liu, S. T., & Hershko, A. (2014). Disassembly of mitotic checkpoint complexes by the joint action of the AAA-ATPase TRIP13 and p31comet. *Proceedings of the National Academy of Sciences of the United States of America*, *111*(33), 12019–12024. https://doi.org/10.1073/PNAS.1412901111/-/DCSUPPLEMENTAL/PNAS.201412901SI.PDF

Faesen, A. C., Thanasoula, M., Maffini, S., Breit, C., Müller, F., Van Gerwen, S., Bange, T., & Musacchio, A. (2017). Basis of catalytic assembly of the mitotic checkpoint complex. *Nature*, *542*(7642), 498. https://doi.org/10.1038/NATURE21384

Faragher, A. J., & Fry, A. M. (2003). Nek2A kinase stimulates centrosome disjunction and is required for formation of bipolar mitotic spindles. *Molecular Biology of the Cell*, *14*(7), 2876. https://doi.org/10.1091/MBC.E03-02-0108

Foltz, D. R., Jansen, L. E. T., Black, B. E., Bailey, A. O., Yates, J. R., & Cleveland, D. W. (2006). The human CENP-A centromeric nucleosome-associated complex. *Nature Cell Biology 2006 8:5*, *8*(5), 458–469. https://doi.org/10.1038/ncb1397

Fulcher, L. J., Sobajima, T., Batley, C., Gibbs-Seymour, I., & Barr, F. A. (2025). MDM2 functions as a timer reporting the length of mitosis. *Nature Cell Biology 2025 27:2*, *27*(2), 262–272. https://doi.org/10.1038/s41556-024-01592-8

Funabiki, H., Yamano, H., Kumada, K., Nagao, K., Hunt, T., Yanagida, M., & Elledge, S. J. (1996). Cell cycle checkpoints: preventing an identity crisis. *Science (New York, N.Y.)*, *274*(5293), 1664–1672. https://doi.org/10.1126/SCIENCE.274.5293.1664

Gascoigne, K. E., Takeuchi, K., Suzuki, A., Hori, T., Fukagawa, T., & Cheeseman, I. M. (2011). Induced Ectopic Kinetochore Assembly Bypasses the Requirement for CENP-A Nucleosomes. *Cell*, *145*(3), 410–422. https://doi.org/10.1016/J.CELL.2011.03.031

Gautier, J., Solomon, M. J., Booher, R. N., Bazan, J. F., & Kirschner, M. W. (1991). cdc25 is a specific tyrosine phosphatase that directly activates p34cdc2. *Cell*, *67*(1), 197–211. https://doi.org/10.1016/0092-8674(91)90583-K

Girdler, F., Gascoigne, K. E., Eyers, P. A., Hartmuth, S., Crafter, C., Foote, K. M., Keen, N. J., & Taylor, S. S. (2006). Validating Aurora B as an anti-cancer drug target. *Journal of Cell Science*, *119*(17), 3664–3675. https://doi.org/10.1242/JCS.03145

Goldenson, B., & Crispino, J. D. (2014). The Aurora Kinases in Cell Cycle and Leukemia. *Oncogene*, *34*(5), 537. https://doi.org/10.1038/ONC.2014.14

Goto, H., Yasui, Y., Nigg, E. A., & Inagaki, M. (2002). Aurora-B phosphorylates Histone H3 at serine28 with regard to the mitotic chromosome condensation. *Genes to Cells : Devoted to Molecular & Cellular Mechanisms*, *7*(1), 11–17. https://doi.org/10.1046/J.1356-9597.2001.00498.X

Gould, K. L., & Nurse, P. (1989). Tyrosine phosphorylation of the fission yeast cdc2+ protein kinase regulates entry into mitosis. *Nature*, *342*(6245), 39–45. https://doi.org/10.1038/342039A0

Grimm, J. B., Brown, T. A., English, B. P., Lionnet, T., & Lavis, L. D. (2017). Synthesis of Janelia Fluor HaloTag and SNAP-Tag Ligands and Their Use in Cellular Imaging Experiments BT - Super-Resolution Microscopy: Methods and Protocols. *Methods in Molecular Biology*, *1663*, 179–188. https://pubmed.ncbi.nlm.nih.gov/28924668/

Grimm, J. B., Xie, L., Casler, J. C., Patel, R., Tkachuk, A. N., Falco, N., Choi, H., Lippincott-Schwartz, J., Brown, T. A., Glick, B. S., Liu, Z., & Lavis, L. D. (2021). A General Method to Improve Fluorophores Using Deuterated Auxochromes. *JACS Au*, *1*(5), 690–696. https://doi.org/10.1021/JACSAU.1C00006/SUPPL_FILE/AU1C00006_SI_002.MP4

Gruneberg, U., Neef, R., Honda, R., Nigg, E. A., & Barr, F. A. (2004). Relocation of Aurora B from centromeres to the central spindle at the metaphase to anaphase transition requires MKlp2. *The Journal of Cell Biology*, *166*(2), 167. https://doi.org/10.1083/JCB.200403084

Guo, Y., Kim, C., Ahmad, S., Zhang, J., & Mao, Y. (2012). CENP-E–dependent BubR1 autophosphorylation enhances chromosome alignment and the mitotic checkpoint. *The Journal of Cell Biology*, *198*(2), 205. https://doi.org/10.1083/JCB.201202152

Hadders, M. A., Hindriksen, S., Truong, M. A., Mhaskar, A. N., Pepijn Wopken, J., Vromans, M. J. M., & Lens, S. M. A. (2020). Untangling the contribution of Haspin and Bub1 to Aurora B function during mitosis. *The Journal of Cell Biology*, *219*(3), e201907087. https://doi.org/10.1083/JCB.201907087

Hammond, D., Zeng, K., Espert, A., Bastos, R. N., Baron, R. D., Gruneberg, U., & Barr, F. A. (2013). Melanoma-associated mutations in protein phosphatase 6 cause chromosome instability and DNA damage owing to dysregulated Aurora-A. *Journal of Cell Science*, *126*(15), 3429–3440. https://doi.org/10.1242/JCS.128397/263484/AM/MELANOMA-ASSOCIATED-MUTATIONS-IN-PROTEIN

Hanks, S., Coleman, K., Reid, S., Plaja, A., Firth, H., FitzPatrick, D., Kidd, A., Méhes, K., Nash, R., Robin, N., Shannon, N., Tolmie, J., Swansbury, J., Irrthum, A., Douglas, J., & Rahman, N. (2004). Constitutional aneuploidy and cancer predisposition caused by biallelic mutations in BUB1B. *Nature Genetics 2004 36:11*, *36*(11), 1159–1161. https://doi.org/10.1038/ng1449

Hartwell, L. H., & Weinert, T. A. (1989). Checkpoints: controls that ensure the order of cell cycle events. *Science (New York, N.Y.)*, *246*(4930), 629–634. https://doi.org/10.1126/SCIENCE.2683079

Hayward, D., Roberts, E., & Gruneberg, U. (2022). MPS1 localizes to end-on microtubule-attached kinetochores to promote microtubule release. *Current Biology*, *32*(23), 5200-5208.e8. https://doi.org/10.1016/j.cub.2022.10.047

Heald, R., & Yckeon, F. (1990). Mutations of Phosphorylation Sites in Lamin A That Prevent Nuclear Lamina Disassembly in Mitosis. *Cell*, *61*, 579–589.

Hein, B., Willig, K. I., & Hell, S. W. (2008). Stimulated emission depletion (STED) nanoscopy of a fluorescent protein-labeled organelle inside a living cell. *Proceedings of the National Academy of Sciences of the United States of America*, *105*(38), 14271–14276. https://doi.org/10.1073/PNAS.0807705105/SUPPL_FILE/SM1.AVI

Hell, S. W., & Wichmann, J. (1994). Breaking the diffraction resolution limit by stimulated emission: stimulated-emission-depletion fluorescence microscopy. *OPTICS LETTERS*, *19*(11).

Hirota, T., Lipp, J. J., Toh, B. H., & Peters, J. M. (2005). Histone H3 serine 10 phosphorylation by Aurora B causes HP1 dissociation from heterochromatin. *Nature*, *438*(7071), 1176–1180. https://doi.org/10.1038/NATURE04254

Hiruma, Y., Sacristan, C., Pachis, S. T., Adamopoulos, A., Kuijt, T., Ubbink, M., Von Castelmur, E., Perrakis, A., & Kops, G. J. P. L. (2015). Competition between MPS1 and microtubules at kinetochores regulates spindle checkpoint signaling. *Science*, *348*(6240), 1264–1267. https://doi.org/10.1126/SCIENCE.AAA4055/SUPPL_FILE/HIRUMA.SM.PDF

Ho, C. C., Siu, W. Y., Lau, A., Chan, W. M., Arooz, T., & Poon, R. Y. C. (2006). Stalled Replication Induces p53 Accumulation through Distinct Mechanisms from DNA Damage Checkpoint Pathways. *Cancer Research*, *66*(4), 2233–2241. https://doi.org/10.1158/0008-5472.CAN-05-1790

Holder, J., Miles, J. A., Batchelor, M., Popple, H., Walko, M., Yeung, W., Kannan, N., Wilson, A. J., Bayliss, R., & Gergely, F. (2024). CEP192 localises mitotic Aurora-A activity by priming its interaction with TPX2. *EMBO Journal*, *43*(22), 5381–5420. https://doi.org/10.1038/S44318-024-00240-Z/SUPPL_FILE/44318_2024_240_MOESM11_ESM.PDF

Holder, J., Mohammed, S., & Barr, F. A. (2020). Ordered dephosphorylation initiated by the selective proteolysis of cyclin B drives mitotic exit. *ELife*, *9*, 1–33. https://doi.org/10.7554/ELIFE.59885

Honda, R., Körner, R., & Nigg, E. A. (2003). Exploring the functional interactions between Aurora B, INCENP, and survivin in mitosis. *Molecular Biology of the Cell*, *14*(8), 3325–3341. https://doi.org/10.1091/MBC.E02-11-0769

Hori, T., Amano, M., Suzuki, A., Backer, C. B., Welburn, J. P., Dong, Y., McEwen, B. F., Shang, W. H., Suzuki, E., Okawa, K., Cheeseman, I. M., & Fukagawa, T. (2008). CCAN Makes Multiple Contacts with Centromeric DNA to Provide Distinct Pathways to the Outer Kinetochore. *Cell*, *135*(6), 1039–1052. https://doi.org/10.1016/j.cell.2008.10.019

Howell, B. J., Hoffman, D. B., Fang, G., Murray, A. W., & Salmon, E. D. (2000). Visualization of Mad2 Dynamics at Kinetochores, along Spindle Fibers, and at Spindle Poles in Living Cells 7. *The Journal of Cell Biology*, *150*(6), 1233–1249. http://www.jcb.org

Howell, B. J., Moree, B., Farrar, E. M., Stewart, S., Fang, G., & Salmon, E. D. (2004). Spindle checkpoint protein dynamics at kinetochores in living cells. *Current Biology*, *14*(11), 953–964. https://doi.org/10.1016/J.CUB.2004.05.053/ATTACHMENT/4F932D17-9EB6-4F6A-A5A0-5996CDEB9B8B/MMC6.MP4

Hunter, T. (2007). The Age of Crosstalk: Phosphorylation, Ubiquitination, and Beyond. *Molecular Cell*, *28*(5), 730–738. https://doi.org/10.1016/j.molcel.2007.11.019

Ivorra-Molla, E., Akhuli, D., McAndrew, M. B. L., Scott, W., Kumar, L., Palani, S., Mishima, M., Crow, A., & Balasubramanian, M. K. (2023). A monomeric StayGold fluorescent protein. *Nature Biotechnology 2023 42:9*, *42*(9), 1368–1371. https://doi.org/10.1038/s41587-023-02018-w

Izawa, D., & Pines, J. (2014). The mitotic checkpoint complex binds a second CDC20 to inhibit active APC/C. *Nature 2014 517:7536*, *517*(7536), 631–634. https://doi.org/10.1038/nature13911

Jema, S., Chen, C., Humphrey, L., Karmarkar, S., Ferrari, F., & Joglekar, A. P. (2023). Signaling protein abundance modulates the strength of the spindle assembly checkpoint. *Current Biology*, *33*(20), 4505-4515.e4. https://doi.org/10.1016/j.cub.2023.08.074

Jeyaprakash, A. A., Basquin, C., Jayachandran, U., & Conti, E. (2011). Structural Basis for the Recognition of Phosphorylated Histone H3 by the Survivin Subunit of the Chromosomal Passenger Complex. *Structure*, *19*(11), 1625–1634. https://doi.org/10.1016/J.STR.2011.09.002

Jeyaprakash, A. A., Klein, U. R., Lindner, D., Ebert, J., Nigg, E. A., & Conti, E. (2007). Structure of a Survivin-Borealin-INCENP Core Complex Reveals How Chromosomal Passengers Travel Together. *Cell*, *131*(2), 271–285. https://doi.org/10.1016/j.cell.2007.07.045

Ji, Z., Gao, H., Jia, L., Li, B., & Yu, H. (2017). A sequential multi-target Mps1 phosphorylation cascade promotes spindle checkpoint signaling. *ELife*, *6*. https://doi.org/10.7554/ELIFE.22513

Ji, Z., Gao, H., & Yu, H. (2015). Kinetochore attachment sensed by competitive Mps1 and microtubule binding to Ndc80C. *Science*, *348*(6240), 1260–1264. https://doi.org/10.1126/SCIENCE.AAA4029/SUPPL_FILE/JI-SM.PDF

Joukov, V., Walter, J. C., & De Nicolo, A. (2014). The Cep192-organized aurora A-Plk1 cascade is essential for centrosome cycle and bipolar spindle assembly. *Molecular Cell*, *55*(4), 578–591. https://doi.org/10.1016/J.MOLCEL.2014.06.016

Ju, L. L., Chen, L., Li, J. H., Wang, Y. F., Lu, R. J., Bian, Z. L., & Shao, J. G. (2017). Effect of NDC80 in human hepatocellular carcinoma. *World Journal of Gastroenterology*, *23*(20), 3675. https://doi.org/10.3748/WJG.V23.I20.3675

Kaeser, M. D., Pebernard, S., & Iggo, R. D. (2004). Regulation of p53 Stability and Function in HCT116 Colon Cancer Cells. *Journal of Biological Chemistry*, *279*(9), 7598–7605. https://doi.org/10.1074/jbc.M311732200

Kallio, M. J., Beardmore, V. A., Weinstein, J., & Gorbsky, G. J. (2002). Rapid microtubule-independent dynamics of Cdc20 at kinetochores and centrosomes in mammalian cells. *The Journal of Cell Biology*, *158*(5), 841. https://doi.org/10.1083/JCB.200201135

Kang, Y. H., Park, C. H., Kim, T. S., Soung, N. K., Bang, J. K., Kim, B. Y., Park, J. E., & Lee, K. S. (2011). Mammalian polo-like kinase 1-dependent regulation of the PBIP1-CENP-Q complex at kinetochores. *Journal of Biological Chemistry*, *286*(22), 19744–19757. https://doi.org/10.1074/jbc.M111.224105

Kelly, A. E., Ghenoiu, C., Xue, J. Z., Zierhut, C., Kimura, H., & Funabiki, H. (2010). Survivin reads phosphorylated histone H3 threonine 3 to activate the mitotic kinase Aurora B. *Science (New York, N.Y.)*, *330*(6001), 235–239. https://doi.org/10.1126/SCIENCE.1189505

Kemmler, S., Stach, M., Knapp, M., Ortiz, J., Pfannstiel, J., Ruppert, T., & Lechner, J. (2009). Mimicking Ndc80 phosphorylation triggers spindle assembly checkpoint signalling. *The EMBO Journal*, *28*(8), 1099–1110. https://doi.org/10.1038/EMBOJ.2009.62

Kettenbach, A. N., Schweppe, D. K., Faherty, B. K., Pechenick, D., Pletnev, A. A., & Gerber, S. A. (2011). Quantitative Phosphoproteomics Identifies Substrates and Functional Modules of Aurora and Polo-Like Kinase Activities in Mitotic Cells. *Science Signaling*, *4*(179), 10.1126/scisignal.2001497. https://doi.org/10.1126/SCISIGNAL.2001497

Kim, T. (2022). Recent Progress on the Localization of PLK1 to the Kinetochore and Its Role in Mitosis. *International Journal of Molecular Sciences*, *23*(9). https://doi.org/10.3390/IJMS23095252

Kitajima, T. S., Sakuno, T., Ishiguro, K. I., Iemura, S. I., Natsume, T., Kawashima, S. A., & Watanabe, Y. (2006). Shugoshin collaborates with protein phosphatase 2A to protect cohesin. *Nature 2006 441:7089*, *441*(7089), 46–52. https://doi.org/10.1038/nature04663

Kiyomitsu, T., Obuse, C., & Yanagida, M. (2007). Human Blinkin/AF15q14 is required for chromosome alignment and the mitotic checkpoint through direct interaction with Bub1 and BubR1. *Developmental Cell*, *13*(5), 663–676. https://doi.org/10.1016/J.DEVCEL.2007.09.005

Klein, U. R., Nigg, E. A., & Gruneberg, U. (2006). Centromere targeting of the chromosomal passenger complex requires a ternary subcomplex of borealin, survivin, and the N-terminal domain of INCENP. *Molecular Biology of the Cell*, *17*(6), 2547–2558. https://doi.org/10.1091/MBC.E05-12-1133/ASSET/IMAGES/LARGE/ZMK0060676650010.JPEG

Kline, S. L., Cheeseman, I. M., Hori, T., Fukagawa, T., & Desai, A. (2006). The human Mis12 complex is required for kinetochore assembly and proper chromosome segregation. *Journal of Cell Biology*, *173*(1), 9–17. https://doi.org/10.1083/JCB.200509158

Kreis, N.-N., Friemel, A., Zimmer, B., Roth, S., Rieger, M. A., Rolle, U., Louwen, F., & Yuan, J. (2016). Mitotic p21Cip1/CDKN1A is regulated by cyclin-dependent kinase 1

phosphorylation. *Oncotarget*, *7*(31), 50215–50228. https://doi.org/10.18632/oncotarget.10330
Krenn, V., & Musacchio, A. (2015). The Aurora B Kinase in Chromosome Bi-Orientation and Spindle Checkpoint Signaling. *Frontiers in Oncology*, *5*(OCT), 225. https://doi.org/10.3389/FONC.2015.00225
Kuijt, T. E. F., Lambers, M. L. A., Weterings, S., Ponsioen, B., Bolhaqueiro, A. C. F., Staijen, D. H. M., & Kops, G. J. P. L. (2020). A Biosensor for the Mitotic Kinase MPS1 Reveals Spatiotemporal Activity Dynamics and Regulation. *Current Biology*, *30*(19), 3862-3870.e6. https://doi.org/10.1016/J.CUB.2020.07.062
Lampson, M. A., & Cheeseman, I. M. (2010). Sensing centromere tension: Aurora B and the regulation of kinetochore function. *Trends in Cell Biology*, *21*(3), 133. https://doi.org/10.1016/J.TCB.2010.10.007
Lara-Gonzalez, P., Pines, J., & Desai, A. (2021). Spindle assembly checkpoint activation and silencing at kinetochores. *Seminars in Cell & Developmental Biology*, *117*, 86. https://doi.org/10.1016/J.SEMCDB.2021.06.009
Levine, M. S., & Holland, A. J. (2018). *The impact of mitotic errors on cell proliferation and tumorigenesis*. https://doi.org/10.1101/gad.314351
Li, S., Garcia-Rodriguez, L. J., & Tanaka, T. U. (2023). Chromosome biorientation requires Aurora B's spatial separation from its outer kinetochore substrates, but not its turnover at kinetochores. *Current Biology*, *33*(21), 4557-4569.e3. https://doi.org/10.1016/j.cub.2023.09.006
Liu, D., Vader, G., Vromans, M. J. M., Lampson, M. A., & Lens, S. M. A. (2009). Sensing chromosome bi-orientation by spatial separation of Aurora B kinase from kinetochore substrates. *Science*, *323*(5919), 1350–1353. https://doi.org/10.1126/SCIENCE.1167000/SUPPL_FILE/LIU_SOM.PDF
Liu, D., Vleugel, M., Backer, C. B., Hori, T., Fukagawa, T., Cheeseman, I. M., & Lampson, M. A. (2010). Regulated targeting of protein phosphatase 1 to the outer kinetochore by KNL1 opposes Aurora B kinase. *The Journal of Cell Biology*, *188*(6), 809–820. https://doi.org/10.1083/JCB.201001006
Liu, H., Rankin, S., & Yu, H. (2013). Phosphorylation-enabled binding of SGO1-PP2A to cohesin protects sororin and centromeric cohesion during mitosis. *Nature Cell Biology*, *15*(1), 40–49. https://doi.org/10.1038/NCB2637
Logarinho, E., Resende, T., Torres, C., & Bousbaa, H. (2008). The Human Spindle Assembly Checkpoint Protein Bub3 Is Required for the Establishment of Efficient Kinetochore–Microtubule Attachments. *Molecular Biology of the Cell*, *19*(4), 1798. https://doi.org/10.1091/MBC.E07-07-0633
Lok, T. M., Wang, Y., Xu, W. K., Xie, S., Ma, H. T., & Poon, R. Y. C. (2020). Mitotic slippage is determined by p31comet and the weakening of the spindle-assembly checkpoint. *Oncogene 2020 39:13*, *39*(13), 2819–2834. https://doi.org/10.1038/s41388-020-1187-6
London, N., Ceto, S., Ranish, J. A., & Biggins, S. (2012). Phosphoregulation of Spc105 by Mps1 and PP1 Regulates Bub1 Localization to Kinetochores. *Current Biology*, *22*(10), 900–906. https://doi.org/10.1016/J.CUB.2012.03.052
Losada, A., Hirano, M., & Hirano, T. (2002). Cohesin release is required for sister chromatid resolution, but not for condensin-mediated compaction, at the onset of mitosis. *Genes & Development*, *16*(23), 3004–3016. https://doi.org/10.1101/GAD.249202
Magnaghi-Jaulin, L., Eot-Houllier, G., Gallaud, E., & Giet, R. (2019). Aurora A Protein Kinase: To the Centrosome and Beyond. *Biomolecules*, *9*(1), 28. https://doi.org/10.3390/BIOM9010028
Maresca, T. J., & Salmon, E. D. (2009). Intrakinetochore stretch is associated with changes in kinetochore phosphorylation and spindle assembly checkpoint activity. *The Journal of Cell Biology*, *184*(3), 373–381. https://doi.org/10.1083/JCB.200808130
Marescal, O., & Cheeseman, I. M. (2020). Cellular Mechanisms and Regulation of Quiescence. *Developmental Cell*, *55*(3), 259. https://doi.org/10.1016/J.DEVCEL.2020.09.029

Mazzagatti, A., Engel, J. L., & Ly, P. (2024). Boveri and beyond: Chromothripsis and genomic instability from mitotic errors. *Molecular Cell*, *84*(1), 55–69. https://doi.org/10.1016/j.molcel.2023.11.002

McHugh, T., & Welburn, J. P. I. (2017). Dynein at kinetochores: Making the connection. *The Journal of Cell Biology*, *216*(4), 855. https://doi.org/10.1083/JCB.201703054

McHugh, T., Zou, J., Volkov, V. A., Bertin, A., Talapatra, S. K., Rappsilber, J., Dogterom, M., & Welburn, J. P. I. (2019). The depolymerase activity of MCAK shows a graded response to Aurora B kinase phosphorylation through allosteric regulation. *Journal of Cell Science*, *132*(4). https://doi.org/10.1242/JCS.228353

McKinley, K. L., & Cheeseman, I. M. (2015). The molecular basis for centromere identity and function. *Nature Reviews Molecular Cell Biology 2015 17:1*, *17*(1), 16–29. https://doi.org/10.1038/nrm.2015.5

Mckinley, K. L., Sekulic, N., Guo, L. Y., Tsinman, T., Black, B. E., Cheeseman Correspondence, I. M., & Cheeseman, I. M. (2015). The CENP-L-N Complex Forms a Critical Node in an Integrated Meshwork of Interactions at the Centromere-Kinetochore Interface Molecular Cell The CENP-L-N Complex Forms a Critical Node in an Integrated Meshwork of Interactions at the Centromere-Kinetochore Interface. *Molecular Cell*, *60*, 886–898. https://doi.org/10.1016/j.molcel.2015.10.027

McVey, S. L., Cosby, J. K., & Nannas, N. J. (2021). Aurora B Tension Sensing Mechanisms in the Kinetochore Ensure Accurate Chromosome Segregation. *International Journal of Molecular Sciences*, *22*(16), 8818. https://doi.org/10.3390/IJMS22168818

Meppelink, A., Kabeche, L., Vromans, M. J. M., Compton, D. A., & Lens, S. M. A. (2015). Shugoshin-1 Balances Aurora B Kinase Activity via PP2A to Promote Chromosome Bi-orientation. *Cell Reports*, *11*(4), 508. https://doi.org/10.1016/J.CELREP.2015.03.052

Michaelis, C., Ciosk, R., & Nasmyth, K. (1997). Cohesins: Chromosomal proteins that prevent premature separation of sister chromatids. *Cell*, *91*(1), 35–45. https://doi.org/10.1016/S0092-8674(01)80007-6

Michel, L. S., Liberal, V., Chatterjee, A., Kirchwegger, R., Pasche, B., Gerald, W., Dobles, M., Sorger, P. K., Murty, V. V. V. S., & Benezra, R. (2001). MAD2 haplo-insufficiency causes premature anaphase and chromosome instability in mammalian cells. *Nature 2001 409:6818*, *409*(6818), 355–359. https://doi.org/10.1038/35053094

Minoshima, Y., Kawashima, T., Hirose, K., Tonozuka, Y., Kawajiri, A., Bao, Y. C., Deng, X., Tatsuka, M., Narumiya, S., May, W. S., Nosaka, T., Semba, K., Inoue, T., Satoh, T., Inagaki, M., & Kitamura, T. (2003). Phosphorylation by Aurora B converts MgcRacGAP to a RhoGAP during cytokinesis. *Developmental Cell*, *4*(4), 549–560. https://doi.org/10.1016/S1534-5807(03)00089-3

Monaco, L., Kolthur-Seetharam, U., Loury, R., Ménissier-De Murcia, J., De Murcia, G., & Sassone-Corsi, P. (2005). Inhibition of Aurora-B kinase activity by poly(ADP-ribosyl)ation in response to DNA damage. *Proceedings of the National Academy of Sciences of the United States of America*, *102*(40), 14244–14248. https://doi.org/10.1073/PNAS.0506252102/SUPPL_FILE/06252FIG7.PDF

Mosalaganti, S., Keller, J., Altenfeld, A., Winzker, M., Rombaut, P., Saur, M., Petrovic, A., Wehenke, A., Wohlgemuth, S., Müller, F., Maffini, S., Bange, T., Herzog, F., Waldmann, H., Raunser, S., & Musacchio, A. (2017). Structure of the RZZ complex and molecular basis of its interaction with Spindly. *Journal of Cell Biology*, *216*(4), 961–981. https://doi.org/10.1083/JCB.201611060

Musacchio, A. (2015). The Molecular Biology of Spindle Assembly Checkpoint Signaling Dynamics. *Current Biology*, *25*(20), R1002–R1018. https://doi.org/10.1016/J.CUB.2015.08.051/ASSET/7E6C69F0-D0AF-4F8A-BDC5-2EECE0AC20BA/MAIN.ASSETS/GR5.JPG

Nabet, B., Ferguson, F. M., Seong, B. K. A., Kuljanin, M., Leggett, A. L., Mohardt, M. L., Robichaud, A., Conway, A. S., Buckley, D. L., Mancias, J. D., Bradner, J. E., Stegmaier, K., & Gray, N. S. (2020). Rapid and direct control of target protein levels with VHL-recruiting dTAG molecules. *Nature Communications 2020 11:1*, *11*(1), 1–8. https://doi.org/10.1038/s41467-020-18377-w

Namura, S., Zhu, J., Fink, K., Endres, M., Srinivasan, A., Tomaselli, K. J., Yuan, J., & Moskowitz, M. A. (1998). Activation and cleavage of caspase-3 in apoptosis induced by experimental cerebral ischemia. *The Journal of Neuroscience : The Official Journal of the Society for Neuroscience*, *18*(10), 3659–3668. https://doi.org/10.1523/JNEUROSCI.18-10-03659.1998

Navarro, A. P., & Cheeseman, I. M. (2021). Kinetochore assembly throughout the cell cycle. *Seminars in Cell & Developmental Biology*, *117*, 62. https://doi.org/10.1016/J.SEMCDB.2021.03.008

Neef, R., Klein, U. R., Kopajtich, R., & Barr, F. A. (2006). Cooperation between Mitotic Kinesins Controls the Late Stages of Cytokinesis. *Current Biology*, *16*(3), 301–307. https://doi.org/10.1016/J.CUB.2005.12.030

Niedzialkowska, E., Wang, F., Porebski, P. J., Minor, W., Higgins, J. M. G., & Stukenberga, P. T. (2012). Molecular basis for phosphospecific recognition of histone H3 tails by Survivin paralogues at inner centromeres. *Molecular Biology of the Cell*, *23*(8), 1457–1466. https://doi.org/10.1091/MBC.E11-11-0904

Nigg, E. A. (2007). Centrosome duplication: of rules and licenses. *Trends in Cell Biology*, *17*(5), 215–221. https://doi.org/10.1016/J.TCB.2007.03.003/ASSET/3E9AF4DA-0DED-4044-9832-7D5090A37024/MAIN.ASSETS/GR2.JPG

Nijenhuis, W., Vallardi, G., Teixeira, A., Kops, G. J. P. L., & Saurin, A. T. (2014). Negative feedback at kinetochores underlies a responsive spindle checkpoint signal. *Nature Cell Biology*, *16*(12), 1257–1264. https://doi.org/10.1038/NCB3065;TECHMETA

Nijenhuis, W., Von Castelmur, E., Littler, D., De Marco, V., Tromer, E., Vleugel, M., Van Osch, M. H. J., Snel, B., Perrakis, A., & Kops, G. J. P. L. (2013). A TPR domain–containing N-terminal module of MPS1 is required for its kinetochore localization by Aurora B. *Journal of Cell Biology*, *201*(2), 217–231. https://doi.org/10.1083/JCB.201210033

Nishino, T., Rago, F., Hori, T., Tomii, K., Cheeseman, I. M., & Fukagawa, T. (2013). CENP-T provides a structural platform for outer kinetochore assembly. *EMBO Journal*, *32*(3), 424–436. https://doi.org/10.1038/EMBOJ.2012.348/SUPPL_FILE/EMBJ2012348.REVIEWER_COMMENTS.PDF

Novak, B., & Tyson, J. J. (1993). Numerical analysis of a comprehensive model of M-phase control in Xenopus oocyte extracts and intact embryos. *Journal of Cell Science*, *106 (Pt 4)*(4), 1153–1168. https://doi.org/10.1242/JCS.106.4.1153

O'Connell, M. J., Raleigh, J. M., Verkade, H. M., & Nurse, P. (1997). Chk1 is a wee1 kinase in the G2 DNA damage checkpoint inhibiting cdc2 by Y15 phosphorylation. *The EMBO Journal*, *16*(3), 545–554. https://doi.org/10.1093/EMBOJ/16.3.545

Okada, M., Cheeseman, I. M., Hori, T., Okawa, K., McLeod, I. X., Yates, J. R., Desai, A., & Fukagawa, T. (2006). The CENP-H–I complex is required for the efficient incorporation of newly synthesized CENP-A into centromeres. *Nature Cell Biology 2006 8:5*, *8*(5), 446–457. https://doi.org/10.1038/ncb1396

Olivier, M., Hollstein, M., & Hainaut, P. (2010). TP53 mutations in human cancers: origins, consequences, and clinical use. *Cold Spring Harbor Perspectives in Biology*, *2*(1). https://doi.org/10.1101/CSHPERSPECT.A001008

Ono, T., Losada, A., Hirano, M., Myers, M. P., Neuwald, A. F., & Hirano, T. (2003). Differential contributions of condensin I and condensin II to mitotic chromosome architecture in vertebrate cells. *Cell*, *115*(1), 109–121. https://doi.org/10.1016/S0092-8674(03)00724-4

Pachis, S. T., & Kops, G. J. P. L. (2018). Leader of the SAC: molecular mechanisms of Mps1/TTK regulation in mitosis. *Open Biology*, *8*(8). https://doi.org/10.1098/RSOB.180109

Pesenti, M. E., Prumbaum, D., Auckland, P., Smith, C. M., Faesen, A. C., Petrovic, A., Erent, M., Maffini, S., Pentakota, S., Weir, J. R., Lin, Y. C., Raunser, S., McAinsh, A. D., & Musacchio, A. (2018). Reconstitution of a 26-Subunit Human Kinetochore Reveals

Cooperative Microtubule Binding by CENP-OPQUR and NDC80. *Molecular Cell*, *71*(6), 923-939.e10. https://doi.org/10.1016/j.molcel.2018.07.038

Pesenti, M. E., Raisch, T., Conti, D., Walstein, K., Hoffmann, I., Vogt, D., Prumbaum, D., Vetter, I. R., Raunser, S., & Musacchio, A. (2022). Structure of the human inner kinetochore CCAN complex and its significance for human centromere organization. *Molecular Cell*, *82*(11), 2113-2131.e8. https://doi.org/10.1016/j.molcel.2022.04.027

Petrovic, A., Keller, J., Liu, Y., Overlack, K., John, J., Dimitrova, Y. N., Jenni, S., van Gerwen, S., Stege, P., Wohlgemuth, S., Rombaut, P., Herzog, F., Harrison, S. C., Vetter, I. R., & Musacchio, A. (2016). Structure of the MIS12 Complex and Molecular Basis of Its Interaction with CENP-C at Human Kinetochores. *Cell*, *167*(4), 1028. https://doi.org/10.1016/J.CELL.2016.10.005

Petrovic, A., Mosalaganti, S., Keller, J., Mattiuzzo, M., Overlack, K., Krenn, V., DeAntoni, A., Wohlgemuth, S., Cecatiello, V., Pasqualato, S., Raunser, S., & Musacchio, A. (2014). Modular Assembly of RWD Domains on the Mis12 Complex Underlies Outer Kinetochore Organization. *Molecular Cell*, *53*(4), 591–605. https://doi.org/10.1016/j.molcel.2014.01.019

Petrovic, A., Pasqualato, S., Dube, P., Krenn, V., Santaguida, S., Cittaro, D., Monzani, S., Massimiliano, L., Keller, J., Tarricone, A., Maiolica, A., Stark, H., & Musacchio, A. (2010). The MIS12 complex is a protein interaction hub for outer kinetochore assembly. *The Journal of Cell Biology*, *190*(5), 835. https://doi.org/10.1083/JCB.201002070

Piano, V., Alex, A., Stege, P., Maffini, S., Stoppiello, G. A., Huis In'T Veld, P. J., Vetter, I. R., & Musacchio, A. (2021). CDC20 assists its catalytic incorporation in the mitotic checkpoint complex. *Science*, *371*(6524), 67–71. https://doi.org/10.1126/SCIENCE.ABC1152

Pleuger, R., Cozma, C., Hohoff, S., Denkhaus, C., Dudziak, A., Kaschani, F., Kaiser, M., Musacchio, A., Vetter, I. R., & Westermann, S. (2024). Microtubule end-on attachment maturation regulates Mps1 association with its kinetochore receptor. *Current Biology*, *34*(11), 2279-2293.e6. https://doi.org/10.1016/J.CUB.2024.03.062

Polley, S., Raisch, T., Ghetti, S., Körner, M., Terbeck, M., Gräter, F., Raunser, S., Aponte-Santamaría, C., Vetter, I. R., & Musacchio, A. (2024). Structure of the human KMN complex and implications for regulation of its assembly. *Nature Structural and Molecular Biology*, *31*(6), 861–873. https://doi.org/10.1038/S41594-024-01230-9;SUBJMETA

Pomerening, J. R., Sontag, E. D., & Ferrell, J. E. (2003). Building a cell cycle oscillator: hysteresis and bistability in the activation of Cdc2. *Nature Cell Biology*, *5*(4), 346–351. https://doi.org/10.1038/NCB954

Primorac, I., Weir, J. R., Chiroli, E., Gross, F., Hoffmann, I., van Gerwen, S., Ciliberto, A., & Musacchio, A. (2013). Bub3 reads phosphorylated MELT repeats to promote spindle assembly checkpoint signaling. *ELife*, *2*(2). https://doi.org/10.7554/ELIFE.01030

Qian, J., García-Gimeno, M. A., Beullens, M., Manzione, M. G., Van der Hoeven, G., Igual, J. C., Heredia, M., Sanz, P., Gelens, L., & Bollen, M. (2017). An Attachment-Independent Biochemical Timer of the Spindle Assembly Checkpoint. *Molecular Cell*, *68*(4), 715-730.e5. https://doi.org/10.1016/j.molcel.2017.10.011

Risteski, P., Jagrić, M., Pavin, N., & Tolić, I. M. (2021). Biomechanics of chromosome alignment at the spindle midplane. *Current Biology*, *31*(10), R574–R585. https://doi.org/10.1016/J.CUB.2021.03.082

Roshan, P., Kuppa, S., Mattice, J. R., Kaushik, V., Chadda, R., Pokhrel, N., Tumala, B. R., Biswas, A., Bothner, B., Antony, E., & Origanti, S. (2023). An Aurora B-RPA signaling axis secures chromosome segregation fidelity. *Nature Communications 2023 14:1*, *14*(1), 1–19. https://doi.org/10.1038/s41467-023-38711-2

Ruchaud, S., Carmena, M., & Earnshaw, W. C. (2007). Chromosomal passengers: Conducting cell division. *Nature Reviews Molecular Cell Biology*, *8*(10), 798–812. https://doi.org/10.1038/NRM2257;KWRD

Russell, P., & Nurse, P. (1986). cdc25+ functions as an inducer in the mitotic control of fission yeast. *Cell*, *45*(1), 145–153. https://doi.org/10.1016/0092-8674(86)90546-5

Ruza, R. R., Chung, C. W., Gold, D. B. H., Serena, M., Roberts, E., Gruneberg, U., & Barr, F. A. (2025). A pivot-tether model for nucleosome recognition by the chromosomal passenger complex. *EMBO Reports*. https://doi.org/10.1038/S44319-025-00523-4

Samejima, K., Platani, M., Wolny, M., Ogawa, H., Vargiu, G., Knight, P. J., Peckham, M., & Earnshaw, W. C. (2015). The inner centromere protein (INCENP) coil is a single α-helix (SAH) domain that binds directly to microtubules and is important for chromosome passenger complex (CPC) localization and function in mitosis. *Journal of Biological Chemistry*, *290*(35), 21460–21472. https://doi.org/10.1074/JBC.M115.645317/ASSET/063F82AF-E3A6-4D93-AB02-85F3FBA27F2C/MAIN.ASSETS/GR7.JPG

Sanchez, Y., Elledge, S. J., results, unpublished, Weinert, thank T., Murray, A., Carr, A., Sherr, C., Walworth, N., Harper, J. W., Sazer, S., Kuroda, M., & Sherr, C. J. (1996). Cancer Cell Cycles. *Science*, *274*(5293), 1672–1674. https://doi.org/10.1126/SCIENCE.274.5293.1672

Saurin, A. T., Van Der Waal, M. S., Medema, R. H., Lens, S. M. A., & Kops, G. J. P. L. (2011). Aurora B potentiates Mps1 activation to ensure rapid checkpoint establishment at the onset of mitosis. *Nature Communications 2011 2:1*, *2*(1), 1–9. https://doi.org/10.1038/ncomms1319

Schermelleh, L., Heintzmann, R., & Leonhardt, H. (2010). A guide to super-resolution fluorescence microscopy. *The Journal of Cell Biology*, *190*(2), 165. https://doi.org/10.1083/JCB.201002018

Screpanti, E., De Antoni, A., Alushin, G. M., Petrovic, A., Melis, T., Nogales, E., & Musacchio, A. (2011). Direct binding of Cenp-C to the Mis12 complex joins the inner and outer kinetochore. *Current Biology*, *21*(5), 391–398. https://doi.org/10.1016/j.cub.2010.12.039

Serena, M., Bastos, R. N., Elliott, P. R., & Barr, F. A. (2020). Molecular basis of MKLP2-dependent Aurora B transport from chromatin to the anaphase central spindle. *Journal of Cell Biology*, *219*(7). https://doi.org/10.1083/JCB.201910059/151730

Sessa, F., Mapelli, M., Ciferri, C., Tarricone, C., Areces, L. B., Schneider, T. R., Stukenberg, P. T., & Musacchio, A. (2005). Mechanism of Aurora B activation by INCENP and inhibition by hesperadin. *Molecular Cell*, *18*(3), 379–391. https://doi.org/10.1016/j.molcel.2005.03.031

Shepperd, L. A., Meadows, J. C., Sochaj, A. M., Lancaster, T. C., Zou, J., Buttrick, G. J., Rappsilber, J., Hardwick, K. G., & Millar, J. B. A. (2012). Phosphodependent recruitment of Bub1 and Bub3 to Spc7/KNL1 by Mph1 kinase maintains the spindle checkpoint. *Current Biology*, *22*(10), 891–899. https://doi.org/10.1016/j.cub.2012.03.051

Sherr, C. J. (1994). Gl Phase Progression: Cycling on Cue. *Cell*, *79*, 551–555.

Sherr, C. J., & Roberts, J. M. (1999). CDK inhibitors: positive and negative regulators of G1-phase progression. *Genes & Development*, *13*(12), 1501–1512. https://doi.org/10.1101/GAD.13.12.1501

Simpson, L. M., Macartney, T. J., Nardin, A., Fulcher, L. J., Röth, S., Testa, A., Maniaci, C., Ciulli, A., Ganley, I. G., & Sapkota, G. P. (2020). Inducible Degradation of Target Proteins through a Tractable Affinity-Directed Protein Missile System. *Cell Chemical Biology*, *27*(9), 1164. https://doi.org/10.1016/J.CHEMBIOL.2020.06.013

Sinha, D., Duijf, P. H. G., & Khanna, K. K. (2019). Mitotic slippage: an old tale with a new twist. *Cell Cycle*, *18*(1), 7. https://doi.org/10.1080/15384101.2018.1559557

Sivakumar, S., & Gorbsky, G. J. (2015). Spatiotemporal regulation of the anaphase-promoting complex in mitosis. *Nature Reviews. Molecular Cell Biology*, *16*(2), 82–94. https://doi.org/10.1038/NRM3934

Sobajima, T., Kowalczyk, K. M., Skylakakis, S., Hayward, D., Fulcher, L. J., Neary, C., Batley, C., Kurlekar, S., Roberts, E., Gruneberg, U., & Barr, F. A. (2023). PP6 regulation of Aurora A-TPX2 limits NDC80 phosphorylation and mitotic spindle size. *The Journal of Cell Biology*, *222*(5). https://doi.org/10.1083/JCB.202205117

Steigemann, P., Wurzenberger, C., Schmitz, M. H. A., Held, M., Guizetti, J., Maar, S., & Gerlich, D. W. (2009). Aurora B-Mediated Abscission Checkpoint Protects against Tetraploidization. *Cell*, *136*(3), 473–484. https://doi.org/10.1016/j.cell.2008.12.020

Stucke, V. M., Silljé, H. H. W., Arnaud, L., & Nigg, E. A. (2002). Human Mps1 kinase is required for the spindle assembly checkpoint but not for centrosome duplication. *The EMBO Journal*, *21*(7), 1723–1732. https://doi.org/10.1093/EMBOJ/21.7.1723

Sudakin, V., Chan, G. K. T., & Yen, T. J. (2001). Checkpoint inhibition of the APC/C in HeLa cells is mediated by a complex of BUBR1, BUB3, CDC20, and MAD2. *The Journal of Cell Biology*, *154*(5), 925–936. https://doi.org/10.1083/JCB.200102093

Sundin, L. J. R., Guimaraes, G. J., & DeLuca, J. G. (2011). The NDC80 complex proteins Nuf2 and Hec1 make distinct contributions to kinetochore-microtubule attachment in mitosis. *Molecular Biology of the Cell*, *22*(6), 759–768. https://doi.org/10.1091/MBC.E10-08-0671/ASSET/IMAGES/LARGE/759FIG6.JPEG

Suzuki, A., Badger, B. L., & Salmon, E. D. (2015). A quantitative description of Ndc80 complex linkage to human kinetochores. *Nature Communications*, *6*, 8161. https://doi.org/10.1038/NCOMMS9161

Takenoshita, Y., Hara, M., & Fukagawa, T. (2022). Recruitment of two Ndc80 complexes via the CENP-T pathway is sufficient for kinetochore functions. *Nature Communications*, *13*(1), 1–19. https://doi.org/10.1038/S41467-022-28403-8;TECHMETA

Taylor, S. S., Hussein, D., Wang, Y., Elderkin, S., & Morrow, C. J. (2001). Kinetochore localisation and phosphorylation of the mitotic checkpoint components Bub1 and BubR1 are differentially regulated by spindle events in human cells. *Journal of Cell Science*, *114*(Pt 24), 4385–4395. https://doi.org/10.1242/JCS.114.24.4385

Thevathasan, J. V., Kahnwald, M., Cieśliński, K., Hoess, P., Peneti, S. K., Reitberger, M., Heid, D., Kasuba, K. C., Hoerner, S. J., Li, Y., Wu, Y. Le, Mund, M., Matti, U., Pereira, P. M., Henriques, R., Nijmeijer, B., Kueblbeck, M., Sabinina, V. J., Ellenberg, J., & Ries, J. (2019). Nuclear pores as versatile reference standards for quantitative superresolution microscopy. *Nature Methods 2019 16:10*, *16*(10), 1045–1053. https://doi.org/10.1038/s41592-019-0574-9

Thompson, S. L., & Compton, D. A. (2010). Proliferation of aneuploid human cells is limited by a p53-dependent mechanism. *Journal of Cell Biology*, *188*(3), 369–381. https://doi.org/10.1083/JCB.200905057

Tovell, H., Testa, A., Maniaci, C., Zhou, H., Prescott, A. R., Macartney, T., Ciulli, A., & Alessi, D. R. (2019). Rapid and Reversible Knockdown of Endogenously Tagged Endosomal Proteins via an Optimized HaloPROTAC Degrader. *ACS Chem. Biol*, *14*, 35. https://doi.org/10.1021/acschembio.8b01016

Uchida, K. S. K., Jo, M., Nagasaka, K., Takahashi, M., Shindo, N., Shibata, K., Tanaka, K., Masumoto, H., Fukagawa, T., & Hirota, T. (2021). Kinetochore stretching-mediated rapid silencing of the spindle-assembly checkpoint required for failsafe chromosome segregation. *Current Biology*, *31*(8), 1581-1591.e3. https://doi.org/10.1016/j.cub.2021.01.062

Uchida, K. S. K., Takagaki, K., Kumada, K., Hirayama, Y., Noda, T., & Hirota, T. (2009). Kinetochore stretching inactivates the spindle assembly checkpoint. *The Journal of Cell Biology*, *184*(3), 383–390. https://doi.org/10.1083/JCB.200811028

Umbreit, N. T., Gestaut, D. R., Tien, J. F., Vollmar, B. S., Gonen, T., Asbury, C. L., & Davis, T. N. (2012). The Ndc80 kinetochore complex directly modulates microtubule dynamics. *Proceedings of the National Academy of Sciences of the United States of America*, *109*(40), 16113–16118. https://doi.org/10.1073/PNAS.1209615109/SUPPL_FILE/SM01.AVI

Vassilev, L. T., Vu, B. T., Graves, B., Carvajal, D., Podlaski, F., Filipovic, Z., Kong, N., Kammlott, U., Lukacs, C., Klein, C., Fotouhi, N., & Liu, E. A. (2004). In Vivo Activation of the p53 Pathway by Small-Molecule Antagonists of MDM2. *Science*, *303*(5659), 844–848. https://doi.org/10.1126/SCIENCE.1092472/SUPPL_FILE/VASSILEV.SOM.PDF

Vleugel, M., Hoek, T. A., Tromer, E., Sliedrecht, T., Groenewold, V., Omerzu, M., & Kops, G. J. P. L. (2015). Dissecting the roles of human BUB1 in the spindle assembly checkpoint. *Journal of Cell Science*, *128*(16), 2975–2982. https://doi.org/10.1242/JCS.169821/260349/AM/DISSECTING-THE-ROLES-OF-HUMAN-BUB1-IN-THE-SPINDLE

Vleugel, M., Omerzu, M., Groenewold, V., Hadders, M. A., Lens, S. M. A., & Kops, G. J. P. L. (2015). Sequential Multisite Phospho-Regulation of KNL1-BUB3 Interfaces at Mitotic Kinetochores. *Molecular Cell*, *57*(5), 824–835. https://doi.org/10.1016/j.molcel.2014.12.036

Vleugel, M., Tromer, E., Omerzu, M., Groenewold, V., Nijenhuis, W., Snel, B., & Kops, G. J. P. L. (2013). Arrayed BUB recruitment modules in the kinetochore scaffold KNL1 promote accurate chromosome segregation. *Journal of Cell Biology*, *203*(6), 943–955. https://doi.org/10.1083/JCB.201307016

Volkov, V. A., Huis In 'T Veld, P. J., Dogterom, M., & Musacchio, A. (2018). Multivalency of NDC80 in the outer kinetochore is essential to track shortening microtubules and generate forces. *ELife*, *7*. https://doi.org/10.7554/ELIFE.36764

Waizenegger, I. C., Giménez-Abián, J. F., Wernic, D., & Peters, J. M. (2002). Regulation of human separase by securin binding and autocleavage. *Current Biology*, *12*(16), 1368–1378. https://doi.org/10.1016/S0960-9822(02)01073-4

Wang, F., Dai, J., Daum, J. R., Niedzialkowska, E., Banerjee, B., Stukenberg, P. T., Gorbsky, G. J., & Higgins, J. M. G. (2010). Histone H3 Thr-3 phosphorylation by Haspin positions Aurora B at centromeres in mitosis. *Science (New York, N.Y.)*, *330*(6001), 231–235. https://doi.org/10.1126/SCIENCE.1189435

Wei, R. R., Al-Bassam, J., & Harrison, S. C. (2006). The Ndc80/HEC1 complex is a contact point for kinetochore-microtubule attachment. *Nature Structural & Molecular Biology 2007 14:1*, *14*(1), 54–59. https://doi.org/10.1038/nsmb1186

Weinberg, R. A. (1995). The retinoblastoma protein and cell cycle control. *Cell*, *81*(3), 323–330. https://doi.org/10.1016/0092-8674(95)90385-2

Welburn, J. P. I., Vleugel, M., Liu, D., Yates, J. R., Lampson, M. A., Fukagawa, T., & Cheeseman, I. M. (2010). Aurora B Phosphorylates Spatially Distinct Targets to Differentially Regulate the Kinetochore-Microtubule Interface. *Molecular Cell*, *38*(3), 383–392. https://doi.org/10.1016/j.molcel.2010.02.034

Wheatley, S. P., Carvalho, A., Vagnarelli, P., & Earnshaw, W. C. (2001). INCENP is required for proper targeting of Survivin to the centromeres and the anaphase spindle during mitosis. *Current Biology*, *11*(11), 886–890. https://doi.org/10.1016/S0960-9822(01)00238-X

Wong, K. M., Micel, L. N., Selby, H. M., Tan, A. C., Pitts, T. M., Bagby, S. M., Spreafico, A., Klauck, P. J., Blakemore, S. J., Smith, P. F., McDonald, A., Berger, A., Tentler, J. J., & Eckhardt, S. G. (2016). Targeting the Protein Ubiquitination Machinery in Melanoma by the NEDD8-Activating Enzyme Inhibitor Pevonedistat (MLN4924). *Investigational New Drugs*, *35*(1), 11. https://doi.org/10.1007/S10637-016-0398-8

Xu, Z., Ogawa, H., Vagnarelli, P., Bergmann, J. H., Hudson, D. F., Ruchaud, S., Fukagawa, T., Earnshaw, W. C., & Samejima, K. (2009). INCENP–aurora B interactions modulate kinase activity and chromosome passenger complex localization. *Journal of Cell Biology*, *187*(5), 637–653. https://doi.org/10.1083/JCB.200906053

Yamagishi, Y., Honda, T., Tanno, Y., & Watanabe, Y. (2010). Two histone marks establish the inner centromere and chromosome bi-orientation. *Science (New York, N.Y.)*, *330*(6001), 239–243. https://doi.org/10.1126/SCIENCE.1194498

Yamagishi, Y., Yang, C. H., Tanno, Y., & Watanabe, Y. (2012). MPS1/Mph1 phosphorylates the kinetochore protein KNL1/Spc7 to recruit SAC components. *Nature Cell Biology*, *14*(7), 746–752. https://doi.org/10.1038/NCB2515

Yang, Y. H., Wei, Y. L., & She, Z. Y. (2024). Kinesin-7 CENP-E in tumorigenesis: Chromosome instability, spindle assembly checkpoint, and applications. *Frontiers in Molecular Biosciences*, *11*, 1366113. https://doi.org/10.3389/FMOLB.2024.1366113/XML

Yatskevich, S., Muir, K. W., Bellini, D., Zhang, Z., Yang, J., Tischer, T., Predin, M., Dendooven, T., McLaughlin, S. H., & Barford, D. (2022). Structure of the human inner kinetochore bound to a centromeric CENP-A nucleosome. *Science (New York, N.Y.)*, *376*(6595), 844–852. https://doi.org/10.1126/SCIENCE.ABN3810

Yatskevich, S., Yang, J., Bellini, D., Zhang, Z., & Barford, D. (2024). Structure of the human outer kinetochore KMN network complex. *Nature Structural & Molecular Biology*, *31*(6), 874–883. https://doi.org/10.1038/S41594-024-01249-Y

Ye, A. A., Deretic, J., Hoel, C. M., Hinman, A. W., Cimini, D., Welburn, J. P., & Maresca, T. J. (2015). Aurora A kinase contributes to a pole-based error correction pathway. *Current Biology : CB*, *25*(14), 1842. https://doi.org/10.1016/J.CUB.2015.06.021

Zeng, K., Bastos, R. N., Barr, F. A., & Gruneberg, U. (2010). Protein phosphatase 6 regulates mitotic spindle formation by controlling the T-loop phosphorylation state of Aurora A bound to its activator TPX2. *The Journal of Cell Biology*, *191*(7), 1315–1332. https://doi.org/10.1083/JCB.201008106

Zhang, G., Kruse, T., López-Méndez, B., Sylvestersen, K. B., Garvanska, D. H., Schopper, S., Nielsen, M. L., & Nilsson, J. (2017). Bub1 positions Mad1 close to KNL1 MELT repeats to promote checkpoint signalling. *Nature Communications*, *8*(1), 1–12. https://doi.org/10.1038/NCOMMS15822;TECHMETA